Numerical Assessment for Long-term Behavior of the Pleistocene Marine Foundations Due to Construction of Large-scale Offshore Airport Fill

ByungGon JEON

Numerical Assessment for Long-term Behavior of the Pleistocene Marine Foundations Due to Construction of Large-scale Offshore Airport Fill

By

ByungGon JEON

A thesis submitted for the Degree of Doctor of Engineering at the Kyoto University

Graduate School of Engineering,
Department of Civil and Earth Resources Engineering
Kyoto University
Kyoto, Japan
2012

Abstract

Kansai International Airport (KIX) was constructed 5km offshore in Osaka Bay to minimize noise and pollution in residential areas. The large-scale offshore reclamation such as KIX in Osaka Bay has undergone much difficulty in the ground settlement due to the unforeseen occurrence. Such a large-scale offshore reclamation has caused a large amount of settlement even in the stiff Pleistocene clay deposits as well as in the soft Holocene clay deposits. The distinguished structure called “quasi-overconsolidation” for the Pleistocene clay layers and insufficient permeability for the Pleistocene sand gravel layers make the prediction of ground settlement due to the offshore reclamation very difficult. The adjacent construction of the twin airport fills on the marine foundations that have insufficient permeability of the Pleistocene sand gravel layers is another significant factor for the difficulty in predicting the ground settlement because of the complicated mechanism of the interactive behavior between two islands associated with the effect of the propagation of excess pore water pressure through the Pleistocene sand gravel layers.

In the foundation ground of KIX having the Holocene clay underlain by the alternating Pleistocene clay and sand gravel layers, the Pleistocene clay layers exhibit the characteristic of the quasi-overconsolidated clay with OCR of 1.1 to 1.6 in average without definite mechanical overconsolidation, and the Pleistocene sand gravel layers exhibit the non-uniform distribution with occasional discontinuity in the horizontal direction. Therefore, the primary and secondary consolidation for those Pleistocene clay layers is observed to occur at the same time caused by time-dependent compression for the quasi-overconsolidated clay layers and insufficient permeability of the Pleistocene sand gravel layers.

A plane-strain elasto-viscoplastic constitutive model proposed on the basis of the concept of

"non-stationary flow surface" is adopted to assess the time-dependent behavior of the Pleistocene clay layers that actually has taken place in the field of KIX. The compression model for the quasi-overconsolidated Pleistocene clays is also adopted for the finite element analysis to consider the time-dependent behavior even in the overconsolidated region. The mechanism of the propagation and dissipation of excess pore water pressure due to insufficient permeability of the Pleistocene sand gravel layers is investigated.

A series of elasto-viscoplastic finite element analyses is performed to develop the numerical procedure with the simple foundation model as the first step. The concept of "mass permeability" is introduced by considering the sedimentation environment to evaluate the representative permeable capacity for the Pleistocene sand gravel layers in the foundation ground of KIX. The proposed numerical procedure is validated by comparing with the measured results.

A series of elasto-viscoplastic finite element analysis is also performed to assess the long-term and the interactive behavior of the reclaimed Pleistocene deposits due to the adjacent construction of the twin airport fills of the 1st and 2nd phase islands. The mechanism for the propagation and dissipation of excess pore water pressure is carefully investigated with the concept of "mass permeability" for the Pleistocene sand gravel layers. The long-term settlement associated with the mode of excess pore water pressure is also investigated with the compression model for the quasi-overconsolidated clays. The predictive accuracy for the proposed numerical procedure is validated by comparing with the measured results at the monitoring point 1 and 2 located in the 1st and 2nd phase islands respectively.

The geologically genuine foundation model has been developed to evaluate the realistic in situ behavior of stress and strain because the geometry of the foundations such as the inclination of the base and the horizontal variation of thickness of the individual clays is one of the most influential factors for numerical analysis. The effect of the drastic change in thickness of

permeable sand gravel layers is investigated based on the finite element analysis. It is found that the thickness as well as the permeability of the sand gravel layers plays a significant role for the behavior of excess pore water pressure. The concept of “standard hydraulic gradient” is also introduced to evaluate the mass permeability for the Pleistocene sand gravel layers of the geologically genuine foundation model. The concept of “standard hydraulic gradient” is found to well reproduce the representative permeable capacity that is evaluated as the concept of mass permeability for the ideal foundation model having the horizontally even layers with constant thickness.

The compression model for the quasi-overconsolidated Pleistocene clays and the representative permeable capacity as the concept of “mass permeability” for the Pleistocene sand gravel layers is applied to the additional review sections with the concept of “standard hydraulic gradient”. The objectivity of the proposed procedure is confirmed through the descriptive accuracy of the measured results even at the additional sections.

On the basis of the above-mentioned findings, the proposed numerical procedure is found to well describe the large and long-term settlement together with the slow dissipation and remarkable propagation of excess pore water pressure in the Pleistocene clay and sand gravel layers that actually has taken place at the site of large-scale offshore reclamation.

Key words: elasto-viscoplasic finite element analysis, reclaimed marine foundation, large- scale offshore reclamation, quasi-overconsolidated Pleistocene clay, Pleistocene sand gravel, long-term behavior, interactive behavior, mass permeability, standard hydraulic gradient

Acknowledgments

First of all, I would like to express my gratitude to the Almighty God and Jesus Christ, who is my savior and everything to me, for giving me the ability to undertake this work.

The research reported in this dissertation was carried out while I was a doctoral student at the Department of Civil and Earth Resources Engineering, Graduate School of Engineering, Kyoto University, Japan. It would be impossible for this dissertation to have been accomplished without the support and encouragement of dear professors, colleagues and my family, to whom I would like to express my gratitude.

I am deeply indebted to my supervisor Professor Mamoru Mimura for his warm encouragement and insightful guidance throughout my study. I greatly appreciate the opportunities he has given me to undertake my graduate studies with his extensive support. I learned many things, academic and non-academic, from my professor. I will keep in mind his sound advice and various teachings for the last four years.

Grateful acknowledgements are also extended to another supervisor, Professor Susumu Iai for welcoming me into his laboratory to work on my study, and for his critical and insightful review of the manuscript and valuable comments. I also wish to thank Professor Makoto Kimura for his constructive suggestions and critical discussions as a committee member for my doctoral degree.

I would like to express my sincere gratitude to the officers of Kansai International Airport Co. Ltd. for their support for providing the information of the in-situ measured data and technical advice. Thanks are also extended to Dr. Koji Yamamoto and the technical staffs of Geo- Research Institute for their earnest cooperation.

I want to thank the members of the Iai Lab. for their support and friendship; Tetsuo Tobita,

Assistant Professor, Mr. Hiroki Shimizu and Mr. Kazuhide Tomisaka, Technicians, Ms. Waka Yuyama, Secretary, and all students. I received a lot of help and advice from them. I will never forget the wonderful time we had together in the Iai Lab.

I would also like to express my special gratitude to my master advisor, Professor SeBoong Oh of Yeungnam University (Korea) for his continuous encouragement and good advice. My sincere appreciation is extended to Associate Professor YoungSang Kim of Chonnam National University (Korea) for recommending me to begin studying at Kyoto University. I am deeply grateful to all the members of Kyoto Nambu Church who have been my another family during my stay in Japan.

Last, but not least, I would like to dedicate this dissertation to my lovely wife, SeoYeon and my lovely daughter, AhIn. My wife has given me continuous support and devoted encouragement through it all. Without her understanding, I would not be able to achieve my PhD endeavor. Finally, I want to thank my parents, my brother and two sisters for their love, warm encouragement and belief.

Table of Contents

List of Figures

List of Tables

1. Introduction

1.1 Background

The development of coastal area accomplished in Japan has been outstanding. Kansai International Airport (KIX) was constructed in Osaka Bay as two man-made reclaimed islands to minimize noise and pollution in residential areas as well as to meet the increasing demand for air transportation. The project of "the second airport in Kansai" was instituted in 1960's on the basis of the assumption that the existing Itami Airport could not cope with the expanding demand for air transportation such as the increase in cruising range, arrival and departure ability, and the number of customers. As for "the second airport in Kansai", the coast of Izumisano City was selected to the construction site among the candidates such as the offing of Osaka south port, the coast of Kobe, the coast of Akashi, Awaji Island, and the coast of Izumisano City. The first stage construction of Kansai International Airport (KIX) including the one runway and the terminal building was started by constructing an offshore reclaimed island of 515 hectares at 5km offing of the Izumisano City in 1987. The 1st phase island began to be operated as the first 24-hour airport in Japan on September 4, 1994. In 2001, after 13years since the start of the 1st phase island construction, reclamation of the 2nd phase island was started to develop an offshore reclaimed island of 545 hectares at 200m offing of the existing 1st phase island and upgrade various facilities concerned with the 4,000m parallel runway, which has been used from 2007.

Figure 1.1 shows the location map for Kansai International Airport (KIX) constructed 5km in the offing of Izumisano City, southern Osaka. Such a large-scale offshore reclamation in Osaka Bay is accompanied with large and rapid settlement of deep Pleistocene clay deposits (Mimura et al., 2003). Long-term settlement of the Pleistocene marine foundations due to huge reclamation load has been of great concern in this project. Akai and Tanaka (1999) also reported that large and rapid settlement had occurred without significant dissipation of excess pore water

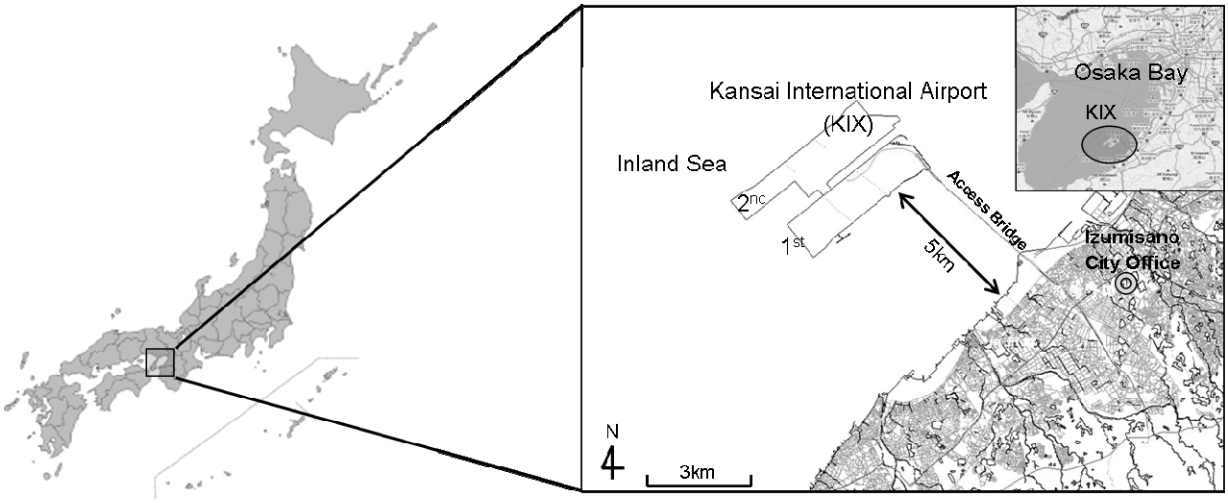

Fig. 1.1 Location map for Kansai International Airport (KIX)

pressure in the Pleistocene clay and sand gravel deposits in the foundation ground of Kansai International Airport (KIX). In the sense, the phenomenon taking place due to the reclamation of KIX seems too curious to explain by adopting the conventional concept of consolidation in which deformation advances associated with the dissipation of excess pore water pressure.

Itoh et al. (2001) summarized on the basis of the data from elastic wave exploration and in-situ boring logs that the Pleistocene sand gravel deposits are not always distributed uniformly in thickness, consistently and that the amount of fine contents included in them is significant. The most serious problem originating from these sand gravel deposits is the "permeability" that controls the rate of consolidation of sandwiched Pleistocene clays because the net values of the coefficient of permeability based on laboratory experiments do not necessarily function as representatives for such non-uniform sand gravel layers with occasional horizontal discontinuity and/or variation of thickness. The quantitative contribution of the Pleistocene sand gravel layers to the long-term settlement of the Pleistocene deposits was shown by Jang and Mimura (2005). The Pleistocene clays have distinguished structure due to the long term effect of diagenesis. The compression behavior of this kind of clay has a strong resemblance to that of Canadian clay with highly developed structure (Leroueil et al., 1985) where no linear relationship is found between

the void ratio and the logarithm of the applied overburden within the range of virgin compression. On the basis of these findings, Mimura et al. (1994) proposed the tri-linear compression model for the Pleistocene clays of KIX construction site. This modeling provided a rapid advance in settlement without any significant dissipation of excess pore water pressure, which has actually occurred in the field. Mimura and Jang (2004) proposed a concept of compression in which viscoplastic behavior is assumed to occur even in the quasi-overconsolidated region than p_c for the Pleistocene clays in Osaka Bay. The procedure has been found to be versatile and allows for the long-term settlement monitored in the reclaimed islands in Osaka Port to be described (Mimura and Jang, 2005a).

The coming problem encountered is the interactive behavior between the 1st and 2nd phase islands. The generated excess pore water pressure due to construction of the 2nd phase island is expected to propagate to the foundation beneath the existing 1st phase island through the Pleistocene sand gravel layers. Such phenomenon as the propagation of excess pore water pressure to the foundation beneath the 1st phase island causes the decrease in effective stress and the induced deformation of the Pleistocene clay layers. It is of importance to evaluate the interactive behavior between the reclaimed Pleistocene foundations of the 1st and 2nd phase islands of KIX for the stable operation and strategic system for maintenance of the offshore airport. There is no precedent for such achievement.

1.2 Previous researches on KIX

An exploratory committee was established to address the geotechnical problems with Kansai International Airport project from 1980 to 1983, collating opinions with regard to settlement predictions based on the results of previous surveys and other data. In pre-survey before construction of the 1st phase island in 1983, amount of settlement of 6.0m for the Holocene layer and 1.5m for the Pleistocene layer was predicted after 50yers from the start of construction by considering the sand gravel layers (Ds1, 8, 9, and 10) having thickness more than 3m as perfectly permeable ones (Nakase, 1992). However, it was recognized that the rate of settlement in the Pleistocene layers is faster than the prediction in the pre-survey through in-situ measurement. The prediction of the long-term settlement for the Pleistocene layers was revised in 1989 by considering all Pleistocene sand gravel layers as perfectly permeable (Suzuki, 2008).

To improve the accuracy of settlement predictions, studies in several categories have been continuously performed by many researches. First, geological survey of KIX has been studied (Takemura and Nakaseko, 2005; Kitada et al., 2011; Inoue et al., 2011). Second, the characteristics of the Pleistocene clay layers have been evaluated through the laboratory and in-situ tests and numerical analyses (Imai et al., 2005; Duncan et al., 2005; Oda et al, 2005; Tsuchida, 2005). Third, the permeability of the Pleistocene sand gravel layers has been evaluated through a series of three-dimensional seepage analyses around the marine foundations of KIX (Kansai International Airport Co., 2002; Nishigaki and Imai, 2005).

On the basis of those studies, numerical assessment of the long-term settlement of the reclaimed Pleistocene marine deposits at KIX has been conducted based on the elasto-viscoplastic or elasto-plastic finite element analyses considering the Pleistocene sand gravel layers as perfectly or partially permeable (Sekiguchi et al., 1988, 1991; Endo et al., 1991; Akai and Tanaka, 1999; Kobayashi et al., 2005; Mimura and Jang, 2005b; Shibata and Karube,

2005).

It is true those studies provided the successful description of the actual state of settlement of KIX for the Pleistocene deposits, but the interactive behavior due to the adjacent construction of the 1st and 2nd phase islands and the mechanism of propagation and dissipation of excess pore water pressure have not been definitely interpreted yet. It is strongly required that the actual interactive behavior such as the propagation of excess pore water pressure through the partially drained Pleistocene sand gravel layers as well as the retardation and restarting of settlement should be rationally explained.

1.3 Objectives

The objective of the study is to assess the long-term behavior of the Pleistocene marine foundations due to the large-scale offshore reclamation such as KIX. The settlement has become a significant technical issue in KIX because the unforeseen settlement has continuously advanced even after the completion of the reclamation, which was not expected in the early stage of the project. It is so difficult to predict the settlement in the Pleistocene layers of KIX in the following several reasons.

First, the reclaimed marine foundation is composed of very complicated geological layers alternating the clay and sand gravel deposits due to the effect of transgression and regression.

Second, because it is not easy to confirm the mode of distribution of the sand gravel layers that have occasional horizontal discontinuity, variation of thickness and various fine contents, it is very difficult to evaluate the permeability of sand gravel layers that controls the rate of consolidation in the clay layers. In the sense, depending on the permeability of sand gravel layers, the indistinguishable primary and secondary consolidation in the clay layers has even occurred at the same time in the filed. Sekiguchi et al. (1988, 1991) showed that long-term

settlement is expected in the Pleistocene deposits due to the construction of KIX based on a calculated performance by considering the perfectly drained sand gravel layers with a series of elasto-viscoplastic finite element analyses, however, the sand gravel layers at KIX were recognized not to function as perfectly drained layer through the in-situ measurement of excess pore water pressure.

Third, the Pleistocene clays called "quasi-overconsolidated clays" (Akai and Sano, 1981) in Osaka Bay have the distinguished structure due to long-term effect of diagenesis without definite mechanical overconsolidation history. In particular, it is difficult to predict the time-dependent long-term settlement of the Pleistocene clay deposits in Osaka Bay because the time-dependent behavior occurs even in the overconsolidated region less than p_c. It was reported that the predicted settlement by the conventional approach was underestimated for the Pleistocene clays, the stress sate of which remained less than p_c (Research Committee on Ground in Osaka Bay, 2002)

Finally, the mechanism of long-term behavior in the Pleistocene marine foundation of KIX is very complicated because of the interactive behavior due to the adjacent construction of the 1st and 2nd phase airport fills. The propagation of excess pore water pressure and the retardation of settlement in the foundation beneath the 1st phase island due to the construction of the 2nd phase island have been identified through the in-situ measurement. The interactive behavior should be definitely investigated to evaluate the long-term behavior after completion of the 2nd phase reclamation.

Because of the above-mentioned complicated factors, the measured behavior in the field has been found to be difficult to explain with the conventional consolidation theory for the Pleistocene deposits. The settlement of the Holocene clay deposit has reasonably been explained by the conventional framework because the rate of consolidation has been accelerated due to the effect of vertical drains. However, in the Pleistocene deposits, the excess pore water pressure in

the sand gravel layers as well as the clay layers have not been well dissipated. Althogh the sand gravel layers keep a large amount of excess pore water pressure, settlement of the Pleistocene clay layers has advanced faster than the pre-calculated results at the early stage of the project.

In this study, in order to investigate the phenomena taking place due to the reclamation at KIX, the numerical framework in terms of the elasto-viscoplastic finite element analysis. First of all, the subsurface stratigraphy of KIX is investigated based on the consideration of the sedimentary environment and in-situ acoustic exploration data. On the basis of the distribution characteristics of the individual Pleistocene sand gravel deposits and the measurements of excess pore water pressure, the permeability for the individual Pleistocene sand gravel layers is provisionally evaluated. The monitored time-dependent behavior taking place in the field for the quasi-overconsolidated Pleistocene clay deposits of KIX is also investigated by assessing the in-situ measurements.

A series of elasto-viscoplastic finite element analyses is performed to assess the long-term behavior of the Pleistocene marine foundations due to construction of the airport fill. The proposed procedure by Mimura and Jang (2004) is adopted to evaluate the time-dependent behaviors of the quasi-overconsolidated Pleistocene clays in Osaka Bay. The procedure has been introduced assuming that the deformation in the quasi-overconsolidated region is no longer elastic but elasto-viscoplastic on the basis of the fact that the quasi-overconsolidated Osaka Pleistocene clays can be considered as normally consolidated aged ones. The concept of “mass permeability” is introduced to evaluate the practical permeability of the sand gravel deposits playing a significant role as permeable layers to control the rate of consolidation of sandwiched Pleistocene clay deposits. The concept of “mass permeability” is proposed to evaluate the permeability not of each element but of the whole layer in one body for the finite element analysis. Therefore, the mass permeability is regarded as the macroscopic capability of permeability for the individual sand gravel layers by considering the horizontal continuity, the

change of thickness horizontally, the degree of fine contents and three-dimensional distribution for the individual sand gravel deposits.

The interactive behavior of the Pleistocene marine foundations due to the adjacent construction of the two airport islands of KIX is also investigated based on the elasto-viscoplastic finite element analyses using the two concepts such as “quasi-overconsolidated clays” and “mass permeability”. Due attention is paid to the mechanism of the generation/ dissipation and propagation of excess pore water pressure though the permeable Pleistocene sand gravel layers subjected to the construction of the adjacent two airport islands. The mode of advance in settlement of the Pleistocene clays associated with the process of excess pore water pressure is carefully discussed.

The geologically genuine foundation model is developed based on the stratigraphic information by the boring logs and extension of the individual layers through acoustic exploration. It is important to develop the exact stratigraphy at the target point for the accurate numerical description but the behavior of the surrounding area such as propagation of excess pore water pressure is influential to the one occurring at the target point in the present particular case. In the sense, the realistic geologically genuine foundation model is indispensable for assessing the long-term interactive behavior of the alternating reclaimed Pleistocene sand gravel and clay deposits at KIX. The concepts of “quasi-overconsolidated compression model” as well as “mass permeability” are implemented into the adopted numerical procedure. The equivalent coefficient of permeability determined for the horizontally even foundation model with the constant thickness is first applied directly to the geologically genuine foundation model. The effect of the change and constriction in thickness of the sand gravel layers on the mode of dissipation and propagation of excess pore water pressure in the reclaimed Pleistocene deposits is discussed. The descriptive accuracy of the long-term compression of the individual Pleistocene clay layers is also discussed considering the geometrical difference between the

horizontally even foundation model and the geologically genuine foundation model.

Finally, the proposed numerical procedure for the representative section is adopted to perform the numerical analyses for the geologically genuine foundation model that is completed for the additional review sections. The validity and objectivity of the proposed numerical procedure is investigated by applying them to the additional review sections including a lot of monitoring points at KIX.

Based on trial calculations, the author shows how to assess the actual behavior of the foundation ground that is taking place in the case of large-scale offshore reclamation such as KIX.

1.4 Scope and Organization

This dissertation is composed of 8 chapters. Figure 1.2 shows contents and flow of this study. The outline of each chapter is described below.

In chapter 1, the background, the objectives, the scope and the organization of the thesis are described in the introductory remarks.

In chapter 2, the subsurface stratigraphy of KIX is described with the geological sedimentary environment in Osaka Bay. The characteristics of the quasi-overconsolidated clays and the permeability of sand gravel layers in the Pleistocene deposits are investigated based on the in-situ measured data in the reclaimed foundations of KIX and the geological distribution characteristics in the sedimentary deposits.

In chapter 3, the elasto-viscoplastic constitutive model based on the non-stationary flow

surface model adopted to assess the time-dependent behavior of the quasi-overconsolidated Pleistocene clays is introduced with the matrix form for the finite element analysis of a plane-strain version. The elasto-plastic constitutive model transformed from the elasto-viscoplastic constitutive model is also introduced to evaluate the effect of time-dependent behavior by comparing with the performed results for the two constitutive models. The concrete form for the coupled stress-flow analysis using the Christian method is also introduced to assess the long-term behavior associated with the mode of excess pore water pressure.

In chapter 4, the numerical procedure to assess the actual behavior in the foundation ground of KIX due to construction of airport fill is proposed based on the finite element analysis for the representative foundation model. The foundation model is developed by assuming to have horizontally continuous even layers with constant thickness based on the stratigraphy at the monitoring point 1, where the settlement of the individual Pleistocene clay layers as well as the excess pore water pressure both in the clay and the sand gravel layers have been measured. Applicability of the time-dependent model for the quasi-overconsolidated clay in the marine foundation of KIX is validated by comparing the in-situ measurements with the calculated results by the two constitutive models, namely, the elasto-viscoplastic and elasto-plastic constitutive models. A new concept of “mass permeability” is proposed to evaluate the permeability of the Pleistocene sand gravel deposit. The effect on the inclination of the layers considered based on the stratigraphy in site is investigated by comparing with the calculated results for the horizontally even foundation model. The long-term behavior of the deeper Pleistocene foundations below Ds10 layer is also investigated based on the elasto- viscoplastic finite element analyses.

In chapter 5, a series of elasto-viscoplastic finite element analyses with the proposed

numerical procedure is performed to assess the interactive behavior of the Pleistocene marine foundations of KIX due to the adjacent construction of the 1st and 2nd phase airport fills. The marine foundations modeled independently for the 1st and 2nd phase islands considering the increase in thickness of the individual layers towards the offing are proposed for the finite element analysis. The mechanism for the propagation and dissipation of excess pore water pressure due to construction of the adjacent two reclamations is carefully discussed through the numerical procedure considering the concept of "mass permeability" introduced to model the actual process of dissipation of excess pore water pressure in the filed. The mode of advance in settlement of the Pleistocene clays associated with the mode of excess pore water pressure is also carefully discussed. The calculated performance is validated by comparing with the measured results for over 20 years from start of construction.

In chapter 6, the geologically genuine foundation model that has the inclined base overlain by the inclined Pleistocene deposits with irregular thickness is adopted for the numerical analyses. Due attention is paid to the mechanism of the generation/dissipation and propagation of excess pore water pressure by the drastic change in thickness of the permeable Pleistocene sand gravel layers for the numerical analyses considering the "equivalent coefficient of permeability" introduced as representative of "mass permeability" for the horizontally even ground foundation. The effect of the hydraulic boundary condition for the finite element analysis is also investigated by considering the drastic change of thickness near the boundary. Finally, a new procedure to apply the concept of "mass permeability", which is evaluated for the representative foundation ground, to the geologically genuine foundation model is proposed by introducing the concept of "standard hydraulic gradient". Applicability of the proposed numerical procedure for the two-dimensional finite element analysis in the geologically genuine foundation model is discussed by comparing the calculated results for the geologically genuine

and the representative foundation models with the in-situ measurements.

In chapter 7, on the basis of the data from the elastic wave exploration and geological survey, the geologically genuine foundation models are developed for the additional review sections. The proposed numerical procedure for the representative section, which is the assumption of non-elastic behavior in the quasi-overconsolidated region for the Pleistocene clays and the evaluated permeable capacity in the concepts of “mass permeability” for the Pleistocene sand gravel layers, is adopted for the numerical analyses. The applicability of the proposed numerical procedure in the representative foundation model is carefully discussed to assess the long-term behavior including the interactive behavior not only in the representative section but also in the overall reclaimed marine Pleistocene deposits with a lot of monitoring points at KIX.

In chapter 8, the conclusions of this dissertation and recommendations for the future work are summarized.

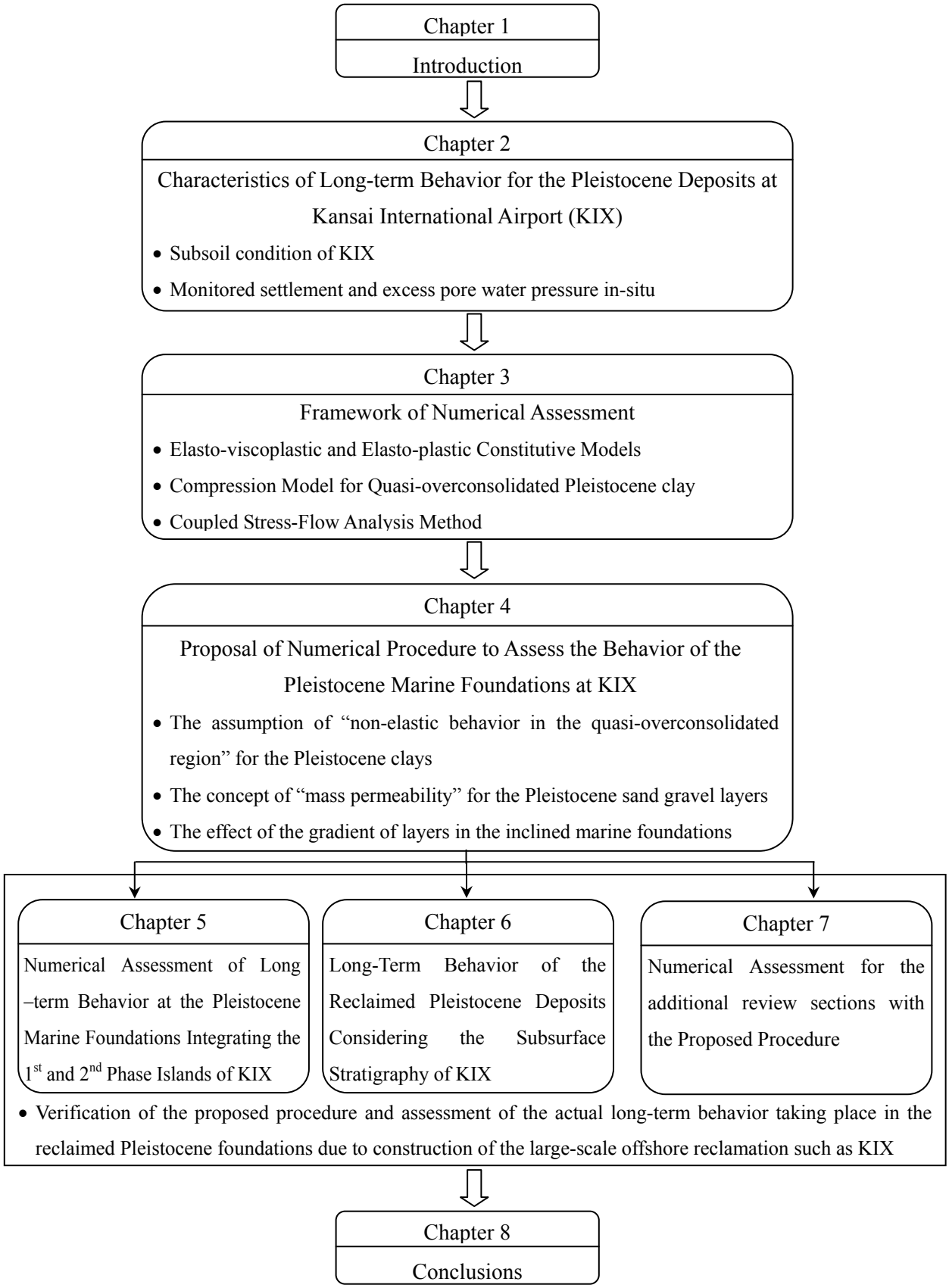

Fig. 1.2 Framework of this study

2. Characteristics of Long-term Behavior for the Pleistocene Deposits at Kansai International Airport (KIX)

2.1 General Description of Osaka Bay

Figure 2.1 shows the location map and oval shape of Osaka Bay. This beautiful creation was shaped by the couple of rising of the surrounding mountains and subsidence of the base ground in the center of the bay. It is also reported that this sedimentary basin aligned in the central part of Japan during Quaternary time (Takemura, 1985). The Quaternary Osaka sedimentary basin has developed at an eastern contractional bend of a major transcurrent fault system named the Median Tectonic Line, which divides the southwest Japan arc. The thickness of the Pleistocene sediments reaches to 3,500m at the deepest part (Yokokura et al., 1998). These sequences are called the Osaka Group and are distributed in Osaka Bay. The seabed deposits of Osaka Bay have been formed due to the soil supply from the rivers on the sinking base (Kobayashi et al., 2001). In Osaka Bay, the sedimentary deposits consist of the Holocene clay underlain by the alternated Pleistocene clay and sand gravel deposits due to transgression and regression of the sea. These marine clay deposits are formed as 15 layers at least around middle Osaka area. Inoue et al. (2001) summarized integrated subsurface structure by gravity and seismic reflection survey in Osaka Bay region and stratigraphy of Kobe district with that of KIX region.

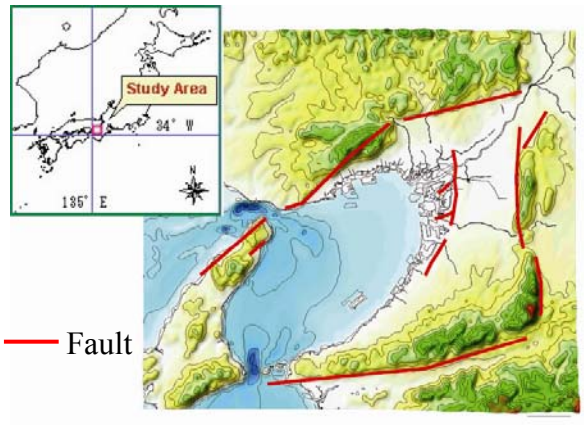

Fig. 2.1 Location map and plan view of Osaka Bay

2.2 Subsoil Conditions of KIX

2.2.1 Subsurface stratigraphy of KIX

The subsurface stratigraphy of KIX has been updated to the present ones based on the geological findings from the boring KIX 18-1, where the boring investigation was executed by digging up about 1,350m in 2006 (Kitada et al., 2011a). Figure 2.2 shows the borehole distribution of KIX including the boring KIX 18-1 near the 2nd runway of KIX. In the boring KIX 18-1, the basement rock was confirmed at the depth 1328.65m by appearing the granodiorite. Basically, the Pleistocene clay and sand gravel deposits were continuously distributed until basement rock. The subsurface stratigraphy of KIX summarized by Kitada et al. (2011a) is shown in Fig. 2.3 by exhibiting the upper sediment part within 500m. Here, Ma and Ds denote marine clay and Pleistocene sand gravel layers respectively. Ma13 is the Holocene marine clay whereas others are the Pleistocene origin. The author considers soil layers only until Ds10 layer for finite element analysis because the 1st and 2nd reclamation loads are expected as not affecting the stress and deformation and there is no measured data in the deeper soil layers than Ds10.

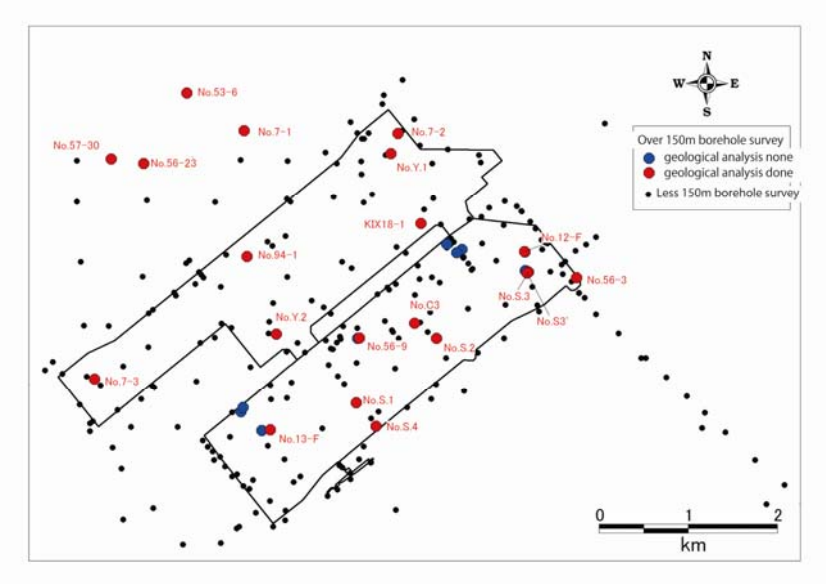

Fig. 2.2 Borehole distribution of KIX including KIX18-1

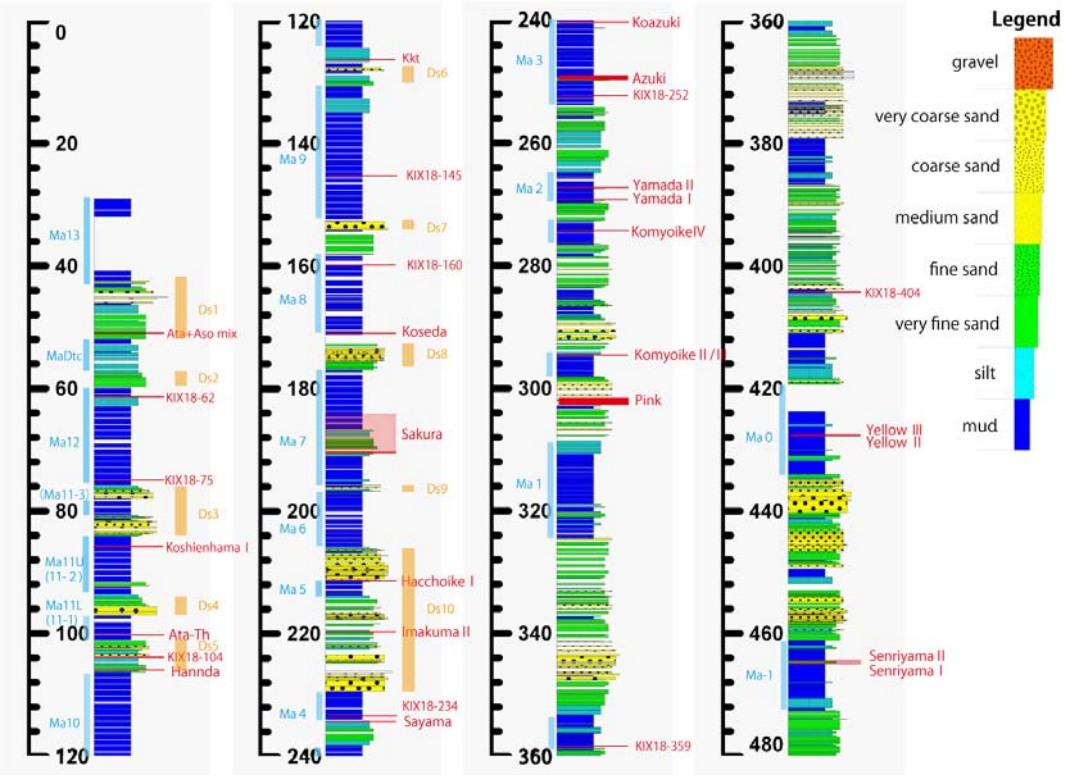

Fig. 2.3 Stratigraphy of upper deposits within 500m at KIX18-1

2.2.2 Geotechnical property of the Pleistocene clays

As is also stated, the seabed deposits of Osaka Bay have been formed due to the soil supply from the rivers on the sinking base. Although it is common that the clay deposits formed under this environment should be normally consolidated, the Pleistocene clays in Osaka Bay exhibit slight overconsolidation with OCR of 1.2 to 1.5 in average. This seeming overconsolidation is thought not to arise from the mechanical reason but to be subjected to the effect of diagenesis, such as aging effect and/or development of cementation among clay particles. In the sense, the Pleistocene clays deposited in Osaka Bay is so-called “quasi-overconsolidated clays” without definite mechanical overconsolidation history and can also be regarded as “normally consolidated aged clays” with seeming overconsolidation. Akai and Sano (1981) called those clays “quasi-overconsolidated clays” by distinguishing them from mechanical overconsolidated clays.

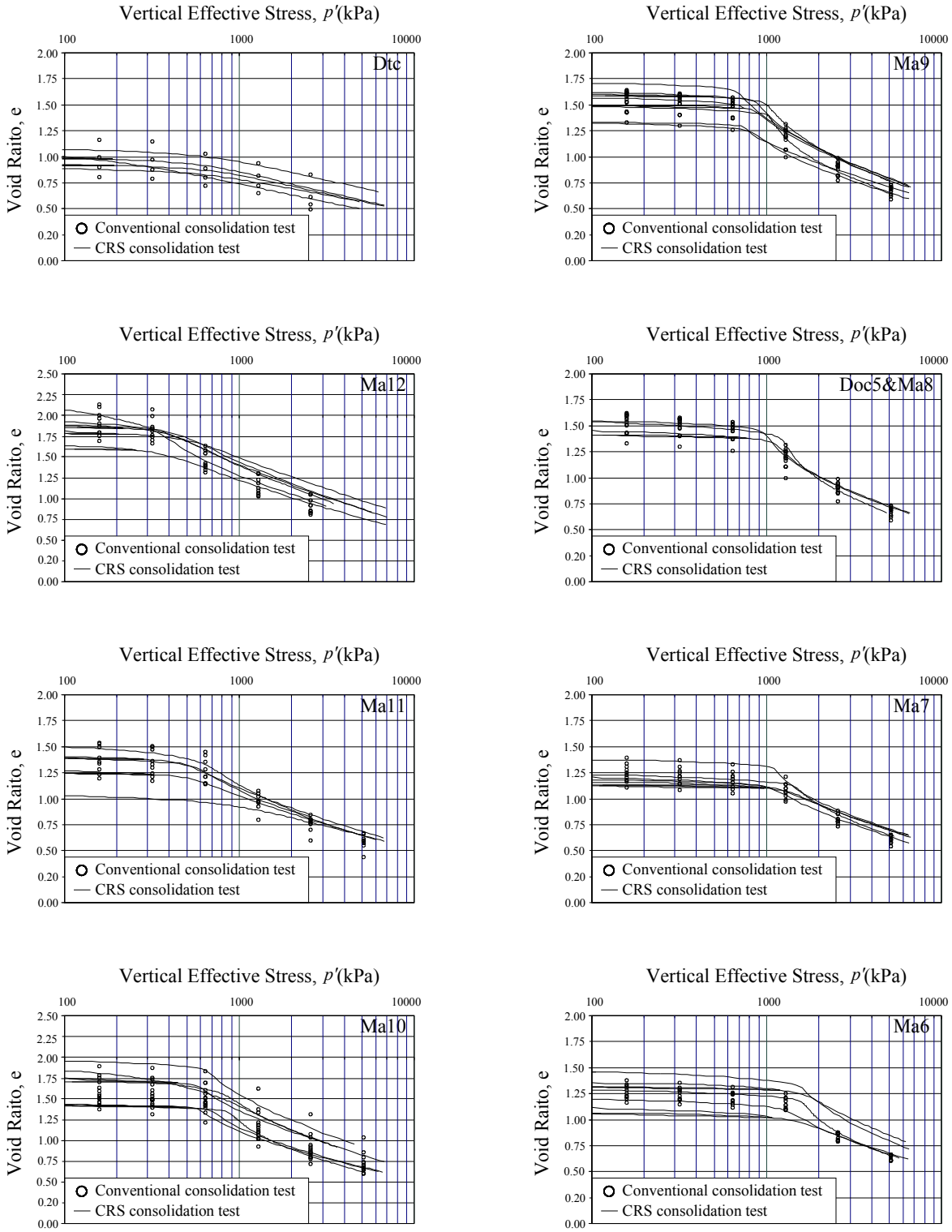

Fig. 2.4 Plots of e-log*p* from laboratory tests for the individual Pleistocene clays of KIX

It was shown that the overshoot behavior occurred associated with plastic yielding during consolidation tests on the aged Kaolin in the laboratory and concluded that the characteristic behavior such as stress overshoot was attributed to the stress and time dependency of clays that had been constructed due to long-term consolidation (Akai et al., 1984). The same behavior of structured clays due to aging or cementation was also pointed out by Leonards and Altschaeffl (1964) and Leroueil et al. (1979). Figure 2.4 shows the plots of e-log$p$ from conventional step loading and CRS consolidation tests for the Pleistocene clays of KIX. Figure 2.5 shows the distribution of OCR with depth in the Pleistocene clay deposits beneath the 1st and 2nd phase islands at KIX. The values of OCR are the results derived from laboratory tests as seen in Fig.2.4. The distribution of values also exhibits slight overconsolidation with OCR of 1.1 to 1.6 in average, showing the tendency that is decreasing with depth.

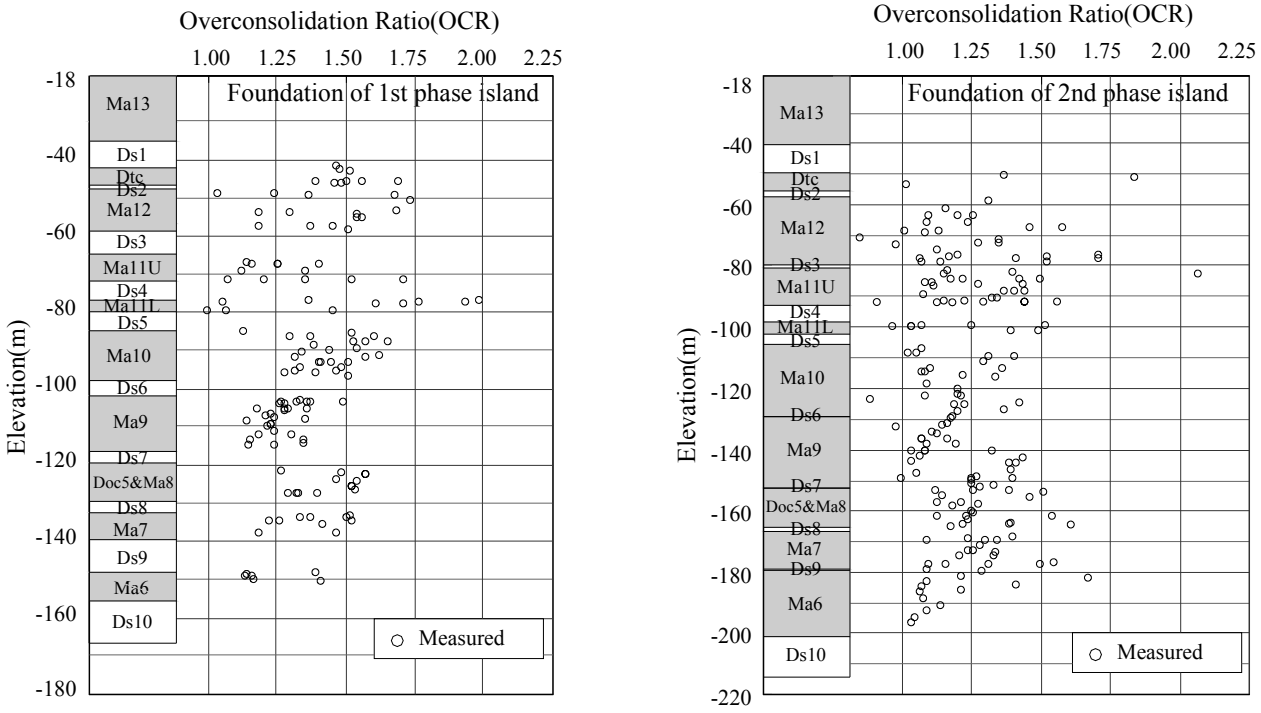

Fig. 2.5 Distribution of overconsolidation ratio (OCR) with depth for the Pleistocene clays

Long-term and large deformation has been a serious issue because the loading increment, Δp, has become large for the quasi-overconsolidated Pleistocene clay enough to undergo plastic yielding due to large-scale reclamation in a deep-sea area. Furthermore, technical and economical difficulties to adopt ground improvement methods for the Pleistocene deposits leave them unimproved, which also caused time-dependent long-term deformation of the Pleistocene clay deposits. Along Osaka Bay, this problem was found in the Port Island where the unforeseen settlement advanced at the time the reclaimed ground appeared above the sea level in 1971. Mikasa and Takada (1977) confirmed that the unforeseen settlement was attributed to the compression of the Pleistocene clay layers based on the in-situ record by the differential settlement gauges. Kiyama (1991) also pointed out that non-disregarded settlement had continued in the long run at the reclaimed islands in Osaka Bay, such as Osaka South Port (Sakishima Reclaimed Island) and Rokko Island with the contribution of compression of the Pleistocene clay layers. Mimura et al. (2003) also showed that a large-scale offshore reclamation in Osaka Bay is accompanied with large and rapid settlement of deep Pleistocene clay deposits.

2.2.3 Distribution characteristics of the Pleistocene sand gravel deposits

The sand gravel deposits play a significant role as permeable layers to control the rate of consolidation of the sandwiched Pleistocene clay deposits. The distribution of sand gravel deposits not only in the reclaimed load area but also in the area that can affect the process of dissipation of excess pore water pressure should be investigated to evaluate the permeability of them. Therefore, the distribution characteristics of the Pleistocene sand gravel layers are evaluated by considering the sedimentary environment and in-situ survey data. Itoh et al. (2001) summarized for the foundation ground of KIX on the basis of the data from elastic wave exploration and in-situ boring logs that the Pleistocene sand gravel deposits are not always

distributed uniformly in thickness, consistently and that the amount of fine contents included in them is significant. On the basis of the findings by Itoh et al. (2001), Takemura and Nakaseko (2005) summarized the status of the Pleistocene sand gravel deposits at KIX based on the geophysical and geological investigation. The brief evaluation for the individual sand gravel layers (Ds) is explained as follows:

Ds1: This unit is correlated with the Tenma Formation at Osaka Plain. The seismic reflection profile shows that Ds1 is widely distributed continuously beneath KIX.

Ds2: This unit is deposited in marine environment at temporal lower sea level stage during the Last Interglacial Period and has a narrow distribution parallel to the present shoreline.

Ds3: This unit includes the sediments deposited in river floor and flood plain at lower sea level stages and widely distributed particularly beneath the 2nd phase island.

Ds4: This unit is deposited under deltaic condition. The mode of distribution is similar to Ds3.

Ds5: This unit is widely distributed particularly beneath the 2nd phase island. Relatively coarse materials are situated in the old river floor and flood plain towards the main land.

Ds6: The distributed area of this unit is relatively narrow with definite limitation of existence offshore. It is deposited in the river floor and flood pain.

Ds7: Blackish environment during regression produced relatively fine sand layers. This unit includes small-scale river floor deposits to land direction with definite limitation of existence offshore.

Ds8: This unit includes the sediments in the flood plain and small-scale river floor deposits. Definite distribution is expected beneath the airport islands.

Ds9: This unit has the river floor deposits indicating lower sea level stage. Similar distribution is expected as Ds8.

Ds10: This coarser unit is called “basal gravel of Kukojima Formation”. Flood plain deposits are observed in the sequence. Definite distribution is found towards the main land with occasional

sandwiched clay layers. This layer is thought to be function as a predominant permeable one as same as Ds1.

Figure 2.6 shows the distribution characteristics of the individual Pleistocene sand gravel deposits on the plan view summarized by Kitada et al. (2011a) and Inoue et al. (2011). The distribution characteristics for the individual sand gravel layers (Ds) are explained as follows:

Ds1: The sand gravel layer is widely and continuously distributed beneath the foundation of KIX. The distribution of gravel layer is predominant in the area of the 1st phase island and the distribution of sand layer is predominant in the area of the 2nd phase island.

Ds2: The relatively thin sand layer is distribution in the area of the both islands.

Ds3: The sand layer is generally widely distributed and the sand layer mixed with gravel is partially distributed.

Ds4: The complicated distribution of layer is found. Basically, the sand layer is widely distributed but the sand layer is not partially distributed in the both edges of the both islands or the sand layer mixed with gravel is partially distributed in the area where there are the monitoring points shown in Fig.2.7.

Ds5: The sand layer is widely distributed in the area of the 2nd phase island and the sand layer mixed with gravel is widely distributed in the area of the 1st phase island.

Ds6: The thin sand layer is widely distributed in the area of the 1st phase island whereas the sand layer is almost not distributed in the area of the 2nd phase island.

Ds7: The sand layer is not partially distributed or the sand layer mixed with gravel is partially distributed. However, in the area of the 2nd phase island, the sand layer is not distributed in most areas beneath the 2nd phase island and the sand layer is distributed towards the outside of the 2nd phase island.

Ds8: The relatively thin sand layer is distributed in the area of the both islands.

Ds9: The sand layer is so not widely distributed in the area of the both islands and the layer

decreases in distribution towards the 2nd phase island. Even the sand layer is not distributed in the area outside of the 2nd phase island.

Ds10: The relatively thick sand layer is widely and continuously distributed in the area of the both islands.

On the basis of the results summarized by Takemura and Nakaseko (2005), Kitada et al. (2011a) and Inoue et al. (2011), the permeability of the Pleistocene sand gravel layers at KIX is qualitatively evaluated as having relatively good permeability for Ds1, 10 and poor permeability for Ds6, 7, 9 and normal permeability for the other Pleistocene sand gravel layers. It can be also evaluated that the permeability of the Pleistocene sand gravel layers beneath the foundation of the 1st phase island may be generally good than that beneath the foundation of the 2nd phase island.

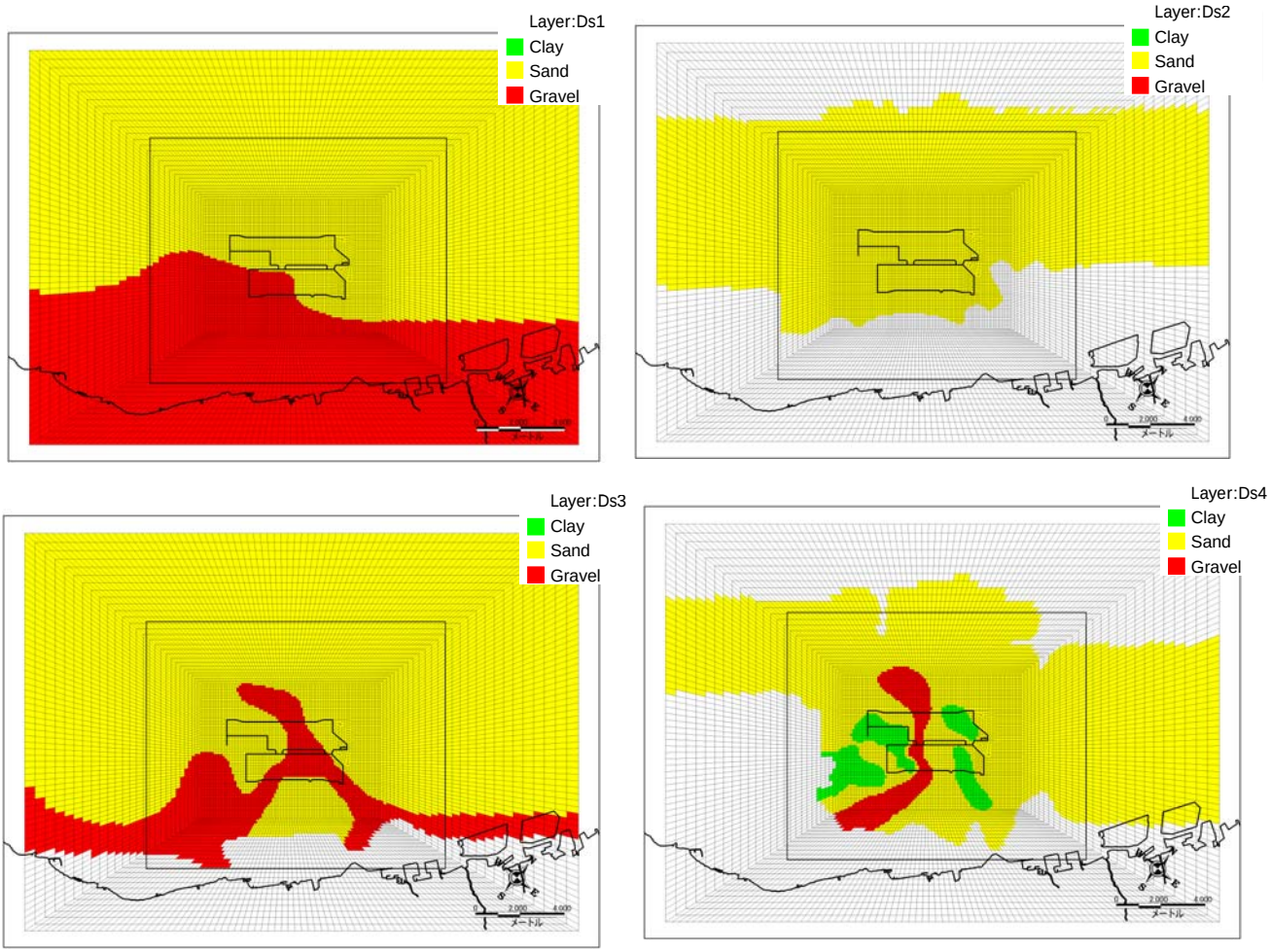

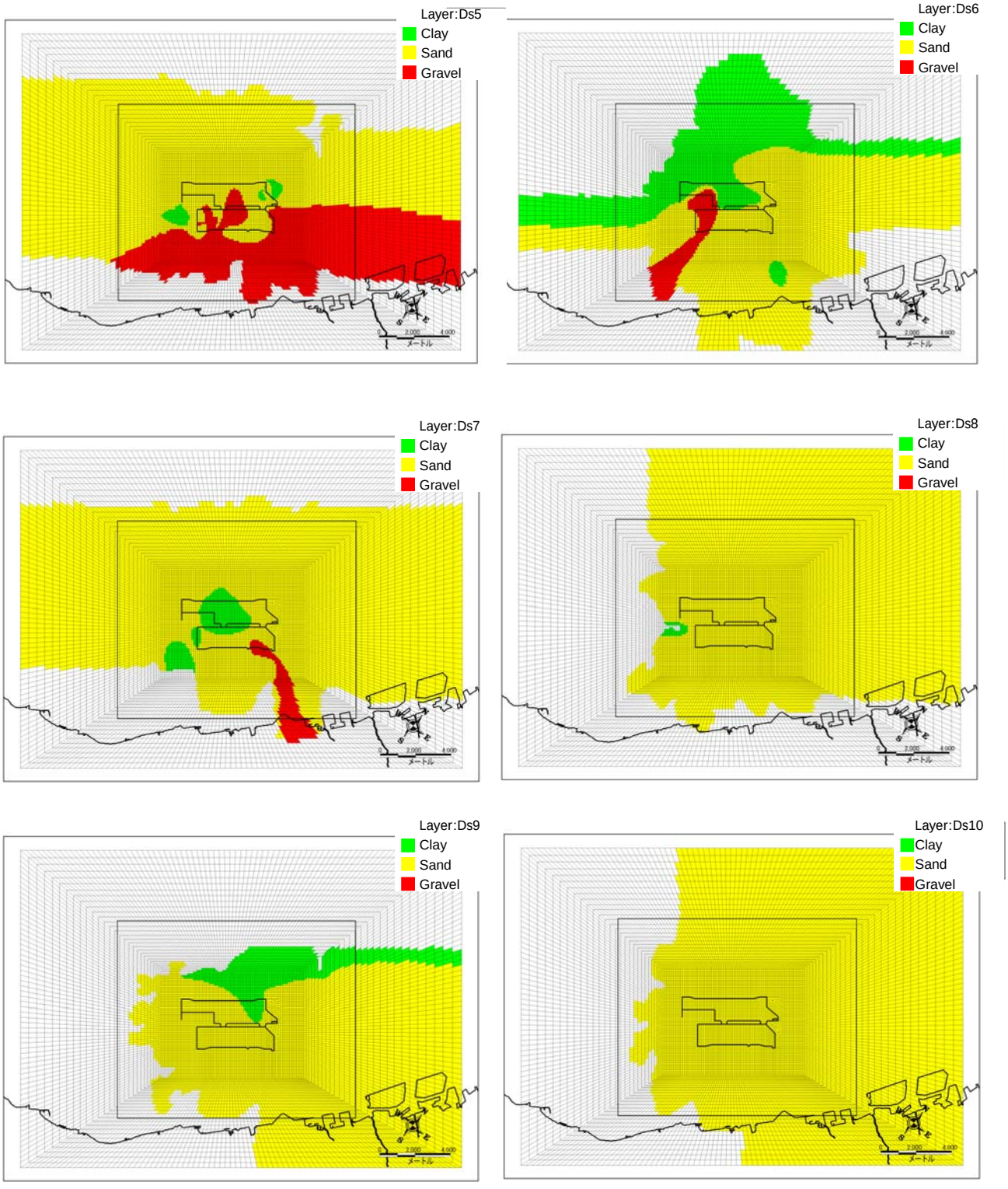

Fig. 2.6 Distribution of the individual Pleistocene sand gravel deposits on the plan view

2.3 Construction Sequence of KIX

Figure 2.7 shows the plan view of the both islands of KIX together with the locations of monitoring point 1 for the 1st phase island and 2 for the 2nd phase island where the differential settlement of the individual Pleistocene clay layers as well as the excess pore water pressure at various depths, both in the clay and the sand gravel layers, have been measured. The construction sequence along the section by A-A' in Fig 2.7 is shown in Fig 2.8 with the increasing process of the applied stress due to reclamation for two airport fills. Figure 2.9 shows the reclaimed stress measured at the monitoring points of the both islands respectively. The prescribed final overburden due to airport fill construction amounts to about 430kPa for the 1st phase island and about 530kPa for the 2nd phase island respectively. The 2nd phase reclamation is started after about 13years from the 1st reclamation.

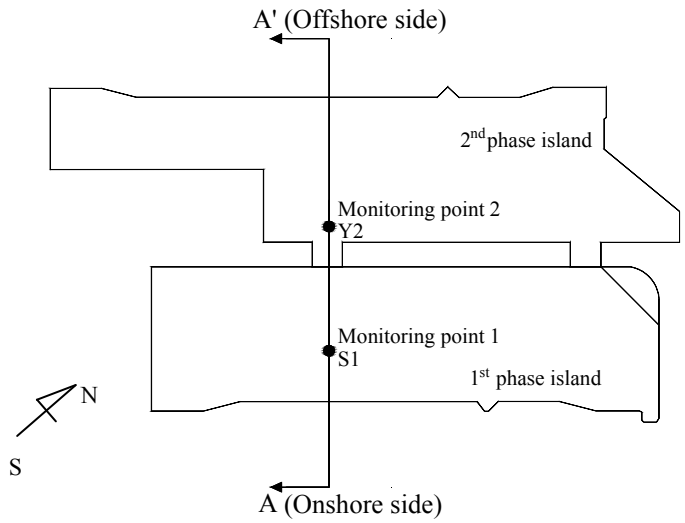

Fig. 2.7 Plan view of the 1st and 2nd phase islands of Kansai International Airport with the locations of the monitoring points

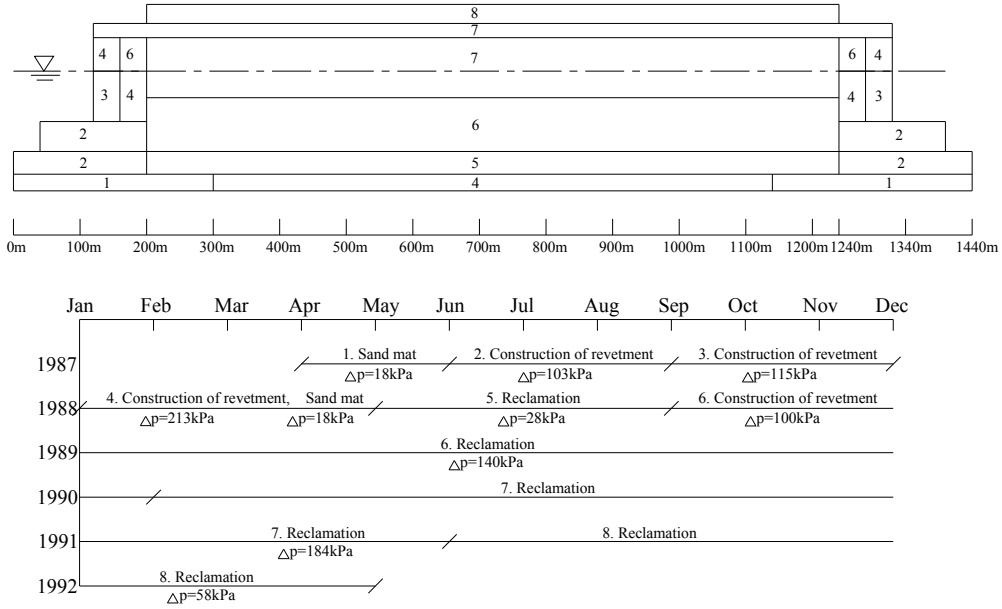

(a) 1st phase island

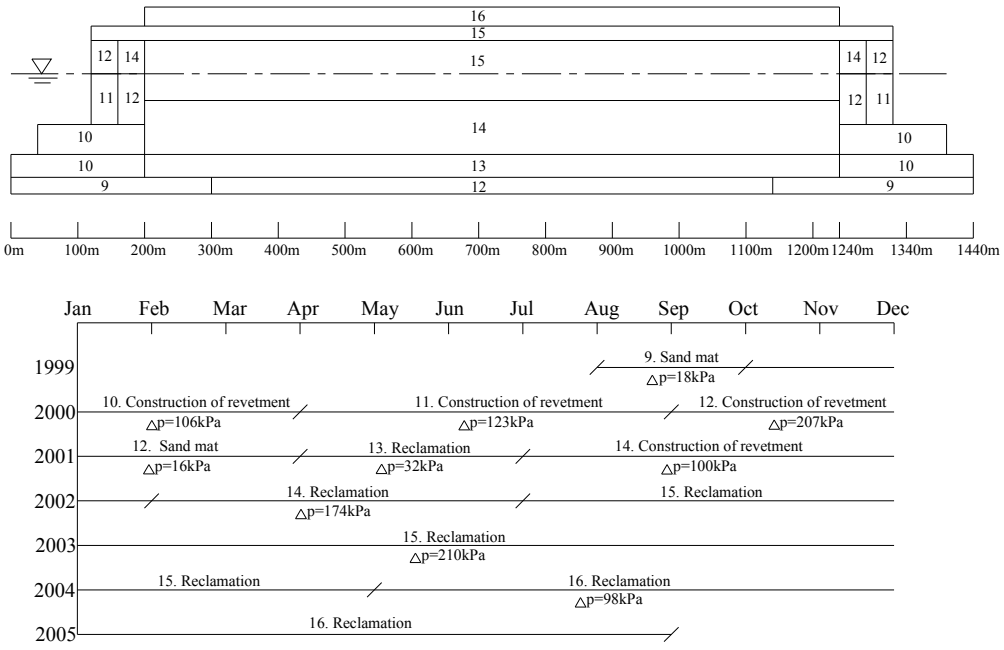

(b) 2nd phase island

Fig. 2.8 Schematic cross-section of the airport fills and the construction sequence

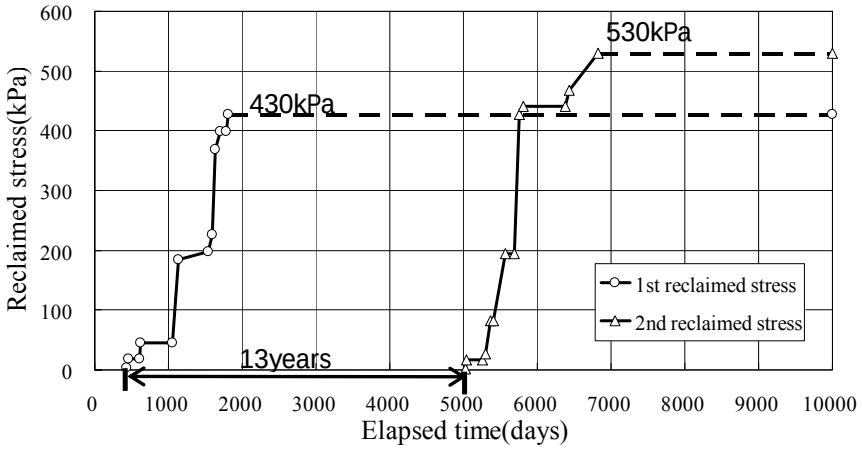

Fig. 2.9 Reclaimed stress with time for the 1st and 2nd phase reclamations

2.4 Monitored Settlement and Excess Pore Water Pressure at KIX

2.4.1 Outline of the in-situ measurement

Measurement at KIX has been continuously conducted for the differential settlement of the individual Pleistocene clay layers as well as the excess pore water pressure at various depths both in the clay and the sand gravel layers. There are a lot of monitoring points at KIX, however, the two monitoring points shown in Fig. 2.7 are considered in this section. Figure 2.10 shows the locations of surviving gauges with geological stratigraphy at the monitoring points 1 and 2 respectively. It is noteworthy that we sometimes could not have the measured information at all or good results due to the damage of them.

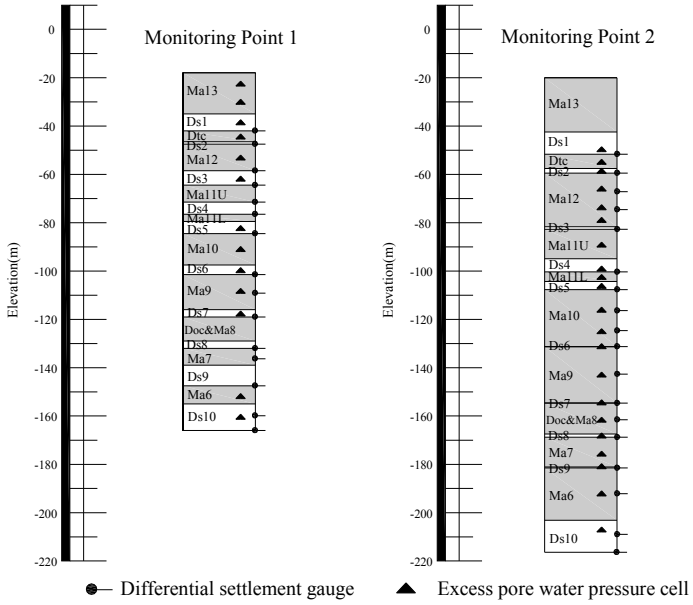

Fig. 2.10 Locations of gauges with geological stratigraphy at the monitoring points 1 and 2

2.4.2 Measured excess pore water pressure

In general, sand gravel layers are assumed to be fully drained for consolidation problems. However, the Pleistocene sand gravel layers at KIX do not have sufficient function as permeable layer because they are not always distributed uniformly in thickness, continuously and that they often include a large amount of fine contents. Figure 2.11 shows the measured distributions of excess pore water pressure with depth at the monitoring point 1 and 2 respectively. The trend line is also marked together with measured results in Fig.2.11 to estimate the distribution of excess pore water pressure in the layers where the pore water pressure cells do not have survived. Figure 2.11(a) shows the measured results at the monitoring point 1 at the time after 5years (the completion of the construction of the 1st phase island), after 13years (before the start of the construction of the 2nd phase island) and after 19years from the start of the project (the completion of the construction of the 2nd phase island) respectively. At the completion of the 1st phase reclamation, a large amount of excess pore water pressure is measured in the upper Pleistocene layers from Dtc to Ds5. Then, it dissipates steadily until before the construction of

the 2nd phase island. The upper Pleistocene sand gravel layers from Ds1 to Ds5 are thought to function as permeable layers from this phenomenon. On other hand, in the middle Pleistocene layers from Ma10 to Doc5&Ma8, a large amount of excess pore water pressure that generates at the completion of the 1st reclamation dose not remarkably decrease until before the construction of the 2nd phase island. It is thought that Ds6 and 7 have insufficient permeability to promote dissipation of excess pore water pressure. In the lower Pleistocene layers from Ds8 to Ds10, it is so difficult to evaluate the permeability of the sand gravel layers through the measured results because we could not have the measured information from Ds8 to Da9 due to the damage of pressure cells. However, by using the measured results of Ds10, 7 and Ma6 in the vicinity, the behavior of excess pore water pressure dissipation is inferred to be similar to the upper Pleistocene layers. Then, it can be summarized that Ds10 has a good permeability while Ds8 and 9 have ordinary permeability. At the completion of the 2nd phase reclamation, the increase in excess pore water pressure due to construction of the 2nd phase island is observed in the upper and the lower Pleistocene layers such as Ds3, 5 and 10. On the other hand, the increase of them is not observed in middle Pleistocene layers such as Ma9, Ds 7 and 6.

Figure 2.11 (b) shows the measured distribution at the monitoring point 2 at the time after of 14years (start of measurement), after 19years (the completion of the construction of the 2nd phase island), after 20years and after 24years from the start of the project respectively. Due attention should be paid to the fact that although little reclaimed stress was measured at the start of measurement (after 5200days (see Fig.2.9)), not a small amount of excess pore water pressure is measured from initial ground condition because the propagation of them generated due to the construction of the 1st phase island. In particular, a larger amount of excess pore water pressure is measured from the initial ground foundation in the middle Pleistocene layers that is expected to have poor permeability for sand gravel layers, Ds6 and 7. It is thought that excess pore water

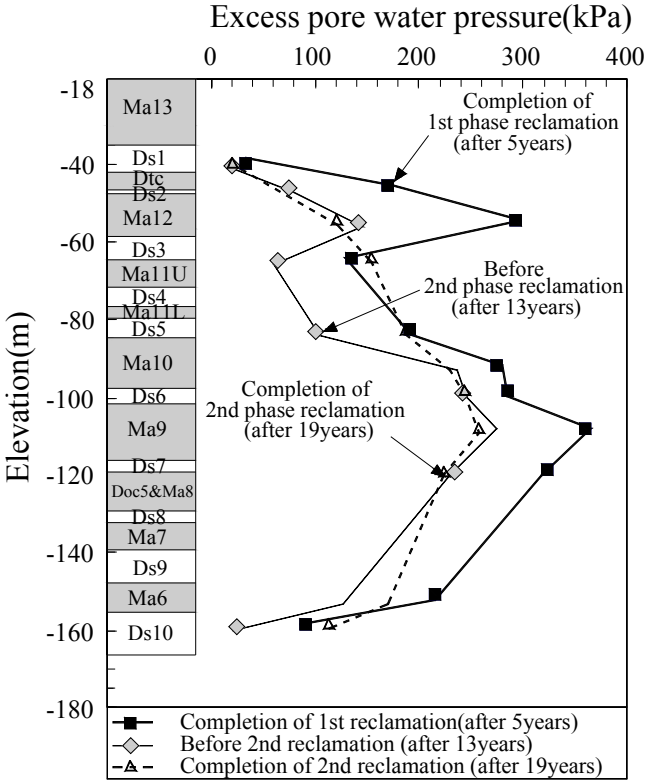

(a) Monitoring point 1

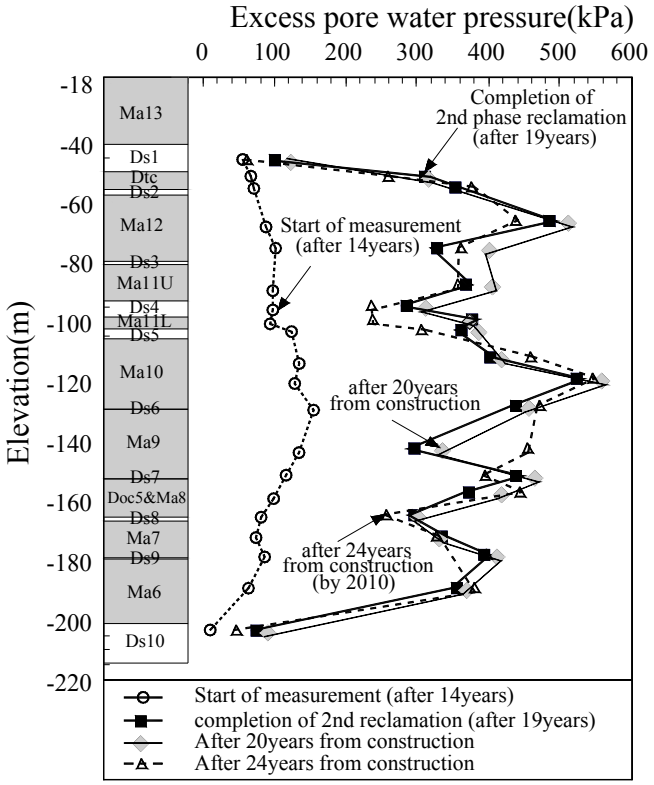

(b) Monitoring point 2

Fig. 2.11 Measured distribution of excess pore water pressure with depth

pressure generated due to construction of the 1st phase island remains undissipated in the ground foundation beneath the 2nd phase island until before the construction the 2nd phase island because of the poor permeability of the Pleistocene sand gravel layer, Ds6 and7. In the upper and lower Pleistocene layers from Ds1 to Ds5 and from Ds8 to Ds10, the generated excess pore water pressure at the completion of the 2nd phase reclamation slightly increases undissipated until after 20 years from the start of the project and then, it steadily dissipates with the lapse of time as shown at after 24years. On the other hand, in the middle Pleistocene layers from Ma10 to Doc5&Ma8, the generated excess pore water pressure due to construction of the 2nd phase island exhibits the continuously increasing distribution with the lapse of time even after the completion of the construction of the 2nd phase island. A larger amount of excess pore water pressure than the reclaimed stress (530kPa) is even observed in Ma10 because the initial stress condition in the ground foundation beneath the 2nd phase island is changed due to propagation of excess pore water pressure from the 1st reclaimed foundation.

Figure 2.12 shows the measured excess pore water pressure-time relations of the individual Pleistocene layers together with trend lines estimated from the measured data at the monitoring point 1. The trend lines of Ds2, 4, 8, 9 and Ma11, 7 and Doc5&Ma8, where there is no the measured information due to damage of the pressure cells, are proportionally inferred using the trend line in the adjoining layer and distribution trend line with depth in Fig 2.11. The trend lines will be used to calculate the settlement depending on the dissipation of excess pore water pressure based on the Terzaghi's consolidation theory in the next section. The measured process of excess pore water pressure in the upper and lower Pleistocene layers such as Ds1, 3, 5, 10 and Dtc, Ma12, 6 exhibits to be steadily dissipated with the lapse of time and the increase of excess pore water pressure due to construction of the 2nd phase island is observed in these layers. On the other hand, a large amount of excess pore water pressure is observed not only in the clay layers but also in the permeable sand gravel layers in the middle Pleistocene layers such as Ds6,

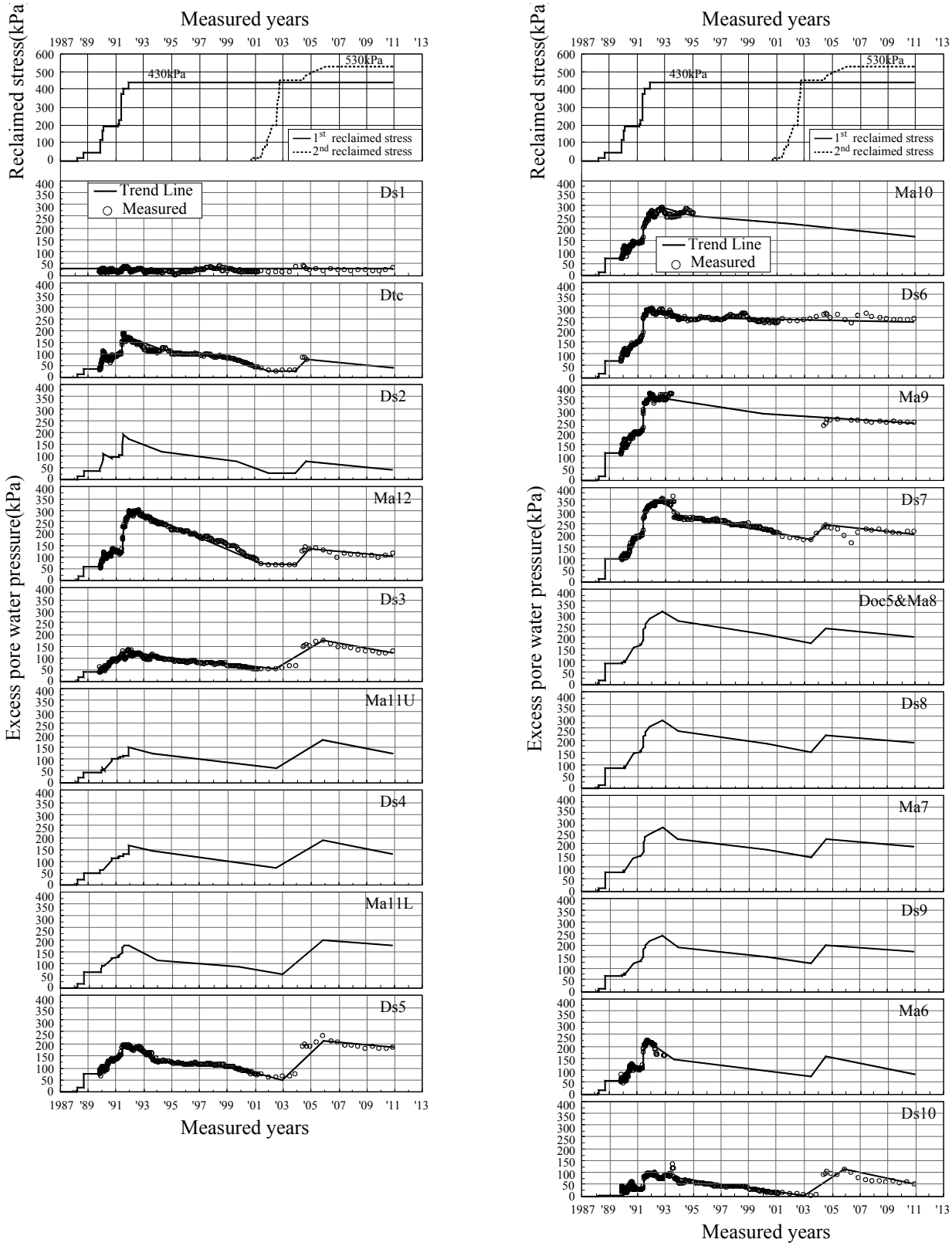

Fig. 2.12 Measured excess pore water pressure - time relations at the monitoring point 1

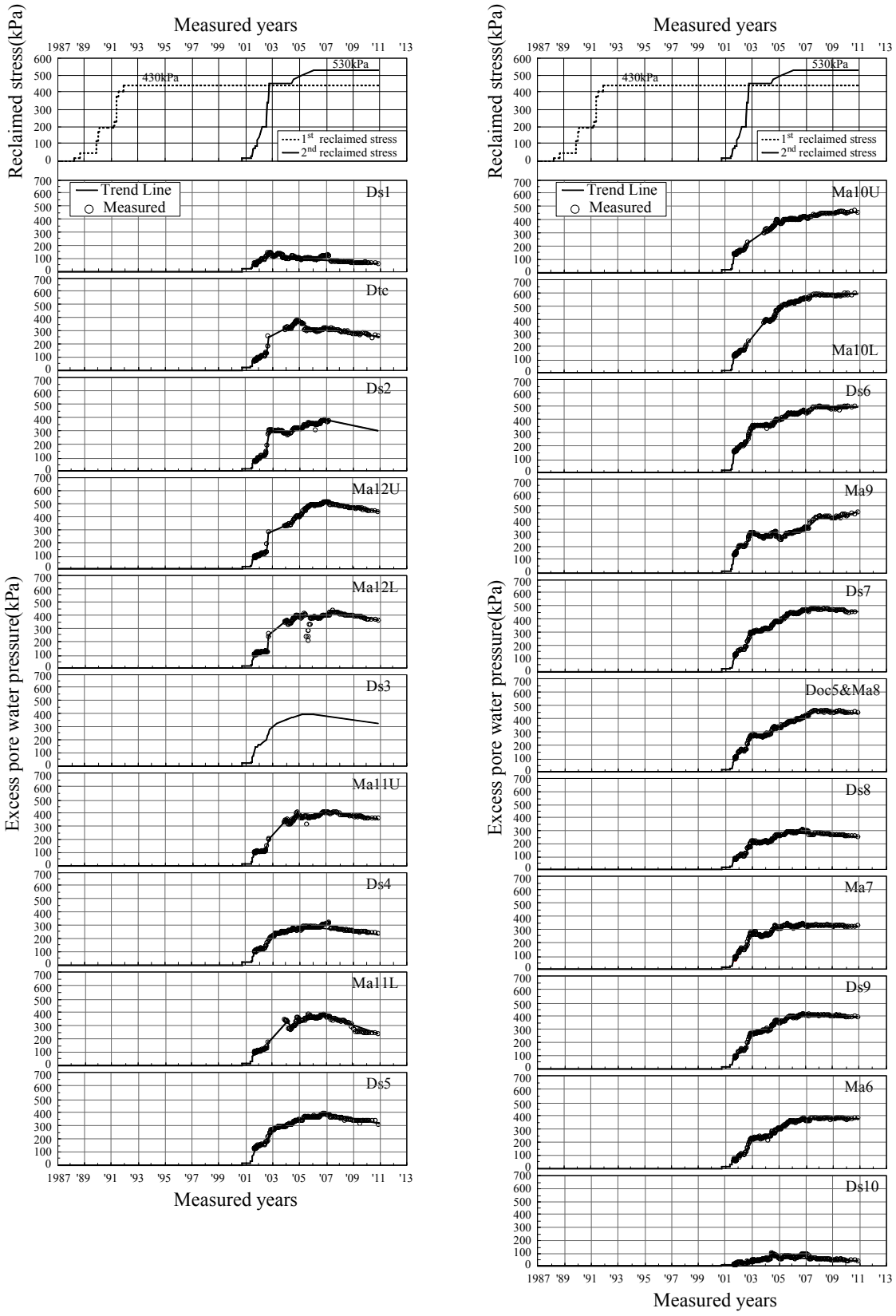

Fig. 2.13 Measured excess pore water pressure - time relations at the monitoring point 2

7 and Ma10, 9 until the present (the year 2011) and the increase of them due to construction of the 2nd phase island is not observed.

Figure 2.13 shows the measured excess pore water pressure - time relations of the individual Pleistocene layers together with trend lines estimated from the measured data at the monitoring point 2. The trend line of Ds3 with no measured information was also inferred. In the upper Pleistocene layers from Dtc to Ds5, the increased excess pore water pressure in the foundation beneath the 2nd phase island due to construction of the 2nd phase island is dissipated with the lapse of time after the completion of construction of the 2nd phase island. However, a rate of excess pore water pressure dissipation is very slow compared to the one of monitoring point 1. In the middle and lower Pleistocene layers from Ma10 to Ma6, the excess pore pressure is not almost dissipated or even increases after the completion of construction of the 2nd phase island. It is clear that a little amount of excess pore water pressure is only observed in the Pleistocene sand gravel layers, Ds1 and 10, whereas a large amount of excess pore water pressure is observed undissipated even after the completion of construction of the 2nd phase island in the other Pleistocene sand gravel layers. It is thought that the Pleistocene sand gravel layers besides Ds1 and 10 in the ground foundation beneath the 2nd phase island do not seem to function well as permeable layers.

2.4.3 Measured settlement

The compression of the Pleistocene clay layers due to the reclaimed load could be considered in three terms, which the first term is a compression associated with dissipation of excess pore water pressure, the second term is the shear-induced dilatancy and the third term is time-dependent behavior associated with strain rate or the secondary compression. In this section, the settlement behavior that has taken place in the Pleistocene clay deposits of KIX is

roughly investigated by comparing between the calculated and the measured results. The calculation of the consolidated settlement associated with dissipation of excess pore water pressure is conducted using the measured excess pore water pressure and trend lines shown in Fig. 2.12 and 2.13. The one-dimensional consolidation formulation used in the calculation of settlement is expressed as follows:

If $p_o + \Delta p' \le p_c$, then

$$S_c = \frac{C_s H}{1+e_0} \cdot log \frac{p_o + \Delta p'}{p_o} \tag{2.1}$$

If $p_o + \Delta p' > p_c$, then

$$S_c = \frac{C_s H}{1+e_0} \cdot log \frac{p_c}{p_0} + \frac{C_c H}{1+e_0} \cdot log \frac{p_o + \Delta p'}{p_c} \tag{2.2}$$

Where S_c is the consolidated settlement, C_c is the compression index for normally consolidated clay, C_s is the compression and swelling index for overconsolidated clay, H is the thickness of clay layer, e_o and p_o denote the initial value of void ratio and vertical effective stress respectively. p_c means the preconsolidation stress and $\Delta p'$ is the increase of vertical effective stress due to reclamation. The increase of vertical effective stress, $\Delta p'$ can be

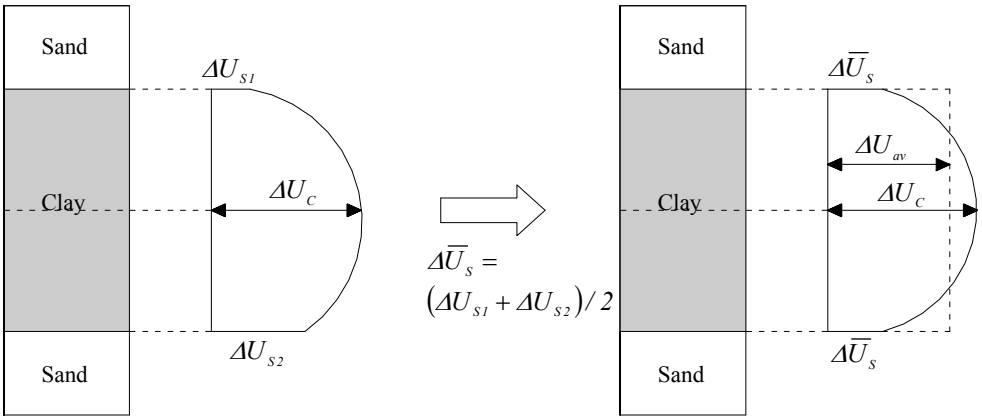

Fig. 2.14 Diagram to determine the mean excess pore water pressure in CRS consolidation test

yielded by using the measured excess pore water pressure and reclaimed stress in the individual layers (see Fig. 2.12 and 2.13). The trend lines are used in the layers where there is no measured information. Figure 2.14 schematically shows the diagram to determine the mean excess pore water pressure in the CRS consolidation test. The mean excess pore water pressure ΔU_{av} is expressed as follows:

$$\Delta U_{av} = \frac{2}{3}\left(\Delta U_C - \Delta \overline{U}_S\right) + \Delta \overline{U}_S = \frac{2}{3}\Delta U_C + \frac{1}{3}\Delta \overline{U}_S \tag{2.3}$$

Here,

$$\Delta \overline{U}_S = \frac{\Delta U_{S1} + \Delta U_{S2}}{2} \tag{2.4}$$

Where ΔU_C and ΔU_S denote the excess pore water pressure for the individual clay and sand gravel layers respectively. The increase of vertical effective stress, $\Delta p'$ in the clay layer is then obtained as follows:

$$\Delta p' = \Delta p - \Delta U_{av} \tag{2.5}$$

in which, Δp means the reclaimed stress shown in Fig 2.9. The other soil parameters derived from conventional step loading consolidation test is shown in Table 2.1.

Table 2.1 Principle consolidation parameters for the Pleistocene clay deposits of KIX

Name of layers	The 1st reclaimed foundation						The 2nd reclaimed foundation					
	C_c	C_s	e_0	p_0 (kPa)	p_c (kPa)	H (m)	C_c	C_s	e_0	p_0 (kPa)	p_c (kPa)	H (m)
Dtc-1	0.5510	0.0551	1.16	156.8	250.9	1.50	0.6291	0.0629	1.22	208.5	312.7	2.00
Dtc-2	0.5028	0.0503	1.16	167.9	268.7	1.50	0.8663	0.0866	1.40	222.2	333.3	2.00
Dtc-3	0.7848	0.0785	1.55	178.4	285.5	1.50	0.6405	0.0641	1.22	236.3	354.4	2.00
Ma12U-1	1.5761	0.1576	2.21	198.3	297.5	2.00	1.7172	0.1717	2.24	272.1	380.9	4.00
Ma12U-2	1.5915	0.1592	2.10	208.3	312.5	2.00	1.4393	0.1439	2.01	292.3	409.2	4.00
Ma12U-3	1.3818	0.1382	1.94	218.9	328.4	2.00	1.4853	0.1485	1.89	313.5	438.9	4.00
Ma12U-4	1.4122	0.1412	1.76	230.3	345.4	2.00	1.3747	0.1375	1.72	336.3	470.8	4.00
Ma12L-1	1.1487	0.1149	1.59	239.8	359.6	1.00	0.7545	0.0755	1.36	355.5	497.7	2.00
Ma12L-2	1.1764	0.1176	1.59	246.9	370.4	1.00	0.8486	0.0849	1.32	370.2	518.2	2.00
Ma12L-3	1.2044	0.1204	1.59	254.1	381.1	1.00	0.5080	0.0508	1.11	384.9	538.9	2.00
Ma11U-1	1.0083	0.1008	1.46	315.4	425.8	1.50	0.9923	0.0992	1.46	411.6	555.7	2.60
Ma11U-2	1.0610	0.1061	1.51	326.6	440.9	2.00	1.1210	0.1121	1.49	431.7	582.8	3.50
Ma11U-3	0.7058	0.0706	1.25	340.0	459.0	2.00	0.7393	0.0739	1.17	455.7	615.2	3.50
Ma11U-4	0.2360	0.0236	0.99	353.6	477.3	1.50	0.2938	0.0294	0.71	480.0	648.1	2.60
Ma11L-1	1.4045	0.1404	1.54	412.3	556.6	1.00	1.4537	0.1454	1.51	549.3	741.5	1.30
Ma11L-2	0.7154	0.0715	1.33	418.8	565.4	1.00	1.2697	0.1270	1.44	558.1	753.5	1.30
Ma11L-3	1.0385	0.1038	1.29	425.8	574.8	1.00	0.9491	0.0949	1.16	567.9	766.6	1.30
Ma10-1	0.9066	0.0907	1.15	489.9	612.4	2.00	0.8023	0.0802	1.09	627.0	815.2	5.40
Ma10-2	1.1929	0.1193	1.44	508.3	635.3	2.00	1.1713	0.1171	1.30	660.9	859.1	3.60
Ma10-3	1.3315	0.1332	1.54	521.3	651.6	2.00	1.5386	0.1539	1.51	684.9	890.4	3.60
Ma10-4	1.7369	0.1737	1.80	533.1	666.3	2.00	1.8082	0.1808	1.69	707.2	919.3	3.60
Ma10-5	1.8109	0.1811	1.76	544.6	680.7	2.00	1.7048	0.1705	1.48	729.6	948.5	3.60
Ma10-6	1.2952	0.1295	1.40	557.1	696.4	2.00	1.1944	0.1194	1.22	754.2	980.4	3.60
Ma9-1	1.2961	0.1296	1.40	611.4	764.2	2.50	1.0277	0.1028	1.24	782.1	977.6	4.00
Ma9-2	1.4708	0.1471	1.49	627.7	784.6	2.50	1.1488	0.1149	1.35	809.9	1012.3	4.00
Ma9-3	1.6627	0.1663	1.58	643.4	804.2	2.50	1.2542	0.1254	1.44	836.4	1045.5	4.00
Ma9-4	1.7617	0.1762	1.58	658.9	823.7	2.50	1.2720	0.1272	1.46	862.4	1078.0	4.00
Ma9-5	1.5186	0.1519	1.41	675.1	843.9	2.50	1.1159	0.1116	1.32	889.3	1111.6	4.00
Ma9-6	1.1808	0.1181	1.27	690.5	863.2	2.00	0.9047	0.0905	1.14	915.2	1144.1	3.20
Doc5&Ma8-1	3.6645	0.3664	2.55	733.6	880.4	3.00	0.9859	0.0986	1.21	941.9	1130.3	3.80
Doc5&Ma8-2	1.2458	0.1246	1.43	750.3	900.3	3.00	1.5175	0.1518	1.67	967.3	1160.7	3.80
Doc5&Ma8-3	0.8474	0.0847	1.09	775.0	930.0	4.00	1.3510	0.1351	1.47	996.5	1195.8	5.10
Ma7-1	0.9394	0.0939	1.17	828.3	994.0	2.50	0.9335	0.0934	1.10	1043.4	1252.1	4.40
Ma7-2	1.3456	0.1346	1.52	845.5	1014.6	2.50	0.9752	0.0975	1.14	1077.2	1292.7	4.40
Ma7-3	0.7903	0.0790	1.04	861.3	1033.6	2.00	1.3472	0.1347	1.48	1105.0	1326.0	3.50
Ma6-1	1.0173	0.1017	1.23	961.4	1153.7	2.50	1.0618	0.1062	1.13	1147.6	1319.7	7.20
Ma6-2	0.8914	0.0891	1.15	979.4	1175.3	2.50	1.4222	0.1422	1.39	1198.5	1378.3	7.20
Ma6-3	1.5283	0.1528	1.23	997.4	1196.9	2.50	1.0000	0.1000	1.08	1250.3	1437.8	7.20

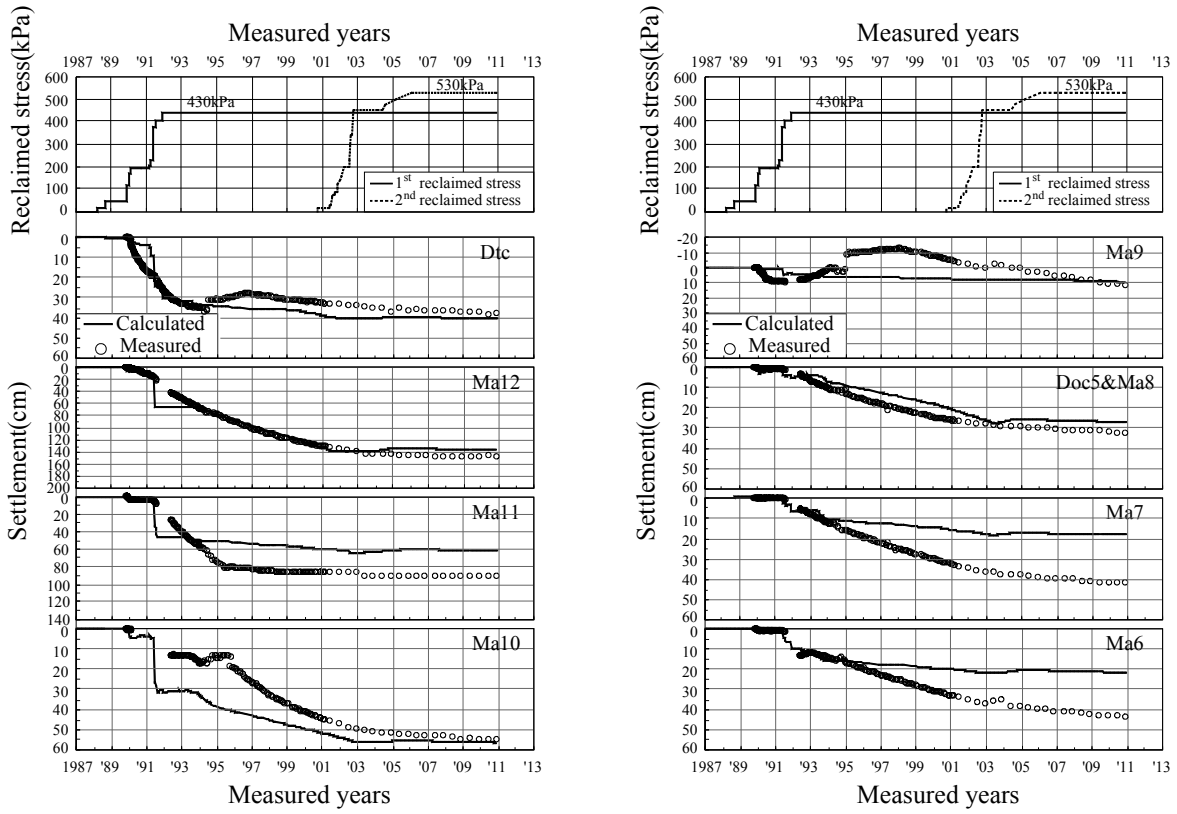

Fig. 2.15 Measured and calculated settlement - time relations at the monitoring point 1

The measured settlement - time relations for the individual Pleistocene layers at the monitoring point 1 are shown in Fig. 2.15 together with the calculated results from the measured excess pore water pressure. As seen from Fig. 2.12, the measured excess pore water pressure in the upper and lower Pleistocene layers such as Ds1, 3, 5, 10 and Dtc, Ma12, 6 has steadily dissipated with the lapse of time. As seen in Fig. 2.15, the calculated settlements in terms of one-dimensional consolidation correspond with the measured data in Dtc and Ma12. It is thought that the consolidation behavior associated with dissipation of excess pore water pressure is predominant in Dtc and Ma12. In Ma11, 7 and 6, the calculated results underestimate the measured data, namely, a larger compression than the one associated with dissipation of excess pore water pressure has occurred in the field. It is thought that the secondary compression is predominant after the completion of the primary consolidation in the early stage of the project.

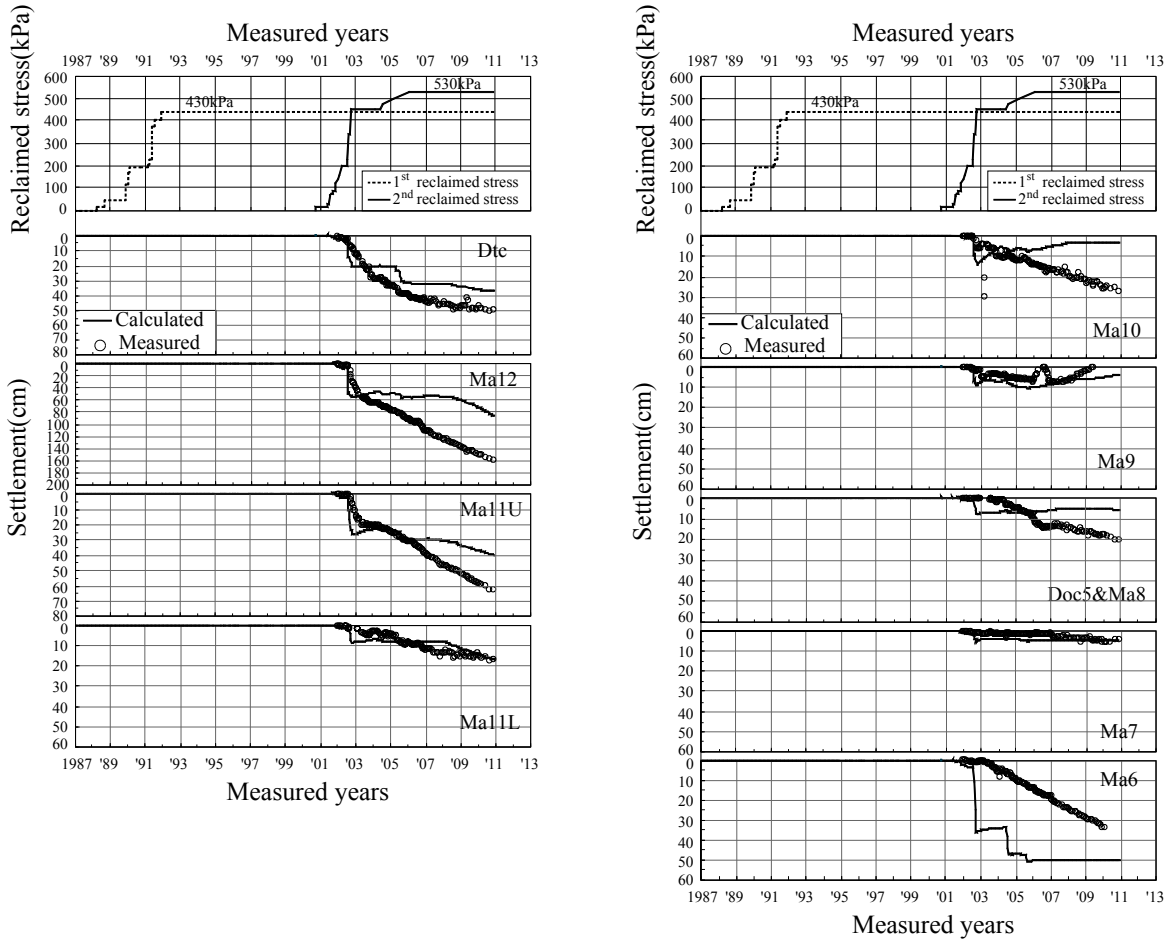

Fig. 2.16 Measured and calculated settlement – time relations at the monitoring point 2

In Ma10 layer, the rate of calculated compression is faster than the measured value with early plastic yielding, and then, the rate of calculated compression becomes much lower with insufficient dissipation of excess pore water pressure (see Fig. 2.12). Although the settlement behaviors in Ma9, Doc5&Ma8 can not be exactly evaluated due to uncertain measured data of settlement and absence of measured excess pore water pressure, it is thought that in Ma9, the time-dependent behavior without significant dissipation of them is predominant because of the poor permeability of the adjoining Pleistocene sand gravel layers Ds6 and 7, whereas the time-dependent behavior in Doc5&Ma8 is not predominant due to non-marine clay, Doc5.

Figure 2.16 shows the measured settlement - time relations for the individual Pleistocene clay layers at the monitoring point 2 together with the calculated results from the measured excess pore water pressure. As shown from Fig. 2.13, the remarkable dissipation of excess pore water pressure has not been observed in the all Pleistocene layers besides Ds1 and 10. However a larger compression than the calculated one from the measured excess pore water pressure has occurred in the most of the Pleistocene clay layers. The settlement in the foundation beneath the 2nd phase island seems to exhibit the predominant time dependent behavior not associated with dissipation of excess pore water pressure. However, it is difficult to explain from the soil parameters used in present because the initial ground condition may be changed due to effect of the adjacent 1st phase reclamation. Although the settlement behaviors can not be exactly evaluated due to uncertain measured data of settlement and change of the initial ground condition, it is thought that a large compression takes place in the upper layers such as Dtc, Ma12 and 11 by undergoing the plastic yielding in the early stage of the project due to large reclamation load and in the other layers from Ma10 to Ma6, the time-dependent behavior is predominant. The calculated result in Ma6 exhibits uncertain behavior due to extreme difference of excess pore water pressure between Ma6 and Ds10.

2.5 Summary

Kansai International Airport was constructed on the marine foundations that have the complicated deposits in Osaka Bay. The marine deposits consist of the Holocene clay underlain by the alternated Pleistocene clay and sand gravel layers due to transgression and regression of the sea. The Pleistocene clay deposits in Osaka Bay are problematic for long-term settlement because they have distinguished structure so-called "quasi-overconsolidated clay". It was confirmed that the Pleistocene clay deposits in KIX exhibit slight overconsolidation with OCR of 1.1 to 1.6 in average, showing the tendency that is decreasing with depth in the results derived from conventional step loading consolidation test.

The sand gravel deposits play a significant role as permeable layer to control the rate of consolidation of sandwiched Pleistocene clay deposits. The distribution characteristics of the individual Pleistocene sand gravel layers at KIX were evaluated by considering the sedimentary environment and in-situ acoustic exploration data. On the basis of the evaluation for the distribution characteristics of the Pleistocene sand gravel layers, the permeability was qualitatively evaluated as having relatively good permeability for Ds1, 10 and poor permeability for Ds6, 7, 9 and ordinary permeability for the other Pleistocene sand gravel layers. In general, the sand gravel deposits beneath the 1st phase island are more widely and thickly distributed compared to the one beneath the 2nd phase island.

Considering the qualitative evaluation for permeability of the Pleistocene sand gravel deposits, the process of the measured excess pore water pressure at the monitoring point 1 and 2 was evaluated. At the monitoring point 1 of the 1st phase island, the excess pore water pressure has been observed to steadily dissipate with the lapse of time in the upper and lower Pleistocene layer. On the other hand, in the middle Pleistocene layer, a large amount of excess pore water pressure has been observed undissipated even now because of poor permeability of sand gravel

layers, Ds6 and 7. At the monitoring point 2 of the 2nd phase island, a large amount of excess pore water pressure has been observed undissipated in the all Pleistocene layers besides Ds1 and 10. It was found that even excess pore water pressure has been increasing continuously after the completion of the construction of the 2nd phase island in the middle Pleistocene layers.

The long-term settlement behavior that has been measured in the Pleistocene clay deposits of KIX was roughly investigated by comparing with the calculation of one-dimensional consolidation from the measured excess pore water pressure. On the basis of the findings by investigation, it was thought that the time-dependent behavior associated with insufficient dissipation of excess pore water pressure or the secondary compression after the completion of the primary consolidation in the early stage of the project is predominant in the reclaimed marine foundation of KIX.

Therefore, it is necessary that the elaso-viscoplastic finite element analyses considering the time-dependent behavior is performed to assess the long-term settlement that have been taking place in the foundation of KIX. The coupled stress-flow analyses should be also performed to assess the mechanism for the propagation and dissipation of excess pore water pressure with the permeability in the individual Pleistocene sand gravel layers.

3. CONSTITUTIVE MODEL AND FORMULATION

3.1 Introduction

Clay is a strain hardening, rate sensitive material that has remarkable characteristics such as rate sensitivity of strength, secondary compression, creep and stress relaxation. Various Elasto-viscoplastic constitutive models have been proposed to describe the rheological behavior of clay. Murayama and Shibata (1956) proposed a rheology model based on the rate process theory, the leading study in this filed. Elasto-viscoplastic constitutive models can be classified into "overstress type model" and "non-stationary flow surface model" (Sekiguchi, 1985) based on the theoretical structures.

Perzyna (1963) proposed an elastic viscoplastic constitutive model with the assumption that viscous effects become pronounced only after the material undergoes yielding. The concept of overstress is involved in the theory proposed by Perzyna. Existence of a static yield surface and a dynamic loading surface is assumed in the stress space. Then the static yield function, F is defined as follows:

$$F\left(\sigma_{ij},\varepsilon_{kl}^{vp}\right)=\frac{f\left(\sigma_{ij},\varepsilon_{kl}^{vp}\right)}{k_s}-1 \tag{3.1}$$

Here, f is a dynamic loading function, ks is a hardening parameter $k_s=\int \sigma_{ij}d\varepsilon_{ij}^{vp}$ prescribed by the viscoplastic work.

The most elaborate assumption for "overstress model" is that the viscoplastic strain rate obeys the following form of the associated viscoplastic flow rule:

$$\dot{\varepsilon}_{ij}^{vp}=\gamma\left\langle\Phi\left(F\right)\right\rangle\frac{\partial f}{\partial\sigma_{ij}} \tag{3.2}$$

Here, γ is a material constant called the fluidity parameter, $\dot{\varepsilon}_{ij}^{vp}$ is a viscoplastic strain rate, Φ(F) is

a scalar function called the viscoplastic flow function that has the overstress function F as its argument. The flow function is assumed as follows:

$$\langle \Phi(F) \rangle = \begin{Bmatrix} \Phi(F), for F > 0 \\ 0, for F \le 0 \end{Bmatrix} \tag{3.3}$$

It is clear that the flow function Φ(F) for a strain hardening material should be monotonically increasing function of F when F is positive. The principal models of this type are proposed by Adachi and Oka (1982), Katona (1984), Baladi and Rohani (1984) etc.

Olszak and Perzyna (1966) proposed a non-stationary flow surface model that has the time-dependent loading surface by introducing the internal variable controlling the viscosity and time-dependency of clays. The non-stationary flow surface is assumed in the following form:

$$F = F(\sigma_{ij}, \varepsilon_{kl}^{vp}, \beta) = 0 \tag{3.4}$$

Here, β is a scalar parameter which embodies time dependent alteration of the material property. Identifying the non-stationary flow surface with a viscoplastic potential leads to the following flow rule:

$$\dot{\varepsilon}_{ij}^{vp} = \Lambda \frac{\partial F}{\partial \sigma_{ij}} \tag{3.5}$$

Here, Λ is a non-negative multiplier. It should also be emphasized that the stress rate term is appeared in this type model whereas the overstress type model does not contain it. The main difference between the overstress model and non-stationary flow surface model consists in the existence of the stress rate term. The principal models of this type are proposed by Sekiguchi (1977), Dragon and Mroz (1979), Nova (1982), Matsui and Abe (1985) etc.

The Pleistocene clays in Osaka Bay have the distinguished structure so-called “quasi-overconsolidated clays” without definite mechanical overconsolidation history. Akai and Tanaka (1999) reported that large and rapid settlement had been proceeding without significant

dissipation of excess pore water pressure in the Pleistocene clay and sand gravel deposits in the foundation ground of Kansai International Airport (KIX). In the sense, elasto-vicoplastic constitutive model under the normally consolidated clay proposed by Sekiguchi (1977) and time dependent behavior model for “quasi-overconsolidated clay” proposed by Mimura and Jang (2004) are introduced in the present study.

Due attention should be also paid to the fact that the generated excess pore water pressure due to construction of airport fill has remained undissipated in the Pleistocene clay layers as well as the Pleistocene sand gravel layers for a long time in the foundation ground of KIX. In general, the sand gravel layers are assumed to be fully permeable layer for consolidation analysis. However, the Pleistocene sand gravel layers in the foundation of KIX are not considered to function as the fully permeable layers. The coupled stress-flow analysis should be hence performed to assess the long-term behavior associated with the process of excess pore water pressure not only in the Pleistocene clay layers but also in the Pleistocene sand gravel layers.

In this chapter, the coupled stress-flow analysis using Christian method (1968) is also introduced and the matrix form for the finite element analysis is described for the further details.

3.2 Elasto-viscoplastic Constitutive Model

3.2.1 Original elasto-viscoplastic constitutive model

The elasto-viscoplastic constitutive model used in this study was originally proposed by Sekiguchi (1977). In order to obtain the stress-strain-time relation relevant to the process of one-dimensional consolidation of clay exhibiting creep under constant effective stress, Sekiguchi and Toriihara (1976) have derived the relation for sustained loading as follow:

$$v = \frac{\lambda}{1+e_0} \cdot ln\frac{p}{p_0} + D\left\{\frac{q}{p} - \frac{q_0}{p_0}\right\} - \alpha \cdot ln\left(\frac{\dot{v}}{\dot{v}_o}\right) \tag{3.6}$$

Where v is the volumetric strain, λ is the compression index, e_o is the initial value of void ratio, q and p are the principal stress difference and mean effective stress, D and $\dot{v}$ are the dilatancy coefficient and the volumetric strain rate, α and $\dot{v}_o$ denote the secondary compression index and the reference volumetric strain rate. q_o and p_o mean the values of q and p at the reference state respectively. It may be noted that if no time effect exists, i.e. if α tends zero, the resulting relation reduces to that derived by Shibata (1963). Let the elastic component of v^e be expressed in the following form:

$$v^e = \frac{\kappa}{1+e_0} \cdot ln\frac{p}{p_0} \tag{3.7}$$

Here, κ is the compression and swelling index. Subtracting this elastic volumetric strain, v^e from v after obtaining the solution to Eq. (3.6), the viscoplastic potential F is defined as follows:

$$F = \alpha \cdot ln\left[1 + \frac{\dot{v}_0 \cdot t}{\alpha} exp\left(\frac{f}{\alpha}\right)\right] = v^p \tag{3.8}$$

in which v^p is the viscoplastic volumetric strain, f is the function in terms of the effective stress and expressed in the following form:

$$f = \frac{\lambda - \kappa}{1 + e_0} \cdot ln \frac{p}{p_0} + D\left\{\frac{q}{p} - \frac{q_0}{p_0}\right\} \tag{3.9}$$

Here, the stress parameters q and p are redefined as follows:

$$q = \sqrt{(3/2)s_{ij}s_{ij}} \; ; \quad p = \sigma'_{ij}\delta_{ij}/3 \tag{3.10}$$

Where s_{ij} is the deviatoric stress tensor, σ'_{ij} and δ'_{ij} are the effective stress tensor and unit tensors, and the summation convention is used.

3.2.2 Plane-strain elasto-viscoplastic constitutive model

A plane-strain elasto-viscoplastic constitutive model modified by Sekiguchi(et al., 1982) was used to assess the long-term behavior of the Pleistocene marine foundation at KIX through the two dimension finite element analysis. Note that the plan-strain version is capable of evaluation of K_o value at rest (Sekiguchi, 1983). This is so significant because the calculated performance for geotechnical events can be much influenced by the initial stress condition. The mathematical structure of the plane-strain version of the viscoplastic constitutive model is shown in Table 3.1 together with the original model. Note that the dilatancy function induced by assuming the strain –rate paramerter $(\dot{\gamma}^p / \dot{v}^p)$, $g(\xi)$ in the plane-strain version has been specified in the following equation.

$$g(\xi) = \frac{(\lambda - \kappa)}{2(1 + e_0)} \cdot ln\left[\frac{\xi^2 - \xi + \mu}{\xi_o^2 - \xi_o + \mu}\right] + \frac{(\lambda - \kappa)}{2(1 + e_0)\sqrt{\mu - 1/4}}\left[arctan\left(\frac{\xi - 1/2}{\sqrt{\mu - 1/4}}\right) - arctan\left(\frac{\xi_o - 1/2}{\sqrt{\mu - 1/4}}\right)\right] \tag{3.11}$$

where ξ and μ denote the stress ratio (s/r) and the failure criterion ($s_f / r_f = sin\phi'$), ξ_o stands for its initial value. It is evident from Table 3.1 that the mathematical structure of each model is essentially the same. A principal difference lies in that, as its name implies, the plane- strain version is based on the two-dimensional stress parameters, r and s, instead of their

counterpart, p and q. Another point to be made here is that the plane-strain version leads to generally better predictions for K_o values ; that is a direct consequence of the specific relation between $\dot{\gamma}^p / \dot{v}^p$ and $\xi(=s/r)$ indicated in Table 3.1

Table 3.1 Features of two elasto-viscoplastic constitutive models

Subject	Sekiguchi (1977)	Plane-strain Version (1982)
Viscoplastic Flow Rule	$\dot{\varepsilon}_{ij}^{p} = \Lambda \frac{\partial F}{\partial \sigma_{ij}^{'}}$	
Viscoplastic Potential	$F = \alpha \cdot ln\left[1 + \frac{\dot{v}_0 \cdot t}{\alpha} exp\left(\frac{f}{\alpha}\right)\right] = v^p$	
Consistency Condition	$\dot{F} = \frac{\partial F}{\partial \sigma_{ij}^{'}} \cdot \partial \dot{\sigma}_{ij}^{'} + \frac{\partial F}{\partial t} = \dot{v}^p$	
Static Yield Function	$f = \frac{\lambda - \kappa}{1+e_0} \cdot ln\frac{p}{p_0} + D\left\{\frac{q}{p} - \frac{q_0}{p_0}\right\}$ where, $p = \sigma_{ij}^{'}\delta_{ij}/3$; $q = \sqrt{(3/2)s_{ij}s_{ij}}$ $(i, j = 1, 3)$	$f = \frac{\lambda - \kappa}{1+e_0} \cdot ln\frac{r}{r_0} + g\left\{\frac{s}{r}\right\}$ where, $r = \sigma_{ij}^{'}\delta_{ij}/2$; $s = \sqrt{(1/2)s_{ij}s_{ij}}$ $(i, j = 1, 2)$
Strain-rate Parameters	$\frac{\dot{\varepsilon}^p}{\dot{v}^p} = \frac{1}{M - q/p}$ where, $*\ \dot{\varepsilon}^p = \frac{2}{3}(\dot{\varepsilon}_1^p - \dot{\varepsilon}_3^p)$, $\dot{v}^p = \dot{\varepsilon}_1^p + \dot{\varepsilon}_2^p + \dot{\varepsilon}_3^p$	$\frac{\dot{\gamma}^p}{\dot{v}^p} = \frac{s/r}{sin\phi^{'} - s/r}$ where, $\dot{\gamma}^p = \dot{\varepsilon}_1^p - \dot{\varepsilon}_3^p$, $\dot{v}^p = \dot{\varepsilon}_1^p + \dot{\varepsilon}_3^p$

* For the purpose of illustration the particular expression valid for ax symmetric strain conditions is listed here.

3.2.3 Concrete form of elasto-viscoplastic constitutive model for FEM

This sub-section presents the concrete forms of the basic for the elasto-viscoplastic constitutive model mentioned above. The viscoplastic flow rule for the model is generally expressed as follows:

$$\dot{\varepsilon}_{ij}^{p} = \Lambda \frac{\partial F}{\partial \sigma_{ij}^{'}} \tag{3.12}$$

in which F is the viscoplastic potential defined by Eq. (3.8) and Λ is a proportional coefficient. To determine the proportional coefficient Λ, the consistency condition has been introduced by Sekiguchi (1977) as follows form:

$$\dot{F} = \frac{\partial F}{\partial \sigma_{ij}^{'}} \dot{\sigma}_{ij}^{'} + \frac{\partial F}{\partial t} = \dot{v}^{p} \tag{3.13}$$

From Eq. (3.12), it follows that

$$\dot{v}^{p} = \Lambda \frac{\partial F}{\partial \sigma_{ij}^{'}} \delta_{ij} \tag{3.14}$$

Eqs. (3.13) and (3.14) permit Λ to be expressed as

$$\Lambda = \frac{\dfrac{\partial F}{\partial \sigma_{ij}^{'}} \dot{\sigma}_{ij}^{'} + \dfrac{\partial F}{\partial t}}{H} = \frac{\dfrac{\partial F}{\partial \sigma_{ij}^{'}} D_{ijkl}^{e} \dot{\varepsilon}_{kl} + \dfrac{\partial F}{\partial t}}{\dfrac{\partial F}{\partial \sigma_{ij}^{'}} D_{ijkl}^{e} \dfrac{\partial F}{\partial \sigma_{kl}^{'}} + H} \tag{3.15}$$

where, D_{ijkl}^{e} is the tangent elasticity constitutive tensor and H is as follows:

$$H = \frac{\partial F}{\partial \sigma_{ij}^{'}} \delta_{ij} \tag{3.16}$$

In general, the stress-strain relation is expressed as follows:

$$\dot{\sigma}_{ij}^{'} = D_{ijkl}^{e} \dot{\varepsilon}_{kl}^{e} = D_{ijkl}^{e} \left(\dot{\varepsilon}_{kl} - \dot{\varepsilon}_{kl}^{p} \right) = D_{ijkl}^{e} \left(\dot{\varepsilon}_{kl} - d\Lambda \frac{\partial F}{\partial \sigma_{kl}^{'}} \right) \tag{3.17}$$

Substitution of Eq. (3.15) into Eq. (3.17) leads to the original elasto-viscoplasic constitutive model proposed by Sekiguchi (1977) as follows:

$$\dot{\sigma}'_{ij} = \left[\left(K - \frac{2}{3} G \right) \delta_{ij} \delta_{kl} + G\left(\delta_{ik} \delta_{jl} + \delta_{il} \delta_{jk} \right) - \frac{\left(\frac{3 s_{ij}}{q} G + \beta K \delta_{ij} \right) \left(\frac{3 s_{kl}}{q} G + \beta K \delta_{kl} \right)}{3G + K\beta^2 + \frac{p'}{C_1 D} \beta} \right] \dot{\varepsilon}_{kl} - \dot{\sigma}^r_{ij} \tag{3.18}$$

where

$$\dot{\sigma}^r_{ij} = \frac{\frac{C_2}{C_1} \left(\frac{3 s_{ij}}{q} G + \beta K \delta_{ij} \right)}{3G + K\beta^2 + \frac{p'}{C_1 D} \beta} \tag{3.19}$$

$$C_1 = 1 - exp\left(- \frac{\varepsilon^{vp}_v}{\alpha} \right), \qquad C_2 = \dot{v}_o \, exp\left(\frac{f - \varepsilon^{vp}_v}{\alpha} \right) \tag{3.20}$$

$$\beta = M - \frac{q}{p'} = \frac{\lambda - \kappa}{D(1 + e_o)} - \frac{q}{p'} \tag{3.21}$$

in which $\dot{\sigma}^r_{ij}$ is the relaxation stress tensor, K and G are the bulk modulus and the shear modulus, M is the soil constant which expresses the ultimate frictional resistance of a given soil (Schofield and Wroth, 1968). The concrete form of the model for plane-strain version is shown in the reference (Mimura and Sekiguchi, 1986). The resulting constitutive relations are implemented into the finite element analysis procedure through the following incremental form:

$$\{\Delta\sigma'\} = [D^{evp}]\{\Delta\varepsilon\} - \{\Delta\sigma^R\} \tag{3.22}$$

Where $\{\Delta\sigma'\}$ and $\{\Delta\varepsilon\}$ are the associated sets of the effective stress increments and the strain increments respectively, and $[D^{evp}]$ stands for the elasto-viscoplastic coefficient matrix. The term $\{\Delta\sigma^R\}$ represents a set of 'relaxation stress', which increases with time when the strain is held constant. In detail, the concrete matrix form for finite element analysis used in this study is given in the Appendix A of the present thesis.

3.3 Elasto-plastic Constitutive Model

The elasto-viscoplastic constitutive model proposed by Sekiguchi (1977) was used in this study to assess the long-term behavior of the Pleistocene marine foundation due to construction of the reclaimed island of KIX in Osaka Bay. In this section, the concrete form of elasto-plastic model is defined to quantitatively assess the time-dependent behavior in the elasto-viscoplastic constitutive model by comparing performance results of two constitutive models.

It may be noted that if the third term on the right-hand side of Eq. (3.6) expressed in the previous section (3.2.1) is not considered, the viscoplastic potential F expressed in Eq. (3.8) is consistent with yield function f of Eq. (3.9). The plastic flow rule for the model is then expressed as follows:

$$\dot{\varepsilon}_{ij}^{p} = \Lambda \frac{\partial f}{\partial \sigma_{ij}^{'}} \tag{3.23}$$

To determine the proportional coefficient Λ, the consistency condition is defined as follows form:

$$\frac{\partial f}{\partial \sigma_{ij}^{'}} d\sigma_{ij}^{'} = d\varepsilon_{v}^{p} \tag{3.24}$$

From Eq. (3.23), it follows that

$$d\varepsilon_{v}^{p} = \Lambda \frac{\partial f}{\partial \sigma_{ij}^{'}} \delta_{ij} \tag{3.25}$$

Eqs. (3.24) and (3.25) permit Λ to be expressed as

$$\Lambda = \frac{\dfrac{\partial f}{\partial \sigma_{ij}^{'}} d\sigma_{ij}^{'}}{h} = \frac{\dfrac{\partial f}{\partial \sigma_{ij}^{'}} D_{ijkl}^{e} d\varepsilon_{kl}}{\dfrac{\partial f}{\partial \sigma_{ij}^{'}} D_{ijkl}^{e} \dfrac{\partial f}{\partial \sigma_{kl}^{'}} + h} \tag{3.26}$$

where, D_{ijkl}^{e} is the tangent elasticity constitutive tensor and h is as follows:

$$h = \frac{\partial f}{\partial \sigma_{ij}^{'}} \delta_{ij} \tag{3.27}$$

In general, the stress-strain relation is expressed as follows:

$$d\sigma_{ij}^{'} = D_{ijkl}^{e} d\varepsilon_{kl}^{e} = D_{ijkl}^{e} \left(d\varepsilon_{kl} - d\varepsilon_{kl}^{p} \right) = D_{ijkl}^{e} \left(d\varepsilon_{kl} - d\Lambda \frac{\partial f}{\partial \sigma_{kl}^{'}} \right) \tag{3.28}$$

Substitution of Eq. (3.26) into Eq. (3.28) leads to the elasto-plasic constitutive model as follows:

$$d\sigma_{ij}^{'} = \left[\left(K - \frac{2}{3} G \right) \delta_{ij} \delta_{kl} + G \left(\delta_{ik} \delta_{jl} + \delta_{il} \delta_{jk} \right) - \frac{\left(\frac{3 s_{ij}}{q} G + \beta K \delta_{ij} \right) \left(\frac{3 s_{kl}}{q} G + \beta K \delta_{kl} \right)}{3G + K\beta^{2} + \frac{p^{'}}{D} \beta} \right] d\varepsilon_{kl} \tag{3.29}$$

where

$$\beta = M - \frac{q}{p^{'}} = \frac{\lambda - \kappa}{D(1 + e_{o})} - \frac{q}{p^{'}} \tag{3.30}$$

The concrete form of the model for plane-strain version is shown in the following incremental form:

$$\{ \Delta \sigma^{'} \} = [D^{ep}] \{ \Delta \varepsilon \} \tag{3.31}$$

where $\{ \Delta \sigma^{'} \}$ and $\{ \Delta \varepsilon \}$ are the associated sets of the effective stress increments and the strain increments respectively, and $[D^{ep}]$ stands for the elasto-plastic coefficient matrix. In detail, the concrete matrix form for finite element analysis used in this study is given in the Appendix B of the present thesis. The performed results for two constitutive models will be discussed in chapter 4.

3.4 Compression Model for Quasi-overconsolidated Pleistocene Clays

Based on the in-situ measured data, the long-term settlement has been found to take place in the reclaimed islands of Osaka Port even in the Pleistocene clay layers that do not undergo the plastic yielding (Mimura et al., 2001), As it is also stated, the seabed deposits of Osaka Bay have been formed due to the soil supply from the rivers on the sinking base. Therefore, those sediments such as the Pleistocene clays should be normally consolidated although they exhibit the apparent overconsolidation with OCR of 1.1 to 1.6. The author considers those quasi-overconsolidated Pleistocene clays as "normally consolidated aged clays" with seeming overconsolidation due to diagenesis effect. In the sense, the compression modeling for quasi-overconsilidated Pleistocene clays proposed by Mimura and Jang (2004) is introduced with the following assumption:

The Pleistocene clays in Osaka Bay are "normally consolidated aged clays" that exhibit the elasto-viscoplastic behavior even in the region $p_o + \Delta p \le p_c$, while an elastic behavior is assumed

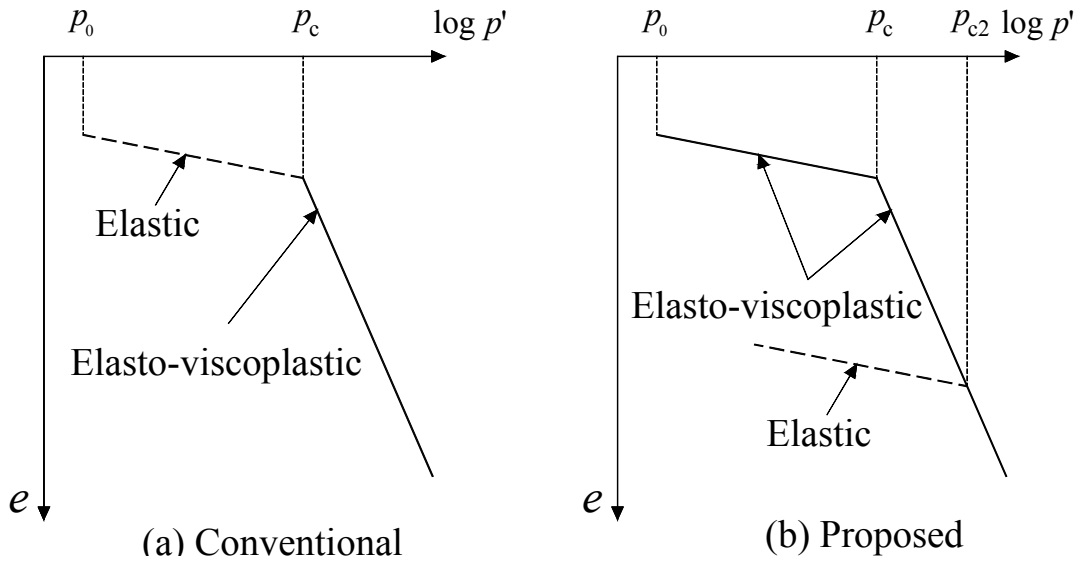

Fig. 3.1 Compression model for the quasi-overconsolidated Pleistocene clays

to occur in this region by the conventional constitutive models. Figure 3.1 shows the conventional and the compression models proposed by Mimura and Jang (2004) schematically. Here, the Pleistocene clays are assumed to exhibit the time-dependent behavior not only in the normally consolidated region but also in the overconsolidated region when the positive loading increment Δp is applied ($p' > p_o$). The stress, p_c in the proposed model does not denote the conventional yield stress but is regarded as the one changing the phase of clay deformation on the reference consolidation curve for monotonic compression due to fading the structural effect. However, once those clays undergo additional loading surpassing p_c, the corresponding stress, p_{c2} in Fig. 3.1 (b) should be new p_c and in the unloading – reloading region the Pleistocene clays exhibit elastic behavior as it is conventionally assumed.

The procedure with the proposed concept is found to provide descriptive accuracy for predicting long-term deformation of the reclaimed Pleistocene deposits in Osaka Port (Mimura and Jang, 2004, 2005a). In the present study, the elasto-viscoplastic finite element code with the proposed compression model is also used for investigation of the stress-deformation characteristics of the Pleistocene deposits due to offshore airport fill of KIX.

3.5 Coupled Stress-Flow Analysis Method in Terms of Finite Element

In the coupled stress-flow finite element analysis used in the present study, note that each quadrilateral element consists of four constant strain triangles and the nodal displacement increments and the element pore water pressure is taken as the primary unknowns of the problem. The finite element equations governing those unknowns are established on the basis of Biot's formulation (Christian, 1968, Akai and Tamura, 1976), and are solved numerically by using the semi-band method of Gaussian elimination.

3.5.1 Equilibrium equation for consolidation

The well-known equilibrium equation of consolidation stress is expressed as follows:

$$\sigma_{ij,j} + \rho g_i = 0 \tag{3.32}$$

in which ρ is defined as the density of the soil plus fluid, g_i represents the vector of gravity accelerations. The total stress tensor σ_{ij} is expressed as follows by dividing into the effective stress tensor $\sigma_{ij}^{'}$ and pore water pressure p_w.

$$\sigma_{ij} = \sigma_{ij}^{'} + \delta_{ij} p_w \tag{3.33}$$

Here, the compressive stress is taken as positive.

From Eq. (3.32), the principle of virtual work is given as follows:

$$\int_v \{\delta\varepsilon\}^T \{\sigma^{'}\} dV + \int_v \{\delta\varepsilon\}^T \{p_w\} dV = \int_v \{\delta u\}^T \{\gamma\} dV \tag{3.34}$$

where $\{\varepsilon\}$ and $\{u\}$ denote the virtual strain and displacement vector, δ indicates an arbitrarily small increment, $\{\sigma^{'}\}$ and $\{p_w\}$ denote the effective stress and pore water pressure vector, and $\{\gamma\}$ is the body force vector. For the discretization of the weak form of the equilibrium equation, the following relations are defined.

$$\{\varepsilon\} = [B]\{u\} \tag{3.35}$$

$$\{\sigma^{'}\} = [D]\{\varepsilon\} = [D][B]\{u\} \tag{3.36}$$

where $[B]$ is the strain – displacement transformation matrix, and $[D]$ is the stress – strain or constitutive matrix as mentioned in the previous section.

By substituting the Eqs. (3.35) and (3.36) into the Eq. (3.34), the following relation will be obtained:

$$\int_v ([B]\{\delta u\})^T [D][B]\{u\} dV + \int_v ([B]\{\delta u\})^T \{p_w\} dV = \int_v \{\delta u\}^T \{\gamma\} dV \tag{3.37}$$

or

$$\{\delta u\}^T \int_v [B]^T [D][B]\{u\}dV + \{\delta u\}^T \int_v [B]^T \{p_w\}dV = \{\delta u\}^T \int_v \{\gamma\}dV \tag{3.38}$$

hence

$$\int_v [B]^T [D][B]\{u\}dV + \int_v [B]^T \{p_w\}dV = \int_v \{\gamma\}dV \tag{3.39}$$

Eq. (3.39) can be written as follows:

$$[K_1]\{u\} + [K_2]\{p_w\} = \{F\} \tag{3.40}$$

in which

$$[K_1] = \int_v [B]^T [D][B]dV \tag{3.41}$$

$$[K_2] = \int_v [B]^T dV \tag{3.42}$$

$$\{F\} = \int_v \{\gamma\}dV \tag{3.43}$$

Finally, the concrete form for finite element analysis in terms of calculation step is expressed as follows:

$$[K_1]\{\Delta u\}_j + [K_2]\{p_w\}_j = \{\Delta F\} + [K_2]\{p_w\}_{j-1} \tag{3.44}$$

where, subscript j means the calculated step for time increment.

3.5.2 Equilibrium equation for fluid flow

The pore water flow is assumed to obey isotropic Darcy's law in the following form:

$$\dot{w}_i = k_{ij}\left(-p_{w,j} + \rho_f g_i\right) \tag{3.45}$$

where w_i is the average relative displacement of the fluid vis-à-vis the solid skeleton and $\dot{w}_i$

denotes the discharge velocity corresponding to w_i, ρ_f denotes the density of the fluid, and the matrix k_{ij} known as the permeability matrix is expressed as follows:

$$k_{ij} = \delta_{ij} k \tag{3.46}$$

in which k is a single value of permeability coefficient.

3.5.3 Continuity equation for fluid flow

Note that the divergence of the flow velocity vector $\dot{w}_{i,i}$ must be equal to the rate of decrease of the pore space and the fluid expansion rate. Thus the mass balance is expressed in the following form:

$$\dot{w}_{i,i} = \dot{\varepsilon}_{ii} - \dot{p}_w \left(n / k_f \right) \tag{3.47}$$

where ε_{ii} denotes the volumetric strain $\varepsilon_v = \varepsilon_x + \varepsilon_y + \varepsilon_z$, n is the porosity of the solid phase, and k_f denotes the bulk modulus of the fluid. The second term of the right-hand-side of Eq. (3.47) can be negligible by considering the fluid as incompressibility. Then, Eq. (3.47) can be newly written as follows:

$$\dot{w}_{i,i} = \dot{\varepsilon}_{ii} \tag{3.48}$$

Similarly, Eq. (3.48) is expressed in terms of the divergence of the vector of flow rate $q_{i,i}$ in the following from:

$$q_{i,i} = \int_v \dot{\varepsilon}_{ii} dV \tag{3.49}$$

or

$$\int_v \frac{\partial \varepsilon_v}{\partial t} dV - \left(\frac{\partial q_x}{\partial x} + \frac{\partial q_y}{\partial y} + \frac{\partial q_z}{\partial z} \right) = 0 \tag{3.50}$$

hence

$$\int_v \Delta\varepsilon_v dV - \Delta t q_{i,i} = 0 \tag{3.51}$$

here,

$$\int_v \Delta\varepsilon_v dV = \int_v [B]\{\Delta u\} dV \tag{3.52}$$

Substituting Eq. (3.42) into Eq. (3.52) yields

$$\int_v \Delta\varepsilon_v dV = \int_v [B]\{\Delta u\} dV = [K_2]^T \{\Delta u\} \tag{3.53}$$

The second term of the left-hand-side of Eq. (3.51) can be expressed as follows:

$$-\Delta t q_{i,i} = [K_3] p_w \tag{3.54}$$

here, the matrix $[K_3]$ is defined as follows:

$$[K_3] p_w = B p_w + \sum_{i=1}^{4} B_i p_{wi} \tag{3.55}$$

in which, the derivation of coefficient B to determine $[K_3]$ is given in Appendix C.

Finally, the concrete form for finite element analysis in terms of fluid flow is expressed as follows:

$$[K_2]^T \{\Delta u\}_j + [K_3]\{p_w\}_j = 0 \tag{3.56}$$

3.5.4 Combination equation for coupled stress-flow analysis

Combining Eqs. (3.44) and (3.56) gives the governing equation for the finite element formulation as follows:

$$\begin{bmatrix} [K_1] & [K_2] \\ [K_2]^T & [K_3] \end{bmatrix} \begin{bmatrix} \{\Delta u\}_j \\ \{p_w\}_j \end{bmatrix} = \begin{bmatrix} \{\Delta F\} + [K_2]\{p_w\}_{j-1} \\ \{0\} \end{bmatrix} \tag{3.57}$$

where $\{\Delta u\}$ and $\{p_w\}$ are taken as the primary unknowns of the problem.

3.6 Summary

The elasto-viscoplastic constitutive model based on the concept of non-stationary flow surface proposed by Sekiguchi (1977) was introduced in this chapter. The plan-strain version to consider the initial stress condition was also introduced. The concrete form for the finite element analysis was described with the viscoplasitc flow rule for the constitutive model.

The elasto-plastic version was also described by not considering the time dependent behavior in the given elasto-viscoplastic constitutive model. The elasto-plastic version will be used to quantitatively assess the time-dependent behavior in the performed results for the elasto-viscoplastic finite element analysis by comparing the performed results for two constitutive models.

A procedure proposed by Mimura and Jang (2004) was also introduced to describe the time-dependent compression of the quasi-overconsolidated Pleistocene clays at the foundation of KIX.

The concrete form for the coupled stress-flow analysis using Christian method was also described to assess the mechanism for the propagation and dissipation of excess pore water pressure. The pore water flow is assumed to obey isotropic Darcy's law and the thickness in the Pleistocene sand gravel layers, which is the important component in Darcy's law, is considered to be significant factor with their permeability to assess the mechanism for process of excess pore water pressure in this coupled stress-flow analysis.

4. Proposal of Numerical Procedure to Assess the Long-term Behavior of the Pleistocene Marine Foundations at KIX

4.1 Introduction

As is already pointed out in the previous chapter, description of the long-term behavior of the Pleistocene marine foundations at KIX is not easy because of the difficulty in the evaluation of the mechanical properties of the quasi-overconsolidated clays and permeability for the Pleistocene sand gravels. Furthermore, the complexity of the geometrical structure of the alternating strata with changing thickness of the individual layers makes the problem still more difficult. Due attention should hence be paid to the compression modeling for the Pleistocene clays and the permeability for the Pleistocene sand gravels in order to rationally describe the in situ behavior of excess pore water pressure and compression of the Pleistocene deposits.

In this chapter, the time-dependent behavior of the Pleistocene deposits of the reclaimed foundation of the 1st phase island of KIX is investigated based on the elasto-viscoplastic finite element analysis. A series of elasto-viscoplastic finite element analyses is performed as the first step to propose the appropriate numerical procedure for the construction of the 1st phase island. Attention is paid to the modeling of permeability for Pleistocene sand gravel layers considering the sedimentation environment because the performance of excess pore water pressure is strongly dependent on the extent of distribution as well as the change in thickness of those permeable sand gravel layers. The concept of “mass permeability” is introduced to model the actual process of dissipation of excess pore water pressure in the field. Another attention is given to the modeling of the compressibility of the highly structured Pleistocene clay layers, exhibiting already significant visco-plastic deformations even in the quasi-overconsolidated effective stress range. Here, the performance of excess pore water pressure propagation in the Pleistocene deposits is highlighted. The mass permeability of the Pleistocene sand gravel deposits

is selected as one of the parameters controlling the deformation of the foundation ground. It is of importance to know how far the generated excess pore water pressure will propagate in permeable sand gravel layers because it directly influences the performance of the adjacent structures. The effect of the existence of excess pore water pressure in the permeable Pleistocene sand gravel layers on the subsequent advance in settlement of the Pleistocene deposits is of great concern for predicting the long-term settlement of the offshore-reclaimed marine foundations. The adopted elasto-viscoplastic finite element analysis is also evaluated in terms of the time-dependent behavior associated with stress overshoot and the secondary compression by comparing with elasto-plastic finite element analysis. The horizontally even ground foundation model is adopted for the finite element analysis to confirm the numerical procedure. However, the ground foundations of KIX have the inclined Pleistocene deposits increasing in thickness towards the offing. Accordingly, the effect of inclination in the ground foundation model is also investigated by comparing with calculated for the horizontally even and inclined ground foundation models. The validity of the adopted ground foundation model in terms of depth is also discussed by assessing the behavior of the deeper Pleistocene Marine foundations than the modeled foundations (until Ds10 layer) in the present study to propose the numerical pressure. The calculated performance due to construction of the 1st phase island of KIX is validated by comparing with the in-situ measured results at monitoring point 1 on the 1st phase island (see Fig. 2.7).

4.2 Evaluation of Soil Parameters for Numerical Analysis

4.2.1 Parameters for the clay deposits

The alternating deposits of KIX have been formed due to sedimentation of clayey soils during transgression and of sandy to gravelly soils during regression on the sinking base of Osaka Bay. The thickness of the individual Pleistocene clay layers generally increases towards offshore caused by the more preferable environment of sufficient depth of the sea in the offing. On the other hand, it is true the Pleistocene sand gravel layers naturally tends to decrease in thickness towards offshore but the mode of distribution of them varies dependent upon the topographical characteristics, such as the location of old river channel, the existence of the ridge and trench and the old river scale etc (Kitada et al, 2011b). The physical and mechanical soil properties hence vary with the places that have undergone different sedimentary environment. In this present study, as shown in Fig. 4.1, the parameters for the Pleistocene clay layers are

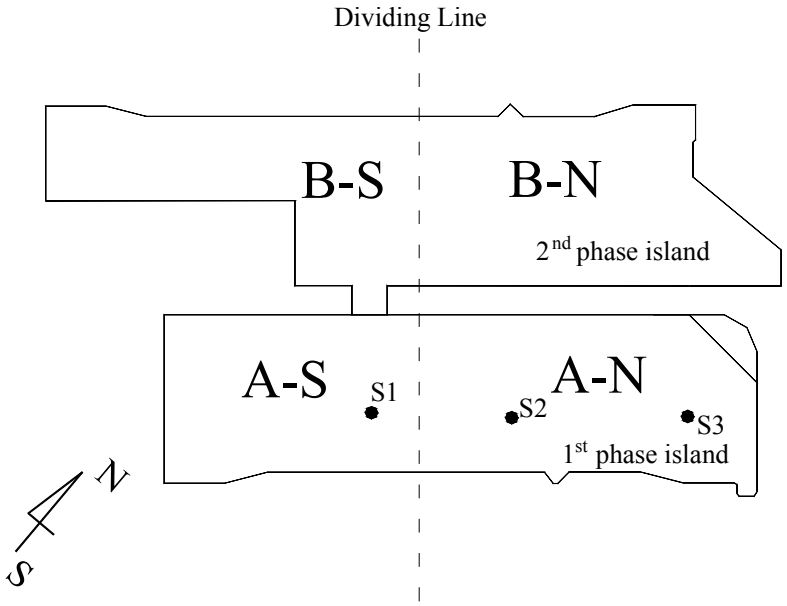

Fig. 4.1 Distinguished blocks for the parameters of the Pleistocene clay deposits at KIX

distinguished into 4 blocks based on the laboratory experimental results for the Pleistocene clays obtained from the corresponding blocks. However, the values of OCR for the quasi-overconsolidated Pleistocene clays are only distinguished into 2 blocks, namely, one from the offshore boundary to the monitoring point 2 of the 2nd phase island and another from the onshore boundary to the monitoring point 1 of the 1st phase island, by adopting the average value.

The Pleistocene clays in Osaka Bay exhibit slight overconsolidation due to the effect of diagenesis such as aging effect and/or development of cementation among clay particles. In this present analysis, the Pleistocene clay layers are assumed to be lightly overconsolidated, and the values of OCR are assumed to about 1.2 to 1.6 for the foundation of the 1st reclaimed island and about 1.15 to 1.5 for the foundation of the 2nd reclaimed island based on the results derived from conventional step loading consolidation test. Figure 4.2 shows the distribution of p_c with depth in the Pleistocene clay deposits for the foundations of the both islands at KIX. According to the report by Akai and Sano (1981), the values of p_c - p_o are almost constant for the upper to middle Pleistocene clays. Based on the facts, the mean values of the scattered data of the consolidation yield stresses are selected as the representative values of p_c shown by the solid line in Fig. 4.2. Although the initial vertical effective stress p_o values for the soil parameters of two groups are different because of the difference of the foundation thickness of the both islands, the values of p_c - p_o show almost constant distribution with depth for the soils of two groups. Here, the values of OCR are assumed to be identical for the individual Pleistocene clay layers. The resultant profile of OCR for the Pleistocene clay layers is shown in Fig. 4.3 for the soils of both groups. The values of OCR are decreasing with depth, showing the largest at the top of the Pleistocene clay and the smallest at the bottom.

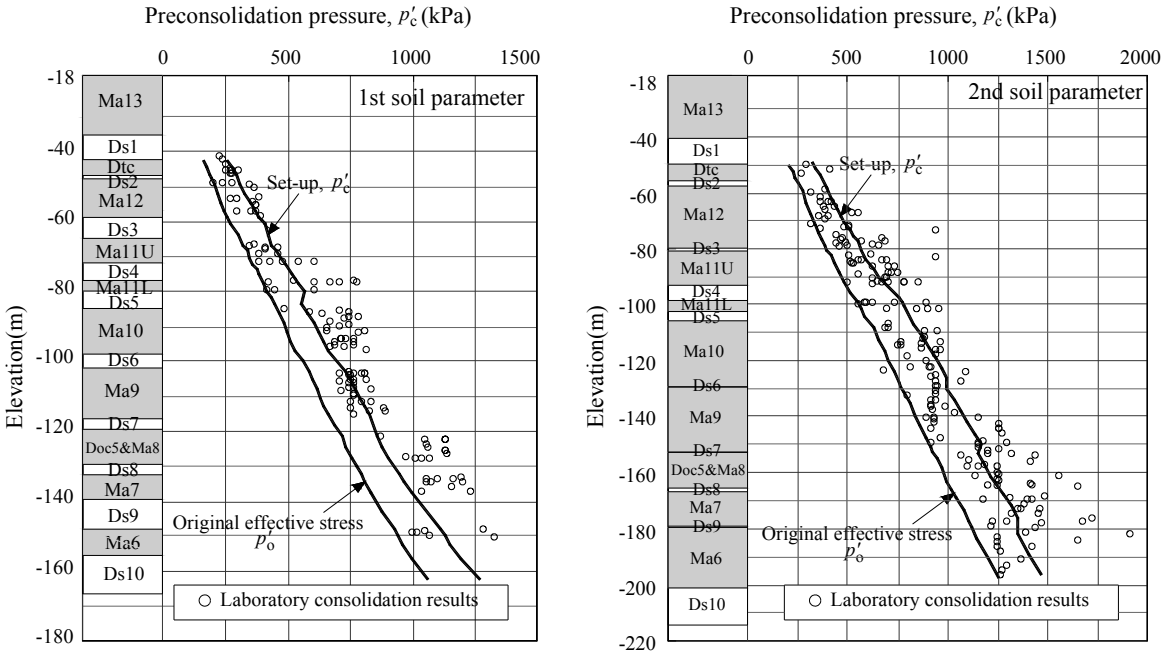

Fig. 4.2 Distribution of preconsolidation pressure (p_c) with depth for the foundations of the 1st and 2nd phase islands

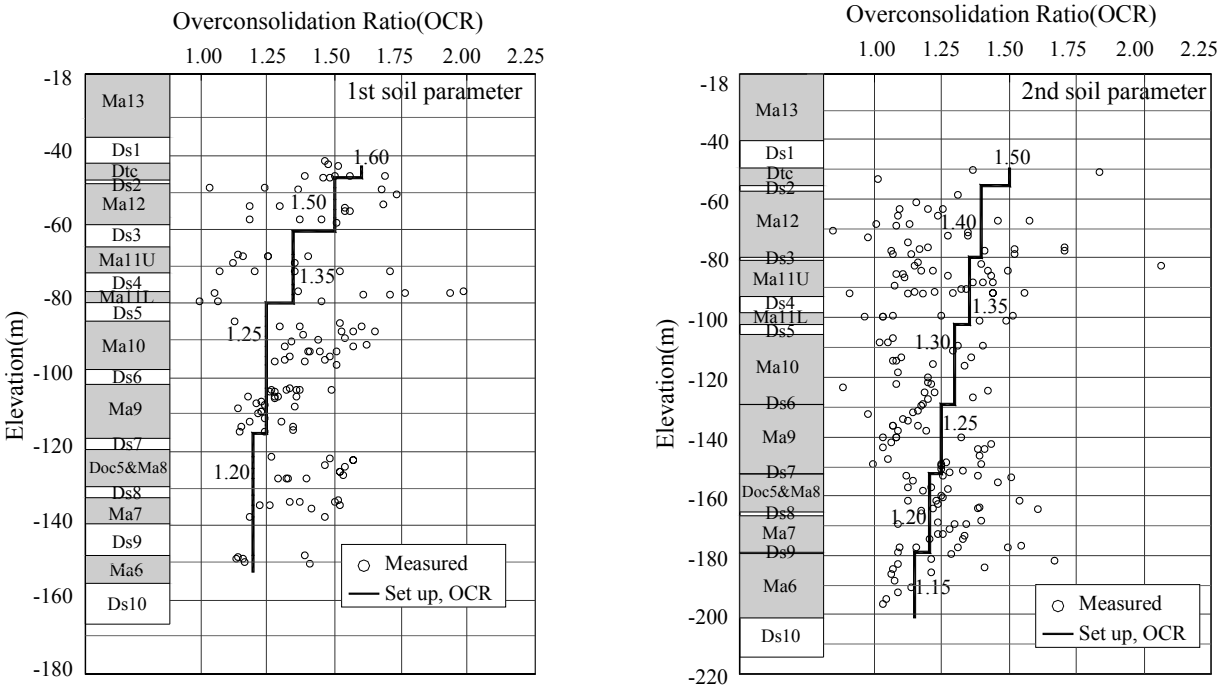

Fig. 4.3 Setup overconsolidation ratio (OCR) for the Pleistocene clays at the foundations of the 1st and 2nd phase islands

The other parameters for the clay deposits used in the constitutive model are rationally determined based on the prescribed determination methods (Mimura et al., 1990, Mimura and Jang, 2004). The determination of principal soil parameters for analysis with proposed procedure is explained as follows:

(a) Compression index λ in the normally consolidated region.

The definition of compression index λ in the NC region is

$$\lambda = 0.434 C_c \tag{4.1}$$

Here, C_c is a compression index in terms of the common logarithms of consolidation pressure, which can be derived by conventional oedometer test. In general, the value of C_c is not constant, but non-linear against consolidation pressure particularly for clays with developed structure.

(b) Recompression index κ

The definition of recompression index κ

$$\kappa = 0.434 C_s \tag{4.2}$$

Here, C_s is a recompression index in terms of the common logarithms of consolidation pressure, which can be also derived by conventional step loading consolidation test. Based on the fact that most values of the ratio C_s / C_c (κ / λ) are in the range of 0.02 to 0.2 (Terzaghi et al.,1996), it is assumed that C_s is one-tenth of C_c as a representative in the present study.

(c) Compression index λ_{QOC} and recompression index κ_{QOC} in the quasi-overconsolidation region

In the present analysis, the above-mentioned procedure is adopted, namely, the compression curve in the quasi- overconsolidated region with inclination of κ is assumed to have

elasto-viscoplastic component the same as in the NC region. As *e*-log *p* relations are adopted as reference consolidation curves for clays, the recompression index, κ is assumed to be the compression index in the quasi-overconsolidated region($p_0 \le p \le p_c$). Here, p_0, p_c and p denote the initial vertical stress, the consolidation yield stress and the current stress respectively. Therefore, the compression index in the quasi-overconsolidated region, λ_{QOC} is introduced in the present study as follows:

$$\lambda_{QOC} = \kappa \tag{4.3}$$

Calladaine (1971) showed that the ratio κ/λ is directly related to a coefficient of friction $\mu\,(=\tan\phi')$ that is constant irrespective of a consolidation state. Here, ϕ' denotes an angle of shear resistance. Karube (1975) also confirmed that the relation of the ratio Λ $(=1-\kappa/\lambda)$ and slope of critical state line M is constant for some clays. As M is constant irrespective of the stress state, the ratio κ/λ is constant for the specific clay. Based on those findings, κ_{QOC} is defined in the following relation as is already discussed in the previous section (b):

$$\kappa_{QOC} = \frac{\kappa}{\lambda}\lambda_{QOC} \tag{4.4}$$

(d) Secondary compression index α

Secondary compression index α_{NC} governing the time-dependant behavior is determined in the NC region using the relationship between $C_{\alpha e}$ and C_c for Osaka Pleistocene clays (Ishii et al., 1984), that is,

$$C_{\alpha e} = 0.05C_c \tag{4.5}$$

Here, $C_{\alpha e}$ denotes the secondary compression index in terms of void ratio. A similar relation between $C_{\alpha e}$ and C_c was reported by Marques et al (2004). The value of α_{NC} then can be determined as follows:

$$\alpha_{NC} = 0.434 \frac{C_{\alpha e}}{1+e_0} \tag{4.6}$$

Mesri and Godlewski (1977) showed that the value of α was small at effective stresses less than the consolidation yield stress, and it increased as the consolidation yield stress was approached. Murayama and Shibata (1966) explained that $C_{\alpha e}$ for the Pleistocene clays increased linearly with consolidation pressure in the quasi-overconsolidated region, but which became to be constant in the NC region. In the present analysis, it is assumed that α_{QOC} at p_0 is one-tenth of the prescribed value in the NC region on the basis of the fact that the adopted ratio of C_s and C_c is 0.1 in this particular case and the adopted relationship between C_c and α (Eq. (4.5)). Figure 4.4 shows the assumed modeling for the secondary compression index together with the co-ordinates of the modeling curve based on the experimental findings in terms of relative yield stress index defined by $(p-p_o)/(p_c-p_o)$. It is set up that α increases gradually with the relative yield stress index in the quasi-overconsolidated region thereafter remains constant irrespective of the stress level in the NC region.

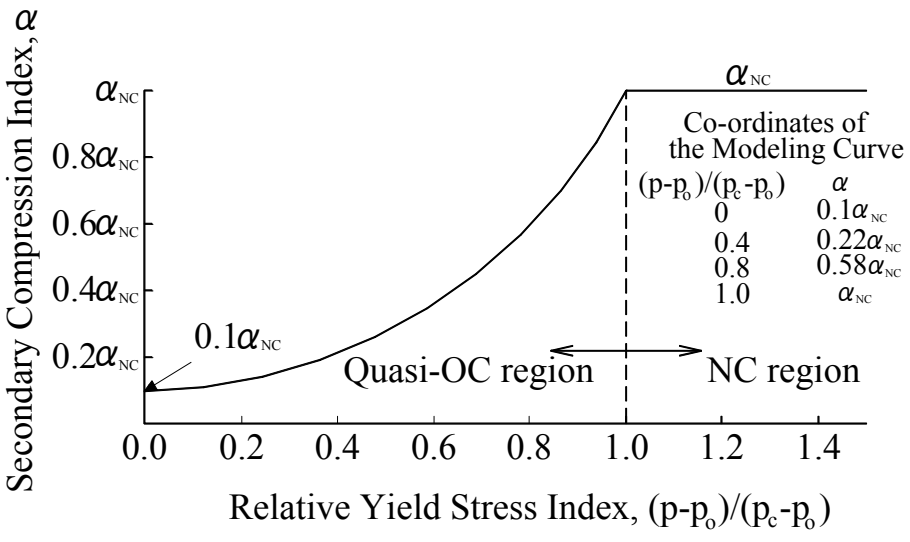

Fig. 4.4 Assumed model for secondary compression index

(e) Reference volumetric strain rate $\dot{v}_o$

The rate of consolidation is another significant factor which controls the process of deformation. The ratio of secondary compression index α to the reference volumetric strain rate $\dot{v}_o$ ($\alpha / \dot{v}_o$) refers to the characteristic time related to the completion of the primary consolidation. The characteristic time t_c in the constitutive model is closely related to a coefficient of consolidation c_v . The value of t_c is determined both for the quasi-overconsolidated region and the NC region as a dissipation time of excess pore water pressure, which is calculated using c_v in the NC region obtained from conventional oedometer test. It is because of the fact that c_v in the quasi- overconsolidated region approaches that of the NC region, although c_v in the OC ($p \le p_0$) region is sufficiently large compared to that in the NC region (Research Committee on Ground in Osaka Bay, 2002). Based on these findings, the same values for t_c are introduced for both in quasi-overconsolidated and NC region in the present study. Based on the parameters, α and t_c , the reference volumetric strain rate, $\dot{v}_o$

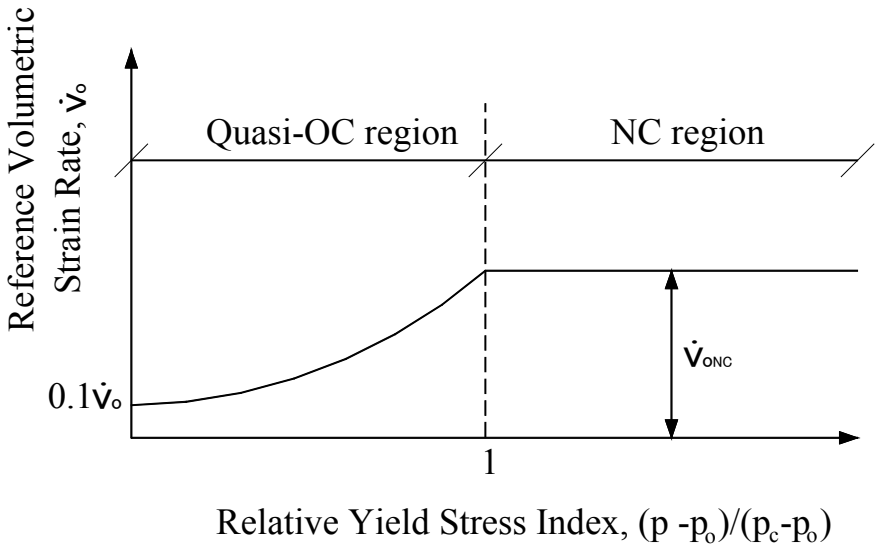

Fig. 4.5 Relationship between the reference volume strain rate and the relative yield stress

becomes a constant maximum value in the NC region. In the quasi-overconsolidated region, $\dot{v}_o$ decreases with the decrease in the relative yield stress index, and at $p = p_0$ the value becomes one-tenth of that in the NC region as schematically shown in Fig. 4.5.

(f) Coefficient of permeability for the clay deposits k

The pore water flow is assumed to obey isotropic Darcy's law. In relation to this, it is further assumed that the coefficient of permeability, k, depends on the void ratio, e, in the following form:

$$k = k_0 \cdot \exp\left(\frac{e - e_0}{\lambda_k}\right) \tag{4.7}$$

in which k_0 is the initial value of k at e=e_0 and λ_k is a material constant governing the rate of change in permeability subjected to a change in the void ratio under the condition that the coefficients of consolidation, c_v are constant for the individual Pleistocene clays. The values of the principal soil parameters for the distinguished Pleistocene clay layers into 4 blocks are summarized in Table 4.1~4.4.

Table 4.1 Principal clayey soil parameters for the foundation of KIX in the A-S block

MTYP	Quasi-OC region				NC region				M	ν'	K_0	p_0 (kPa)	p_c (kPa)	e_0	k_0 (m/day)	λ_k	Name of layers
	λ_{QOC}	κ_{QOC}	α_{QOC}	$\dot{v}_{0\,QOC}$ (day^{-1})	λ	κ	α_{NC}	$\dot{v}_{0\,NC}$ (day^{-1})									
1	0.0509	0.0051	6.06E-04	6.06E-07	0.5093	0.0509	6.06E-03	6.06E-06	1.40	0.35	0.540	4.0	19.1	3.20	8.64E-04	0.509	Ma13U-1
2	0.0532	0.0053	6.65E-04	6.65E-07	0.5321	0.0532	6.65E-03	6.65E-06	1.40	0.35	0.540	12.3	25.3	3.00	8.64E-04	0.532	Ma13U-2
3	0.0532	0.0053	6.99E-04	6.99E-07	0.5316	0.0532	6.99E-03	6.99E-06	1.40	0.35	0.540	20.8	31.6	2.80	8.64E-04	0.532	Ma13U-3
4	0.0518	0.0052	7.09E-04	7.09E-07	0.5178	0.0518	7.09E-03	7.09E-06	1.40	0.35	0.540	29.6	39.2	2.65	8.64E-04	0.518	Ma13U-4
5	0.0493	0.0049	7.14E-04	7.14E-07	0.4927	0.0493	7.14E-03	7.14E-06	1.40	0.35	0.540	38.9	47.9	2.45	8.64E-04	0.493	Ma13U-5
6	0.0510	0.0051	7.61E-04	7.61E-07	0.5097	0.0510	7.61E-03	7.61E-06	1.40	0.35	0.540	48.7	57.6	2.35	8.64E-04	0.510	Ma13U-6
7	0.0418	0.0042	6.86E-04	6.86E-07	0.4184	0.0418	6.86E-03	6.86E-06	1.40	0.35	0.540	57.7	66.9	2.05	8.64E-04	0.418	Ma13L-1
8	0.0489	0.0049	8.02E-04	8.02E-07	0.4889	0.0489	8.02E-03	8.02E-06	1.40	0.35	0.540	65.9	80.5	2.05	8.64E-04	0.489	Ma13L-2
9	0.0405	0.0040	6.98E-04	6.98E-07	0.4046	0.0405	6.98E-03	6.98E-06	1.40	0.35	0.540	76.2	91.7	1.90	8.64E-04	0.405	Ma13L-3
10	0.0239	0.0024	5.53E-04	4.12E-07	0.2392	0.0239	5.53E-03	4.12E-06	1.10	0.38	0.607	156.8	250.9	1.16	1.73E-04	0.239	Dtc-1
11	0.0218	0.0022	5.04E-04	3.76E-07	0.2182	0.0218	5.04E-03	3.76E-06	1.10	0.38	0.607	167.9	268.7	1.16	2.07E-04	0.218	Dtc-2
12	0.0341	0.0034	6.69E-04	4.99E-07	0.3406	0.0341	6.69E-03	4.99E-06	1.10	0.38	0.607	178.4	285.5	1.55	1.81E-04	0.341	Dtc-3
13	0.0684	0.0068	1.07E-03	1.75E-07	0.6840	0.0684	1.07E-02	1.75E-06	1.30	0.36	0.561	198.3	297.5	2.21	1.90E-04	0.684	Ma12U-1
14	0.0691	0.0069	1.11E-03	1.83E-07	0.6907	0.0691	1.11E-02	1.83E-06	1.30	0.36	0.561	208.3	312.5	2.10	1.47E-04	0.691	Ma12U-2
15	0.0600	0.0060	1.02E-03	1.68E-07	0.5997	0.0600	1.02E-02	1.68E-06	1.30	0.36	0.561	218.9	328.4	1.94	9.07E-05	0.600	Ma12U-3
16	0.0613	0.0061	1.11E-03	1.83E-07	0.6129	0.0613	1.11E-02	1.83E-06	1.30	0.36	0.561	230.3	345.4	1.76	9.50E-05	0.613	Ma12U-4
17	0.0499	0.0050	9.63E-04	1.58E-07	0.4985	0.0499	9.63E-03	1.58E-06	1.25	0.36	0.572	239.8	359.6	1.59	5.62E-05	0.499	Ma12L-1
18	0.0511	0.0051	9.87E-04	1.62E-07	0.5106	0.0511	9.87E-03	1.62E-06	1.25	0.36	0.572	246.9	370.4	1.59	5.62E-05	0.511	Ma12L-2
19	0.0523	0.0052	1.01E-03	1.66E-07	0.5227	0.0523	1.01E-02	1.66E-06	1.25	0.36	0.572	254.1	381.1	1.59	5.62E-05	0.523	Ma12L-3
20	0.0438	0.0044	8.90E-04	9.51E-07	0.4376	0.0438	8.90E-03	9.51E-06	1.20	0.37	0.583	315.4	425.8	1.46	9.50E-05	0.438	Ma11U-1
21	0.0460	0.0046	9.16E-04	9.79E-07	0.4605	0.0460	9.16E-03	9.79E-06	1.20	0.37	0.583	326.6	440.9	1.51	9.07E-05	0.460	Ma11U-2
22	0.0306	0.0031	6.80E-04	7.27E-07	0.3063	0.0306	6.80E-03	7.27E-06	1.20	0.37	0.583	340.0	459.0	1.25	7.08E-05	0.306	Ma11U-3
23	0.0102	0.0010	2.57E-04	2.75E-07	0.1024	0.0102	2.57E-03	2.75E-06	1.20	0.37	0.583	353.6	477.3	0.99	5.27E-05	0.102	Ma11U-4
24	0.0610	0.0061	1.20E-03	5.65E-06	0.6095	0.0610	1.20E-02	5.65E-05	1.25	0.36	0.572	412.3	556.6	1.54	5.88E-05	0.610	Ma11L-1
25	0.0311	0.0031	6.67E-04	3.15E-06	0.3105	0.0311	6.67E-03	3.15E-05	1.25	0.36	0.572	418.8	565.4	1.33	6.05E-05	0.311	Ma11L-2
26	0.0451	0.0045	9.83E-04	4.64E-06	0.4507	0.0451	9.83E-03	4.64E-05	1.25	0.36	0.572	425.8	574.8	1.29	6.48E-05	0.451	Ma11L-3
27	0.0393	0.0039	9.14E-04	2.55E-07	0.3935	0.0393	9.14E-03	2.55E-06	1.25	0.36	0.572	489.9	612.4	1.15	3.80E-05	0.393	Ma10-1
28	0.0518	0.0052	1.06E-03	2.97E-07	0.5177	0.0518	1.06E-02	2.97E-06	1.25	0.36	0.572	508.3	635.3	1.44	4.49E-05	0.518	Ma10-2
29	0.0578	0.0058	1.14E-03	3.17E-07	0.5779	0.0578	1.14E-02	3.17E-06	1.25	0.36	0.572	521.3	651.6	1.54	7.60E-05	0.578	Ma10-3
30	0.0754	0.0075	1.35E-03	3.76E-07	0.7538	0.0754	1.35E-02	3.76E-06	1.25	0.36	0.572	533.1	666.3	1.80	6.13E-05	0.754	Ma10-4
31	0.0786	0.0079	1.42E-03	3.97E-07	0.7859	0.0786	1.42E-02	3.97E-06	1.25	0.36	0.572	544.6	680.7	1.76	5.23E-05	0.786	Ma10-5
32	0.0562	0.0056	1.17E-03	3.27E-07	0.5621	0.0562	1.17E-02	3.27E-06	1.25	0.36	0.572	557.1	696.4	1.40	5.18E-05	0.562	Ma10-6
33	0.0563	0.0056	1.17E-03	3.18E-07	0.5625	0.0563	1.17E-02	3.18E-06	1.25	0.36	0.572	611.4	764.2	1.40	9.50E-05	0.563	Ma9-1
34	0.0638	0.0064	1.28E-03	3.48E-07	0.6383	0.0638	1.28E-02	3.48E-06	1.25	0.36	0.572	627.7	784.6	1.49	9.07E-05	0.638	Ma9-2
35	0.0722	0.0072	1.40E-03	3.79E-07	0.7216	0.0722	1.40E-02	3.79E-06	1.25	0.36	0.572	643.4	804.2	1.58	9.50E-05	0.722	Ma9-3
36	0.0765	0.0076	1.48E-03	4.02E-07	0.7646	0.0765	1.48E-02	4.02E-06	1.25	0.36	0.572	658.9	823.7	1.58	9.07E-05	0.765	Ma9-4
37	0.0659	0.0066	1.37E-03	3.71E-07	0.6591	0.0659	1.37E-02	3.71E-06	1.25	0.36	0.572	675.1	843.9	1.41	7.34E-05	0.659	Ma9-5
38	0.0512	0.0051	1.13E-03	3.07E-07	0.5125	0.0512	1.13E-02	3.07E-06	1.25	0.36	0.572	690.5	863.2	1.27	6.91E-05	0.512	Ma9-6
39	0.1590	0.0159	2.24E-03	1.58E-06	1.5904	0.1590	2.24E-02	1.58E-05	1.25	0.36	0.572	733.6	880.4	2.55	2.85E-05	1.590	Doc5&Ma8-1
40	0.0541	0.0054	1.11E-03	7.86E-07	0.5407	0.0541	1.11E-02	7.86E-06	1.25	0.36	0.572	750.3	900.3	1.43	7.78E-05	0.541	Doc5&Ma8-2
41	0.0368	0.0037	8.81E-04	6.23E-07	0.3678	0.0368	8.81E-03	6.23E-06	1.25	0.36	0.572	775.0	930.0	1.09	1.30E-05	0.368	Doc5&Ma8-3
42	0.0408	0.0041	9.41E-04	1.36E-06	0.4077	0.0408	9.41E-03	1.36E-05	1.25	0.36	0.572	828.3	994.0	1.17	1.30E-05	0.408	Ma7-1
43	0.0584	0.0058	1.16E-03	1.67E-06	0.5840	0.0584	1.16E-02	1.67E-05	1.25	0.36	0.572	845.5	1014.6	1.52	2.42E-05	0.584	Ma7-2
44	0.0343	0.0034	8.42E-04	1.22E-06	0.3430	0.0343	8.42E-03	1.22E-05	1.25	0.36	0.572	861.3	1033.6	1.04	3.02E-05	0.343	Ma7-3
45	0.0442	0.0044	9.91E-04	1.25E-06	0.4415	0.0442	9.91E-03	1.25E-05	1.25	0.36	0.572	961.4	1153.7	1.23	3.54E-05	0.442	Ma6-1
46	0.0387	0.0039	8.99E-04	1.13E-06	0.3869	0.0387	8.99E-03	1.13E-05	1.25	0.36	0.572	979.4	1175.3	1.15	4.49E-05	0.387	Ma6-2
47	0.0663	0.0066	1.49E-03	1.87E-06	0.6633	0.0663	1.49E-02	1.87E-05	1.25	0.36	0.572	997.4	1196.9	1.23	2.59E-05	0.663	Ma6-3

Table 4.2 Principal clayey soil parameters for the foundation of KIX in the B-S block

MTYP	Quasi-OC region				NC region				M	ν'	K_0	p_0 (kPa)	p_c (kPa)	e_0	k_0 (m/day)	λ_k	Name of layers
	λ_{QOC}	κ_{QOC}	α_{QOC}	$\dot{v}_{0\,QOC}$ (day^{-1})	λ	κ	α_{NC}	$\dot{v}_{0\,NC}$ (day^{-1})									
1	0.0447	0.0045	5.20E-04	5.20E-07	0.4474	0.0447	5.20E-03	5.20E-06	1.40	0.35	0.540	4.9	8.2	3.30	8.64E-04	0.447	Ma13U-1
2	0.0486	0.0049	6.07E-04	6.07E-07	0.4858	0.0486	6.07E-03	6.07E-06	1.40	0.35	0.540	15.4	20.9	3.00	8.64E-04	0.486	Ma13U-2
3	0.0483	0.0048	6.52E-04	6.52E-07	0.4826	0.0483	6.52E-03	6.52E-06	1.40	0.35	0.540	26.8	33.6	2.70	8.64E-04	0.483	Ma13U-3
4	0.0492	0.0049	6.93E-04	6.93E-07	0.4924	0.0492	6.93E-03	6.93E-06	1.40	0.35	0.540	38.7	48.8	2.55	8.64E-04	0.492	Ma13U-4
5	0.0492	0.0049	7.23E-04	7.23E-07	0.4917	0.0492	7.23E-03	7.23E-06	1.40	0.35	0.540	51.1	60.7	2.40	8.64E-04	0.492	Ma13U-5
6	0.0465	0.0046	7.26E-04	7.26E-07	0.4649	0.0465	7.26E-03	7.26E-06	1.40	0.35	0.540	64.2	73.7	2.20	8.64E-04	0.465	Ma13U-6
7	0.0425	0.0042	7.20E-04	7.20E-07	0.4248	0.0425	7.20E-03	7.20E-06	1.40	0.35	0.540	76.4	86.1	1.95	8.64E-04	0.425	Ma13L-1
8	0.0432	0.0043	7.38E-04	7.38E-07	0.4325	0.0432	7.38E-03	7.38E-06	1.40	0.35	0.540	87.5	97.0	1.93	8.64E-04	0.432	Ma13L-2
9	0.0323	0.0032	6.46E-04	6.46E-07	0.3231	0.0323	6.46E-03	6.46E-06	1.40	0.35	0.540	102.2	117.0	1.50	8.64E-04	0.323	Ma13L-3
10	0.0273	0.0027	6.15E-04	2.37E-07	0.2730	0.0273	6.15E-03	2.37E-06	1.10	0.38	0.607	208.5	312.7	1.22	1.73E-04	0.273	Dtc-1
11	0.0376	0.0038	7.83E-04	3.01E-07	0.3760	0.0376	7.83E-03	3.01E-06	1.10	0.38	0.607	222.2	333.3	1.40	2.07E-04	0.376	Dtc-2
12	0.0278	0.0028	6.27E-04	2.41E-07	0.2780	0.0278	6.27E-03	2.41E-06	1.10	0.38	0.607	236.3	354.4	1.22	1.81E-04	0.278	Dtc-3
13	0.0745	0.0075	1.15E-03	9.92E-08	0.7453	0.0745	1.15E-02	9.92E-07	1.30	0.36	0.561	272.1	380.9	2.24	1.90E-04	0.745	Ma12U-1
14	0.0625	0.0062	1.04E-03	8.96E-08	0.6246	0.0625	1.04E-02	8.96E-07	1.30	0.36	0.561	292.3	409.2	2.01	1.47E-04	0.625	Ma12U-2
15	0.0645	0.0064	1.11E-03	9.61E-08	0.6446	0.0645	1.11E-02	9.61E-07	1.30	0.36	0.561	313.5	438.9	1.89	9.07E-05	0.645	Ma12U-3
16	0.0597	0.0060	1.10E-03	9.45E-08	0.5966	0.0597	1.10E-02	9.45E-07	1.30	0.36	0.561	336.3	470.8	1.72	9.50E-05	0.597	Ma12U-4
17	0.0327	0.0033	6.93E-04	5.97E-08	0.3275	0.0327	6.93E-03	5.97E-07	1.25	0.36	0.572	355.5	497.7	1.36	7.34E-05	0.327	Ma12L-1
18	0.0368	0.0037	7.95E-04	6.86E-08	0.3683	0.0368	7.95E-03	6.86E-07	1.25	0.36	0.572	370.2	518.2	1.32	5.62E-05	0.368	Ma12L-2
19	0.0220	0.0022	5.23E-04	4.51E-08	0.2205	0.0220	5.23E-03	4.51E-07	1.25	0.36	0.572	384.9	538.9	1.11	4.49E-05	0.220	Ma12L-3
20	0.0431	0.0043	8.74E-04	3.25E-07	0.4307	0.0431	8.74E-03	3.25E-06	1.20	0.37	0.583	411.6	555.7	1.46	9.50E-05	0.431	Ma11U-1
21	0.0487	0.0049	9.79E-04	3.64E-07	0.4865	0.0487	9.79E-03	3.64E-06	1.20	0.37	0.583	431.7	582.8	1.49	9.07E-05	0.487	Ma11U-2
22	0.0321	0.0032	7.40E-04	2.75E-07	0.3209	0.0321	7.40E-03	2.75E-06	1.20	0.37	0.583	455.7	615.2	1.17	7.08E-05	0.321	Ma11U-3
23	0.0128	0.0013	3.73E-04	1.39E-07	0.1275	0.0128	3.73E-03	1.39E-06	1.20	0.37	0.583	480.0	648.1	0.71	5.27E-05	0.128	Ma11U-4
24	0.0631	0.0063	1.26E-03	4.80E-06	0.6309	0.0631	1.26E-02	4.80E-05	1.25	0.36	0.572	549.3	741.5	1.51	5.88E-05	0.631	Ma11L-1
25	0.0551	0.0055	1.13E-03	4.31E-06	0.5510	0.0551	1.13E-02	4.31E-05	1.25	0.36	0.572	558.1	753.5	1.44	6.05E-05	0.551	Ma11L-2
26	0.0412	0.0041	9.55E-04	3.65E-06	0.4119	0.0412	9.55E-03	3.65E-05	1.25	0.36	0.572	567.9	766.6	1.16	6.48E-05	0.412	Ma11L-3
27	0.0348	0.0035	8.31E-04	8.23E-08	0.3482	0.0348	8.31E-03	8.23E-07	1.25	0.36	0.572	627.0	815.2	1.09	3.80E-05	0.348	Ma10-1
28	0.0508	0.0051	1.11E-03	1.10E-07	0.5084	0.0508	1.11E-02	1.10E-06	1.25	0.36	0.572	660.9	859.1	1.30	4.49E-05	0.508	Ma10-2
29	0.0668	0.0067	1.33E-03	1.32E-07	0.6678	0.0668	1.33E-02	1.32E-06	1.25	0.36	0.572	684.9	890.4	1.51	7.60E-05	0.668	Ma10-3
30	0.0785	0.0078	1.46E-03	1.44E-07	0.7848	0.0785	1.46E-02	1.44E-06	1.25	0.36	0.572	707.2	919.3	1.69	6.13E-05	0.785	Ma10-4
31	0.0740	0.0074	1.49E-03	1.48E-07	0.7399	0.0740	1.49E-02	1.48E-06	1.25	0.36	0.572	729.6	948.5	1.48	5.23E-05	0.740	Ma10-5
32	0.0518	0.0052	1.17E-03	1.16E-07	0.5184	0.0518	1.17E-02	1.16E-06	1.25	0.36	0.572	754.2	980.4	1.22	5.18E-05	0.518	Ma10-6
33	0.0446	0.0045	9.94E-04	1.10E-07	0.4460	0.0446	9.94E-03	1.10E-06	1.25	0.36	0.572	782.1	977.6	1.24	9.50E-05	0.446	Ma9-1
34	0.0499	0.0050	1.06E-03	1.17E-07	0.4986	0.0499	1.06E-02	1.17E-06	1.25	0.36	0.572	809.9	1012.3	1.35	9.07E-05	0.499	Ma9-2
35	0.0544	0.0054	1.12E-03	1.23E-07	0.5443	0.0544	1.12E-02	1.23E-06	1.25	0.36	0.572	836.4	1045.5	1.44	9.50E-05	0.544	Ma9-3
36	0.0552	0.0055	1.12E-03	1.24E-07	0.5520	0.0552	1.12E-02	1.24E-06	1.25	0.36	0.572	862.4	1078.0	1.46	9.07E-05	0.552	Ma9-4
37	0.0484	0.0048	1.04E-03	1.15E-07	0.4843	0.0484	1.04E-02	1.15E-06	1.25	0.36	0.572	889.3	1111.6	1.32	7.34E-05	0.484	Ma9-5
38	0.0393	0.0039	9.19E-04	1.01E-07	0.3926	0.0393	9.19E-03	1.01E-06	1.25	0.36	0.572	915.2	1144.1	1.14	6.91E-05	0.393	Ma9-6
39	0.0428	0.0043	9.69E-04	4.21E-07	0.4279	0.0428	9.69E-03	4.21E-06	1.25	0.36	0.572	941.9	1130.3	1.21	2.85E-05	0.428	Doc5&Ma8-1
40	0.0659	0.0066	1.23E-03	5.36E-07	0.6586	0.0659	1.23E-02	5.36E-06	1.25	0.36	0.572	967.3	1160.7	1.67	7.78E-05	0.659	Doc5&Ma8-2
41	0.0586	0.0059	1.19E-03	5.16E-07	0.5863	0.0586	1.19E-02	5.16E-06	1.25	0.36	0.572	996.5	1195.8	1.47	1.30E-05	0.586	Doc5&Ma8-3
42	0.0405	0.0041	9.65E-04	2.28E-07	0.4051	0.0405	9.65E-03	2.28E-06	1.25	0.36	0.572	1043.4	1252.1	1.10	1.30E-05	0.405	Ma7-1
43	0.0423	0.0042	9.89E-04	2.34E-07	0.4232	0.0423	9.89E-03	2.34E-06	1.25	0.36	0.572	1077.2	1292.7	1.14	2.42E-05	0.423	Ma7-2
44	0.0585	0.0058	1.18E-03	2.79E-07	0.5847	0.0585	1.18E-02	2.79E-06	1.25	0.36	0.572	1105.0	1326.0	1.48	3.02E-05	0.585	Ma7-3
45	0.0461	0.0046	1.08E-03	1.63E-07	0.4608	0.0461	1.08E-02	1.63E-06	1.25	0.36	0.572	1147.6	1319.7	1.13	3.54E-05	0.461	Ma6-1
46	0.0617	0.0062	1.29E-03	1.95E-07	0.6173	0.0617	1.29E-02	1.95E-06	1.25	0.36	0.572	1198.5	1378.3	1.39	4.49E-05	0.617	Ma6-2
47	0.0434	0.0043	1.04E-03	1.57E-07	0.4340	0.0434	1.04E-02	1.57E-06	1.25	0.36	0.572	1250.3	1437.8	1.08	2.59E-05	0.434	Ma6-3

Table 4.3 Principal clayey soil parameters for the foundation of KIX in the A-N block

MTYP	Quasi-OC region				NC region				M	ν'	K_0	p_0 (kPa)	p_c (kPa)	e_0	k_0 (m/day)	λ_k	Name of layers
	λ_{QOC}	κ_{QOC}	α_{QOC}	$\dot{v}_{0\,QOC}$ (day^{-1})	λ	κ	α_{NC}	$\dot{v}_{0\,NC}$ (day^{-1})									
1	0.0531	0.0051	6.18E-04	6.18E-07	0.5308	0.0531	6.18E-03	6.18E-06	1.40	0.35	0.540	4.2	21.5	3.29	8.64E-04	0.531	Ma13U-1
2	0.0528	0.0053	6.43E-04	6.43E-07	0.5279	0.0528	6.43E-03	6.43E-06	1.40	0.35	0.540	12.7	27.1	3.11	8.64E-04	0.528	Ma13U-2
3	0.0509	0.0053	6.58E-04	6.58E-07	0.5088	0.0509	6.58E-03	6.58E-06	1.40	0.35	0.540	21.6	33.5	2.87	8.64E-04	0.509	Ma13U-3
4	0.0505	0.0052	6.73E-04	6.73E-07	0.5054	0.0505	6.73E-03	6.73E-06	1.40	0.35	0.540	31.0	41.5	2.75	8.64E-04	0.505	Ma13U-4
5	0.0494	0.0049	6.89E-04	6.89E-07	0.4937	0.0494	6.89E-03	6.89E-06	1.40	0.35	0.540	40.9	50.8	2.58	8.64E-04	0.494	Ma13U-5
6	0.0488	0.0051	7.06E-04	7.06E-07	0.4877	0.0488	7.06E-03	7.06E-06	1.40	0.35	0.540	51.3	61.1	2.45	8.64E-04	0.488	Ma13U-6
7	0.0420	0.0042	6.56E-04	6.56E-07	0.4203	0.0420	6.56E-03	6.56E-06	1.40	0.35	0.540	62.4	72.6	2.21	8.64E-04	0.420	Ma13L-1
8	0.0487	0.0049	7.54E-04	7.54E-07	0.4874	0.0487	7.54E-03	7.54E-06	1.40	0.35	0.540	74.1	89.9	2.23	8.64E-04	0.487	Ma13L-2
9	0.0405	0.0040	6.58E-04	6.58E-07	0.4049	0.0405	6.58E-03	6.58E-06	1.40	0.35	0.540	86.5	103.0	2.08	8.64E-04	0.405	Ma13L-3
10	0.0130	0.0024	3.04E-04	2.27E-07	0.1302	0.0130	3.04E-03	2.27E-06	1.10	0.38	0.607	124.3	198.8	1.14	1.73E-04	0.130	Dtc-1
11	0.0145	0.0022	3.27E-04	2.44E-07	0.1452	0.0145	3.27E-03	2.44E-06	1.10	0.38	0.607	150.9	241.5	1.22	2.07E-04	0.145	Dtc-2
12	0.0122	0.0034	2.92E-04	2.17E-07	0.1215	0.0122	2.92E-03	2.17E-06	1.10	0.38	0.607	177.0	283.2	1.08	1.81E-04	0.122	Dtc-3
13	0.0747	0.0068	1.04E-03	1.72E-07	0.7473	0.0747	1.04E-02	1.72E-06	1.30	0.36	0.561	204.8	307.2	2.58	1.90E-04	0.747	Ma12U-1
14	0.0772	0.0069	1.11E-03	1.82E-07	0.7721	0.0772	1.11E-02	1.82E-06	1.30	0.36	0.561	212.7	319.1	2.49	1.47E-04	0.772	Ma12U-2
15	0.0638	0.0060	9.66E-04	1.59E-07	0.6377	0.0638	9.66E-03	1.59E-06	1.30	0.36	0.561	221.1	331.6	2.30	9.07E-05	0.638	Ma12U-3
16	0.0707	0.0061	1.13E-03	1.86E-07	0.7068	0.0707	1.13E-02	1.86E-06	1.30	0.36	0.561	229.8	344.8	2.12	9.50E-05	0.707	Ma12U-4
17	0.0365	0.0050	7.10E-04	1.17E-07	0.3646	0.0365	7.10E-03	1.17E-06	1.25	0.36	0.572	240.0	360.0	1.57	5.62E-05	0.365	Ma12L-1
18	0.0365	0.0051	7.11E-04	1.17E-07	0.3650	0.0365	7.11E-03	1.17E-06	1.25	0.36	0.572	251.4	377.0	1.57	5.62E-05	0.365	Ma12L-2
19	0.0365	0.0052	7.11E-04	1.17E-07	0.3654	0.0365	7.11E-03	1.17E-06	1.25	0.36	0.572	262.7	394.0	1.57	5.62E-05	0.365	Ma12L-3
20	0.0461	0.0044	8.22E-04	8.78E-07	0.4605	0.0461	8.22E-03	8.78E-06	1.20	0.37	0.583	321.5	434.1	1.80	9.50E-05	0.461	Ma11U-1
21	0.0549	0.0046	9.59E-04	1.02E-06	0.5492	0.0549	9.59E-03	1.02E-05	1.20	0.37	0.583	330.8	446.6	1.86	9.07E-05	0.549	Ma11U-2
22	0.0401	0.0031	7.67E-04	8.20E-07	0.4011	0.0401	7.67E-03	8.20E-06	1.20	0.37	0.583	340.6	459.8	1.61	7.08E-05	0.401	Ma11U-3
23	0.0086	0.0010	1.98E-04	2.12E-07	0.0862	0.0086	1.98E-03	2.12E-06	1.20	0.37	0.583	352.0	475.2	1.18	5.27E-05	0.086	Ma11U-4
24	0.0618	0.0061	1.07E-03	5.05E-06	0.6178	0.0618	1.07E-02	5.05E-05	1.25	0.36	0.572	366.5	494.7	1.89	5.88E-05	0.618	Ma11L-1
25	0.0587	0.0031	9.95E-04	4.69E-06	0.5870	0.0587	9.95E-03	4.69E-05	1.25	0.36	0.572	379.6	512.5	1.95	6.05E-05	0.587	Ma11L-2
26	0.0448	0.0045	8.55E-04	4.03E-06	0.4481	0.0448	8.55E-03	4.03E-05	1.25	0.36	0.572	393.6	531.3	1.62	6.48E-05	0.448	Ma11L-3
27	0.0396	0.0039	8.00E-04	2.23E-07	0.3958	0.0396	8.00E-03	2.23E-06	1.25	0.36	0.572	452.3	565.3	1.47	3.80E-05	0.396	Ma10-1
28	0.0541	0.0052	9.61E-04	2.68E-07	0.5411	0.0541	9.61E-03	2.68E-06	1.25	0.36	0.572	471.8	589.7	1.82	4.49E-05	0.541	Ma10-2
29	0.0582	0.0058	9.90E-04	2.76E-07	0.5823	0.0582	9.90E-03	2.76E-06	1.25	0.36	0.572	489.7	612.1	1.94	7.60E-05	0.582	Ma10-3
30	0.0792	0.0075	1.20E-03	3.36E-07	0.7915	0.0792	1.20E-02	3.36E-06	1.25	0.36	0.572	505.8	632.2	2.29	6.13E-05	0.792	Ma10-4
31	0.0709	0.0079	1.14E-03	3.18E-07	0.7091	0.0709	1.14E-02	3.18E-06	1.25	0.36	0.572	521.8	652.2	2.11	5.23E-05	0.709	Ma10-5
32	0.0606	0.0056	1.07E-03	3.00E-07	0.6055	0.0606	1.07E-02	3.00E-06	1.25	0.36	0.572	539.5	674.4	1.82	5.18E-05	0.606	Ma10-6
33	0.0608	0.0056	1.07E-03	2.90E-07	0.6078	0.0608	1.07E-02	2.90E-06	1.25	0.36	0.572	584.7	730.9	1.85	9.50E-05	0.608	Ma9-1
34	0.0631	0.0064	1.07E-03	2.89E-07	0.6314	0.0631	1.07E-02	2.89E-06	1.25	0.36	0.572	603.3	754.2	1.96	9.07E-05	0.631	Ma9-2
35	0.0729	0.0072	1.19E-03	3.22E-07	0.7285	0.0729	1.19E-02	3.22E-06	1.25	0.36	0.572	621.2	776.5	2.07	9.50E-05	0.729	Ma9-3
36	0.0765	0.0076	1.23E-03	3.33E-07	0.7652	0.0765	1.23E-02	3.33E-06	1.25	0.36	0.572	638.7	798.4	2.12	9.07E-05	0.765	Ma9-4
37	0.0626	0.0066	1.09E-03	2.97E-07	0.6262	0.0626	1.09E-02	2.97E-06	1.25	0.36	0.572	656.5	820.6	1.86	7.34E-05	0.626	Ma9-5
38	0.0464	0.0051	8.74E-04	2.37E-07	0.4636	0.0464	8.74E-03	2.37E-06	1.25	0.36	0.572	675.7	844.6	1.65	6.91E-05	0.464	Ma9-6
39	0.1799	0.0159	1.99E-03	1.41E-06	1.7985	0.1799	1.99E-02	1.41E-05	1.25	0.36	0.572	728.5	874.3	3.51	2.85E-05	1.799	Doc5&Ma8-1
40	0.0342	0.0054	6.18E-04	4.37E-07	0.3420	0.0342	6.18E-03	4.37E-06	1.25	0.36	0.572	746.9	896.3	1.77	7.78E-05	0.342	Doc5&Ma8-2
41	0.0296	0.0037	6.12E-04	4.33E-07	0.2964	0.0296	6.12E-03	4.33E-06	1.25	0.36	0.572	770.1	924.2	1.42	1.30E-05	0.296	Doc5&Ma8-3
42	0.0534	0.0041	1.03E-03	1.48E-06	0.5339	0.0534	1.03E-02	1.48E-05	1.25	0.36	0.572	853.0	1023.6	1.60	1.30E-05	0.534	Ma7-1
43	0.0848	0.0058	1.37E-03	1.98E-06	0.8482	0.0848	1.37E-02	1.98E-05	1.25	0.36	0.572	877.3	1052.7	2.09	2.42E-05	0.848	Ma7-2
44	0.0331	0.0034	6.79E-04	9.81E-07	0.3308	0.0331	6.79E-03	9.81E-06	1.25	0.36	0.572	901.5	1081.8	1.44	3.02E-05	0.331	Ma7-3
45	0.0695	0.0044	1.26E-03	1.59E-06	0.6945	0.0695	1.26E-02	1.59E-05	1.25	0.36	0.572	997.0	1196.4	1.75	3.54E-05	0.695	Ma6-1
46	0.0451	0.0039	8.87E-04	1.12E-06	0.4506	0.0451	8.87E-03	1.12E-05	1.25	0.36	0.572	1013.6	1216.3	1.54	4.49E-05	0.451	Ma6-2
47	0.0547	0.0066	1.02E-03	1.28E-06	0.5470	0.0547	1.02E-02	1.28E-05	1.25	0.36	0.572	1030.1	1236.1	1.69	2.59E-05	0.547	Ma6-3

Table 4.4 Principal clayey soil parameters for the foundation of KIX in the B-N block

MTYP	Quasi-OC region				NC region				M	ν'	K_0	p_0 (kPa)	p_c (kPa)	e_0	k_0 (m/day)	λ_k	Name of layers
	λ_{QOC}	κ_{QOC}	α_{QOC}	$\dot{v}_{0\,QOC}$ (day^{-1})	λ	κ	α_{NC}	$\dot{v}_{0\,NC}$ (day^{-1})									
1	0.0425	0.0045	4.92E-04	4.92E-07	0.4250	0.0425	4.92E-03	4.92E-06	1.40	0.35	0.540	5.0	8.4	3.32	8.64E-04	0.425	Ma13U-1
2	0.0450	0.0049	5.60E-04	5.60E-07	0.4504	0.0450	5.60E-03	5.60E-06	1.40	0.35	0.540	15.7	21.3	3.02	8.64E-04	0.450	Ma13U-2
3	0.0456	0.0048	6.03E-04	6.03E-07	0.4560	0.0456	6.03E-03	6.03E-06	1.40	0.35	0.540	27.3	34.2	2.78	8.64E-04	0.456	Ma13U-3
4	0.0504	0.0049	6.76E-04	6.76E-07	0.5036	0.0504	6.76E-03	6.76E-06	1.40	0.35	0.540	39.5	49.8	2.73	8.64E-04	0.504	Ma13U-4
5	0.0486	0.0049	6.94E-04	6.94E-07	0.4864	0.0486	6.94E-03	6.94E-06	1.40	0.35	0.540	52.4	62.2	2.50	8.64E-04	0.486	Ma13U-5
6	0.0441	0.0046	6.64E-04	6.64E-07	0.4406	0.0441	6.64E-03	6.64E-06	1.40	0.35	0.540	66.1	75.8	2.32	8.64E-04	0.441	Ma13U-6
7	0.0391	0.0042	6.46E-04	6.46E-07	0.3906	0.0391	6.46E-03	6.46E-06	1.40	0.35	0.540	81.1	90.9	2.02	8.64E-04	0.391	Ma13L-1
8	0.0526	0.0043	8.04E-04	8.04E-07	0.5256	0.0526	8.04E-03	8.04E-06	1.40	0.35	0.540	96.4	111.0	2.27	8.64E-04	0.526	Ma13L-2
9	0.0408	0.0032	7.14E-04	7.14E-07	0.4076	0.0408	7.14E-03	7.14E-06	1.40	0.35	0.540	112.2	127.4	1.85	8.64E-04	0.408	Ma13L-3
10	0.0209	0.0027	4.44E-04	3.31E-07	0.2085	0.0209	4.44E-03	3.31E-06	1.10	0.38	0.607	238.5	357.8	1.35	1.73E-04	0.209	Dtc-1
11	0.0327	0.0038	6.44E-04	4.80E-07	0.3272	0.0327	6.44E-03	4.80E-06	1.10	0.38	0.607	262.1	393.1	1.54	2.07E-04	0.327	Dtc-2
12	0.0226	0.0028	4.86E-04	3.62E-07	0.2257	0.0226	4.86E-03	3.62E-06	1.10	0.38	0.607	285.6	428.4	1.32	1.81E-04	0.226	Dtc-3
13	0.0744	0.0075	1.03E-03	1.70E-07	0.7437	0.0744	1.03E-02	1.70E-06	1.30	0.36	0.561	325.8	456.1	2.60	1.90E-04	0.744	Ma12U-1
14	0.0722	0.0062	1.04E-03	1.71E-07	0.7219	0.0722	1.04E-02	1.71E-06	1.30	0.36	0.561	342.3	479.3	2.48	1.47E-04	0.722	Ma12U-2
15	0.0710	0.0064	1.07E-03	1.75E-07	0.7103	0.0710	1.07E-02	1.75E-06	1.30	0.36	0.561	359.6	503.4	2.33	9.07E-05	0.710	Ma12U-3
16	0.0548	0.0060	9.15E-04	1.51E-07	0.5475	0.0548	9.15E-03	1.51E-06	1.30	0.36	0.561	378.3	529.6	1.99	9.50E-05	0.548	Ma12U-4
17	0.0258	0.0033	5.06E-04	8.34E-08	0.2579	0.0258	5.06E-03	8.34E-07	1.25	0.36	0.572	400.4	560.5	1.55	5.62E-05	0.258	Ma12L-1
18	0.0371	0.0037	7.19E-04	1.18E-07	0.3706	0.0371	7.19E-03	1.18E-06	1.25	0.36	0.572	425.8	596.2	1.58	5.62E-05	0.371	Ma12L-2
19	0.0288	0.0022	5.84E-04	9.61E-08	0.2878	0.0288	5.84E-03	9.61E-07	1.25	0.36	0.572	451.6	632.2	1.47	5.62E-05	0.288	Ma12L-3
20	0.0590	0.0043	1.01E-03	1.08E-06	0.5895	0.0590	1.01E-02	1.08E-05	1.20	0.37	0.583	509.9	688.4	1.92	9.50E-05	0.590	Ma11U-1
21	0.0581	0.0049	1.01E-03	1.08E-06	0.5807	0.0581	1.01E-02	1.08E-05	1.20	0.37	0.583	526.4	710.7	1.87	9.07E-05	0.581	Ma11U-2
22	0.0321	0.0032	6.47E-04	6.91E-07	0.3205	0.0321	6.47E-03	6.91E-06	1.20	0.37	0.583	544.4	735.0	1.48	7.08E-05	0.321	Ma11U-3
23	0.0203	0.0013	4.82E-04	5.15E-07	0.2029	0.0203	4.82E-03	5.15E-06	1.20	0.37	0.583	565.1	762.9	1.11	5.27E-05	0.203	Ma11U-4
24	0.0537	0.0063	9.87E-04	4.66E-06	0.5366	0.0537	9.87E-03	4.66E-05	1.25	0.36	0.572	593.9	801.8	1.72	5.88E-05	0.537	Ma11L-1
25	0.0607	0.0055	1.01E-03	4.78E-06	0.6067	0.0607	1.01E-02	4.78E-05	1.25	0.36	0.572	617.6	833.8	1.99	6.05E-05	0.607	Ma11L-2
26	0.0428	0.0041	8.19E-04	3.86E-06	0.4283	0.0428	8.19E-03	3.86E-05	1.25	0.36	0.572	642.1	866.9	1.62	6.48E-05	0.428	Ma11L-3
27	0.0302	0.0035	6.39E-04	1.78E-07	0.3023	0.0302	6.39E-03	1.78E-06	1.25	0.36	0.572	737.3	958.5	1.37	3.80E-05	0.302	Ma10-1
28	0.0656	0.0051	1.18E-03	3.29E-07	0.6561	0.0656	1.18E-02	3.29E-06	1.25	0.36	0.572	768.9	999.5	1.78	4.49E-05	0.656	Ma10-2
29	0.0748	0.0067	1.26E-03	3.50E-07	0.7484	0.0748	1.26E-02	3.50E-06	1.25	0.36	0.572	797.7	1037.0	1.98	7.60E-05	0.748	Ma10-3
30	0.0840	0.0078	1.31E-03	3.64E-07	0.8398	0.0840	1.31E-02	3.64E-06	1.25	0.36	0.572	824.4	1071.8	2.22	6.13E-05	0.840	Ma10-4
31	0.0771	0.0074	1.28E-03	3.58E-07	0.7708	0.0771	1.28E-02	3.58E-06	1.25	0.36	0.572	851.4	1106.8	2.01	5.23E-05	0.771	Ma10-5
32	0.0531	0.0052	1.00E-03	2.79E-07	0.5313	0.0531	1.00E-02	2.79E-06	1.25	0.36	0.572	881.3	1145.7	1.65	5.18E-05	0.531	Ma10-6
33	0.0505	0.0045	9.79E-04	2.66E-07	0.5051	0.0505	9.79E-03	2.66E-06	1.25	0.36	0.572	935.5	1169.3	1.58	9.50E-05	0.505	Ma9-1
34	0.0652	0.0050	1.13E-03	3.06E-07	0.6520	0.0652	1.13E-02	3.06E-06	1.25	0.36	0.572	965.0	1206.2	1.89	9.07E-05	0.652	Ma9-2
35	0.0700	0.0054	1.18E-03	3.20E-07	0.7001	0.0700	1.18E-02	3.20E-06	1.25	0.36	0.572	992.9	1241.1	1.97	9.50E-05	0.700	Ma9-3
36	0.0795	0.0055	1.32E-03	3.58E-07	0.7954	0.0795	1.32E-02	3.58E-06	1.25	0.36	0.572	1020.4	1275.5	2.02	9.07E-05	0.795	Ma9-4
37	0.0765	0.0048	1.30E-03	3.54E-07	0.7651	0.0765	1.30E-02	3.54E-06	1.25	0.36	0.572	1048.3	1310.4	1.93	7.34E-05	0.765	Ma9-5
38	0.0516	0.0039	9.89E-04	2.69E-07	0.5160	0.0516	9.89E-03	2.69E-06	1.25	0.36	0.572	1078.0	1347.5	1.61	6.91E-05	0.516	Ma9-6
39	0.0476	0.0043	8.84E-04	6.25E-07	0.4755	0.0476	8.84E-03	6.25E-06	1.25	0.36	0.572	1156.6	1387.9	1.69	2.85E-05	0.476	Doc5&Ma8-1
40	0.0889	0.0066	1.16E-03	8.18E-07	0.8888	0.0889	1.16E-02	8.18E-06	1.25	0.36	0.572	1185.2	1422.2	2.85	7.78E-05	0.889	Doc5&Ma8-2
41	0.0594	0.0059	1.01E-03	7.15E-07	0.5938	0.0594	1.01E-02	7.15E-06	1.25	0.36	0.572	1213.1	1455.7	1.94	1.30E-05	0.594	Doc5&Ma8-3
42	0.0381	0.0041	7.59E-04	1.10E-06	0.3812	0.0381	7.59E-03	1.10E-05	1.25	0.36	0.572	1312.8	1575.4	1.51	1.30E-05	0.381	Ma7-1
43	0.0496	0.0042	9.35E-04	1.35E-06	0.4959	0.0496	9.35E-03	1.35E-05	1.25	0.36	0.572	1347.2	1616.6	1.65	2.42E-05	0.496	Ma7-2
44	0.0747	0.0058	1.20E-03	1.73E-06	0.7471	0.0747	1.20E-02	1.73E-05	1.25	0.36	0.572	1378.8	1654.6	2.11	3.02E-05	0.747	Ma7-3
45	0.0534	0.0046	1.01E-03	1.26E-06	0.5340	0.0534	1.01E-02	1.26E-05	1.25	0.36	0.572	1446.9	1663.9	1.66	3.54E-05	0.534	Ma6-1
46	0.0781	0.0062	1.31E-03	1.64E-06	0.7813	0.0781	1.31E-02	1.64E-05	1.25	0.36	0.572	1486.6	1709.6	1.99	4.49E-05	0.781	Ma6-2
47	0.0373	0.0043	7.42E-04	9.33E-07	0.3733	0.0373	7.42E-03	9.33E-06	1.25	0.36	0.572	1526.8	1755.8	1.52	2.59E-05	0.373	Ma6-3

4.2.2 Evaluation of permeability and parameters for the Pleistocene sand gravel deposits

The model foundation for finite element analysis shown in Fig.4.7 is assumed to be horizontally continuous for the sand gravel layers sandwiched by the Pleistocene clay layers. But it was not definitely confirmed how the sand gravel layers under the Pleistocene marine foundation are distributed in practice. Due attention should be paid to the fact that the thickness, the horizontal continuity and the fine contents for the sand gravel layers are the influential factors to control the process of generation and dissipation of excess pore water pressure in the Pleistocene deposits. In present study, the concept of "mass permeability" is introduced. It is true that the values of the coefficient of permeability, k were derived based on the experiments but for such a large scale reclamation, those experimental values are meaningful as far as the distributed structure of the sand gravel layers are rationally modeled over a wide range. At present, the detailed distribution model for them cannot be established. Furthermore, the permeability controlling the advance in consolidation is not the one derived in the laboratory but the one that actually functions in the field. The author considers this practical permeability as "mass permeability" that effectively controls the process of excess pore water dissipation in the field. The "equivalent coefficient of permeability" is hence introduced as a representative of "mass permeability" by considering the horizontal continuity, the change of thickness horizontally and the degree of fine contents for the Pleistocene sand gravel deposits. For convenience, the sand gravel layers are assumed to be level and continuous and the equivalent coefficients of permeability are provided for the individual sand gravel layers following the above-mentioned judgment.

No comprehensive laboratory tests have been conducted for deriving the coefficient of permeability of the Pleistocene sand gravel materials because of the difficulties in obtaining the high quality undisturbed samples from the deep sedimentation. Furthermore, the Pleistocene sand

gravel layers had been considered as perfectly drained ones at the early stage of the projects. The importance of the permeability of the Pleistocene sand gravel layers was recognized through the in-situ measurement of the excess pore water pressure in the individual layers (Akai and Tanaka, 1999). On the basis of the findings by Itoh et al. (2001), Takemura and Nakaseko (2005) summarized the status of the Pleistocene sand gravel deposits at KIX based on the geophysical and geological investigation. Kitada et al. (2011a) and Inoue et al. (2011) also summarized the distribution characteristic of the individual Pleistocene sand gravel deposits based on the soil exploration and geological survey data. The brief evaluation for the individual sand gravel layers (Ds) was explained and the qualitative evaluation for permeability was performed in the previous section 2.2.3. Here, it is important to realize that the geological and geophysical output about the qualitative evaluation for permeability of the Pleistocene sand gravel layers has to be transformed to the quantitative numerical values of the coefficient of permeability to apply to the present elasto-viscoplastic finite element procedure.

On the basis of the above-mentioned evaluation for permeability of the Pleistocene sand gravel layers, a series of three-dimensional seepage analyses around the marine foundations of KIX was conducted (Kansai International Airport Co., 2002, Nishigaki et al., 2005). By providing coefficients of permeability were provided in the order of 10^0 m/day to 10^1 m/day for the individual sand gravel layers to reproduce the in-situ generation and dissipation process of the excess pore water pressure. In the present analyses, those values are introduced as references. The definite numerical values for the equivalent coefficient of permeability as input parameters for the Pleistocene sand gravel layers were adjusted to reproduce the measured results of the individual layers over 14 years as shown in Table 4.5. It is noteworthy to assume that the equivalents of coefficient for Ds6 and Ds7 evaluated poorly permeable were decreased seriously while the ordinary values were set for other sand gravel layers. The evaluated permeability for the individual Pleistocene sand gravel layers is adopted as the identical values in all areas without

distinction of blocks because that is regarded as the representative of the capacity of permeability for the individual Pleistocene sand gravel layers at KIX.

The Pleistocene sand gravel layers, which are expressed by Ds, are also assumed to be linear elastic material for the numerical analysis. The elastic shear modulus for sand deposits is determined by the following empirical relationship in terms of the SPT-N value (Yoshinaka, 1968).

$$G_o\left(tf/m^2\right)=\frac{70}{2\left(1+\nu'\right)}\cdot N \tag{4.8}$$

in which ν' is the Poisson's ratio in terms of effective stress. The values of the principal soil parameters for the Pleistocene sand gravel layers are summarized with the evaluated equivalent coefficient of permeability in Table 4.5.

Table.4.5 Equivalent coefficient of permeability and principal soil parameters for the Pleistocene sand gravel layers

NTYP	ν'	K_o	Go (kPa)	k_o(m/day)	Name of layers
1	0.33	0.50	13,100	2.16E+01	Ds-1
2	0.33	0.50	13100	1.30E+00	Ds-2
3	0.33	0.50	13,100	1.08E+01	Ds-3
4	0.33	0.50	13,100	3.89E+00	Ds-4
5	0.33	0.50	13,100	3.89E+00	Ds-5
6	0.33	0.50	13,100	2.59E-01	Ds-6
7	0.33	0.50	13,100	8.64E-02	Ds-7
8	0.33	0.50	13,100	2.16E+00	Ds-8
9	0.33	0.50	13,100	2.16E+00	Ds-9
10	0.33	0.50	13,100	6.92E+00	Ds-10

4.3 Numerical analysis for Construction of the 1st phase island of KIX

4.3.1 Outline of Numerical analysis

A series of elasto-viscoplastic finite element analyses is performed to be first step to propose the numerical procedure for the assessment of the long-term settlement and the generation /dissipation process of excess pore water pressure due to the offshore reclamation. The modified plane strain version (Sekiguchi et al. 1982) of the elasto-viscoplastic model originally proposed by Sekiguchi (1977) is used for the constitutive model in this finite element analysis. The compression model for quasi-overconsolidated Pleistocene clays (Mimura and Jang, 2004) is also adopted in the present study to assess the non-elastic behavior in the quasi-overconsolidated region. The coupled stress-flow analysis that is established on the basis of Biot's formulation (Christian, 1986, Akai and Tamura, 1976) is also considered in the present study.

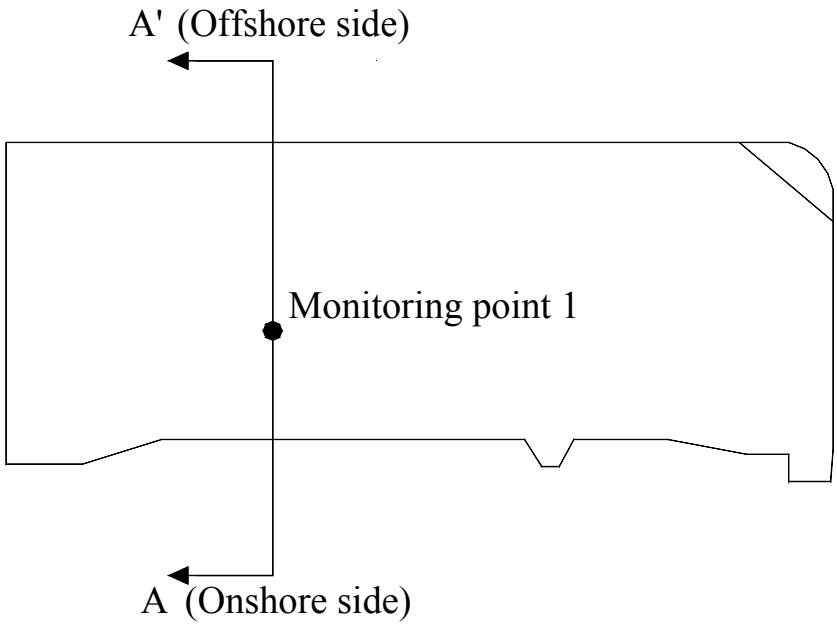

Fig. 4.6 Plan view of the 1st phase island of Kansai International Airport and the location of the monitoring point 1

Figure 4.6 shows the plan view of the 1st phase island of KIX together with the location of monitoring point 1. A series of elasto-viscoplastic finite element analyses is carried out along the section shown by A-A' in Fig. 4.6 to be considered as the representative section to propose the numerical procedure. The construction sequence was shown in Fig. 2.8(a) with the increasing process of the applied stress due to reclamation. As shown in Fig. 2.9, the prescribed final overburden due to the 1st airport fill construction amounts to about 430 kPa at the monitoring point1. The soil parameters for the present numerical analyses are adopted for the A-S block shown in Table 4.1 for the Pleistocene clay deposits and those shown in Table 4.5 for the Pleistocene sand gravel deposits by considering only the construction of the 1st phase island.

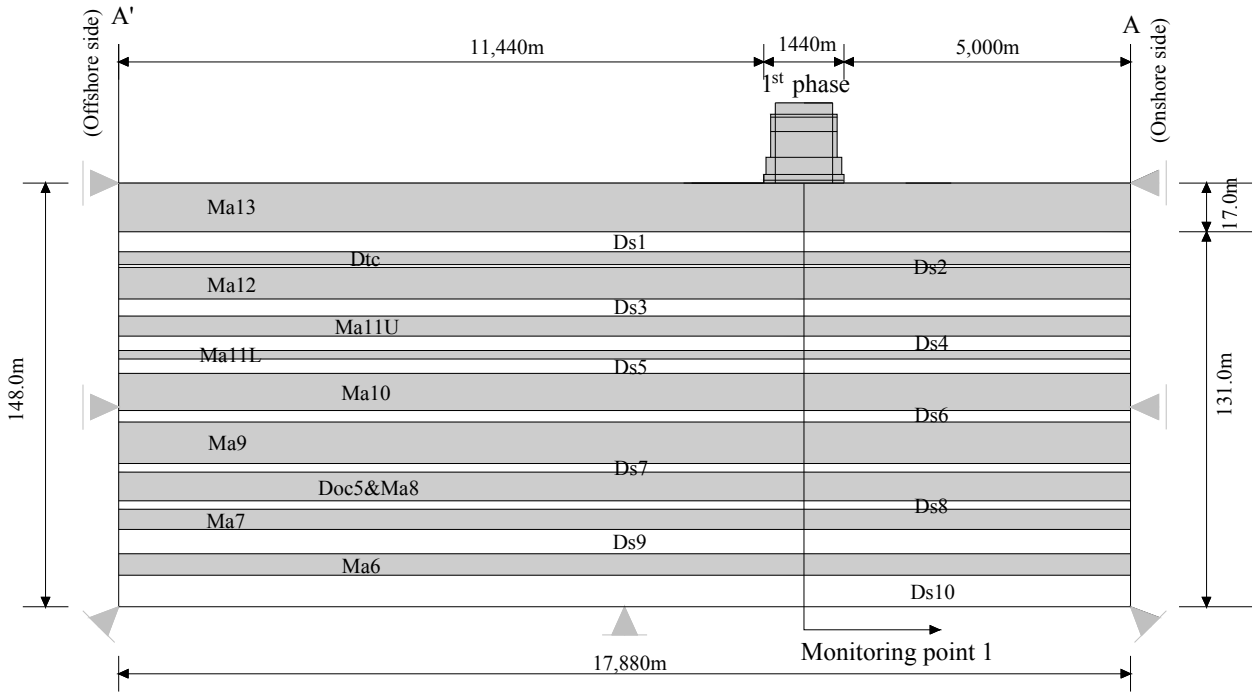

Fig. 4.7 Schematic cross-section of the foundation ground of the 1st phase Kansai International Airport for finite element analysis

4.3.2 Foundation model and hydraulic boundary for horizontally even layer

Figure 4.7 schematically shows the representative foundation model used in the finite element analysis along the section shown by A-A' in Fig.4.6. The foundation model is assumed to be horizontally even layers that have a constant thickness and continuous layer based on the boring data at the monitoring point 1. Here, Ma and Ds denote the marine clay and the Pleistocene sand gravel layer respectively, and the individual names of the Pleistocene clay layers have been updated to the present ones based on the geological findings from the boring KIX18-1 (Kitada et al, 2009). Ma13 is the Holocene marine clay whereas the others are Pleistocene in origin. The original foundation is set from the elevation of -18m to -166m. For the normally consolidated Holocene clay deposit, Ma13, sand drains are driven in a rectangular configuration with a pitch of 2.0 to 2.5 meters to promote the consolidation. The modeling of sand drains is simulated by the macro-element method (Sekiguchi et al., 1986). The lateral boundary of the clay layers (A-A' lines) in Fig. 4.7 is assumed to be undrained while that of the sand gravel layers is assumed to be fully drained. The bottom boundary is hence assumed to be undrained because Ds10 is underlain by Ma3 whose permeability is low enough to be impermeable. Mimura and Sumikura (2000) reported that insufficient distance to the hydraulic boundary causes the dissipation of excess pore water pressure to be overestimated, and that the permeable sand gravel layers play a significant role in controlling the rate of consolidation. It is natural that the calculated results are seriously influenced by the setting of boundary conditions. In the case of KIX, as there are alternating permeable sand gravel layers sandwiched by the Pleistocene clay layers, the propagation of excess pore water pressure through those permeable sand gravel layers should be of concern. Then, the effect of the mesh size in terms of the distance to the seaside boundary merits due consideration with regard to the subsequent deformation.

Mimura and Jang (2005b) reported that when the distance to the boundary is set to be about 10 times of the loading area, the effect of the hydraulic boundary condition can be ruled out.

Based on the findings, the foundation model used in the present study is shown in Fig. 4.7. As shown in Fig. 4.7, while the loading area by reclamation of the 1st phase island is 1,440m, the distance to the right boundary is set to be 5,000m, which is the actual distance from land. For the opposite offshore side boundary, it is set to be 11,440m to make the numerical results free from the effect of the hydraulic boundary. The larger distance for the left boundary was set after considering that the 2nd phase island will be constructed on this side in future.

4.3.3 Simulation results and discussion

4.3.3.1 Performance of excess pore water pressure

Calculated distribution of excess pore water pressure is shown in Fig. 4.8. As shown in Fig. 4.8 (a), at the completion of the 1st reclamation (1800 days from the start of reclamation), little amount of excess pore water pressure remains in the Holocene clay layer because of the effect of sand drains. In contrast, a large amount of excess pore water pressure remains not only in the clay layers but also in the permeable sand gravel layers in the Pleistocene deposits. In particular, more than 200 kPa of excess pore water pressure is kept in the middle Pleistocene clay layers, Ma10 and 9 as well as sand gravel layers, Ds6 and 7. It should also be noted that excess pore water pressure propagates through the sand gravel layers outward from the loaded area even at the completion of reclamation. A remarkable decrease in effective stress hence takes place in the foundation where there is no reclamation load at the time. Here, due attention should be paid to the fact that a slight propagation of excess pore water pressure takes place in Ds6 and 7 because the very low permeability of these sand gravel layers functions to obstruct the sufficient propagation of excess pore water pressure. On the contrary, in the upper and lower Pleistocene deposits where the permeability of sand gravel layers is better than Ds6 and 7, a serious propagation of excess pore water pressure can be seen.

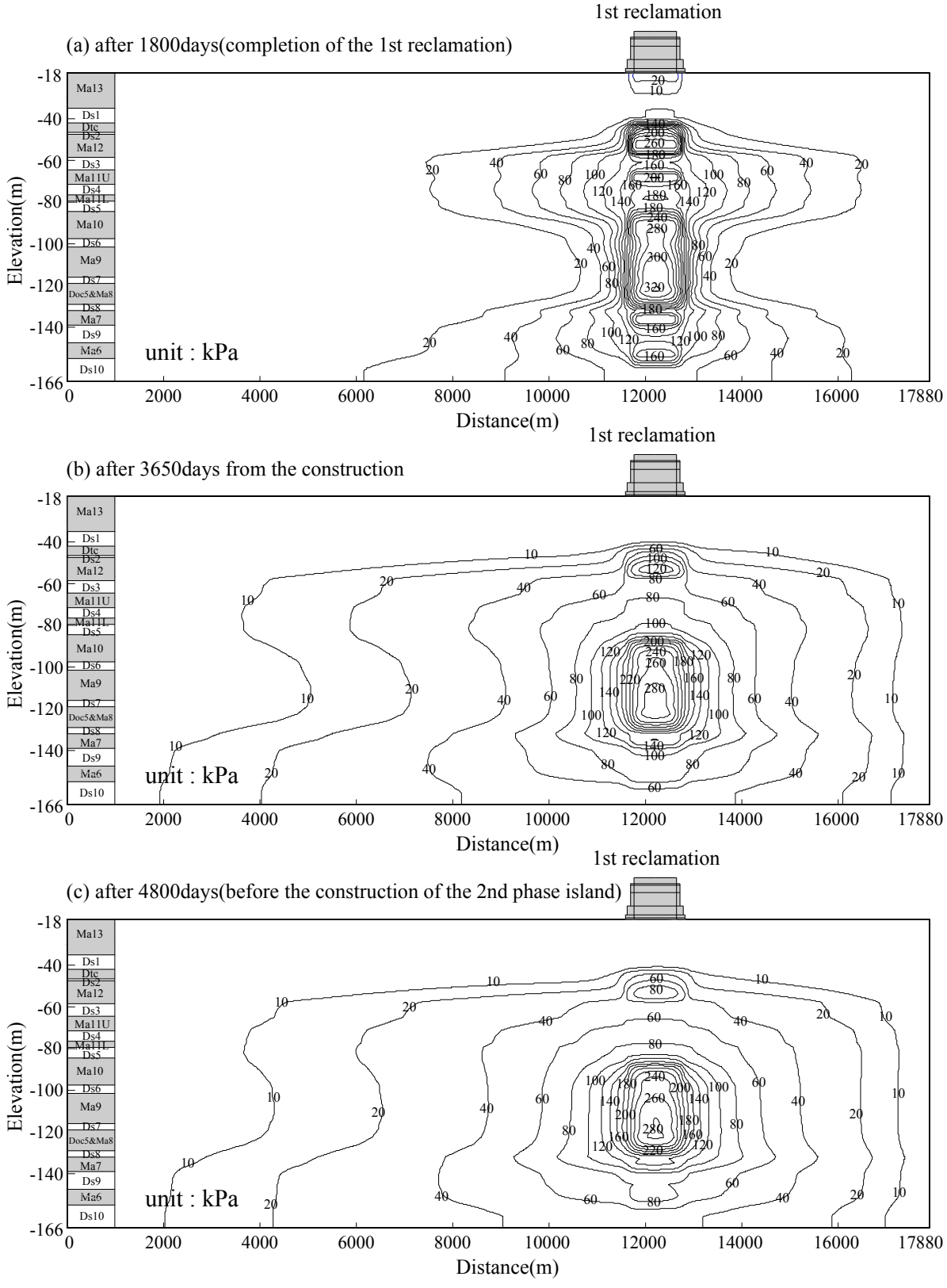

Fig. 4.8 Contours of calculated distribution of excess pore water pressure in terms of construction of the 1st phase island

The propagation of excess pore water pressure in the Pleistocene sand gravel layers of the KIX foundations is associated with the insufficient dissipation of excess pore water pressure in these layers. The phenomenon is caused by insufficient capability of permeability in the Pleistocene sand gravel layers with insufficient thickness for the full dissipation of excess pore water pressure due to the vastness of reclamation load. In fact, almost full dissipation is achieved without any significant propagation of excess pore water pressure both in Ds1 and 10, both of which have sufficient thickness and permeability. With the lapse of time, the excess pore water pressure in the upper Pleistocene clay layers such as Ma 12 and 11 monotonically dissipates, whereas it remains unchanged in the middle Pleistocene layers (see Fig. 4.8 (b)). As is explained in the previous section, the low values of the coefficient of permeability are set for Ds6 and 7 because they are thin, have poorly consistency and are rich in fine contents. This low permeability of Ds6 and 7 causes the remarkable undissipated excess pore water pressure in those layers. It is noteworthy in Fig. 4.8 (c) that the excess pore water pressure in those layers is found not to dissipate even before the construction of the 2nd phase island (after 4800 days since the start of reclamation). It clearly means that the primary consolidation in terms of the process of excess pore water pressure dissipation was not completed in the Pleistocene deposits before the construction of the 2nd phase island.

The distribution of the excess pore water pressure with depth at the monitoring point 1 that is located at the center of the 1st phase island (see Figs. 4.6, 4.7) is shown in Fig. 4.9. Here, the solid line, dotted line and thin solid line denote the distribution at the completion of the reclamation of the 1st phase island, after 3650 days and after 4800 days (before the start of reclamation of the 2nd phase island) respectively. Because the upper Pleistocene clays such as Ma12 and 11 have undergone plastic yielding due to reclaimed load, a large amount of excess pore water pressure generates at the completion of reclamation of the 1st phase island. Then, it dissipates steadily because of the high permeability of the sand gravel layers, Ds1and 3 above and below Ma12.

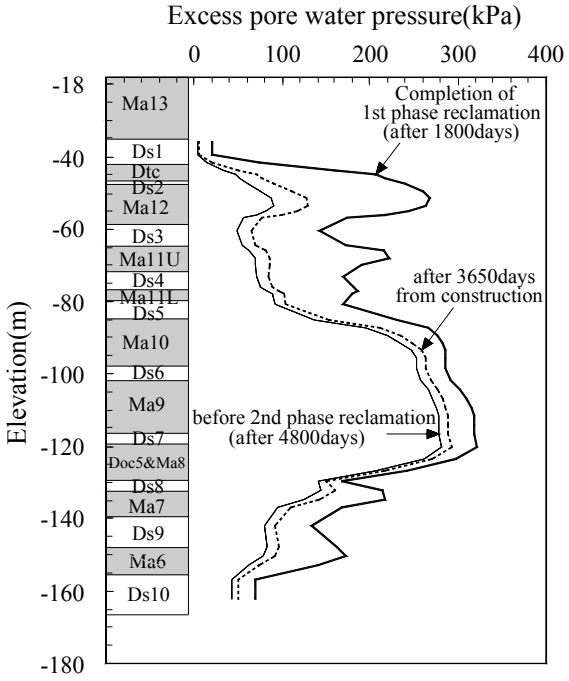

Fig. 4.9 Calculated distribution of the excess pore water pressure with depth at the monitoring point 1 in terms of construction of the 1st phase island

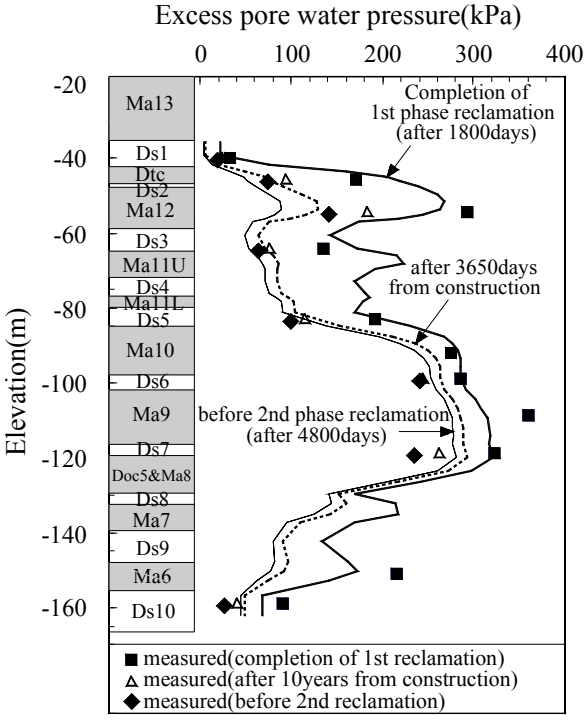

Fig. 4.10 Comparison of calculated and measured excess pore water pressure distribution with depth at the monitoring point 1 in terms of construction of the 1st phase island

Since Ma11 is relatively silty with high permeability, and is divided into 2 layers by the sand intrusion, not only is the generated excess pore water pressure not so large compared to Ma12, but it dissipates faster with time. On the other hand, the mode of excess pore water pressure in the middle Pleistocene layers is different. Because of the poor quality of mass permeability of the sand gravel layers (Ds6, 7), Ma10, 9 and Doc5&Ma8 behave as if they are one continuous clay layer. Here, Ds6 and 7 do not seem to function as permeable layers at all. The rate of excess pore water pressure dissipation is very low in those layers, which results in that a large amount of undissipated excess pore water pressure remains in the middle Pleistocene layers for a long time. The calculated performance provides that even before the construction of the 2nd phase island, more than 200 kPa of excess pore water pressure remains. In the lower Pleistocene layers such as Ma7, 6, the generated excess pore water pressure is not so large compared to the other layers and dissipates faster with time because of the high permeability of the thick sand gravel layer, Ds10 situated below Ma6.

At the monitoring point 1, the excess pore water pressure has been measured at various layers. The calculated performance can be validated by comparing it with the measured data. Figure 4.10 shows the comparison of the excess pore water pressure distribution with depth. The calculated values were compared with the measured values at three different times. The solid line and ■, the dotted line and △, thin solid line and ◆ are the calculated and measured results at the completion of the reclamation of the 1st phase island , after 3650 days and after 4800 days (before the start of the construction of the 2nd phase island) respectively. Although the calculated performance at the completion of the reclamation of the 1st phase island slightly underestimates the measured excess pore water pressure at the layers such as Ma12, 9 and 7, the overall mode of distribution can well be described. With the lapse of time, the discrepancy between the calculated and measured results decreases and both show a good match at after 3650 days from the start of reclamation as well as at after 4800 days(before the start of the construction of the 2nd phase island).

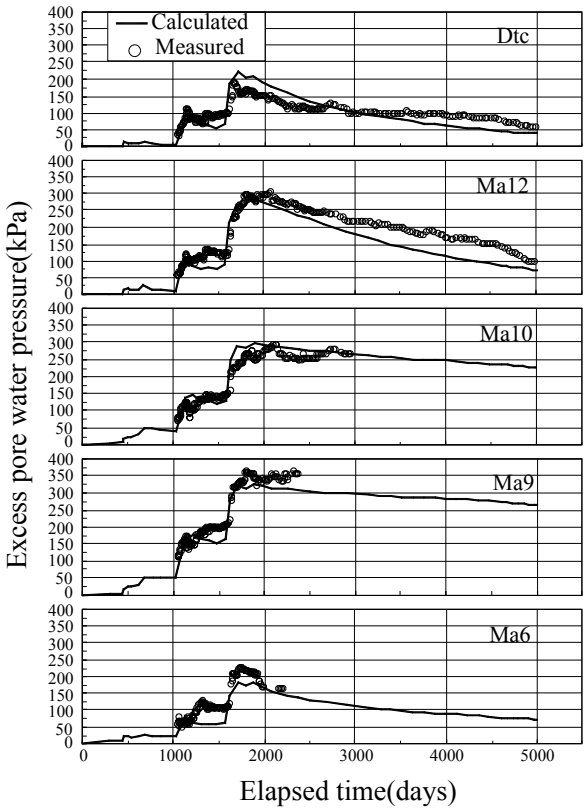

(a) Comparison of measured and calculated excess pore water pressure for the Pleistocene clay layers

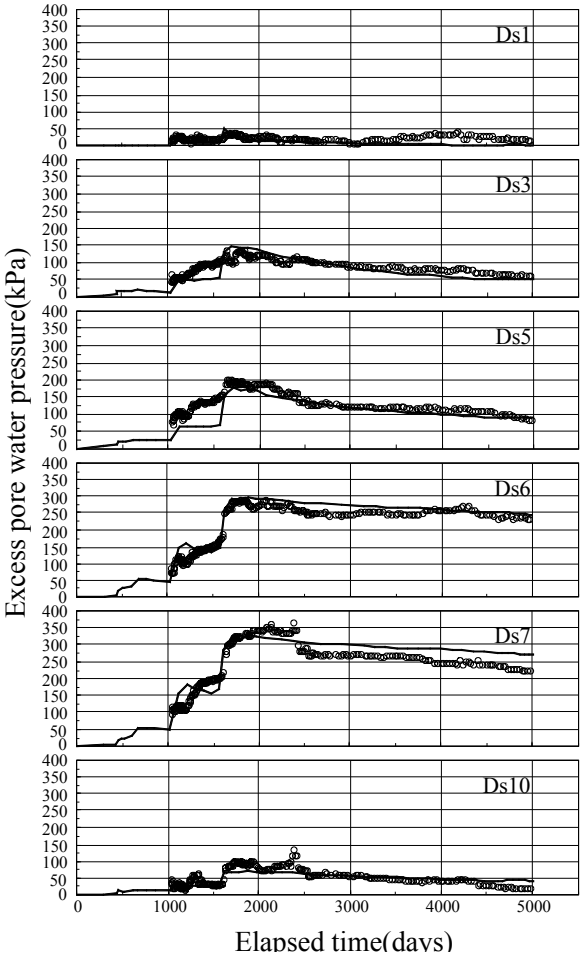

(b) Comparison of measured and calculated excess pore water pressure for the Pleistocene sand gravel layers

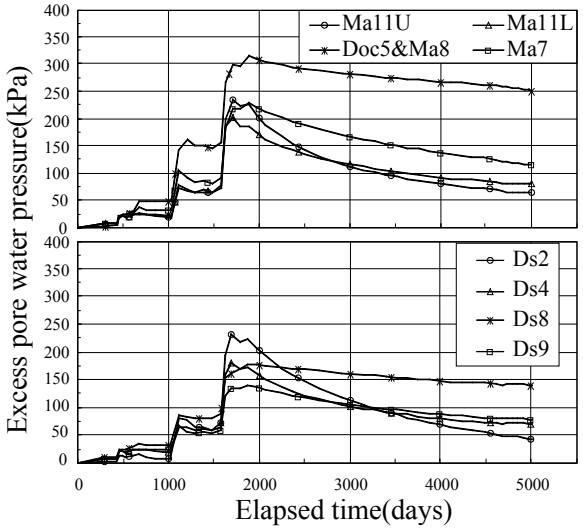

(c) Calculated excess pore water pressure for the Pleistocene clay layers

Fig. 4.11 Calculated and measured excess pore water pressure with time for the individual Pleistocene layers at the monitoring point 1 in terms of construction of the 1st phase island

Long-term behavior of the excess pore water pressure in the Pleistocene deposits is found to be well simulated with the present analyses.

Calculated excess pore water pressure - time relations are shown in Fig. 4.11(a) together with the measured results for the individual Pleistocene clay layers. Note that the comparison is shown for the Pleistocene clay layers where the pore pressure cells have survived. For the selected Pleistocene clay layers, the process of generation and dissipation of excess pore water pressure is well described by the present numerical procedure. Calculated excess pore water pressure-time relations are shown in Fig. 4.11(b) together with the measured results for the individual Pleistocene sand gravel layers. It is clear that little excess pore water pressure is generated in Ds1 and 10, whereas a large amount of excess pore water pressure is generated and kept undissipated in the middle Pleistocene sand gravel layers, such as Ds6 and 7. The phenomenon of undissipation in Ds6 and 7 causes the delay of consolidation for Ma10 and 9 associated with undissipation of excess pore water pressure (see Figure 4.11(a)). This difference reflects the mass permeability of the Pleistocene sand gravel layers remarkably well. The calculated performance can well predict the actual behavior of excess pore water pressure in the all Pleistocene sand gravel layers. Figure 4.11(c) shows the calculated performance of the excess pore water pressure of the Pleistocene clay and sand gravel layers where there is no measured information due to damage of the pressure cells. As seen from Figs. 4.11, the behavior of excess water pressure can be well predicted by the proposed procedure. It is hence confirmed that the adopted procedure in terms of elasto-viscoplastic finite element analysis associated with a compression modeling works well to assess the stress condition of the reclaimed Pleistocene deposits at KIX.

4.3.3.2 Transition of stress state with depth

The stress condition with depth at the monitoring point 1 is shown in Fig 4.12. In Fig. 4.12(a), p_0 denotes the initial vertical effective stress, p_c is the consolidation yield stress, p_f means the final total vertical stress due to the reclamation of the 1st phase island and p' denotes the effective vertical stress at the completion of the reclamation of the 1st phase island. The hatched area exhibits the undissipated excess pore water pressure. The effective stresses already surpass p_c for the Pleistocene clay layers above Ma10, while those still remain below p_c for the middle to lower Pleistocene clay layers such as Ma10, 9 and Doc5&Ma8. Then, the upper Pleistocene clay layers behave as normally consolidated and the middle to lower Pleistocene clay layers behave as overconsolidated at the completion of the reclamation of the 1st phase island. It is interesting that the stress condition of the airport foundations is not so different even before the start of the reclamation of the 2nd phase island as shown in Fig 4.12(b). It is true that the excess pore water pressure at the upper Pleistocene layers is almost dissipated before the construction of the 2nd phase island, but the one at the middle Pleistocene clay layers scarcely dissipates during the period. The one reason of this behavior is that the mass permeability of permeable sand gravel layers, such as Ds6 and 7 is insufficient to promote dissipation of excess pore water pressure and another is that the rate of consolidation for those layers becomes lower because the consolidation coefficients, c_v for Ma10 become much lower due to plastic yielding. From the results shown in Fig. 4.12, the advance in settlement due to consolidation for the middle Pleistocene clay layers is not expected in this period.

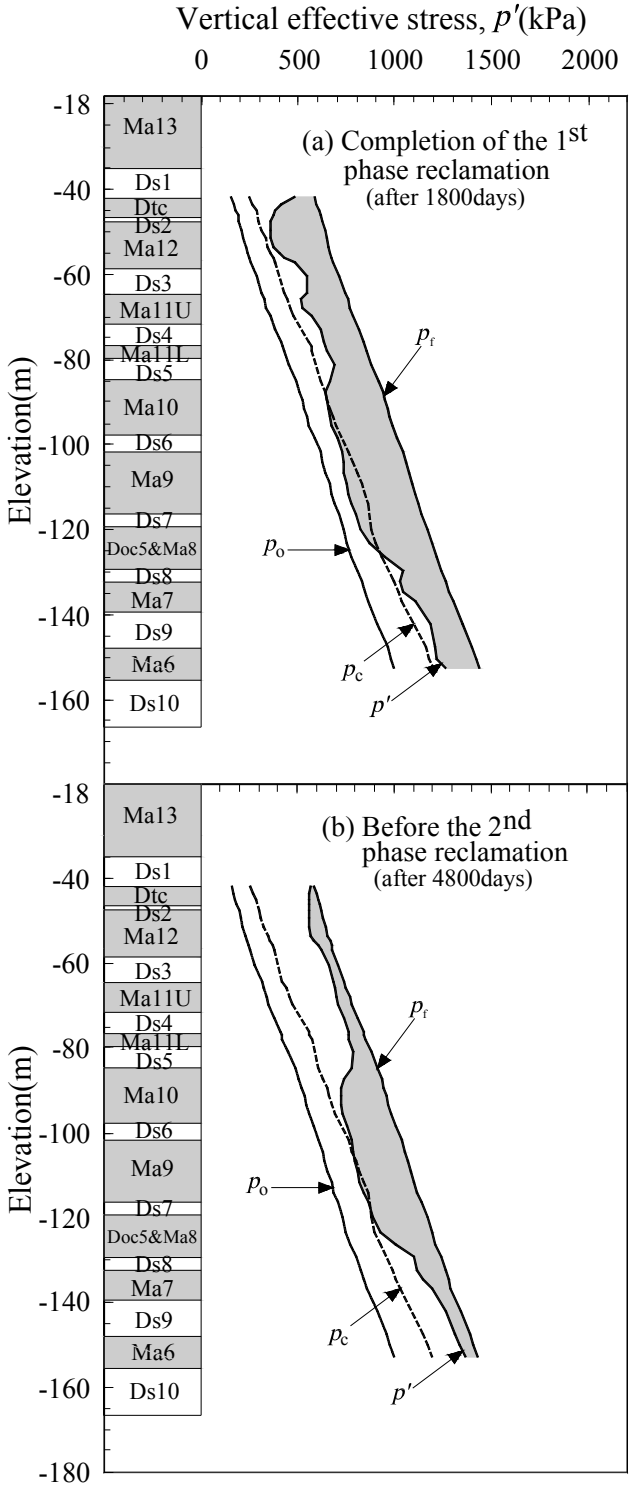

Fig. 4.12 Stress condition with depth at the monitoring point 1 in terms of construction of the 1st phase island

4.3.3.3 Settlement

The calculated and measured settlement - time relations for the individual Pleistocene clay layers are shown in Fig. 4.13. As seen from Fig. 4.9, the excess pore water pressure in the upper Pleistocene layers from Dtc to Ds5 has steadily dissipated with time. This steady dissipation has resulted in the remarkable advance in the compression of the Dtc, Ma12 and 11 clay layers, in particular. On the other hand, in the middle and lower Pleistocene layers such as Ma10 to Ds10, the rate of dissipation of excess pore water pressure is much lower than in the upper Pleistocene layers (see Fig. 4.11) because of the poor permeability of the sand gravel layers in this region. It means that the primary consolidation associated with the dissipation of excess pore water pressure is not predominant in the middle to lower Pleistocene clay layers. Delayed compression, however, occurs during the process of excess pore water pressure dissipation under the condition of insufficient advance in primary consolidation. In all the Pleistocene clay layers in the KIX foundation ground, considerable time dependent compression has hence continued with insufficient dissipation of excess pore water pressure.

The comparison between the calculated and measured settlement is also shown to confirm the validity of the proposed procedure in Fig. 4.13. In the upper Pleistocene clay layers such as Dtc, Ma12 and 11, the clays undergo plastic yielding due to the reclamation load in a short time because of their relatively small initial stresses, p_o. Because the stress surpasses p_c so rapidly due to the reclamation load, the time dependent behavior in the overconsolidated region can be ruled out, and then as a typical behavior for normally consolidated clay, the hyperbolic shape for settlement – time relations is exhibited for Dtc, Ma12 and 11. The calculated performance can well describe the whole process of compression. On the contrary, in the middle Pleistocene clay layers such as Ma10, 9 and Doc5&Ma8, the stress remains within p_c at the completion of the reclamation of the 1st phase island. However, as shown in Fig 4.12, it takes a long time for these layers to become gradually normally consolidated by undergoing plastic yielding due to the

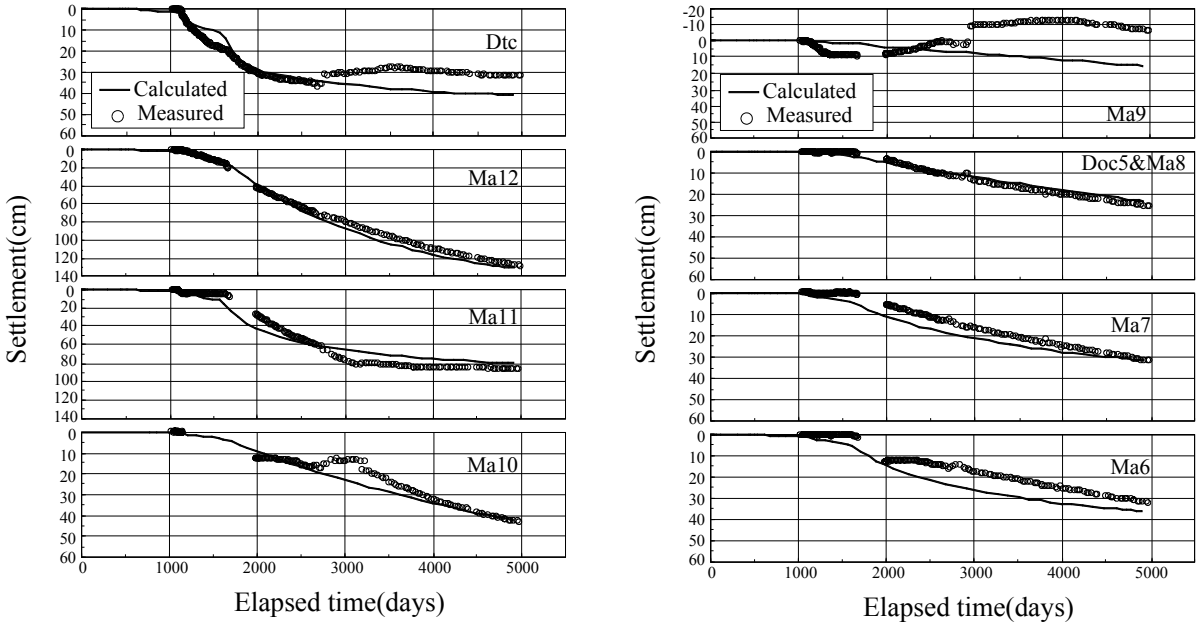

Fig. 4.13 Comparison of measured and predicted settlement for the Pleistocene clay layers at the monitoring point 1 in terms of construction of the 1st phase island

dissipation of excess pore water pressure. During this process, time dependent compression takes place with the insufficient dissipation of excess pore water pressure. The calculated performance can also well describe the whole process of deformation.

In the lower Pleistocene clay layers such as Ma7 and 6, the mode of settlement with time is hyperbolic because of the sufficient permeability of Ds10. Different from the case for the middle Pleistocene clay layers, the dissipation of excess pore water pressure has advanced steadily with time. The calculated performance can well describe the measured settlement of Ma7 and 6.

4.4 Assessment of Time-dependent Behavior through Comparison of Constitutive Models

4.4.1 Outline of numerical analysis

A series of finite element analyses between the elasto-plastic and the elasto-viscoplastic constitutive models is conducted to investigate the time-dependent behavior that has taken place in the Pleistocene clay layers at KIX by comparing with measured results. The approximate assessment for the time-dependent behavior in the Pleistocene clay layers of KIX was performed by using the measured results in section 2.4.

In this section, comparing the calculated results in terms of elasto-viscoplastic and elasto-plastic finite element analysis, the time-dependent behavior associated with stress overshoot just beyond plastic yielding or the secondary compression taking place without increase in an effective stress with insufficient dissipation of excess pore water pressure is significantly discussed. The time-dependent behavior is investigated not only in the normally consolidated region but also in the quasi-overconsolidated region by adopting the compression model for the quasi-overconsolidation clay proposed by Mimura and Jang (2004). The elasto-plastic constitutive model for finite element analysis was concreted in section 3.3 by not considering the secondary compression effect in the elasto-viscoplastic constitutive model.

The all numerical procedure except the constitutive model is exactly the same with the one introduced in the previous section 4.3. The time-dependent behavior until before construction of the 2nd phase island is only discussed because the interactive behavior occurs in the foundation of the 1st phase island due to construction of the adjacent 2nd phase island.

4.4.2 Simulation results and discussion

4.4.2.1 Comparison of calculated *e*-log*p* curve

Calculated stress- strain relations for the two constitutive models in terms of the change in void ratio against effective vertical stress due to construction of the 1st phase island are shown in Fig.4.14 together with the setup *e*-log*p* for the representative elements of the individual Pleistocene clay layers at the monitoring point 1. The setup compression curves in terms of *e*-log*p* are described as reference compression ones with p_o, p_c, κ and λ shown in Table 4.1. In the calculated results in terms of elasto-plastic model, the stress-strain paths following the setup *e*-log*p* curve is shown for the all Pleistocene clay layers. It means that the strain depending upon the consolidation associated with dissipation of excess pore water pressure is mainly calculated in the performance of the elasto-plastic model. On the other hand, the elasto-viscoplastic model gives various stress-strain paths for the individual Pleistocene clays on *e*-log*p* plane depending upon the strain rate mainly controlled by the rate of dissipation of excess pore water pressure. The stress-strain curves for the elasto-viscoplastic model show typical overshoot performance and the time-dependent behavior with insufficient dissipation of excess pore water pressure. For the upper Pleistocene clay layers from Dtc to Ma10, the typical viscoplastic behavior associated with stress overshoot just beyond pre-consolidation stress p_c takes place due to the early plastic yielding with large-scale reclamation load. In contrast, the time-dependent behavior associated with insufficient dissipation of excess pore water pressure is predominant for the middle and lower Pleistocene clay layers from Ma9 to Ma6. It is noteworthy that those behaviors associated with stress overshoot or the secondary compression are found even in the quasi-overconsolidated region.

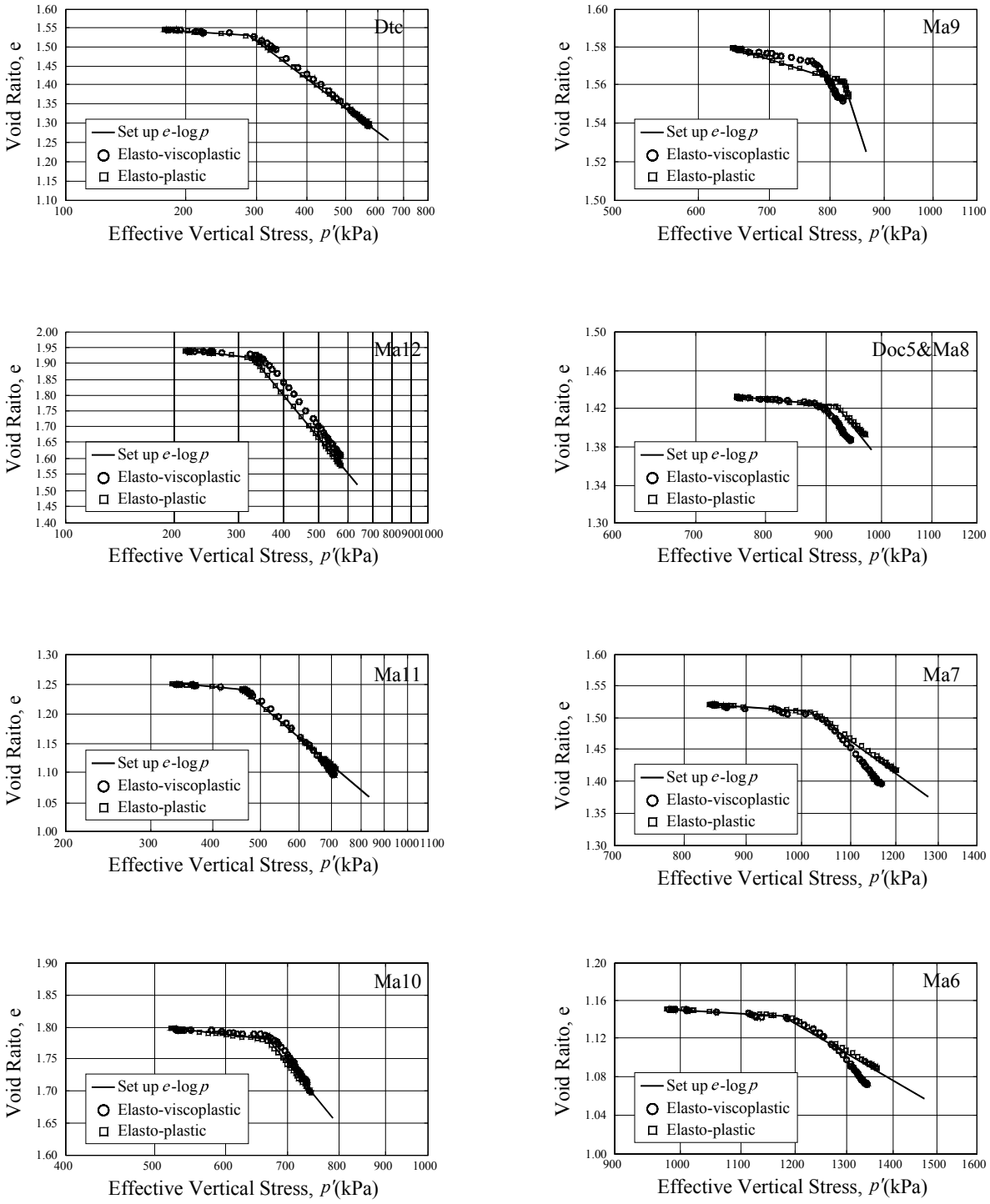

Fig. 4.14 Comparison of calculated stress- strain relations for the two constitutive models

In this section, the stress-strain behavior is briefly discussed to only explain a difference for two constitutive models. However, in the next chapter, the stress-strain relations for the individual Pleistocene clay layers will be discussed in greater detail with the interactive behavior due to construction of the adjacent 2nd phase island. Then, considering a difference of two constitutive models associated with time-dependent behavior, the behavior of excess pore water pressure and settlement with the lapse of time is discussed based on stress-strain relations.

4.4.2.2 Comparison of stress path

Figure 4.15 shows the calculated stress paths in terms of $q - p'$ relations for the representative elements of the individual Pleistocene clay layers at the monitoring point 1. Here, the circle denotes the calculated results by the elasto-viscoplastic constitutive model while the * denotes the one by the elasto-plastic constitutive model. Note that the calculated effective stress paths of all Pleistocene clay elements are found to move along Ko-line. It means that the stress ratio in terms of σ'_3/σ'_1 has not been changed during the process of reclamation and consolidation. It is natural that the almost one-dimensional deformation is expected to occur with little lateral displacement in the selected clay elements because they are located almost at the center of the airport island. The stability of the reclaimed Pleistocene foundation is hence confirmed from these results shown in Fig. 4.15 because the stress state exhibits stable with keeping Ko condition without any signs towards failure. As seen from Fig. 4.14, the time-dependent behavior is predominant for middle and lower Pleistocene clay layers from Ma9 to M6. For those Pleistocene clay elements, larger stress can be derived on the stress paths calculated by the elasto-plastic constitutive model compared to the ones by the elasto-viscoplastic constitutive model in Fig. 4.15 because the effect of the term of the relaxation stress, σ^R is taken into account for the elasto-viscoplastic constitutive model.

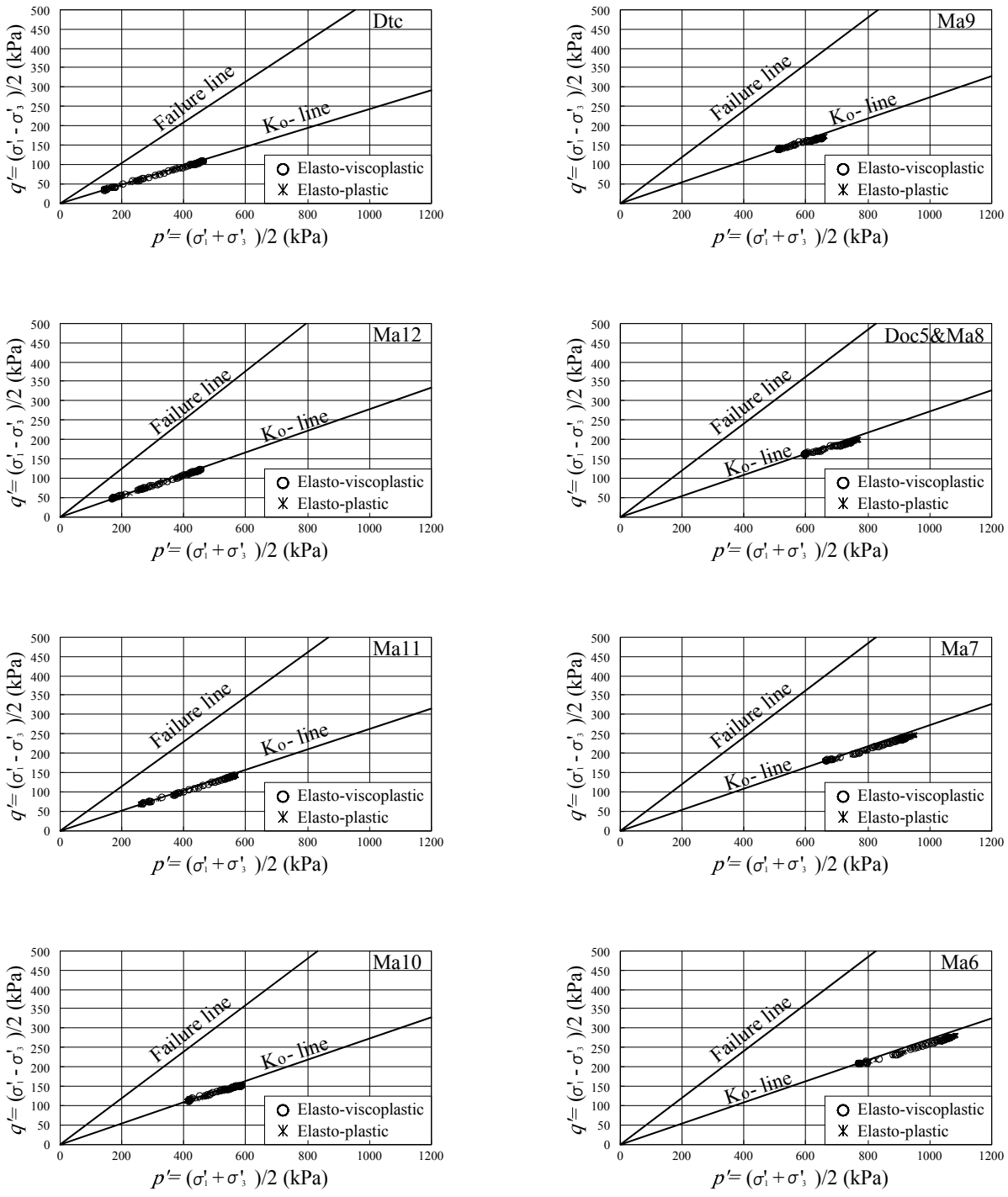

Fig. 4.15 Comparison of calculated stress paths for the two constitutive models

4.4.2.3 Comparison of performance of excess pore water pressure

Figure 4.16(a) shows the calculated excess pore water pressure - time relations for two constitutive models with the measured results for the individual Pleistocene clay layers at the monitoring point 1. The only calculated performance of the excess pore water pressure is also shown in Fig. 4.16(c) for the Pleistocene clay layers. Due attention should be paid to the fact that at the completion of the 1st reclamation, a slightly larger amount of excess pore water pressure for most of the Pleistocene layers is calculated in the results of elasto-plastic model than that of the elasto-viscoplastic model. It is because the calculated strain rate in the elasto-viscoplastic model is lower due to stress overshoot performance at the completion of the 1st phase reclamation not only in the normally consolidated region but also in the quasi-overconsolidated region as shown in Fig. 4.14. After the completion of the 1st reclamation, the mode of compression proceeds with dissipation of excess pore water pressure. It is also noted that although the lower rate of dissipation of excess pore water pressure for the middle and lower Pleistocene clay layers from Ma9 to Ma7 in the results of elasto-viscoplastic model is calculated compared to that of the elasto-plastic model, a larger amount of compression is calculated in the results of elasto-viscoplastic model because of the effect of time-dependent behavior (see Fig. 4.14 and 4.17).

In the present study, the coupled stress-flow analysis taking the nodal displacement increments and the element pore water pressure as the primary unknowns of the problem is adopted. In the elasto-viscoplastic model, the constitutive relations for the finite element analysis were expressed with relaxation stresses, $\{\Delta\sigma^R\}$ as shown eq. 3.22. The relaxation stresses, $\{\Delta\sigma^R\}$ calculates the strain irrespective of the dissipation of excess pore water pressure because this term represents the increasing stresses with time when strains are held constant.

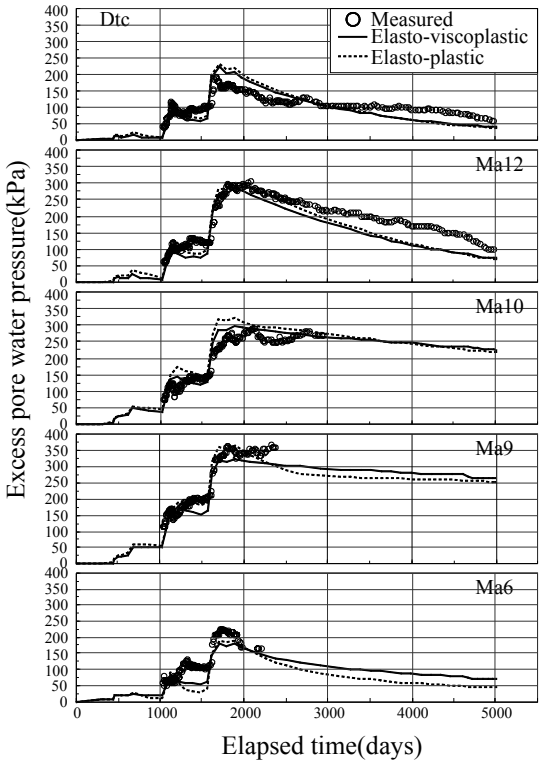

(a) Measured and calculated excess pore water pressure for the Pleistocene clay layers

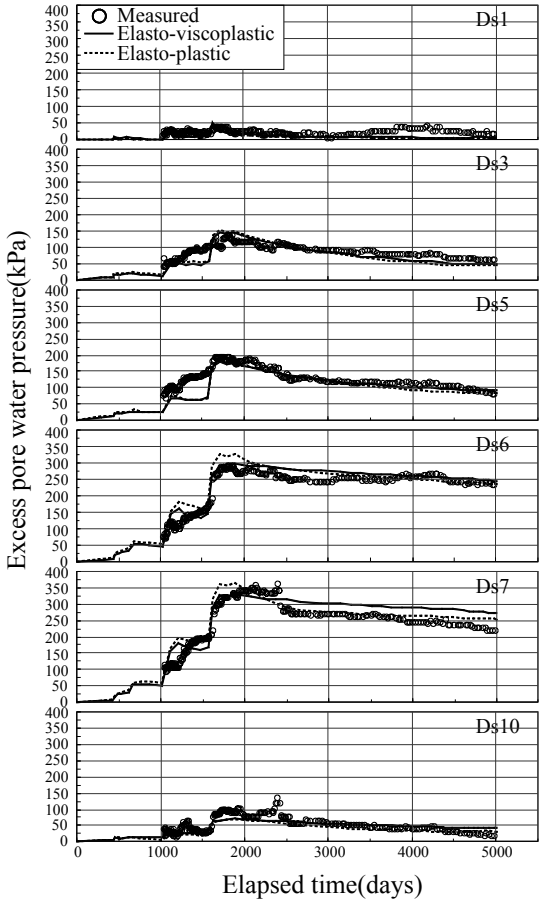

(b) Measured and calculated excess pore water pressure for the Pleistocene sand gravel layers

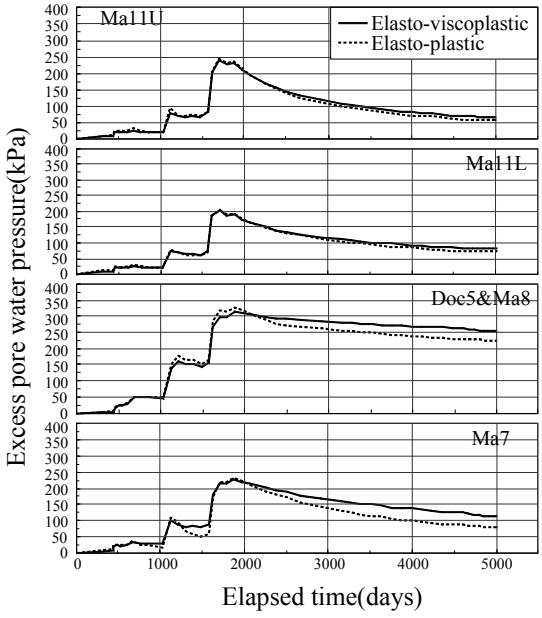

(c) Calculated excess pore water pressure for the Pleistocene clay layers

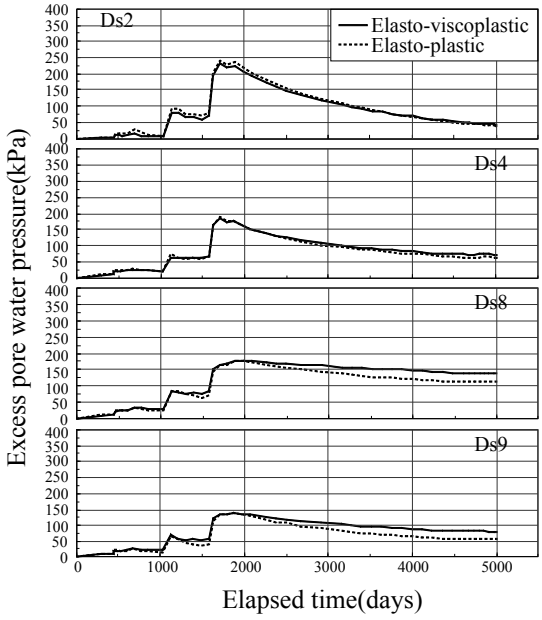

(d) Calculated excess pore water pressure for the Pleistocene sand gravel layers

Fig. 4.16 Comparison of calculated excess pore water pressure for the two constitutive models with time at the monitoring point 1

Therefore, it is natural that a larger amount of compression is calculated in the elasto-viscoplatic model with time although a larger amount of excess pore water pressure still remains. In the Pleistocene sand gravel layers, they exhibit the similar behavior related to the Pleistocene clay layers (see Fig.4.16 (b) and (d)). The calculated performance well describes the measured excess pore water pressure for both constitutive models.

4.4.2.4 Comparison of performance of settlement

Calculated settlement-time relations for two constitutive models are shown in Fig. 4.17 with the measured results for the individual Pleistocene clay layers at the monitoring point 1. For the upper Pleistocene clay layers such as Dtc and Ma 12, 10, a lower rate of consolidation is calculated in the elato-viscoplastic constitutive model compared to that of the elasto-plastic constitutive model because of the stress overshoot as shown in Fig 4.14. In contrast, for the

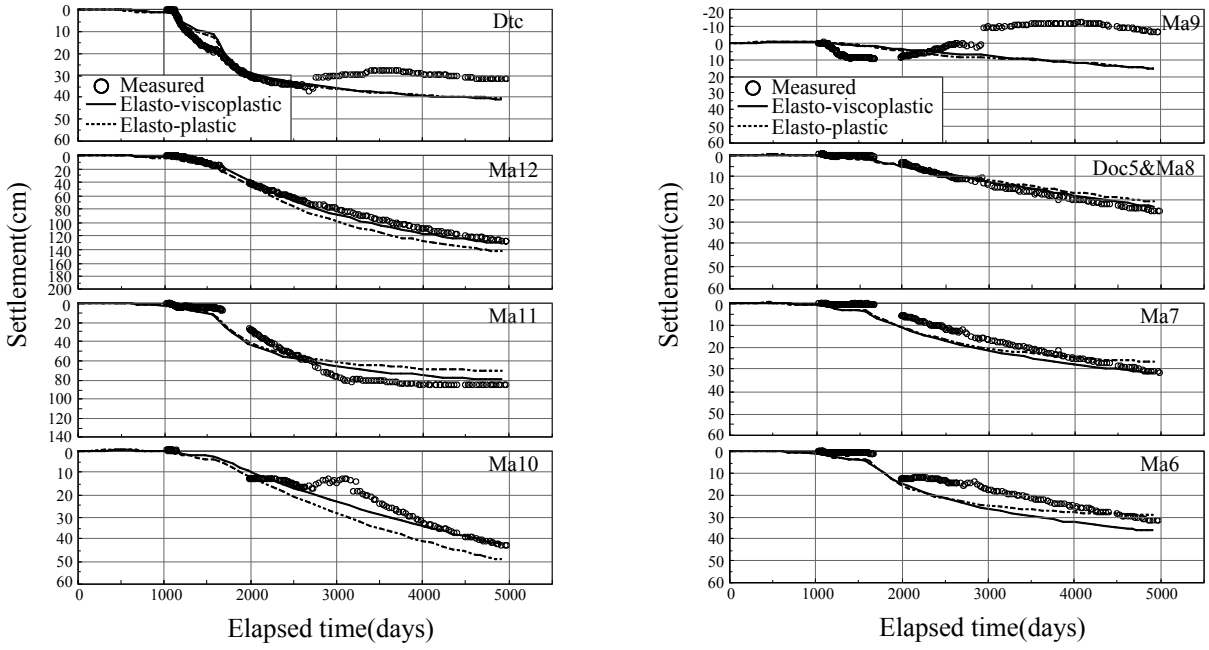

Fig. 4.17 Comparison of measured and predicted settlement in the Pleistocene clay layers for the two constitutive models

others Pleistocene clay layers such as Ma11, 9, 7, 6 and Doc5&Ma8, although a larger amount of excess pore water pressure is calculated to remain undissipated in the elasto-viscoplastic model for the long-term behavior, a larger amount of compression in the elasto-viscoplastic model is calculated with the lapse of time. These contrasting results well explain the time dependent behavior that has taken place in the Pleistocene clays of KIX.

As assessed by using the measured excess pore water pressure in section 2.4, the time-dependent compression has continuously occurred during the process of excess pore water pressure dissipation under the condition of insufficient advance in primary consolidation or after completion of the primary consolidation. It is confirmed that the elasto-viscoplastic model well describes the time dependent compression associated with the stress overshoot for Dtc and Ma12, 11, 10, and the secondary compression after completion of primary consolidation in the early stage for Ma11 and 6, and the creep phenomena with insufficient dissipation of excess pore water pressure for Ma9, 7 and Doc5&Ma8. The long-term settlement can be better predicted by elasto-viscoplastic constitutive model.

4.5 Numerical Assessment for the Long-term Behavior of the Inclined Marine Foundations

4.5.1 Outline of numerical analysis

The geological foundations in the Pleistocene layers of KIX have a downward inclination towards the offing with increase of thickness. However, the numerical procedure was confirmed by the calculated performance considering the ideal foundation model that has horizontally even layers in the previous section 4.3. Therefore, in this section, a series of elasto-viscoplastic finite element analyses is performed for the inclined marine foundations. The applicability of the proposed numerical procedure for the inclined marine foundations is discussed by comparing with the calculated results for the horizontally even layers.

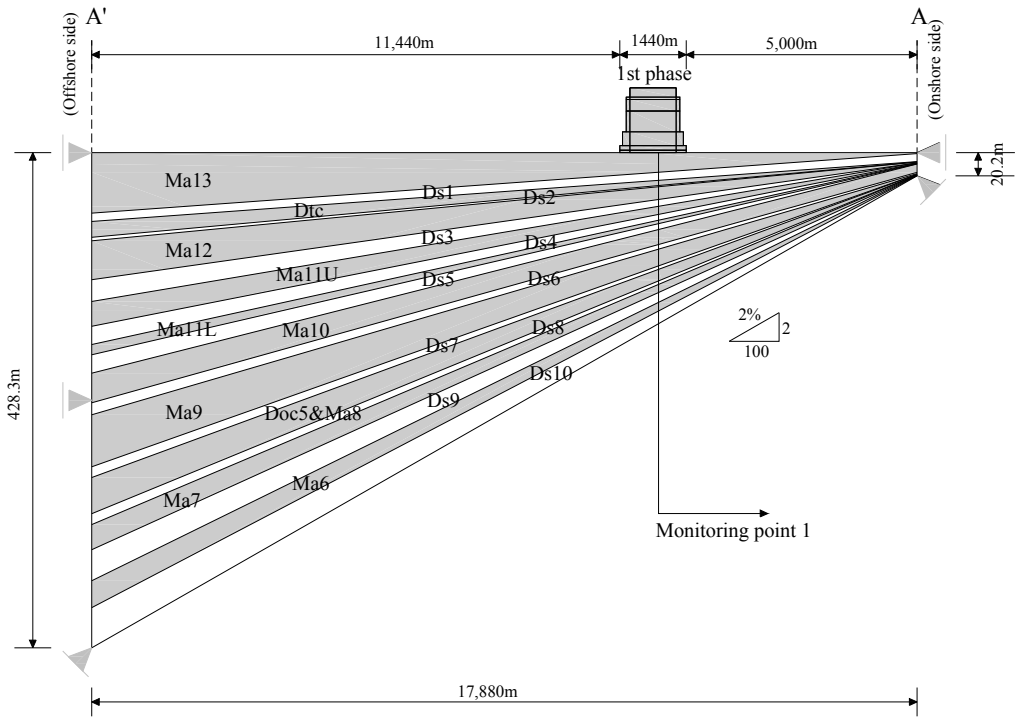

Fig. 4.18 Schematic cross-section of the inclined marine foundation model of the 1st phase Kansai International Airport for finite element analysis

Figure 4.18 shows the inclined foundation model used in the present study. The inclined foundation model is considered by connecting between the individual layers at monitoring point 1 and the corresponding layers at the point of onshore side boundary. The determined gradient of layers is then extended just towards the offing and the inclined foundation model is assumed to be the increasing layer in thickness with a fixed gradient towards the offing. The gradient of layers is assumed to be from 0.3% to 2.0% increasing towards Ds10 layer. The thickness in the individual layers at monitoring point 1 is identical with horizontally even layer foundation model and the other condition for numerical analysis is exactly the same with that used in section 4.3.

4.5.2 Simulation results and discussion

4.5.2.1 Comparison of performance of excess pore water pressure

Calculated excess pore water pressure – time relations for the both foundation models are shown in Fig. 4.19 for the individual Pleistocene layers at the monitoring point 1. Although in the lower Pleistocene layers such as Doc5&Ma8, Ma7, 6 and Ds9, 10, little discrepancies with increase in the gradient towards Ds10 layer is calculated for two foundation models, the calculated performance approximately corresponds to each other. The lower Pleistocene layers with relatively great gradient of layer exhibit that the rate of dissipation of excess pore water pressure in the inclined foundation is slightly lower. However, because the difference of the performed results for two foundation models is very small, the effect of the gradient in layers that consist of the reclaimed marine foundation at KIX in practice could be ignored for performance of excess pore water pressure in the present study.

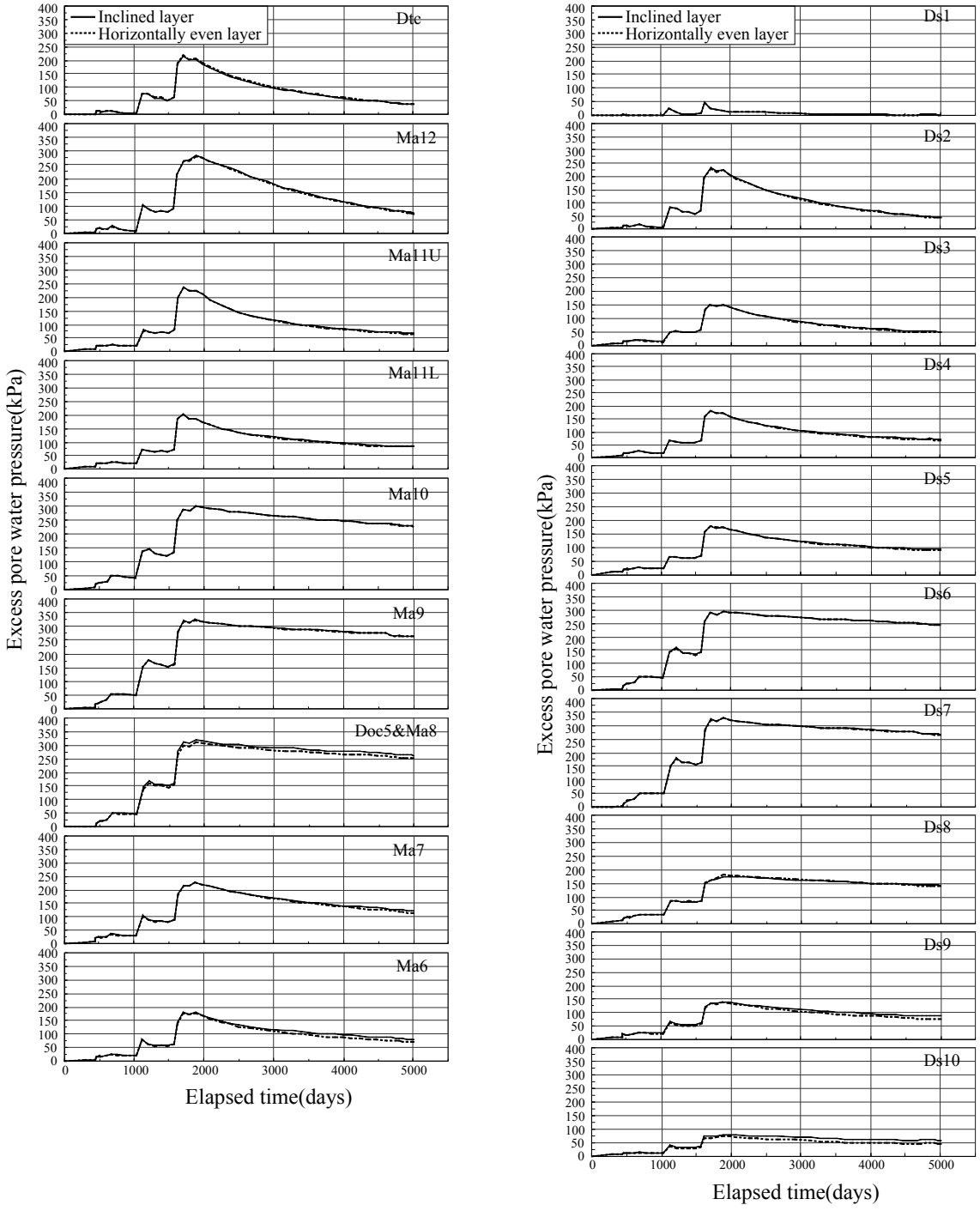

Fig. 4.19 Comparison of calculated excess pore water pressure for the inclined and horizontally even foundation models with time

4.5.2.2 Comparison of performance of settlement

Figure 4.20 shows the calculated compression for the both foundation models with time for individual Pleistocene clay layers at monitoring point 1. The calculated performance shows the similar behavior with performance of excess pore water pressure. They also exhibit little discrepancies in the lower Pleistocene layer such as Doc5&Ma8, Ma7 and 6, however, the discrepancies for two foundation models are as small as negligible. Because the gradient of foundation layers in KIX is not so large to be from 0.3% to 2.0%, the effect of the gradient of foundation layers could also be ignored for the performance of long-term settlement. It is hence confirmed that the adopted procedure in terms of elasto-viscoplastic finite element analysis works well to assess the long-term behavior for the inclined marine foundations at KIX.

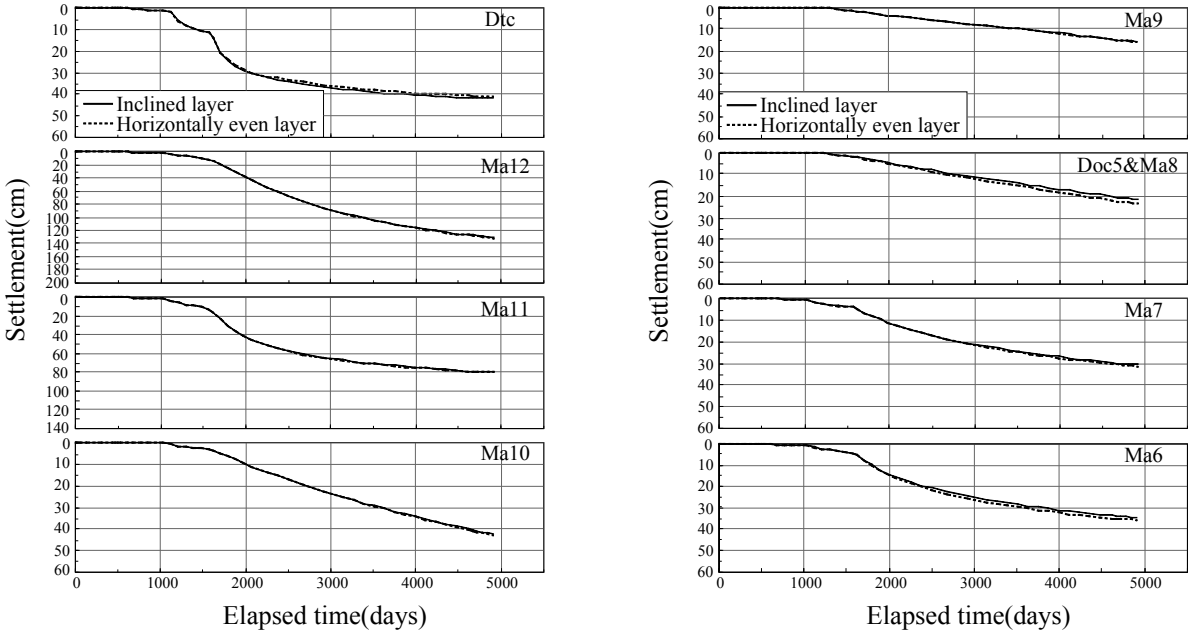

Fig. 4.20 Comparison of calculated settlement for the inclined and horizontally even foundation models with time

4.6 Numerical Assessment for the Behavior of the Deep Pleistocene Marine Foundations below Ds10 Layer at KIX

4.6.1 Outline of numerical analysis

As it is already in chapter 2, it was found on the basis of the boring investigation that the Pleistocene clay and sand gravel deposits overlies the base rock that was confirmed at the depth of 1,320m at KIX. The subsurface foundation of KIX is however modeled from the top of the seabed to the basal sand gravel layer, Ds10 at the depth of 148m in the present study because the mechanical properties below Ma3 overlain by Ds10 drastically change compared to the ones for the deposits above Ds10. The differential settlement gauges and pore water pressure cells have hence been set to monitor the compression of the individual Pleistocene clay layers as well as the excess pore water pressure of the individual Pleistocene sand gravel layers because the main problems in terms of the long-term settlement have been considered to occur in those layers above Ds10. It should be noted that no measurement has been conducted in the individual Pleistocene layers below Ds10 except the total settlement of the soil layers below Ma3 with the settlement gauge set up at the top of Ma3. Because the purpose of the present study consists in the confirmation of the applicability and accuracy of the proposed numerical procedure, the detailed numerical assessment should be conducted to focus on the deformable Pleistocene layers above Ds10 by comparing the calculated performance with the measured information for the individual layers with time. It is true on the other hand that the possible settlement taking place in the layers below Ds10 cannot be ruled out without discussion even if it is not a main purpose of the present study.

In this section, a series of elasto-viscoplastic finite element analyses is performed for the foundation model considering the underlying layers below Ds10. Figure 4.21 shows the foundation model expanding the foundation to the Pleistocene sand gravel layer, Ds15 introduced for the discussion on the contribution of the additional settlement of the foundation at

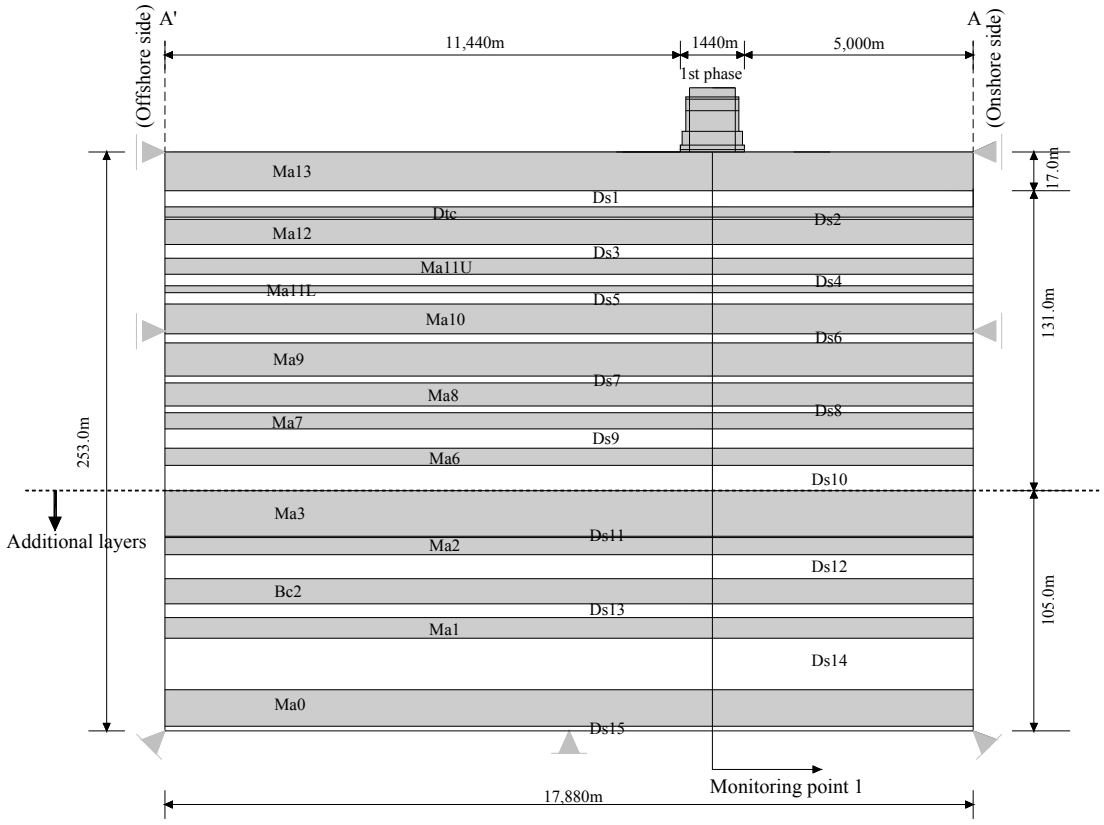

Fig. 4.21 Schematic cross-section of the deep marine foundation model below Ds10 layer for finite element analysis

KIX. The marine foundation is modeled by extending from Ma3 to Ds15 layers beneath Ds10 with the thickness of 105m on the basis of the representative foundation model that was proposed in the previous section. The foundation model is also assumed to be horizontally even layers that have a constant thickness and continuous layer based on the boring data at the monitoring point 1.

4.6.2 Soil parameters

The parameters for the Pleistocene clay layers beneath Ma3 are basically evaluated based on the result derived from conventional step loading consolidation test. However, according to the

experimental results, the condition of effective stress in the clay layers below Ma3 due to the reclamation load remains within overconsolidated region and no comprehensive laboratory tests have been conducted because of the difficulties in obtaining the high quality undisturbed samples from such deep sedimentation. Therefore, the values of OCR in the clay layers beneath Ma3 are assumed to be identical to Ma6 and the compression index *C*c in the normally consolidated region is also assumed to 0.5 by considering the clay layers below Ma3 as the stiff Pleistocene clay deposits. For the Pleistocene sand gravel layers, the values of "equivalent coefficient of permeability" evaluated as the ordinary values in the order of 10^0m/day are used. The values of the principal soil parameters both for the Pleistocene clays and sand gravel layers below Ds10 are summarized in Table 4.6.

Table 4.6 Principal soil parameters for the Pleistocene clay and sand gravel layers below Ds10 of KIX

MTYP	Quasi-OC region				NC region				M	ν'	K_0	p_0 (kPa)	p_c (kPa)	e_0	k_0 (m/day)	λ_k	Name of layers
	λ_{QOC}	κ_{QOC}	α_{QOC}	$\dot{v}_{0\,QOC}$ (day^{-1})	λ	κ	α_{NC}	$\dot{v}_{0\,NC}$ (day^{-1})									
1	0.0217	0.0022	4.68E-04	5.52E-08	0.2170	0.0217	4.68E-03	5.52E-07	1.20	0.36	0.572	1139.7	1367.6	1.32	2.59E-05	0.217	Ma3-1
2	0.0217	0.0022	4.19E-04	4.94E-08	0.2170	0.0217	4.19E-03	4.94E-07	1.20	0.36	0.572	1164.4	1397.3	1.59	2.59E-05	0.217	Ma3-2
3	0.0217	0.0022	4.91E-04	5.79E-08	0.2170	0.0217	4.91E-03	5.79E-07	1.20	0.36	0.572	1203.0	1443.7	1.21	2.59E-05	0.217	Ma3-3
4	0.0217	0.0022	5.16E-04	6.08E-08	0.2170	0.0217	5.16E-03	6.08E-07	1.20	0.36	0.572	1250.1	1500.1	1.10	2.59E-05	0.217	Ma3-4
5	-	-	-	-	-	-	-	-	-	0.36	0.572	1271.2	-	-	2.59E-05	-	Ds11
6	0.0217	0.0022	5.24E-04	6.59E-07	0.2170	0.0217	5.24E-03	6.59E-06	1.20	0.36	0.572	1284.1	1540.9	1.07	2.59E-05	0.217	Ma2-1
7	0.0217	0.0022	5.33E-04	6.70E-07	0.2170	0.0217	5.33E-03	6.70E-06	1.20	0.36	0.572	1303.5	1564.2	1.04	2.59E-05	0.217	Ma2-2
8	0.0217	0.0022	5.42E-04	6.82E-07	0.2170	0.0217	5.42E-03	6.82E-06	1.20	0.36	0.572	1322.7	1587.3	1.00	2.59E-05	0.217	Ma2-3
9	-	-	-	-	-	-	-	-	-	0.33	0.500	1362.4	-	-	2.16E+00	-	Ds12
10	0.0217	0.0022	4.68E-04	3.65E-07	0.2170	0.0217	4.68E-03	3.65E-06	1.20	0.36	0.572	1458.6	1750.3	1.32	2.59E-05	0.217	Bc2-1
11	0.0217	0.0022	4.67E-04	3.64E-07	0.2170	0.0217	4.67E-03	3.64E-06	1.20	0.36	0.572	1494.5	1793.4	1.32	2.59E-05	0.217	Bc2-2
12	0.0217	0.0022	5.56E-04	4.34E-07	0.2170	0.0217	5.56E-03	4.34E-06	1.20	0.36	0.572	1529.1	1834.9	0.95	2.59E-05	0.217	Bc2-3
13	-	-	-	-	-	-	-	-	-	0.33	0.500	1572.7	-	-	2.16E+00	-	Ds13
14	0.0217	0.0022	5.63E-04	6.56E-07	0.2170	0.0217	5.63E-03	6.56E-06	1.20	0.36	0.572	1616.4	1939.6	0.93	2.59E-05	0.217	Ma1-1
15	0.0217	0.0022	5.09E-04	5.93E-07	0.2170	0.0217	5.09E-03	5.93E-06	1.20	0.36	0.572	1646.8	1976.2	1.13	2.59E-05	0.217	Ma1-2
16	0.0217	0.0022	6.57E-04	7.65E-07	0.2170	0.0217	6.57E-03	7.65E-06	1.20	0.36	0.572	1672.9	2007.5	0.65	2.59E-05	0.217	Ma1-3
17	-	-	-	-	-	-	-	-	-	0.33	0.500	1782.3	-	-	2.16E+00	-	Ds14
18	0.0217	0.0022	6.16E-04	2.27E-07	0.2170	0.0217	6.16E-03	2.27E-06	1.20	0.36	0.572	1947.3	2336.8	0.76	2.59E-05	0.217	Ma0-1
19	0.0217	0.0022	4.91E-04	1.81E-07	0.2170	0.0217	4.91E-03	1.81E-06	1.20	0.36	0.572	1996.2	2395.5	1.21	2.59E-05	0.217	Ma0-2
20	0.0217	0.0022	6.74E-04	2.49E-07	0.2170	0.0217	6.74E-03	2.49E-06	1.20	0.36	0.572	2040.0	2448.0	0.61	2.59E-05	0.217	Ma0-3
21	-	-	-	-	-	-	-	-	-	0.33	0.500	2069.4	-	-	2.16E+00	-	Ds15

4.6.3 Simulation results and discussion

4.6.3.1 Performance of excess pore water pressure

Calculated excess pore water pressure – time relations are shown in Fig. 4.22 for the individual Pleistocene layers below Ma3 at the monitoring point1. In general, the excess pore water pressure in the all Pleistocene layers monotonically dissipates with time because the Pleistocene sand gravel layers such as Ds12, 13, and 14 have sufficient thickness to function as permeable layers. Although a relatively large amount of excess pore water pressure generates in Ma3 and Ds11 layers, the generated excess pore water pressure almost dissipates before the construction of the 2nd phase island. On the basis of these performances, it is found that the primary consolidation in terms of the process of excess pore water pressure dissipation is almost completed in the Pleistocene clay layers below Ma3 before the construction of the 2nd phase island.

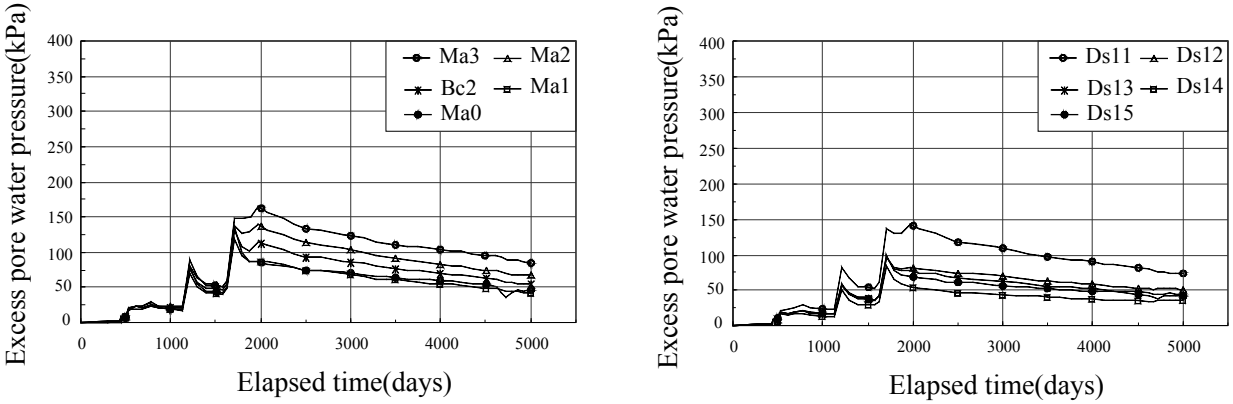

(a) The Pleistocene clay layers

(b) The Pleistocene sand gravel layers

Fig. 4.22 Calculated excess pore water pressure with time for the individual Pleistocene layers below Ma3 at the monitoring point 1

4.6.3.2 Ratio of vertical effective stress increments and vertical strain

Figure 4.23 shows the calculated vertical strain and the ratio of vertical effective stress increments for the individual Pleistocene clay layers below Ma3. The elements located at the mid-depth are selected as representatives for the individual Pleistocene clay layers. Here, the dotted line and solid line denote the increasing process of vertical strain and ratio of vertical effective stress increments to the initial vertical effective stress due to construction of the 1st phase island. The values of ratio of vertical effective stress increments are decreasing with depth, by about 30% at Ma3 and about 20% at Ma0. Because the Pleistocene clay layers below Ma3 have relatively large initial effective stress, the ratio of effective stress increments is found to be not so large compared to the upper layers above Ma3. It is noteworthy that the calculated vertical strain remains within the very small values such as about 0.5% to 1.5%.

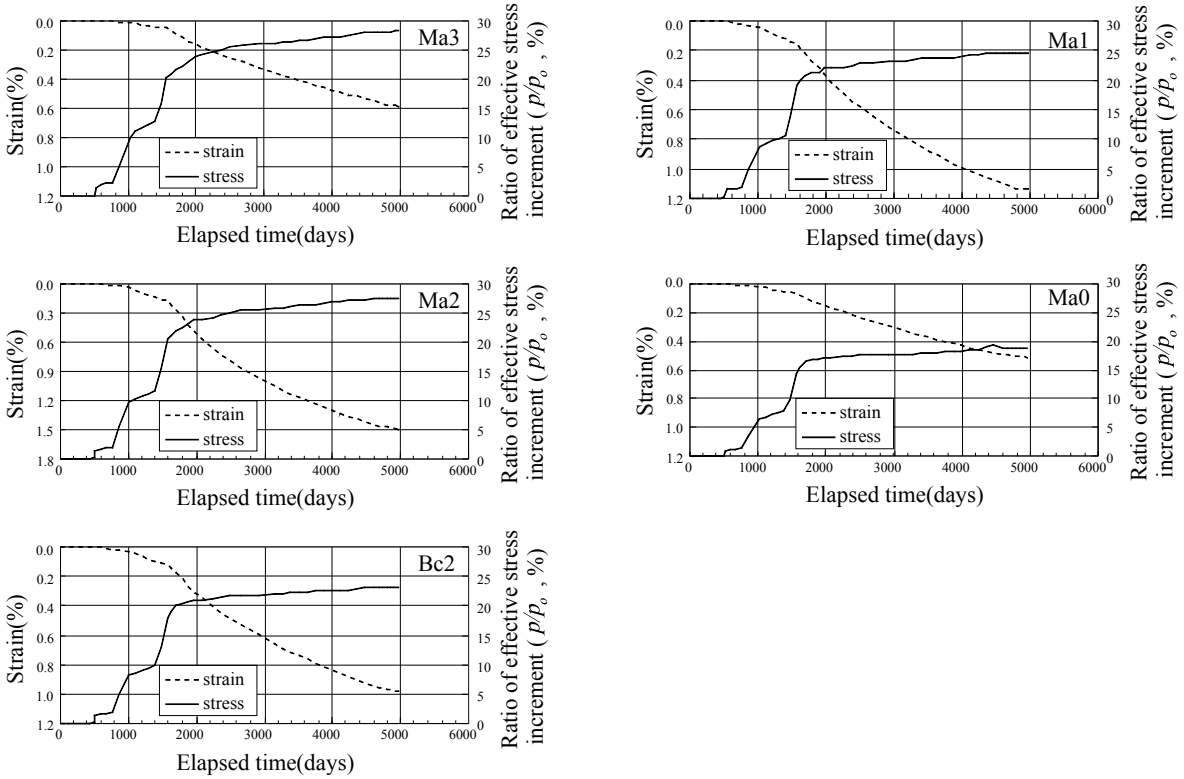

Fig. 4.23 Calculated vertical strain and ratio of vertical effective stress increments with time for the individual Pleistocene layers below Ma3 at the monitoring point 1

4.6.3.3 Settlement

Calculated settlement – time relations for the individual Pleistocene clay layers below Ma3 are shown in Fig. 4.24. As seen from Fig. 4.22, almost full dissipation of excess pore water pressure is achieved before construction of the 2nd phase island in the all Pleistocene layers. However, because the ratio of vertical effective stress increment is not so large relatively as seen from Fig. 4.23, amount of compression is also not so large with about 10cm. It also means that the secondary consolidation is predominant with completion of primary consolidation associated with dissipation of excess pore water pressure in the Pleistocene clay layers below Ma3. Figure 4.25 shows the calculated and measured settlement – time relations for the Pleistocene layers below Ma3. It should be noted that the calculated performance denotes the calculated compression from Ma3 to Ma0, and there is no measurements of the differential settlement of the individual Pleistocene clay layers below Ma3, but the total settlement of the Pleistocene layers below Ma3 has been measured in the field. It is then natural that the measured result is larger than the calculated one. It is so difficult to accurately assess the behavior of the

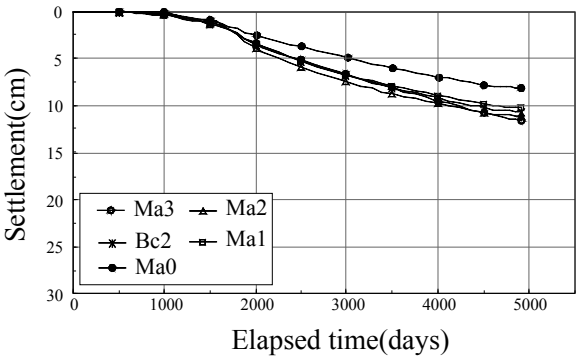

Fig.4.24 Calculated settlement with time for the individual Pleistocene clay layers below Ma3 at the monitoring point 1

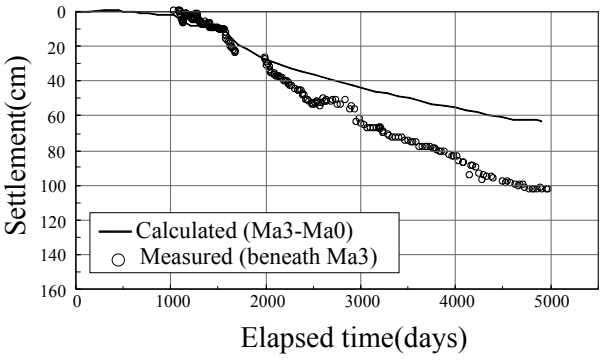

Fig.4.25 Comparison of measured and calculated total settlement with time for the Pleistocene layers below Ma3 at the monitoring point 1

Pleistocene layers below Ma3 in which the relative contribution of the secondary consolidation is predominant because there are no information for the individual differential settlement and excess pore water pressure. It should however be noted that the long-term settlement occurring in the foundation below Ds10 cannot be ruled out for the total settlement of the 1st phase island. The mechanism of such long-term settlement of these layers has to be an important coming issue to be deal with.

4.7 Summary

A series of elasto-viscoplastic finite element analyses was performed to be first step to propose the numerical procedure for the construction of the 1st phase island with the simple foundation model having the horizontally even layer at the representative section. A compression model for the quasi-overconsolidated Pleistocene clays and the concept of mass permeability for the sand gravel deposits have been implemented in the elasto-viscoplastic finite element method to assess the time dependent behavior of the reclaimed Pleistocene deposits of KIX. Because of the existence of the poorly permeable sand gravel layers in the Pleistocene deposits, excess pore water pressure does not dissipate well. The packed excess pore water pressure propagates through the Pleistocene sand gravel layers horizontally. The effect of the propagation of excess pore water pressure on the adjacent foundation ground should be considered to assess the control and maintenance of the offshore twin-islands airport in future. Due to large reclamation load up to about 430 kPa, the upper Pleistocene clay layers underwent the plastic yielding in a short time, the excess pore water pressure however dissipated steadily in these layers because of the existence of highly permeable sand gravel layers (Ds1and 3) in the vicinity. The state of stresses of the middle Pleistocene clays remains in the overconsolidated region at the completion of the construction of the 1st phase island. Due to the insufficient

dissipation of pore water pressure caused by the poor permeability of sand gravel layers in this region, it takes a long time for middle Pleistocene clays to become normally consolidated with dissipation of excess pore water pressure. The time dependent compression hence takes place without the remarkable dissipation of pore water pressure in the middle Pleistocene clay layers. In the lower Pleistocene clay layers such as Ma 7 and 6, high permeability of Ds10 overlain by Ma 6 promotes the dissipation of excess pore water pressure in the clay layers. The calculated performance for excess pore water pressure in the Pleistocene deposits is found to well describe the in-situ measured results by introducing the concept of mass permeability of the sand gravel layers together with the structural effect for the Pleistocene clays.

Long-term settlement is the biggest cause for concern. The highly developed structure of the quasi-overconsolidated Pleistocene clays in Osaka Bay has large room for compression. The author has adopted the compression model for quasi-overconsolidated Pleistocene clays which was found to be versatile to explain the long-term settlement taken place in the Pleistocene clay deposits in Osaka Port. It is found that the numerical analyses with the adopted procedure in terms of the elasto-viscoplastic finite element method functions well to explain the high compressibility associated with insufficient dissipation of excess pore water pressure that has taken place in the Pleistocene clays of the foundation of Kansai International Airport. The calculated performance can quantitatively describe the time - compression relations for the upper Pleistocene clay layers, such as Dtc, Ma12 and 11, that underwent plastic yielding due to the reclamation load. It is natural that the behavior of these clay layers can well be described with the applied constitutive model that was originally developed for normally consolidated clays. It is also found that the calculated results can predict the settlement with time for Ma10, 9 and Doc5&Ma8, which remain in quasi-overconsolidated region even after the completion of reclamation. The behavior of long-term settlement of the lower Pleistocene clays, such as Ma7 and 6, is similar to the one for the upper Pleistocene clays because of the advance in

consolidation due to high permeability of Ds10. Then, it can be summarized that the calculated performance can well describe the compression of the Pleistocene clay layers together with the generation/dissipation process of excess pore water pressure in the permeable Pleistocene sand gravel as well as the Pleistocene clay layers.

The characteristic of time-dependent behavior in the elasto-viscoplastic constitutive model adopted in the present study was evaluated by comparing with the calculated performance in terms of the elasto-plastic constitutive model. Although a lower rate of dissipation of excess pore water pressure was calculated in the elasto-viscoplastic constitutive model for most of the Pleistocene layers, a larger amount of long-term settlement was calculated because of considering the relaxation stresses for finite element analysis. It was also found that the time dependent behavior associated with stress overshoot for Dtc, Ma12, 10 and the secondary compression after the completion of primary consolidation in the early stage for Ma11, 6 and the creep phenomenon with insufficient dissipation of excess pore water pressure for Doc5&Ma8, Ma9, 7 is superiorly calculated in the elasto-viscoplastic finite element analysis with the adopted numerical procedure. The calculated performance of the elasto-viscoplastic constitutive model could better describe the long-term measurements than the one of the elasto-plastic constitutive model.

The applicability of the adopted numerical procedure for the inclined marine foundations at KIX was investigated by comparing with the calculated performance for horizontally even foundation model. The inclined marine foundations were assumed as having the gradient of from 0.3% to 2.0% based on the soil exploration and geological survey data. The calculated performance almost corresponded to the one of horizontally even foundation model. It is thought that not steeply gradient of layers at KIX does not affect the long-term behavior due to large-scale offshore reclamation.

The long-term behavior of the deep Pleistocene deposits below Ds10 layer was investigated

based on the elasto-viscoplastic finite element analyses. It was found that the ratio of vertical effective stress increments due to reclamation load was not so large compared to the upper layers and the calculated compression was not so large in this particular case. Although reliable assessment for the long-term behavior of the deep Pleistocene layers below Ds10 was very difficult because of insufficient measured information, the amount of settlement occurring in those layers is found not to able to be ignored for the operation of the airport fill. The mechanism of such large settlement in those deep Pleistocene layers should be a coming important topic.

Finally, it is noteworthy that the proposed procedure with the elasto-viscoplastic finite element method supported by the compression model for quasi-overconsolidated Pleistocene clays and the concept of “mass permeability” for the Pleistocene sand gravel layers is versatile and capable of explaining the high compressibility associated with the insufficient dissipation of excess pore water pressure that has taken place in the Pleistocene clays of the foundation of Kansai International Airport.

5. Interactive Behavior Due to the Adjacent Construction at the Pleistocene Marine Foundations Integrating the 1st and 2nd Phase Islands of KIX

5.1 Introduction

In the previous chapter 4, author proposed the numerical procedure for the representative foundation ground model to assess the compression of the individual Pleistocene clay layers together with the process of the generation and dissipation of excess pore water pressure. Note that the assumption of non-elastic behavior in the quasi-overconsolidated region for the Pleistocene clays (Mimura and Jang, 2004) and the concept of "mass permeability" of the Pleistocene sand gravel layers that control the consolidation of the reclaimed foundation at KIX have been introduced in the numerical procedure.

In this chapter, a series of elasto-viscoplastic analyses is conducted to assess the overall behavior including the interactive behavior of the reclaimed Pleistocene foundations integrating the 1st and 2nd phase islands at KIX. The adopted procedure for the numerical analysis is the one proposed by Mimura and Jang (2004). It should also be noted that the concept of mass permeability is applied as the reasonable modeling for the Pleistocene sand gravel layers as reported in chapter 4. Attention is paid to the interactive behavior of the reclaimed foundation due to the adjacent construction of the 1st and 2nd phase airport fills. In particular, the behavior of the Pleistocene foundations of the existing 1st phase island due to construction of the adjacent 2nd phase island is carefully discussed. The behavior of the Pleistocene foundations beneath the 2nd phase island that was constructed on the foundations keeping the excess pore water pressure propagated due to construction of the 1st phase island is also carefully discussed.

Considering the increase in thickness of the individual layers towards offshore, the foundations are modeled independently for the 1st and 2nd phase islands on the basis of the

representative subsoil models by the boring information. The homogeneous, horizontally even and continuous soil layers are introduced with different thickness for the foundations to satisfy the continuity of the individual layers. The process of generation, dissipation and propagation of excess pore water pressure due to construction of the both islands is discussed together with the performance of the advance in compression of the individual Pleistocene clay layers. Discussion is focused on the interactive behavior of the Pleistocene foundations subjected to the adjacent offshore reclamation. It is particularly investigated how the propagation of the excess pore water pressure generated due to construction of the adjacent both islands affects the behavior of the foundations beneath the both islands. Here, due attention should be paid to the effect of the decrease in effective stress associated with the propagating excess pore water pressure on the subsequent compression of the individual Pleistocene clay layers beneath the both islands.

Finally, the adopted numerical procedure is validated by comparing with the in-situ measured excess pore water pressure and compression for the individual Pleistocene layers of the reclaimed foundations beneath the both islands of KIX.

5.2 Foundation Model and Soil Parameters

5.2.1 Foundation model

A series of elasto-viscoplastic finite element analyses is performed to assess the long-term settlement and the generation/propagation/dissipation process of excess pore water pressure for the Pleistocene foundations of the 1st and 2nd phase islands of KIX considering the effect of adjacent construction of the both islands. Author proposed the representative foundation ground model in which the continuous, horizontally even layers with constant thickness was assumed based on the boring data at the monitoring point 1 of the 1st phase island. It was confirmed that the adopted numerical procedure using the concepts of "non-elastic behavior in the quasi-overconsolidated region" for the Pleistocene clays and "mass permeability" for the Pleistocene sand gravel layers could describe the overall behavior of the reclaimed Pleistocene foundations due to construction of the 1st phase island of KIX.

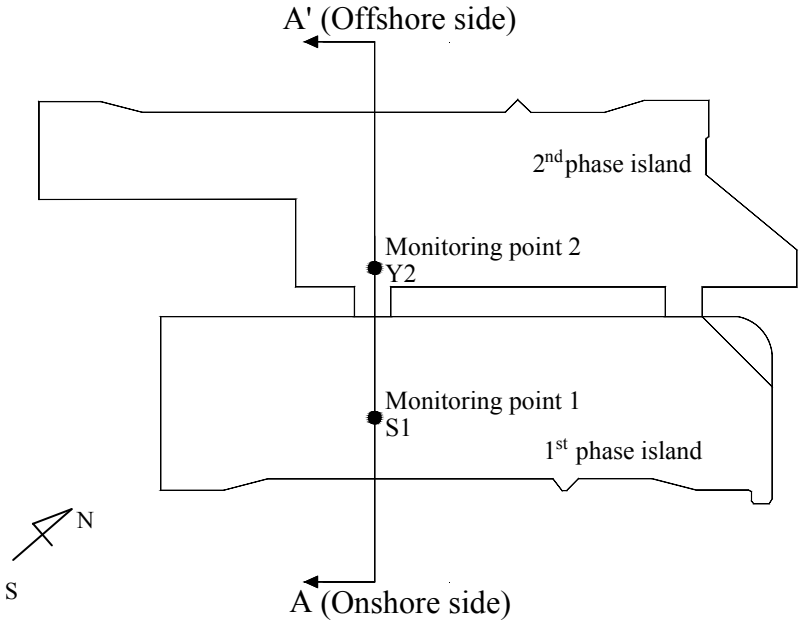

Fig. 5.1 Plan view of the 1st and 2nd phase island of Kansai International Airport with the location of the monitoring points

In the present study, attention is paid to the interactive behavior of the reclaimed Pleistocene foundations of the 1st and 2nd phase islands due to the adjacent construction of the both islands. Figure 5.1 shows the plan view of the both islands of KIX together with the location of monitoring point 1 for the 1st phase island and 2 for the 2nd phase island where the differential settlement of the individual Pleistocene clay layers as well as the excess pore water pressure at various depth both in the clay and the sand gravel layers have been measured.

A series of elasto-viscoplastic finite element analyses is carried out along the section shown by A-A' in Fig. 5.1. Acoustic exploration and geological interpretation of the boring cores provided the horizontal distribution and thickness of the individual Pleistocene layers together

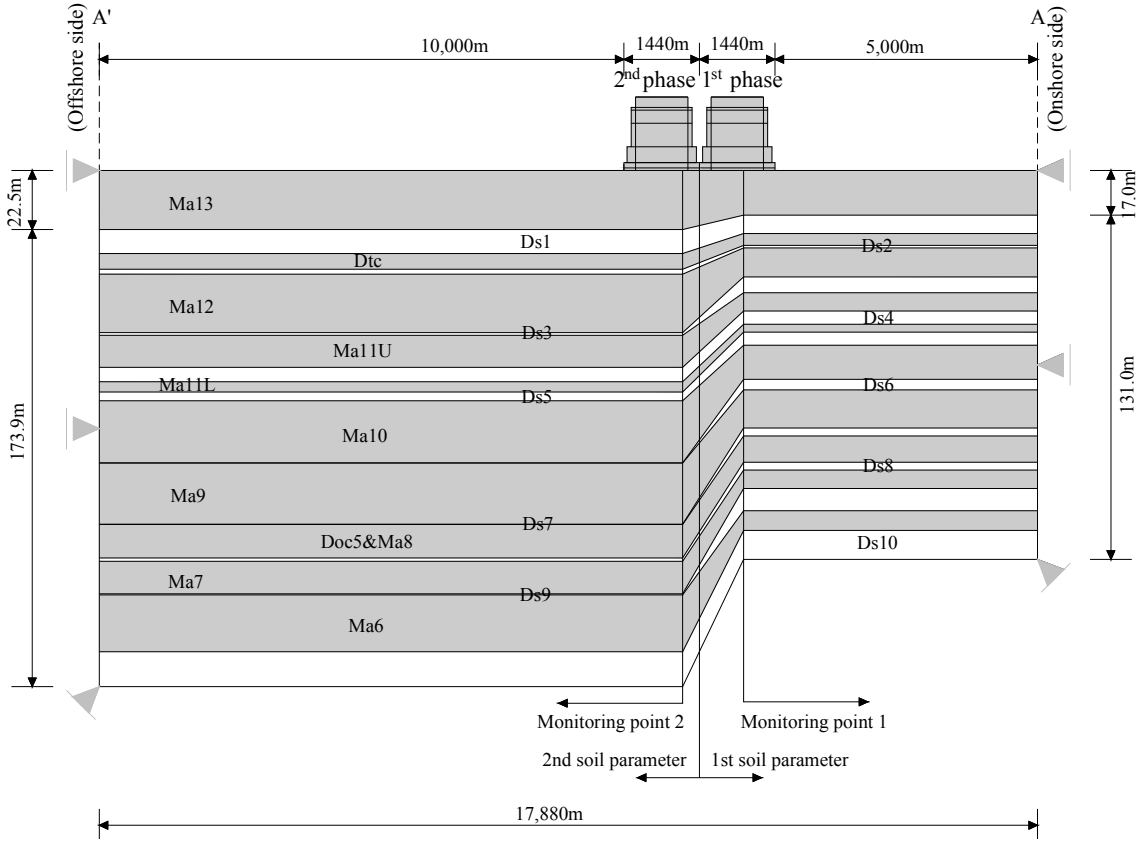

Fig. 5.2 Schematic cross-section of the foundation ground of the 1st and 2nd phase Kansai International Airport for finite element analysis

with the capability of permeability for the Pleistocene sand gravel layers (Kitada et al, 2011a, Inoue et al., 2011). Because the stratigraphy and thickness of the individual layers are different among the foundations of the 1st and 2nd phase islands, the foundation model assuming continuous, horizontally even layers with constant thickness in chapter 4 does not function well when the construction of the 2nd phase island is taken into account. On the other hand, it costs us no slight labor to develop the geologically genuine foundation model that possesses the actual stratigraphy with the inclination of the base and a delicate change in thickness of the individual layers because of the luck of sufficient geo-information to develop the sophisticated subsoil structure model. The author hence introduce the foundation model as schematically shown in Fig. 5.2 considering the increase in thickness of the individual layers towards the offing on the basis of the representative boring information for both airport islands. Here, the individual names of the layers such as Ma and Ds, the condition of ground improvement for Ma13 by sand drains and the assumption of the hydraulic boundary is exactly the same that were used in chapter 4. As shown in Fig. 5.2, the foundation model for the 1st phase island is assumed to be continuous horizontally even layer with constant thickness from the monitoring point 1 to the onshore boundary whereas the foundation model for the 2nd phase island is also assumed to be continuous horizontally even layers with constant thickness from monitoring point 2 to the offshore boundary. The foundation model between both islands is simply modeled by linearly connecting the corresponding layers of the foundations of the 1st and 2nd phase islands. Note here that the thickness of the individual layers of the foundations for the 1st and 2nd phase islands is determined based on the stratigraphy by the boring data at the monitoring point 1 for the 1st phase island and at the monitoring 2 for the 2nd phase island respectively. The construction sequence and the reclaimed stress measured at the monitoring points of the both islands were shown in Fig. 2.8 and 2.9 respectively in chapter 2.

5.2.2 Soil parameters

The parameters for the Pleistocene clay layers at KIX were evaluated for the distinguished 4 blocks in section 4.2 (see Fig. 4.1). In this present study, as shown in Fig. 5.2, the area for analysis are distinguished into 2 blocks along the section shown by A-A' in Fig.5.1, namely, one from the offshore boundary to the monitoring point 2 of the 2nd phase island and another from the onshore boundary to the monitoring point 1 of the 1st phase island. Following the geometrical separation, the representative soil parameters for two blocks are adopted on the basis of the laboratory experimental results for the Pleistocene clays obtained from the corresponding blocks. The parameters of the A-S block for the 1st phase island and the B-S block for the 2nd phase island are adopted for the Pleistocene clay layers. The value of the principal soil parameters of both groups for the Pleistocene clay layers were summarized in Table 4.1 and 4.2.

However, the identical values that were adopted in the previous chapter 4 are introduced for the equivalent coefficient of permeability evaluated on the basis of the concept of "mass permeability" for the individual Pleistocene sand gravel layers irrespective of the blocks. The Pleistocene sand gravel layers, which are expressed by Ds, are also assumed to be linear elastic material. Therefore, the values of soil parameters determined in chapter 4 are identically used for individual Pleistocene sand gravel layers in the present study (see Table 4.5).

5.3 Interactive Behavior of the Pleistocene Marine Foundations of the Existing 1st Phase Island Due to Construction of the 2nd Phase Island

5.3.1 Performance of excess pore water pressure

Calculated distribution of excess pore water pressure is shown in Fig. 5.3. As shown in Fig. 5.3(a), at the completion of the 1st reclamation (5 years from the start of reclamation), little amount of excess pore water pressure remains in the Holocene clay layer, Ma13 because of the effect of sand drains. In contrast, a large amount of excess pore water pressure remains not only in the clay layers but also in the permeable sand gravel layers in the Pleistocene deposits. In particular, more than 200 kPa of excess pore water pressure is kept in the middle Pleistocene clay layers, Ma10 and 9 as well as sand gravel layers, Ds6 and 7. The excess pore water pressure is found to distribute with the inclined shape at the foundation between the both islands reflecting the assumed model geometry. Although the elevation of the corresponding layers is different on the offshore and onshore side, the excess pore water pressure for the individual layers distributes reasonably on the both side of the 1st phase island. It is true that the mode of propagation of excess pore water pressure is qualitatively same that for the continuous horizontally even model foundation shown in the previous chapter 4 but the detailed investigation provides the fact that less propagation takes place towards the offshore side compared to the onshore side. The present foundation model on the side of the 2nd phase island has been developed following the stratigraphy from the boring information at the monitoring point 2 on the 2nd phase island whereas the continuous horizontally even model was developed simply based on the one at the monitoring point 1 on the 1st phase island. According to the boring information at the monitoring point 2, the thickness of the Pleistocene sand gravel layers beneath the 2nd phase island decreases and is small. This reduction in thickness of the permeable Pleistocene sand gravel layers obstructs the smooth propagation of excess pore water pressure toward offshore.

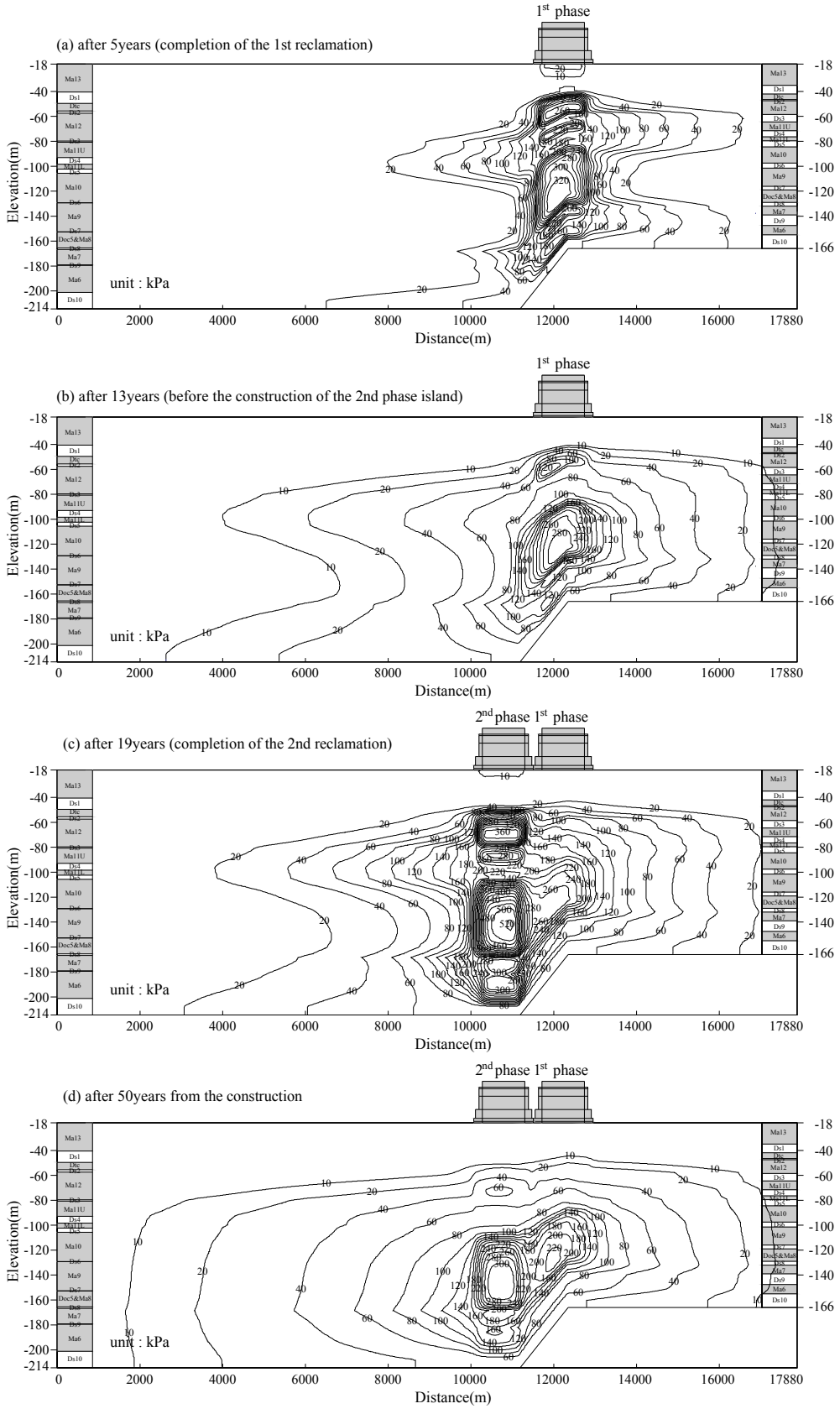

Fig. 5.3 Contours of the calculated distribution of excess pore water pressure in terms of construction of the 1st and 2nd phase islands

The excess pore water pressure is hence propagated more toward the onshore side compared to the direction of the 2nd phase island. Here, due attention should be paid to the fact that a slight propagation of excess pore water pressure takes place in Ds6 and 7 because the very low permeability of these sand gravel layers functions to obstruct sufficient propagation of excess pore water pressure. On the contrary, remarkable propagation of excess pore water pressure occurs in the upper and lower Pleistocene deposits where the permeability of sand gravel layers in these region is better than Ds6 and 7. It is seen that almost full dissipation is achieved without significant propagation of excess pore water pressure both in Ds1 and 10 that have sufficient thickness and permeability. From these results, the performance of excess pore water pressure in the Pleistocene sand gravel layers of the KIX foundations is strongly dependent upon the mass permeability of them. It is very important to note that propagation of excess pore water pressure scarcely occurs in the highly permeable sand gravel layers due to full dissipation as well as in the poorly permeable sand gravel layers due to difficulty of propagation. Remarkable propagation is found to occur through the Pleistocene sand gravel layers having the ordinary coefficient of permeability, such as Ds 3, 5 and 9 in the foundation of KIX.

With the lapse of time, the excess pore water pressure in the upper and lower Pleistocene clay layers such as Dtc, Ma 12,11,7 and 6 monotonically dissipates, whereas the one in the middle Pleistocene layers keeps unchanged (see Fig. 5.3 (b)). As is explained above, the low values of the coefficient of permeability are set for Ds6 and 7 because they are thin, poorly continuous and rich in fine contents. This low permeability of Ds6 and 7 causes the remarkable undissipated excess pore water pressure in these layers. It is noteworthy in Fig. 5.3 (b) that the excess pore water pressure in these layers is found not to dissipate even before the construction of the 2nd phase island (after 13years since the start of reclamation) and remarkable decrease in effective stress takes place in the foundation beneath the 2nd reclaimed island where there is no reclamation load at the time. It clearly means that the primary consolidation in terms of the

process of excess pore water pressure dissipation is not completed in the Pleistocene deposits beneath the 1st phase island before the construction of the 2nd phase island.

Figure 5.3 (c) shows the distribution of excess pore water pressure at the completion of the 2nd reclamation (after 19years since the start of the 1st reclamation). It is natural that a large amount of excess pore water pressure generates in the Pleistocene foundation beneath the 2nd phase island due to construction of the 2nd phase island. The calculated excess pore water pressure generating in the upper and lower Pleistocene layers amounts to 300kPa and that in the middle Pleistocene layers such as Ma10, 9 and Ds6 and 7 becomes almost equivalent to the reclamation load of 530kPa. Because the middle Pleistocene sand gravel layers, Ds6 and 7 have the insufficient capability of permeability and decrease in thickness beneath the 2nd phase island, the generated excess pore water pressure in the middle Pleistocene foundation beneath the 2nd phase island is not well propagated to the foundation beneath the 1st phase island. By comparing the excess pore water pressure remaining in the foundation beneath the 1st phase island (Fig. 5.3 (b) and (c)), it is found that the excess pore water pressure in the middle Pleistocene layers beneath the 1st phase island is slightly dissipated during this period with little propagation of excess pore water pressure although we had the effective event “construction of the 2nd phase island”. In contrast, the generated excess pore water pressure due to construction of the 2nd phase island in the upper and lower Pleistocene foundation of the 2nd phase island is remarkably propagated to the one beneath the 1st phase island. The mode of propagation could be explained likewise by using the concept of “mass permeability” of the Pleistocene sand gravel layers. Detailed investigation from Fig. 5.3 (b) and (c) provides the following quantitative change in excess pore water pressure in the Pleistocene foundation beneath the 1st phase island. The excess pore water pressure in the upper Pleistocene clay layer Ma11 and the lower Pleistocene clay layer Ma6 beneath the 1st phase island increases from 80kPa to 140kPa and 80kPa to 100kPa respectively. The increase in the excess pore water pressure is caused by the propagation of the

excess pore water pressure generated in the foundation beneath the 2nd phase island through the adjoining Pleistocene sand gravel layers with ordinary permeability. On the other hand, the excess pore water pressure in the middle Pleistocene clay layer Ma 9 is almost stable or slightly deceases from 280kPa to 260kPa during the same period. It means that the generated excess pore water pressure in this region is not so well propagated through the adjoining Pleistocene sand gravel layers because of their poor permeability and tends to dissipate slowly toward the onshore side. Excess pore water pressure is scarcely propagated through Ds1 and 10 because of their sufficient function as permeable layers. As long as the rate and the mode of excess pore water pressure propagation and dissipation in the Pleistocene deposits of KIX is concerned, the mass permeability of the Pleistocene sand gravel layers plays a significant role.

It is noteworthy that more than 200kPa of excess pore water pressure in the middle Pleistocene layers beneath the 1st and 2nd phase islands and more than 100kPa of excess pore water pressure in the lower Pleistocene layer beneath the 2nd phase island still remain undissipated even after 50years from the start of the reclamation (Fig. 5.3 (d)). It clearly means that the primary consolidation in terms of the process of excess pore water pressure dissipation is not completed in the Pleistocene deposits for a very long time.

The calculated distribution of the excess pore water pressure with depth at the monitoring point 1 of the 1st phase island (see Figs. 5.1, 5.2) is shown in Fig. 5.4 together with the measured results. The calculated values are compared with the measured one at three different times. Here, the solid line and ■, thin solid line and ◇, the chain dotted line and △ are the calculated and measured results at the completion of the 1st phase reclamation, before the construction of the 2nd phase island and at the completion of the 2nd phase reclamation respectively and the dotted line is only the calculated performance at after 50years from construction. At the completion of the 1st phase reclamation, because the upper Pleistocene clays such as Ma12 and 11 have undergone plastic yielding due to reclaimed load, a large amount of excess pore water pressure

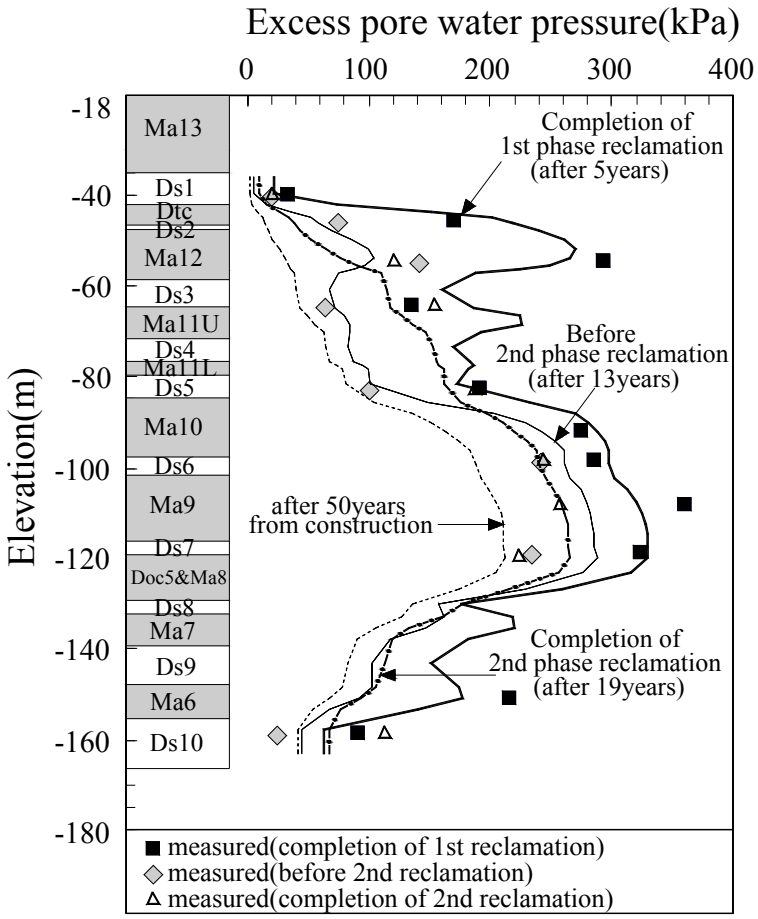

Fig. 5.4 Comparison of the calculated and measured excess pore water pressure distribution with depth at the monitoring point 1 in terms of construction of the 1st and 2nd phase islands

generates. Then, it dissipates steadily until before the construction of the 2nd phase island because of the high permeability of the sand gravel layers, Ds1 and 3 above and below Ma12. On the other hand, the mode of excess pore water pressure in the middle Pleistocene layers is different. Because of the poor quality of mass permeability of the sand gravel layers (Ds6, 7), Ma10, 9 and Doc5&Ma8 behave as if they were one continuous clay layer. Here, Ds6 and 7 does not seem to function as permeable layers at all. The rate of excess pore water pressure dissipation is very low in those layers, which results in that a large amount of undissipated excess pore water pressure remains in the middle Pleistocene layers for a long time. The

calculated performance provides that even after 50years from the construction, more than 200kPa of excess pore water pressure remains around Ma9 layer. In the lower Pleistocene layers such as Ma7 and 6, the generated excess pore water pressure is not so large compared to the other layers and dissipates relatively fast with time because of the high permeability of the thick sand gravel layer, Ds10 situated beneath Ma6.

At the completion of the 2nd phase reclamation, it is quantitatively found that the excess pore water pressure is propagated to the foundation beneath the 1st phase island due to the construction of the 2nd phase island. The excess pore water pressure increased remarkably due to the adjacent construction of the 2nd phase island in the upper Pleistocene layers of around Ma11 because the sand gravel layers, Ds3, 4 and 5 have ordinary permeability as permeable layers with sufficient thickness for propagation at the time. In the lower Pleistocene layers of around Ma7, the excess pore water pressure does not increase remarkably because the propagation of excess pore water pressure from the foundation beneath the 2nd phase island is obstructed due to decrease in thickness of the Pleistocene sand gravel layers, Ds8 and 9 between the 1st and 2nd phase islands. It is also found that excess pore water pressure is not remarkably propagated in Dtc, Ma12, Ma6 because of sufficient permeability of Ds1, Ds10 and sand drain for the upper layers. On the other hand, the one does not increase in the middle Pleistocene layer such as Ma 10, 9, Doc5&Ma8 and Ds6, 7 because the sand gravel layers, Ds6 and 7 do not function as well as permeable layers. Although the calculated performance at the completion of the 1st phase reclamation slightly underestimates the measured excess pore water pressure at the layers such as Ma12, 9 and Ma6, the overall mode of distribution can be well described. In particular, the propagation of excess pore water pressure at the completion of the 2nd phase reclamation can be well described. Therefore, the long-term and interactive behavior of the excess pore water pressure in the Pleistocene deposits of the existing 1st phase island due to the adjacent construction of the 2nd phase island is found to be well simulated with the present analyses.

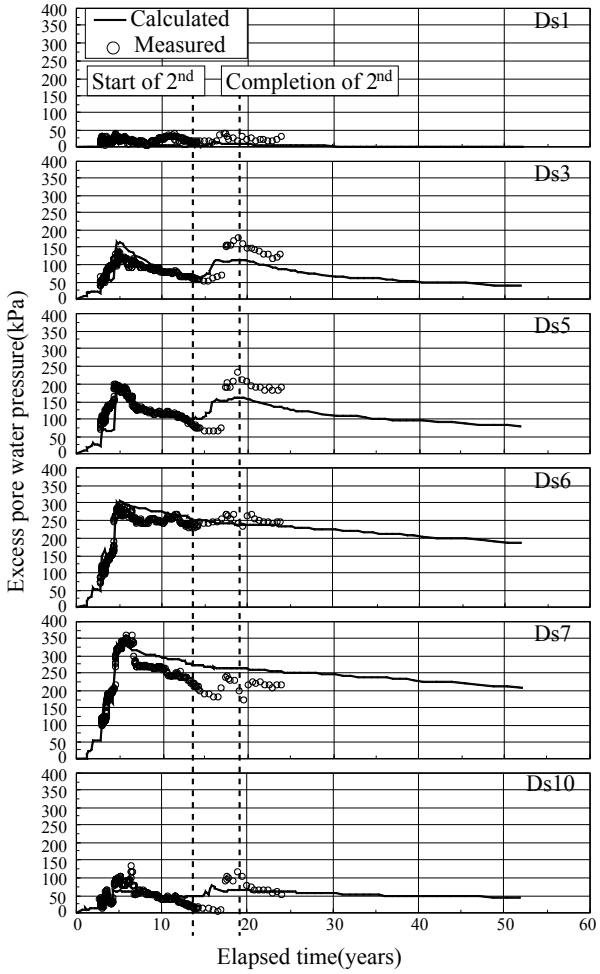

(a) Comparison of measured and calculated excess pore water pressure for the Pleistocene sand gravel layers

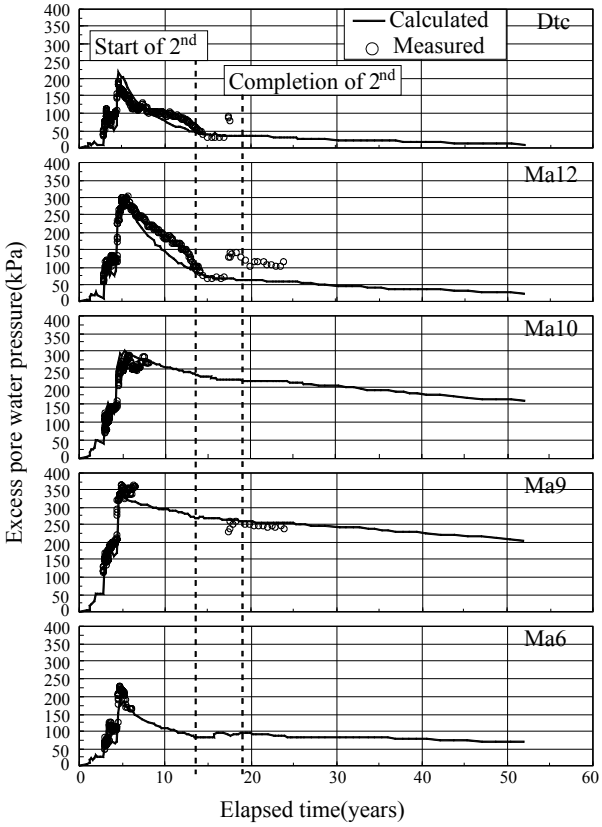

(c) Comparison of measured and calculated excess pore water pressure for the Pleistocene clay layers

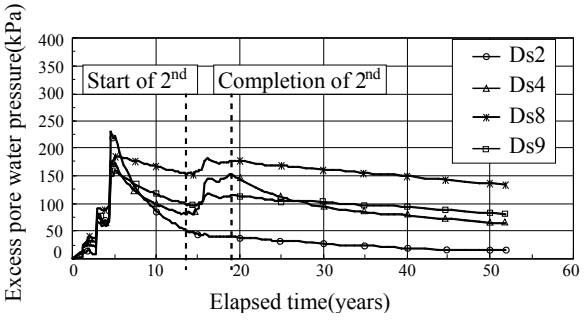

(b) Calculated excess pore water pressure for the Pleistocene sand gravel layers

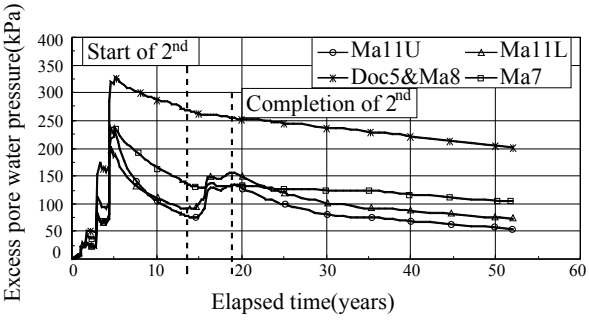

(d) Calculated excess pore water pressure for the Pleistocene clay layers

Fig. 5.5 Calculated and measured excess pore water pressure with time for the individual Pleistocene layers at the monitoring point 1 in terms of construction of the 1st and 2nd phase islands

Calculated excess pore water pressure – time relations are shown in Fig. 5.5 (a) together with the measured results for the individual Pleistocene sand gravel layers. Note that the comparison is shown for the Pleistocene sand gravel layers where the pore pressure cells have survived. It is clear that a little excess pore water pressure generates in Ds1 and 10, whereas a large amount of excess pore water pressure generates and keeps undissipated in the middle Pleistocene sand gravel layers such as Ds6 and 7. The increase in excess pore water pressure due to construction of the 2nd phase island is found in the upper and lower Pleistocene sand gravel layers such as Ds 3, 5 and 10. On the other hand, the excess pore water pressure is not well propagated in the middle Pleistocene layers such as Ds6 and 7. Calculated performance can well predict the actual behavior of excess pore water pressure in the all Pleistocene sand gravel layers. Figure 5.5(b) shows the calculated performance of the excess pore water pressure of the Pleistocene sand gravel layers where there is no measured information due to damage of the pressure cells. The propagation of excess pore water pressure due to the construction of the 2nd phase island is remarkably seen in the Ds4. On the other hand, the excess pore water pressure is slightly propagated through Ds 8 and 9 because the decrease in thickness of these layers beneath the 2nd phase island and at the junction between two islands obstructs the propagation to the foundation beneath the 1st phase island. The excess pore water pressure in Ds2 is well dissipated without remarkable propagation because of the existence of high permeable layer, Ds1 in the vicinity. The behavior of excess pore water pressure in the Pleistocene sand gravel layers is naturally associated with the one in the Pleistocene clay layers.

Calculated excess pore water pressure – time relations for the Pleistocene clay layers are shown in Fig. 5.5(c) together with the measured results for the corresponding layers. For the selected clay layers, the process of generation and dissipation of excess pore water pressure is well described by the present numerical procedure. Figure 5.5(d) shows the calculated performance of the excess pore water pressure of the Pleistocene clay layers where there is no

measured information due to damage of the pressure cells. The process of excess pore water pressure propagation is similar to that of the Pleistocene sand gravel layers. It is also found that a rate of excess pore water pressure dissipation is very slow and the one is not propagated in the middle Pleistocene clay layers such as Ma10 and 9. Insufficient dissipation of excess pore water pressure in Ds6 and 7 causes the delay of consolidation for Ma10 and 9 in which the generated excess pore water pressure is not well dissipated. As seen from Figs. 5.5, the behavior of excess pore water pressure can be well predicted with the proposed procedure. It is hence confirmed that the adopted procedure in terms of elasto-viscoplastic finite element analysis associated with a compression modeling and a concept of "mass permeability" works well to assess the stress condition of the Pleistocene deposits of the existing 1st phase island due to the adjacent construction of the 2nd phase island at KIX.

5.3.2 Transition of stress state with depth at the monitoring point 1

The calculated profiles of stresses with depth at the monitoring point 1 are shown in Fig. 5.6. In the figures the stress profiles at 4 different stages are exhibited, namely, (a) at the completion of reclamation for the 1st phase island, (b) just before the start of reclamation for the 2nd phase island, (c) at the completion of reclamation for the 2nd phase island and (d) after 50years from the start of construction. Here, p_o denotes the initial vertical effective stress, p_c is the consolidation yield stress, p_f means the finial total vertical stress and *p'* denotes the effective vertical stress. The hatched area exhibits the undissipated excess pore water pressure. As shown in Fig. 5.6 (a), at the completion of reclamation for the 1st phase island, the effective stresses already surpass p_c for the Pleistocene clay layers above Ma10, while those still remain below p_c for the middle to lower Pleistocene clay layers such as Ma10, 9 and Doc5&Ma8. The upper Pleistocene clay layers hence behave as normally consolidated and the middle to lower

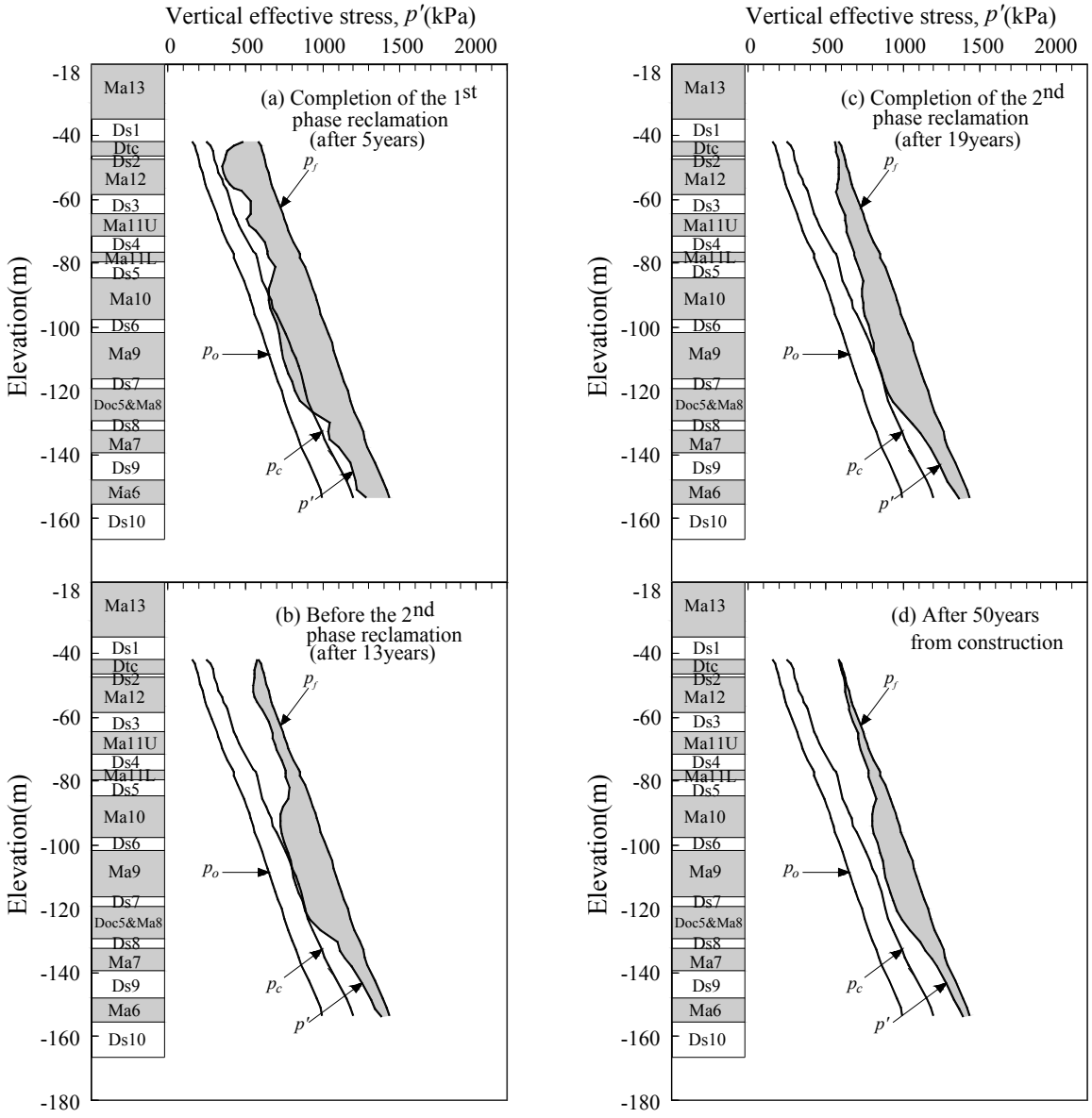

Fig. 5.6 Stress condition with depth at the monitoring point 1 in terms of construction of the 1st and 2nd phase islands

Pleistocene clay layers behave as quasi-overconsolidated during the process of reclamation for the 1st phase island. The stress condition of the reclaimed foundation beneath the 1st phase island just before the start of reclamation for the 2nd phase island is shown in Fig. 5.6 (b). It is true that the excess pore water pressure at the upper Pleistocene layers is steadily dissipated before the construction of the 2nd phase island, but the one at the middle Pleistocene clay layers scarcely

dissipates during the period because of the poor permeability of the adjoining sand gravel layers. It means that the Pleistocene clay layers, Ma9 and Doc5&Ma8 behave as quasi-overconsolidated clays without definite plastic yielding over the period of the 1st phase island construction, whereas other clays become normally consolidated associated with steady dissipation of excess pore water pressure. The profile of stresses at the completion of reclamation for the 2nd phase island is shown in Fig. 5.6 (c). In the upper Pleistocene deposits, excess pore water pressure is found to increase due to the effect of propagation of the excess pore water pressure generated in the foundation beneath the 2nd phase island by the reclamation for the 2nd phase island. It should also be noted that in the middle Pleistocene deposits, the profile of the excess pore water pressure scarcely changed in this particular period because the propagation of the excess pore water pressure is obstructed due to the decrease in thickness and poor permeability of the Pleistocene sand gravel layers, Ds6 and 7. The profile of stresses at 50 years from the start of the project is shown in Fig. 5.6 (d). Emphasis should be placed on the fact that significant amount of excess pore water pressure remains even after 50 years from the start of the project in the middle Pleistocene deposits. One of the most effective reasons for this behavior is that the mass permeability of the permeable Pleistocene sand gravel layers, Ds6 and 7 is insufficient to promote dissipation of excess pore water pressure. In contrast, so-called primary consolidation associated with dissipation of excess pore water pressure steadily advances both in the upper and lower Pleistocene clay layers due to the existence of the well permeable Pleistocene sand gravel layers, such as Ds1 and 10 in the vicinity. From these results about the change in stresses in the reclaimed foundation at the monitoring point 1, it is found that typical consolidation associated with dissipation of excess pore water pressure advances in the upper and lower Pleistocene clay layers associated with definite plastic yielding, whereas in the middle Pleistocene clay layers the consolidation with insufficient dissipation of excess pore water pressure continues for a long time in the region of quasi-overconsolidation.

5.3.3 Stress strain performance for the individual Pleistocene clay layers

Calculated stress – strain relations in terms of the change in void ratio against effective vertical stress due to the construction of the airport islands are shown in Fig. 5.7 together with the setup *e*-log*p* for the representative elements of the individual Pleistocene clay layers at the monitoring point 1. The setup compression curves in terms of *e*-log*p* are described as reference compression ones with p_o, p_c, κ and λ shown in Table 4.1. The elasto-viscoplastic model gives various stress – strain paths for the individual Pleistocene clays on *e*-log*p* plane depending upon the strain rate mainly controlled by the rate of dissipation of excess pore water pressure. The increase in effective stress in clay elements due to reclamation load causes the strain with a certain strain rate. For the upper Pleistocene clay layers such as Dtc, Ma12 and 11, it is clear in Fig. 5.6 that the excess pore water pressure steadily dissipates due to high permeability of the adjoining Pleistocene sand gravel layers, Ds1 and 3 by the time of the start of 2nd phase island construction and the low initial stress, p_o for these layers makes them easily surpass p_c and become normally consolidated in the early stage of the project. The stress-strain curves for these clay layers hence exhibit typical overshoot performance as is usually seen for normally consolidated clays. The range of overshoot occurrence corresponds to the one in which the viscoplastic volumetric strain rate is larger than $\dot{v}_o$ and the volumetric strain rate becomes equivalent to $\dot{v}_o$ at the intersecting point between the calculated and setup *e*-log*p* following the reduction in the strain rate. In the region where the effective stress is larger than the intersecting point, so-called secondary consolidation takes place with little excess pore pressure in the clay elements.

In the middle Pleistocene clay layers (Ma9 and Doc5&Ma8), the viscoplastic overshoot takes place in the quasi-overconsolidated region less than p_c. Here, emphasis should be paid to the introduced assumption that viscoplastic strain also generates even in the quasi-overconsolidated region for the Pleistocene clays. The present peculiar behavior is caused

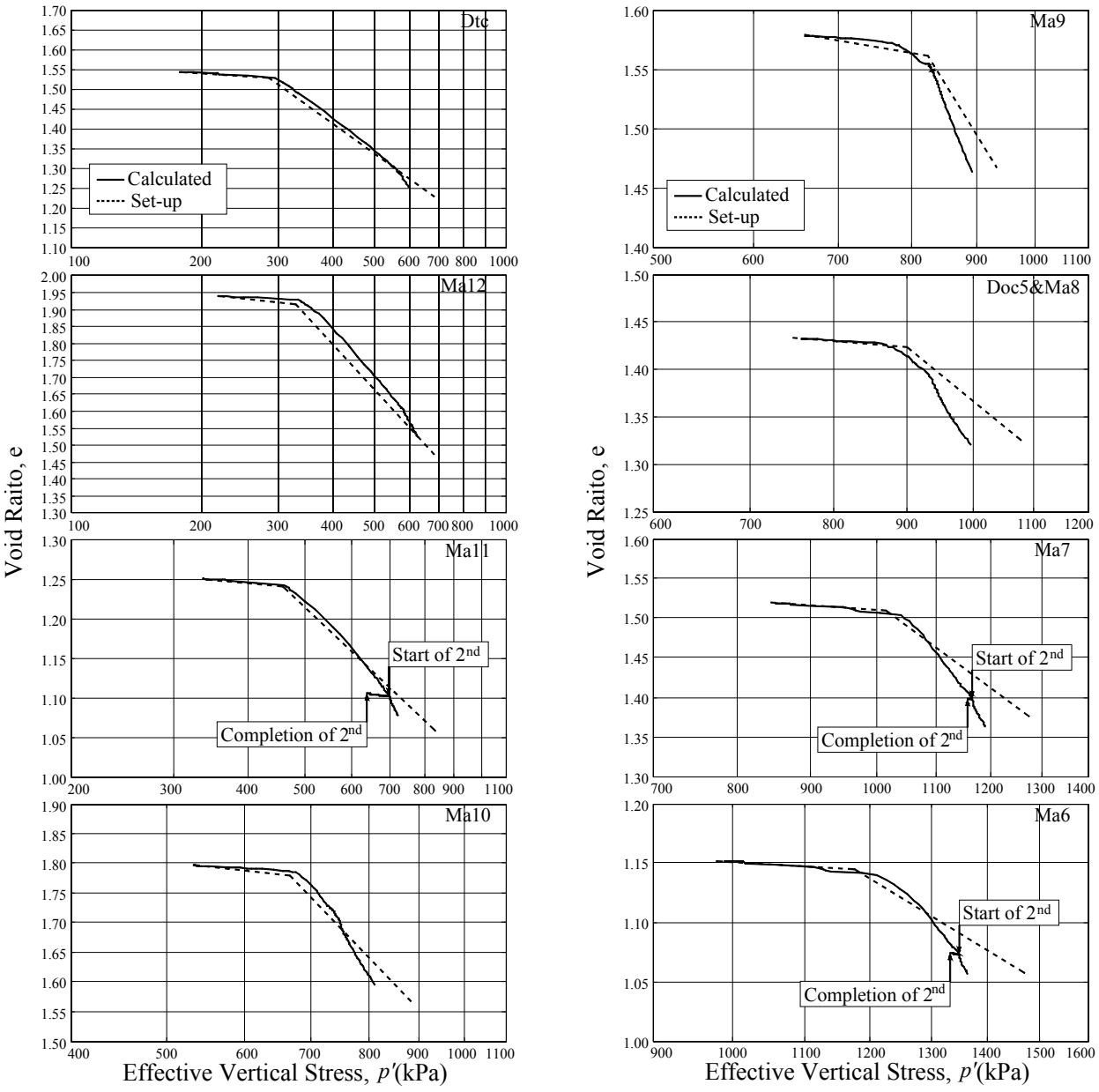

Fig. 5.7 Calculated *e*-log*p* relations for the Pleistocene clay layers at the monitoring point 1 in terms of construction of the 1st and 2nd phase islands

by the occurrence of viscoplastic strain while the stress state remains below p_c for a long time because the gain in effective stress is prolonged due to poor permeability of Ds6 and 7. The calculated stress – strain paths for these clays are below the setup *e*-logp. This mode of stress – strain relations means that the rate of deformation is low and the larger long-term compression is

expected due to strain rate dependency.

The stress strain paths for the lower Pleistocene clays, Ma7 and 6 exhibit the both characteristics of the normally consolidated (upper Pleistocene) and quasi-overconsolidated (middle Pleistocene) clays. The viscoplastic behavior occurs in these clay layers in the quasi-overconsolidated region because the large initial stress, p_o for these clays prevent the effective stress from easily surpassing p_c even after applying the reclamation load. At the same time, however, the adjoining Pleistocene sand gravel layers, Ds10 and 9 with high permeability function well for dissipation of excess pore water pressure from these Pleistocene clay layers. The relatively high rate of excess pore water dissipation gives high rate of deformation for the lower Pleistocene clay layers. Therefore, the combined behavior of normally and quasi-overconsolidated clay takes place in the lower Pleistocene clay layers.

Additional important fact to be discussed here is the effect of the construction of the 2nd phase island on the stress-strain behavior of the Pleistocene clay layers at the monitoring point 1 on the 1st phase island. As is already mentioned, the excess pore water pressure generated due to construction of the 2nd phase island is propagated to the foundation of the 1st phase island through the permeable Pleistocene sand gravel layers. On *e*-log*p* plane, the propagation of the excess pore water pressure affects the stress-strain relations for the Pleistocene clays. Remarkable decrease in effective stress can be seen for Ma11. The point of start and end of rebound on the *e*-log*p* relation corresponds to the start and the completion of the construction of the 2nd phase island respectively. As seen in Fig. 5.4 and 5.5 (a), the excess pore water pressure due to the 2nd phase island construction is definitely propagated to the foundation at the monitoring point 1 in the adjoining sand gravel layers, Ds3, 4 and 5. Ma11 is regarded to be deposited under the relatively cool interglacial stage. Insufficient transgression produced the separated strata (Ma 11U and Ma11L) with coarser components. The relatively high permeability of Ma 11 as well as that of the adjoining sand gravel layers causes the remarkable

rebound on *e*-log*p* plane in terms of serious reduction in effective stress due to propagation of excess pore water pressure generated by the construction of the 2nd phase island. The phenomena can also be seen in the lower Pleistocene clay layers, Ma7 and 6 because of the high permeability of Ds 10 and 9, whereas the middle Pleistocene clays do not undergo such remarkable reduction in effective stress because the low permeability of the adjoining Pleistocene sand gravel layers, such as Ds6 and 7, obstructs to propagate the excess pore water pressure to the monitoring point 1 from the foundation beneath the 2nd phase island.

5.3.4 Compression of the Pleistocene clay layers

Calculated compression - time relations for the individual Pleistocene clay layers are shown in Fig. 5.8 together with the corresponding measured data. Here, the solid line shows the results with the effect of the construction of the 2nd phase island whereas the hatched line shows the one without the construction of the 2nd phase island. The effect of the construction of the 2nd phase island on the reclaimed foundation of the 1st phase island is discussed later. As seen from Fig. 5.5, the excess pore water pressure in the upper and lower Pleistocene layers from Dtc to Ds5 and from Ma7 to Ds10 has steadily dissipated with time. This steady dissipation causes the remarkable advance in compression of these clay layers such as Dtc, Ma12, 11, 7 and 6. During the construction of the 2nd phase island, the settlement of these clay layers is retarded or even slight upheaval can be seen for some layers because the excess pore water pressure is increased or the dissipation of excess pore water pressure is hindered due to propagation of the one from the foundation beneath the 2nd phase island. In the upper and lower Pleistocene clay layers such as Dtc, Ma12, 11, 7 and 6, at the completion of the 2nd phase reclamation, the primary consolidation with steady dissipation of excess pore water pressure is almost completed because of high permeability of sand gravel layers, Ds 1, 2 and 10. It should be noted that the upper

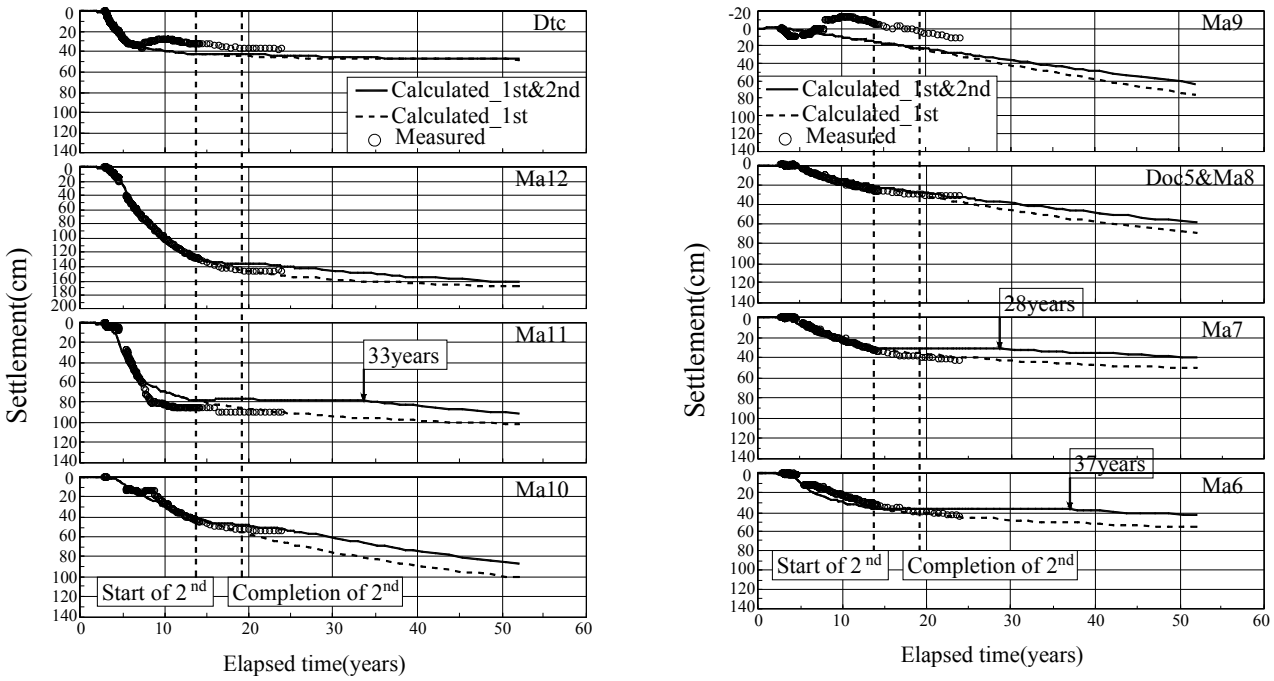

Fig. 5.8 Comparison of measured and predicted settlement for the Pleistocene clay layers at the monitoring point 1 in terms of construction of the 1st and 2nd phase islands

Pleistocene clays undergo plastic yielding due to reclamation load in a short time because of their relatively small initial stresses, p_o. Because the stress surpasses p_c by the reclamation load in the early stage of the project, the time dependent behavior associated with secondary compression in the quasi-overconsolidated region can be ruled out and then as a typical behavior for normally consolidated clay, the hyperbolic shape for settlement-time relations is exhibited with the monotonic dissipation of excess pore water pressure for Dtc, Ma12 and 11. The secondary compression is then predominant after the completion of the 2nd phase reclamation. In the lower Pleistocene clay layers such as Ma7 and 6, although their initial stresses, p_o are relatively large, the stress surpasses p_c relatively rapidly by the reclamation load with the monotonic dissipation of excess pore water pressure because of the sufficient permeability of Ds10 and 9. Therefore, the mode of settlement with time exhibits hyperbolic shape also for Ma7

and 6. As shown in Fig. 5.7, unloading in terms of the decrease in effective stress due to propagation of excess pore water pressure occurs in Ma11, 7 and 6 at the monitoring point 1 of the 1st phase island during the construction of the 2nd phase island. This decrease in effective stress remarkably causes the occurrence of retardation of compression or swelling in these Pleistocene clay layers. The calculated performance shows that the compression is retarded for these clay layers for a long time and begins to restart at after 33 years in Ma11, 28 years in Ma7 and 37 years in Ma6 from the start of the project. The duration and the time to recompression depend upon the mode of propagation and dissipation of excess pore water pressure mainly controlled by "mass permeability" of the adjoining Pleistocene sand gravel layers.

In the middle Pleistocene clay layers such as Ma10, 9 and Doc5&Ma8, the rate of dissipation of excess pore water pressure is much lower compared to the upper and lower Pleistocene layers and excess pore water pressure does not increase during the construction of the 2nd phase island (see Fig.5.5) because of the poor permeability of the sand gravel layers, Ds6 and 7. It is also found that the behavior of unloading and reloading does not take place during the construction of the 2nd phase island and the mode of the secondary compression is predominant from at the relatively low stress level in Fig.5.7. Then, although a rate of compression in these clay layers such as Ma10, 9 and Doc5&Ma8 is getting retarded due to the construction of the 2nd phase island, the process of compression is continues without remarkable dissipation of excess pore water pressure. It means that the primary consolidation associated with dissipation of excess pore water pressure is not predominant in the middle Pleistocene clay layers. But the delayed compression including secondary consolidation occurs during the process of excess pore water pressure dissipation under the condition of insufficient advance in primary consolidation. It is also noteworthy that the stresses in Ma9 and Doc5&Ma8 remain below p_c at the completion of the reclamation of the 1st phase island. However, as shown in Fig.5.6, it takes a long time for these layers to become gradually normally consolidated by

undergoing plastic yielding due to the dissipation of excess pore water pressure. During this process, the time dependent compression including the secondary consolidation takes place with insufficient dissipation of excess pore water pressure in the quasi-overconsolidated region. In the all Pleistocene clay layers of KIX foundation ground, it is found that remarkable time dependent compression has hence continued without remarkable dissipation of excess pore water pressure in the normally consolidated or quasi-overconsolidated region.

The effect of the adjacent construction of the 2nd phase island is found to be remarkable in Fig. 5.8. The total compression with the effect of the 2nd phase island described by the solid lines is delayed because of the decrease in effective stress caused by the propagated excess pore water pressure from the foundation of the 2nd phase island. On the contrary, the one without the 2nd phase island described by the hatched lines progresses steadily associated with the steady dissipation of excess pore water pressure. It is true that the degree of delay of compression due to effect of the 2nd phase island construction is different for the individual Pleistocene clay layers because the mode of migration of excess pore water pressure in the adjoining Pleistocene sand gravel layers is different, but the existence of the 2nd phase island definitely influences the progress in compression of the reclaimed Pleistocene clay layers beneath the 1st phase island.

The comparison between the calculated and measured settlement is also shown in Fig. 5.8 to confirm the validity of the proposed procedure. The calculated performance can well describe the whole process of compression including the interactive behavior due to the construction of the adjacent 2nd phase island although the calculation slightly exaggerates the retardation of compression. Here, due attention should be paid to the coming in-situ compression of the individual Pleistocene clay layers; particularly it is of interest if the interactive behavior such as retardation and/or recompression is surely measured as the present calculated prediction.

5.4 Interactive Behavior of the Pleistocene Marine Foundations beneath the 2nd Phase Island

5.4.1 Performance of excess pore water pressure

The mode of calculated distribution of excess pore water pressure in the Pleistocene marine foundations integrating the 1st and 2nd phase island was already explained in the previous section 5.3.1 using the contours of the calculated distribution of them as shown in Fig.5.3. The calculated distribution of the excess pore water pressure with depth at the monitoring point 2 of the 2nd phase island (see Figs. 5.1, 5.2) is shown in Fig. 5.9 together with the measured results. The calculated values are compared with the measured one at four different times. Here, the solid line and ■, thin solid line and △, the chain dotted line and ◇, the chain two-dotted line and ○ are the calculated and measured results at the completion of the 2nd phase reclamation, at after 20years, at after 24years (by the present (2010)) and at after 14years (start of measurement) from the start of project respectively and the dotted line is only the calculated performance at after 50years from the start of project. As mentioned in section 5.3.1, not a small amount of excess pore water pressure takes place in the foundation beneath the 2nd reclaimed island where there is no reclamation load at start of measurement (after 14years from construction) due to the effect of propagation of the excess pore water pressure generated in the foundation beneath the 1st phase island by the reclamation of the 1st phase island. At start of measurement for the monitoring point 2, a larger amount of excess pore water pressure has remained undissipated in the middle Pleistocene layer compared to the one in the upper and lower Pleistocene layers because the rate of propagation is very low and the dissipation of the propagated excess pore water pressure is also very slow because of the poor permeability of the adjoining sand gravel layers, Ds6 and 7. The mode of the calculated distribution at start of measurement well describes the measured one. However, at the other times, the calculated distribution exhibits the contrast with the measured values. The mode of calculated distribution

is similar to that at the monitoring point 1 for the 1st phase island and steadily dissipates with the lapse of time. The calculated excess pore water pressure after the completion of the 2nd phase reclamation decreases with time for all the Pleistocene layers. On the other hand, in the upper Pleistocene clay layers such as Dtc, Ma12 and 11, the measured excess pore water pressure after the completion of the 2nd phase reclamation (after 19years) increases with the lapse of time at after 20years, and then decreases with the lapse of time at after 24years. In the middle Pleistocene clay layers such as Ma10, 9 and Doc5&Ma8, the measured values continuously increase with the lapse of time at after 20, 24years. For the lower Pleistocene clay layers such as Ma7 and 6, the measured values after the completion of the 2nd phase reclamation almost do not change until after 24years. It should be noted that the measured mode of excess pore water pressure dissipation has the relation to the permeability and thickness of sand gravel layers in the vicinity.

According to the permeability and thickness of sand gravel layers, in the upper Pleistocene sand gravel layer from Ds1 to Ds5 having relatively high permeability without a drastic constriction in thickness toward offshore, they seem to function as permeable layer. However, in the middle Pleistocene sand gravel layers such as Ds6 and 7 having poor permeability with drastic constriction in thickness toward offshore, they do not seem to function as permeable layer at all and the excess pore water pressure rather increases with the lapse of time due to the unended propagation of them from the 1st reclaimed foundation with very low permeability. In the lower Pleistocene sand gravel layer from Ds8 to Ds10, although Ds10 layer has the high permeability and sufficient thickness toward offshore, Ds8 and 9 layers do not seem to well function as permeable layers because of the drastic constriction in thickness toward offshore.

It is also confirmed that the measured values are not well simulated with the finite element analysis in the present study because there is the possibility in change of the initial ground condition in terms of soil parameters used for the numerical analysis due to the effect of

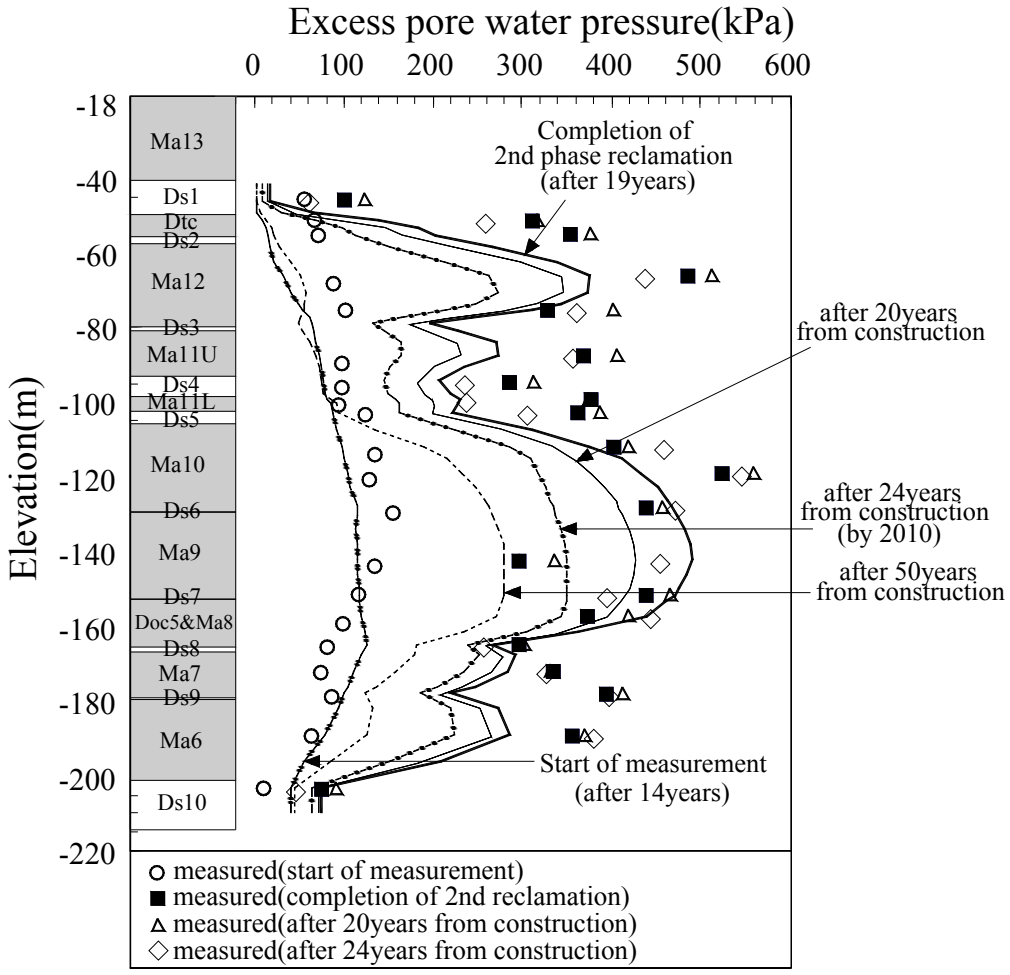

Fig. 5.9 Comparison of the calculated and measured excess pore water pressure distribution with depth at the monitoring point 2 in terms of construction of the 1st and 2nd phase islands

propagation of excess pore water pressure in the foundation beneath the 2nd phase island and the calculated performance could not consider the tri-dimensional distribution for the foundation model.

The calculated performance predicts that even after 50years from the start of project, more than 200kPa of excess pore water pressure remains in the middle Pleistocene layers such as Ma10, 9 and Doc5&Ma8.

Calculated excess pore water pressure – time relations are shown in Fig. 5.10 (a) together with the measured results for the individual Pleistocene sand gravel layers at the monitoring point 2. Similar to the results for the 1st phase island at the monitoring point 1 (see Fig.5.5), it is also calculated that a little amount of excess pore water pressure generates in Ds1 and 10 whereas more than 500kPa of excess pore water pressure generates and keeps undissipated in the middle Pleistocene sand gravel layers such as Ds6 and 7. In the other Pleistocene sand gravel layers, a large amount of excess pore water pressure relatively generates compared to the one at the monitoring point 1 and the rate of excess pore water pressure dissipation is so slow because of decrease in thickness of sand gravel layers toward offshore. Amount of propagation of excess pore water pressure in the foundation beneath the 2nd phase island due to construction of the 1st phase island is about 100kPa before construction of the 2nd phase island in the Pleistocene sand gravel layers from Ds4 to Ds9. However, remarkable propagation is not found in the Pleistocene sand gravel layers such as Ds1, 2 and 10 because of their sufficient thickness and permeability. It is noteworthy that the calculated excess pore water pressure exhibits the mode of increase and dissipation following the construction sequence of the 2nd phase reclamation, whereas the measured values increase even after the completion of the 2nd phase reclamation without remarkable dissipation in the all Pleistocene sand gravel layers except Ds1 and 10. However, it is found that the calculated performance pretty describes the mode of the measured excess pore water pressure at the monitoring point 2 with the evaluated mass permeability of the Pleistocene sand gravel layers. Therefore, the mass permeability of the Pleistocene sand gravel layers also plays a significant role at the foundations of the 2nd reclaimed island.

Figure 5.10 (b) shows the calculated excess pore water pressure – time relations for the individual Pleistocene clay layers together with the measured results at the monitoring point 2. The process of excess pore water pressure propagation and dissipation is similar to that of the Pleistocene sand gravel layers. It is also noteworthy that the calculated excess pore water

pressure dissipates with the lapse of time during the 2nd phase reclamation and after the completion of the 2nd phase reclamation, however, the measured values increase even after the completion of the 2nd phase reclamation without remarkable dissipation. In the upper Pleistocene clay layers from Dtc to Ma11 having the relatively high permeability of the adjoining Pleistocene sand gravel layers, the measured mode of excess pore water pressure dissipates with the lapse of time after the completion of the 2nd phase reclamation. However, in the other Pleistocene clay layers from Ma10 to Ma6, the measured mode of them increases or does not dissipate with the lapse of time until the present time because of the poor permeability and insufficient thickness of the adjoining Pleistocene sand gravel layers.

The calculated performance underestimates the measured values for the all individual Pleistocene layers. However, the tendency of excess pore water pressure dissipation and propagation is well explained depending upon the mass permeability of the Pleistocene sand gravel layers with the present numerical procedure.

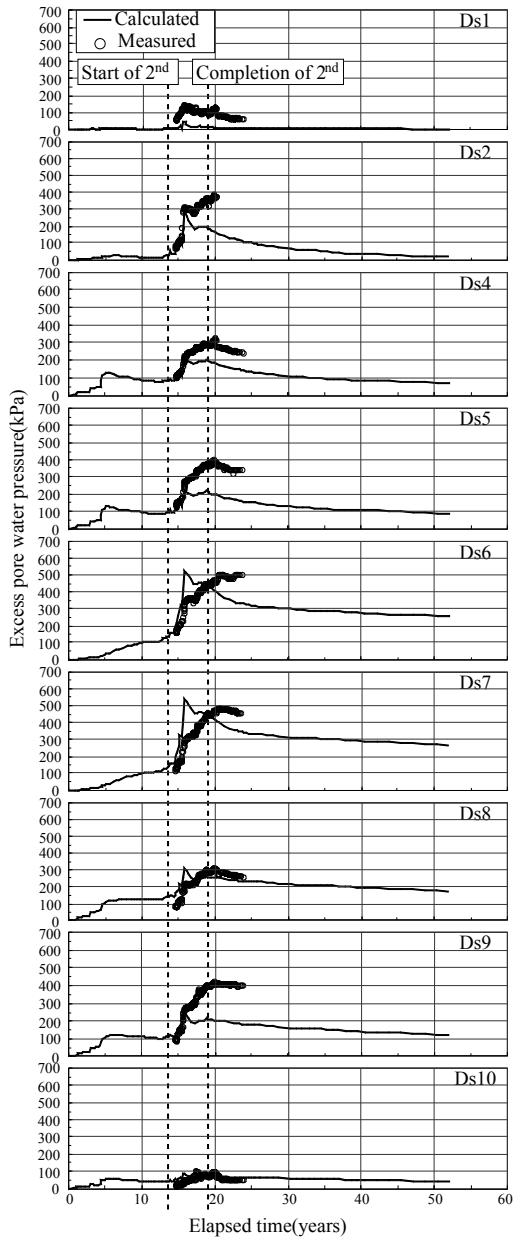

(a) Comparison of measured and calculated excess pore water pressure for the Pleistocene sand gravel layers

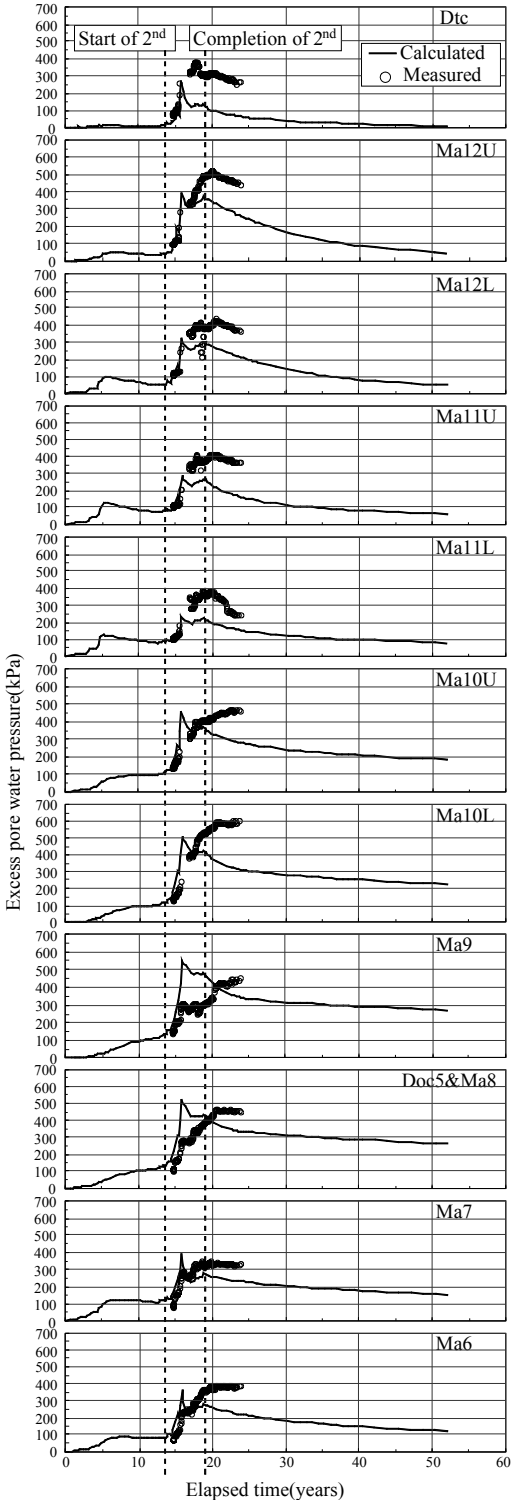

(b) Comparison of measured and calculated excess pore water pressure for the Pleistocene clay layers

Fig. 5.10 Calculated and measured excess pore water pressure with time for the individual Pleistocene layers at the monitoring point 2 in terms of construction of the 1st and 2nd phase islands

5.4.2 Transition of stress state with depth at the monitoring point 2

The calculated profiles of stresses with depth at the monitoring point 2 are shown in Fig. 5.11. In the figures, the stress profiles at 4 different stages are exhibited, namely, (a) just before the start of reclamation for the 2nd phase island, (b) at the completion of reclamation for the 2nd phase island, (c) after 24years (by the present (2010)) and (d) after 50years from the start of project. Here, the individual names such as p_o, p_c, p_f, and p' are exactly the same that were denoted in section 5.3.2 for the monitoring point 1. The hatched area exhibits the propagated excess pore water pressure for Fig.5.11 (a) and the undissipated one for the others (Fig. 5.11 (b, c, d)). As shown in Fig. 5.11 (a), just before the start of reclamation for the 2nd phase island, the effective stresses decrease less than initial effective stress, p_o due to the effect of propagation of excess pore water pressure from the foundations beneath the 1st phase island by the reclamation of the 1st phase island. A slightly larger amount of the propagated excess pore water pressure remains undissipated in the middle Pleistocene layers from Ma10 to Doc5&Ma8 compared to the other Pleistocene layers because of the poor permeability of the Pleistocene sand gravel layers, Ds6 and 7. At the completion of the 2nd phase reclamation in Fig. 5.11 (b), the mode of effective stresses is similar to that at the monitoring point 1 as surpassing p_c for the Pleistocene clay layers above Ma10, while still remaining below p_c for the middle to lower Pleistocene clay layers. However, the stress condition below p_c for the middle Pleistocene clay layers will be lasted for the longer time than that at the monitoring point 1 because of decrease in the initial effective stresses, p_o due to the effect of propagation of excess pore water pressure from the foundations beneath the 1st phase island and decrease in the thickness of permeable sand gravel layer toward offshore. Figure 5.11 (c) shows that the stress condition still remains below p_c for the middle Pleistocene clay layers even after 24 years (by the present (2010)) from the start of project. As shown in Fig. 5.11 (d), due attention should be paid to the fact that although the effective stresses barely surpass p_c for the middle Pleistocene clay layers, a large amount of

excess pore water pressure remains even after 50 years. It means that the middle Pleistocene clay layers such as Ma10, 9 and Doc5&Ma8 behave as quasi-overconsolidated clays without definite plastic yielding for a long time whereas other clays become normally consolidated associated with steady dissipation of excess pore water pressure.

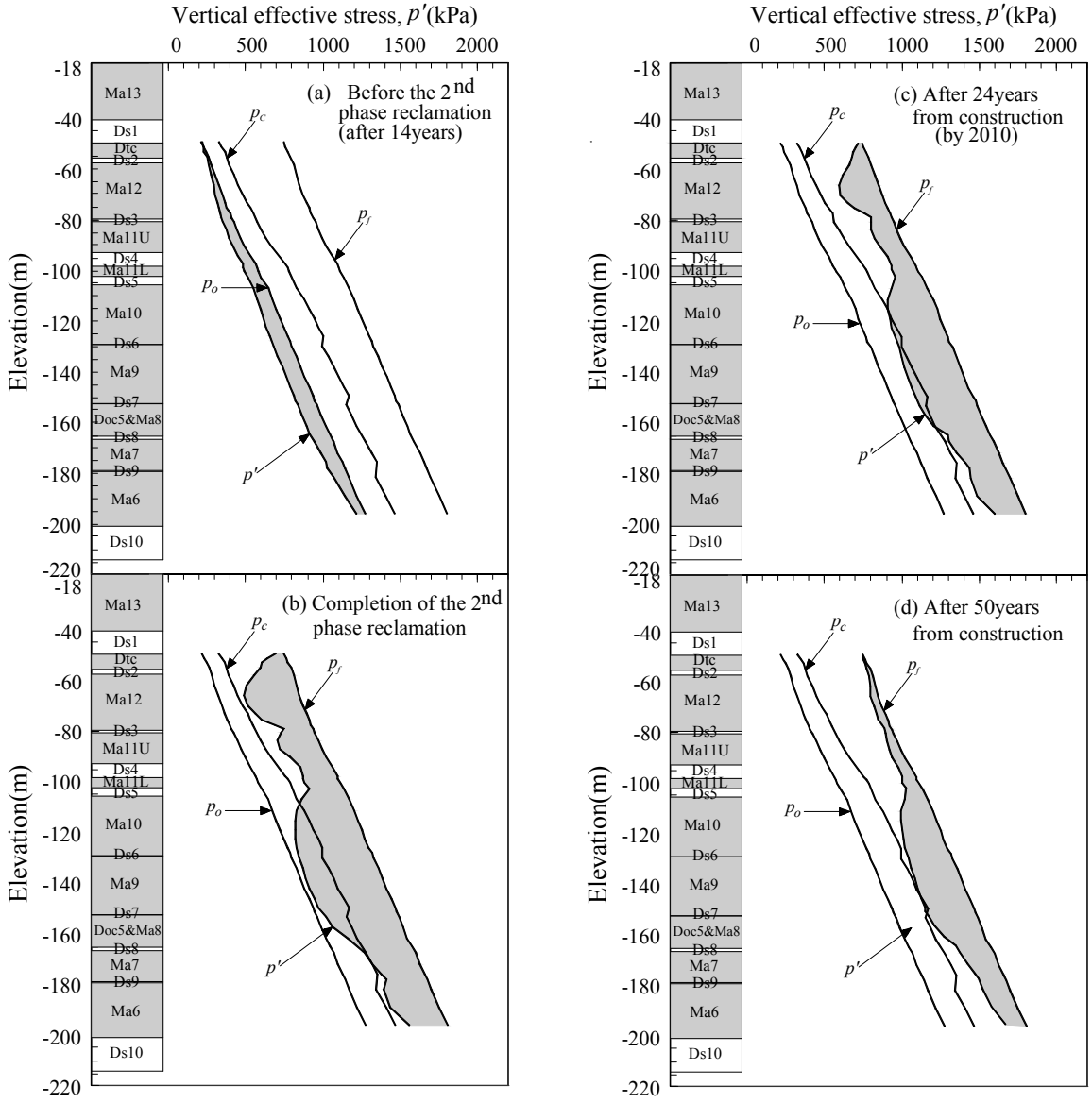

Fig. 5.11 Stress condition with depth at the monitoring point 2 in terms of construction of the 1st and 2nd phase islands

5.4.3 Stress strain performance for the individual Pleistocene clay layers

The calculated stress-strain relations in terms of the change in void ratio against effective vertical stress due to the construction of the airport islands are shown in Fig. 5.12 together with the setup *e*-log*p* for the representative elements of the individual Pleistocene clay layers at the monitoring point 2. The setup compression curves in terms of *e*-log*p* are described as reference compression ones with p_o, p_c, κ and λ shown in Table 4.2. As is already shown in Fig. 5.11 (a), the decrease in effective stress of clay elements before the start of reclamation for the 2nd phase island generates due to the effect of propagation of excess pore water pressure from the foundation beneath the 1st phase island by the reclamation of the 1st phase island. Amount of decrease in effective stress from initial effective stress, p_o is dependent upon the permeability of the adjoining sand gravel layers as shown in stress-strain paths of Fig.5.12. Amount of them in Dtc, Ma12 and 6 is relatively small compared to other clays because of sufficient permeability of Ds1, Ds10 and sand drain for the upper layers. For the Pleistocene clay layers such as Ma11, Ma7, a large trace for decrease in effective stress is exhibited in stress-strain paths because the adjoining sand gravel layers, Ds3, 4, 5, 8 and 9 have proper permeability as permeable layers with sufficient thickness for propagation and dissipation of excess pore water pressure at the time. On the other hand, in the middle Pleistocene clay layers such as Ma10, 9 and Doc5&Ma8, although the rate of excess pore water pressure propagation is very slow because of the poor permeability of Ds6 and 7, because the rate of excess pore water pressure dissipation is also very slow, a large amount of decrease in effective stress generates with steady propagation of excess pore water pressure until before the start of reclamation for the 2nd phase island.

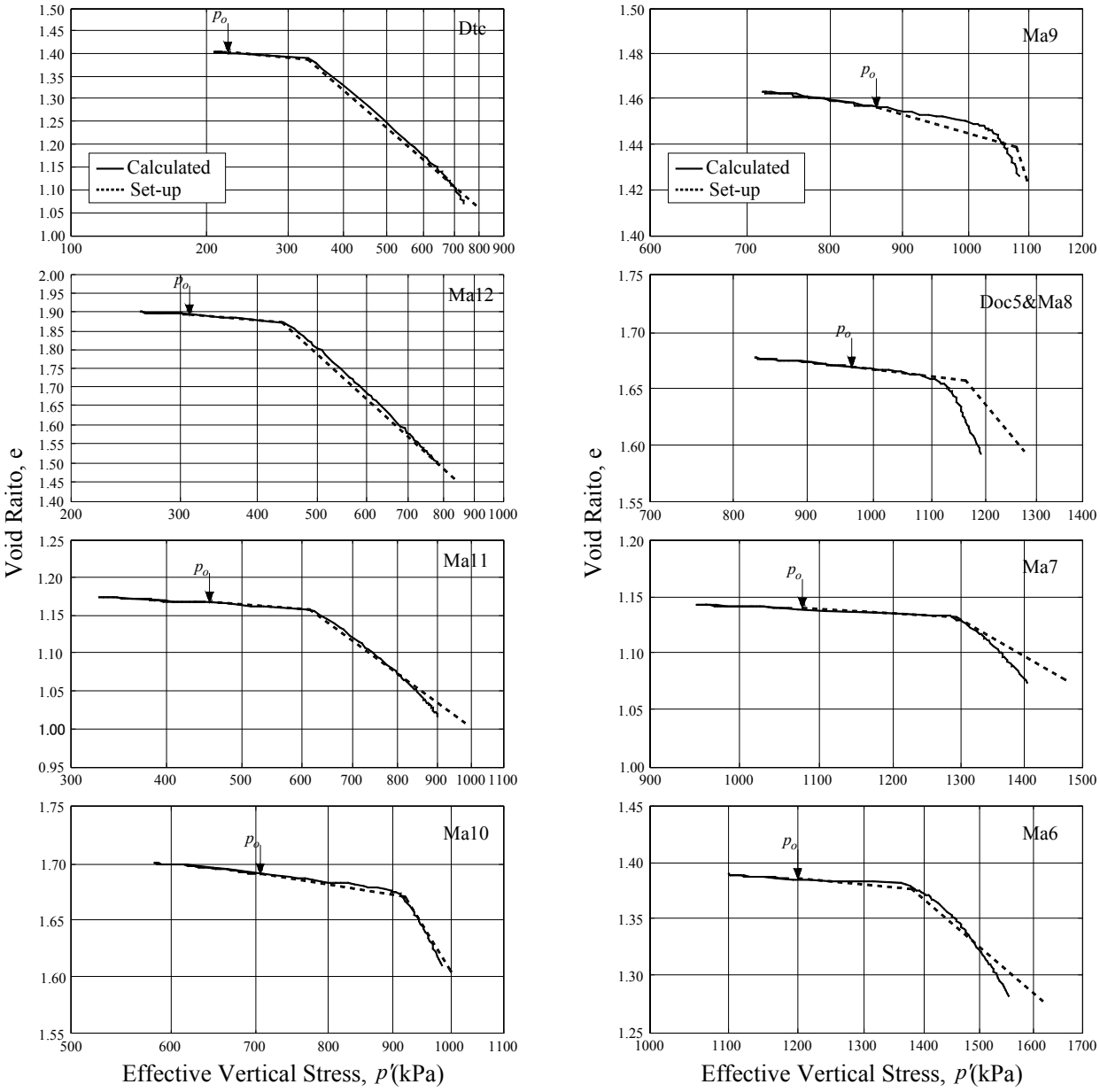

Fig. 5.12 Calculated *e*-log*p* relations for the Pleistocene clay layers at the monitoring point 2 in terms of construction of the 1st and 2nd phase islands

The stress-strain paths below initial effective stress, p_o exhibit the elastic behavior following the inclination of recompression index, κ and the stress-strain paths in the region surpassing p_o exhibit the elasto-viscoplastic behavior depending upon the strain rate mainly controlled by the rate of dissipation of excess pore water pressure in the present study. The stress-strain paths show the similar behavior at the monitoring point 1. For the upper Pleistocene clay layers such as Dtc, Ma12 and 11, the stress-strain curves exhibit typical overshoot performance as usually seen for normally consolidated clays because of the low initial stress, p_o and steady dissipation of excess pore water pressure. On the other hand, in the middle Pleistocene clay layers such as Ma10, 9 and Doc5&Ma8, the viscoplastic overshoot takes place in the quasi-overconsolidated region less than p_c and then the time-dependent behavior associated with insufficient dissipation of excess pore water pressure is predominant even in the quasi-overconsolidated region. The stress strain paths for the lower Pleistocene clays, Ma7 and 6 also exhibit the both characteristics of the normally consolidated and quasi-overconsolidated clays, similar to that at the monitoring point 1. However, after surpassing $p_{c,}$ the time-dependent behavior associated with insufficient dissipation of excess pore water pressure is predominant in the normally consolidated region.

5.4.4 Compression of the Pleistocene clay layers

Calculated compression-time relations for the individual Pleistocene clay layers are shown in Fig. 5.13 together with the corresponding measured data from the start of reclamation for the 2nd phase island at the monitoring point 2. As seen in Fig. 5.5 and 5.10, the mode of the calculated excess pore water pressure dissipation is similar to each other for both the monitoring point 1 and 2 because the same values for permeability of sand gravel layers are applied for the present numerical analysis. Therefore, the mode of the calculated compression is also similar to that at the monitoring point 1 until before occurrence of the interactive behavior due to construction of the 2nd phase island. However, because the rate of excess pore water pressure dissipation at the monitoring point 2 is slower than the one at the monitoring point 1 due to decrease in thickness of sand gravel layers toward offshore, the rate of compression may be also slower compared to that at the monitoring point 1. As seen in Fig. 5.13, the hyperbolic shape for settlement-time relations is also exhibited with the monotonic dissipation of excess pore water pressure for Dtc, Ma12 and 11. However, the primary consolidation is not completed for a short time but lasted for a long time with steady dissipation of excess pore water pressure. As shown in Fig. 5.12, in the middle and lower Pleistocene clay layers, the time dependent behavior is predominant. Although in the Ma6 layer, the behavior of normally consolidated clay is exhibited by surpassing $p_{c,}$ in the early stage, because the rate of excess pore water pressure dissipation is getting low with the lapse of time, the time dependent behavior is also predominant. Therefore, the compression curves in the middle and lower Pleistocene clay layers exhibit not hyperbolic shape but continuously increasing shape with the lapse of time.

It is noteworthy that although the calculated excess pore water pressure underestimates the measured values for the all individual Pleistocene layers, the calculated performance for the compression can well describe the measured values. Because the condition of effective stress remains in the quasi-overconsolidated region for a long time due to decrease in initial effective

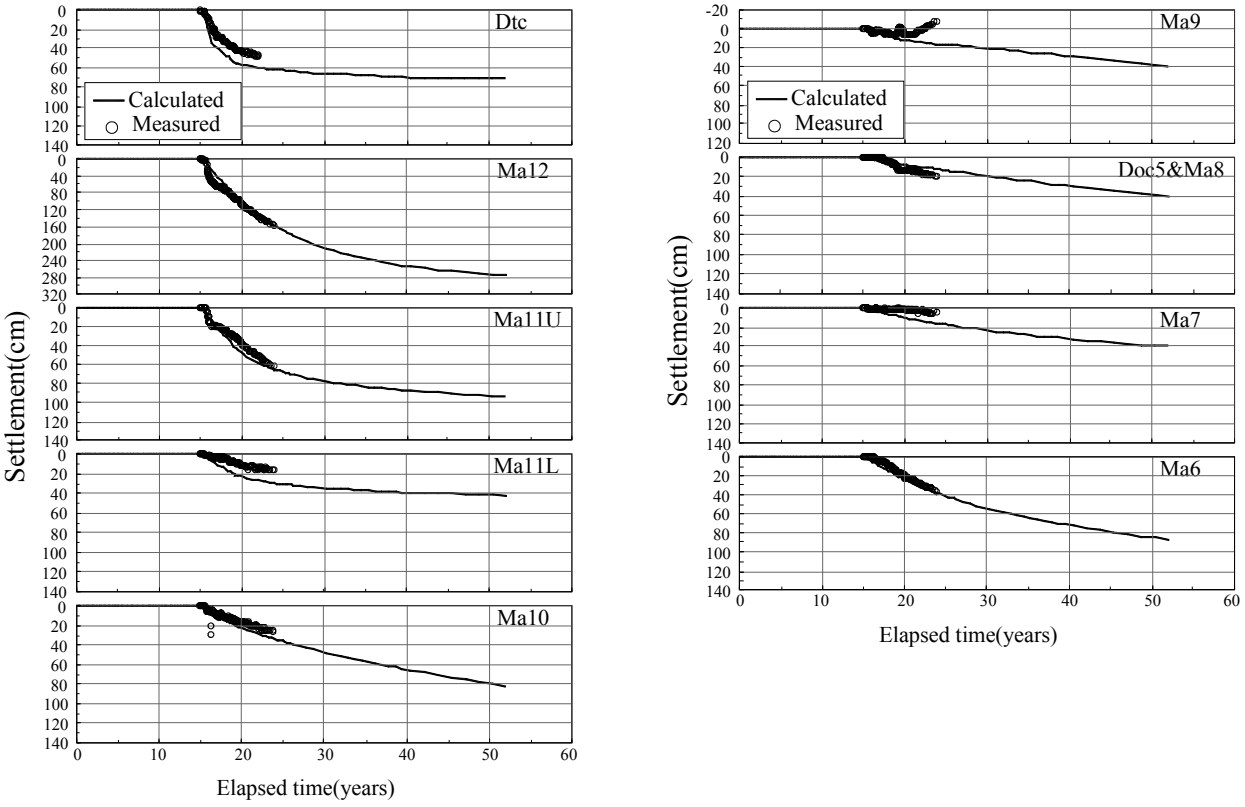

Fig. 5.13 Comparison of measured and predicted settlement for the Pleistocene clay layers at the monitoring point 2 in terms of construction of the 1st and 2nd phase islands

stress $p_{o,}$ generally, the rate of compression is slow and the time dependent compression is predominant in the calculated performance. In the present numerical analysis, the time dependent compression is calculated by expressing the relaxation stress irrespective of the dissipation of excess pore water pressure. Therefore, it is found that although the performance of excess pore water pressure slightly underestimates the measured values, the calculated compression well describes the measured values with the present numerical procedure.

5.5 Summary

The long-term behavior including the interactive behavior due to construction of the adjacent both islands at the Pleistocene marine foundation integrating the 1st and 2nd phase islands of the Kansai International Airport was numerically evaluated using the elasto-viscoplastic finite element method. The original marine foundation was modeled as to have continuous, horizontally even layers with constant thickness independently for the 1st and 2nd phase islands. The stratigraphy at the monitoring points on the 1st and 2nd phase islands was regarded as the representatives for the corresponding foundations. The foundation between both islands is simply modeled by linearly connecting the corresponding layers of the foundations of the 1st and 2nd phase islands.

It is natural that a large excess pore water pressure generated in the Pleistocene clay layers but the emphasis should be focused on the fact that even in the permeable Pleistocene sand gravel layers a large amount of excess pore water pressure was kept undissipated for a long time. Although the upper Pleistocene clay layers underwent the plastic yielding due to reclamation load in a short time, the excess pore water pressure dissipated steadily in these layers because of the existence of highly permeable sand gravel layers (Ds1 and 3) in the vicinity. In contrast, the state of stresses of the middle Pleistocene clays for the foundations of both islands remained in the quasi-overconsolidated region at the completion of the construction of the 1st and 2nd phase islands respectively. Due to the insufficient dissipation of excess pore water pressure caused by the poor permeability of the Pleistocene sand gravel layers in this region, it took a long time for the middle Pleistocene clay layers to become normally consolidated with delayed dissipation of excess pore water pressure.

The calculated stress strain relations in terms of e-log$p$ for the representative elements of the individual Pleistocene clay layers exhibited the characteristic time dependent behavior with

stress overshoot and secondary compression. The mode of compression was strongly influenced by the strain rate of the Pleistocene clays that was controlled by the rate of excess pore water dissipation. In the upper Pleistocene clay layers, typical consolidation associated with excess pore water dissipation took place because the adjoining Pleistocene sand gravel layers with high Permeability such as Ds1, 3 and 5 promoted drainage from the Pleistocene clay layers. In contrast, remarkable compression with low strain rates continued in the middle Pleistocene clay layers with scarce dissipation of excess pore water pressure because of the poor permeability of the adjoining sand gravel layers such as Ds6 and 7. The behavior taking place in the middle Pleistocene clay layers is difficult to be described without the compression model for the quasi-overconsolidated clays and the concept of mass permeability for the Pleistocene sand gravels.

Due attention should be paid to the fact that the foundations of the 1st and 2nd phase islands were seriously affected each other by the reclamation of the adjacent both islands between 200m. The most characteristic and influential phenomenon was “propagation of excess pore water pressure through the permeable sand gravel layers” in this particular case. Here, at the monitoring point 1 for the 1st phase island, it should be noted that the Pleistocene sand gravel layers with poor permeability such as Ds6 and 7 scarcely functioned to propagate the excess pore water pressure generated due to the construction of the 2nd phase island to the adjacent foundation of the 1st island well because of their poor permeability. On the contrary, the propagation of the excess pore water pressure was remarkable through the Pleistocene sand gravel layers with ordinary permeability such as Ds3 and 5. It was also found that excess pore water pressure did not propagate well through the Pleistocene sand gravel layers with high permeability and sufficient thickness as permeable layer such as Ds1 and 10 because of immediate dissipation in them as has been confirmed in the reclaimed foundations in Osaka Port. The calculated performance at the monitoring point 1 was found to well describe the

generation/dissipation and propagation process of the excess pore water pressure subjected to the construction of the offshore islands of KIX.

At the monitoring point 2 for the 2nd phase island, remarkable decrease in effective stress took place before the start of reclamation for the 2nd phase island due to the effect of propagation of excess pore water pressure from the foundation beneath the 1st reclaimed island by the reclamation of the 1st phase island. It was found that a larger amount of the propagated excess pore water pressure in the middle Pleistocene layers remained undissipated before the start of reclamation for the 2nd phase island compared to the other layers because of the poor permeability of sand gravel layers, Ds6 and 7. Although the calculated performance at the monitoring point 2 slightly underestimated the measured value, it could well describe the tendency of dissipation and propagation process of the excess pore water pressure depending upon the mass permeability of the individual Pleistocene sand gravel layers.

Long-term compression of the Pleistocene clay layers associated with the dissipation and propagation of excess pore water pressure was investigated with the present numerical procedure. Here, at the monitoring point 1 for the 1st phase island, retardation and/or slight upheaval were calculated for the Pleistocene clay layers beneath the 1st phase island caused by the propagation of excess pore water pressure generated due to the construction of the 2nd phase island. In particular, for the upper and lower Pleistocene clay layers such as Ma11, 7 and 6, the phenomenon of unloading occurred due to the decease in effective stress induced by the excess pore water pressure propagated from the foundation beneath the 2nd phase island. The long-term compression in these Pleistocene clay layers at the monitoring point 1 was hence retarded for a certain period. However, following the propagated excess pore water pressure started to dissipate, compressive behavior again occurred accordingly. In the middle Pleistocene clay layers, retarding of compression or upheaval were not significant because the poor permeability of the adjoining sand gravel layers, Ds6 and 7 obstructed the propagation of excess pore water

pressure generated due to construction of the 2nd phase island to the foundation of the 1st phase island.

At the monitoring point 2 for the 2nd phase island, the condition of effective stress remained in the quasi-overconsolidated region for the longer time than it was the initial ground condition because of the decrease in the initial effective stress, p_o before the start of reclamation for the 2nd phase island. The rate of excess pore water pressure dissipation was lower compared to that at the monitoring point 1 because of decrease in thickness of sand gravel layers toward offshore. Therefore, it was found that the rate of compression for the Pleistocene clay layers was also low and time dependent compression with insufficient dissipation of excess pore water pressure was generally predominant.

The calculated performance was found to well describe the overall compression over 24 years for the individual Pleistocene clay layers at the monitoring point 1 and 2 on the 1st and 2nd phase islands respectively.

It is noteworthy that the proposed procedure with the elasto-viscoplastic finite element method was found to be versatile to explain the long-term and interactive behavior associated with propagation of excess pore water pressure due to construction of the adjacent both islands at the Pleistocene marine foundations integrating the 1st and 2nd phase islands of Kansai International Airport.

6. Long-term Behavior of the Reclaimed Pleistocene Deposits Considering the Subsurface Stratigraphy of KIX

6.1 Introduction

The foundation ground model that integrates the foundations beneath the 1st and 2nd phase islands of KIX was proposed to assess the long-term behavior including the interactive one due to construction of the adjacent islands in chapter 5. The calculated performance for the proposed foundation ground model rationally described the behavior of the Pleistocene marine foundations that actually takes place in the field. Although the foundation ground model was modeled independently for the 1st and 2nd phase islands on the basis of the representative subsoil models by the boring information, the inclined foundation with irregular thickness for the Pleistocene deposits was not considered in the proposed foundation ground model in chapter 5. On the basis of the data from elastic wave exploration and in-situ boring logs, Kitada et al. (2011a) and Inoue et al. (2011) reported that the foundations at KIX have the inclined base towards the offing overlain by the Pleistocene deposits with irregular thickness. It is also pointed out that the thickness of the Pleistocene clay layers tends to increase towards the offing. Itoh et al. (2001), Kitada et al. (2011a) and Inoue et al. (2011) also summarized that the Pleistocene sand gravel deposits are not always distributed uniformly and continuously in thickness.

In the present chapter, long-term behavior of the inclined Pleistocene deposits at KIX with irregular thickness due to the adjacent construction of the two airport islands is investigated based on the elasto-viscoplastic finite element analyses. The geologically genuine foundation model that has the inclined base overlain by the inclined Pleistocene deposits with irregular thickness is adopted for the numerical analysis. The assumption of non-elastic behavior in the quasi-overconsolidated region for the Pleistocene clays and the equivalent coefficient of permeability that was evaluated as the representative of mass permeability for the Pleistocene

sand gravel layers in the chapter 4 are also adopted for the numerical analysis. Due attention is paid to the mechanism of the generation/dissipation and propagation of excess pore water pressure by the change of thickness in the permeable Pleistocene sand gravel layers. The mode of excess pore water pressure in the inclined Pleistocene foundation with irregular thickness is significantly discussed by comparing with the performed results for the representative ground model that is introduced as the horizontally even ground foundation with constant thickness in chapter 4. The mode of advance in settlement of the Pleistocene deposits associated with the process of the generation/dissipation and propagation of excess pore water pressure is also carefully discussed.

The concept of "mass permeability" for the Pleistocene sand gravel layers was set for the horizontally even ground foundation by considering the horizontal continuity, the change of thickness horizontally and the degree of fine contents. Then, in the present chapter, the concept of "standard hydraulic gradient" is introduced to evaluate "mass permeability" for the Pleistocene sand gravel layers having the irregular thickness with using the "equivalent coefficient of permeability" introduced as representative of "mass permeability" for the horizontally even ground foundation. The calculated performance is validated by comparing with the in-situ measured results at monitoring point 1 on the 1st phase island.

6.2 Foundation Model Considering the Subsurface Stratigraphy

6.2.1 Geological layer configuration

The alternating deposits beneath KIX have been formed due to sedimentation of clayey soils during transgression and of sandy to gravelly soils during regression on the sinking base of Osaka Bay. The thickness of the individual Pleistocene clay layers generally increases towards the offing caused by the more preferable environment of sufficient depth of the sea. On the other hand, it is true that the Pleistocene sand gravel layers naturally tends to decrease in thickness towards the offing but the mode of distribution of them varies dependent upon the topographical characteristics, such as the location of old river channel, the existence of the ridge and trench and the old river scale etc (Kitada et al, 2011b). On the basis of the data from acoustic and elastic wave explorations and in-situ boring logs, Kitada et al. (2011a) and Inoue et al. (2011) have introduced the geological layer configuration for the representative section where there includes the monitoring point 1 as shown by A-A' in Fig. 6.1. In particular, more than 200 boreholes were surveyed to construct KIX around airport fill and Figure 6.1 shows the location of boreholes surveyed near the A-A' line including the boreholes in the offing.

Figure 6.2 shows the geological layer configuration along the section shown by A-A' with the boring logs. As is mentioned above, the mode of distribution exhibits that the Pleistocene clay layers increase in thickness towards the offing and the sand gravel layers drastically change in thickness horizontally. In particular, the mode of distribution in the Pleistocene sand gravel layers exhibits that the thickness of layer partially disappears and the distribution of thickness is relatively sufficient in Ds1, 3 and 10, whereas in Ds6 and 7, that is insufficient. It is also noteworthy that the geological layer configuration outside the airport island where there is no borehole data is developed by only the acoustic and elastic wave explorations. Therefore, the validity of geological layer configuration is discussed by the reproducibility of the in-situ

measured results through the numerical analysis.

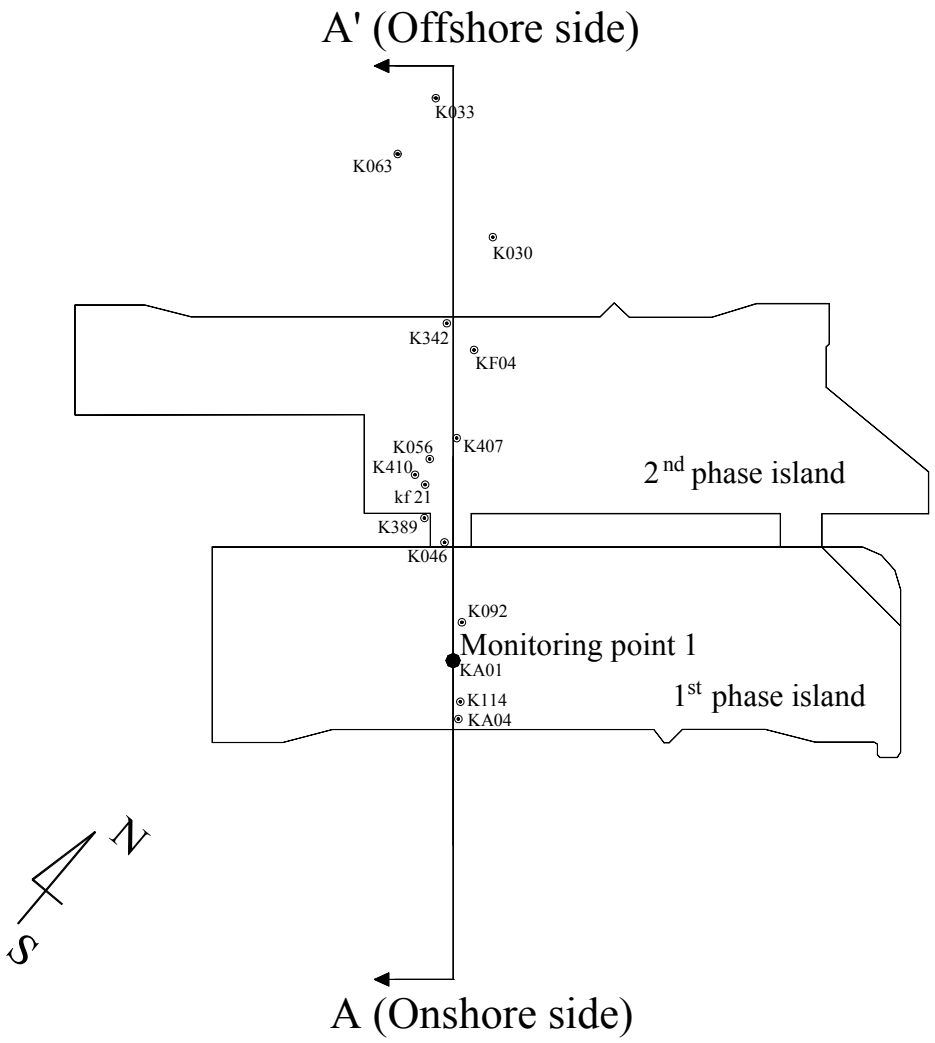

Fig. 6.1 Plan view of the 1st and 2nd phase island of Kansai International Airport and the location of the boreholes

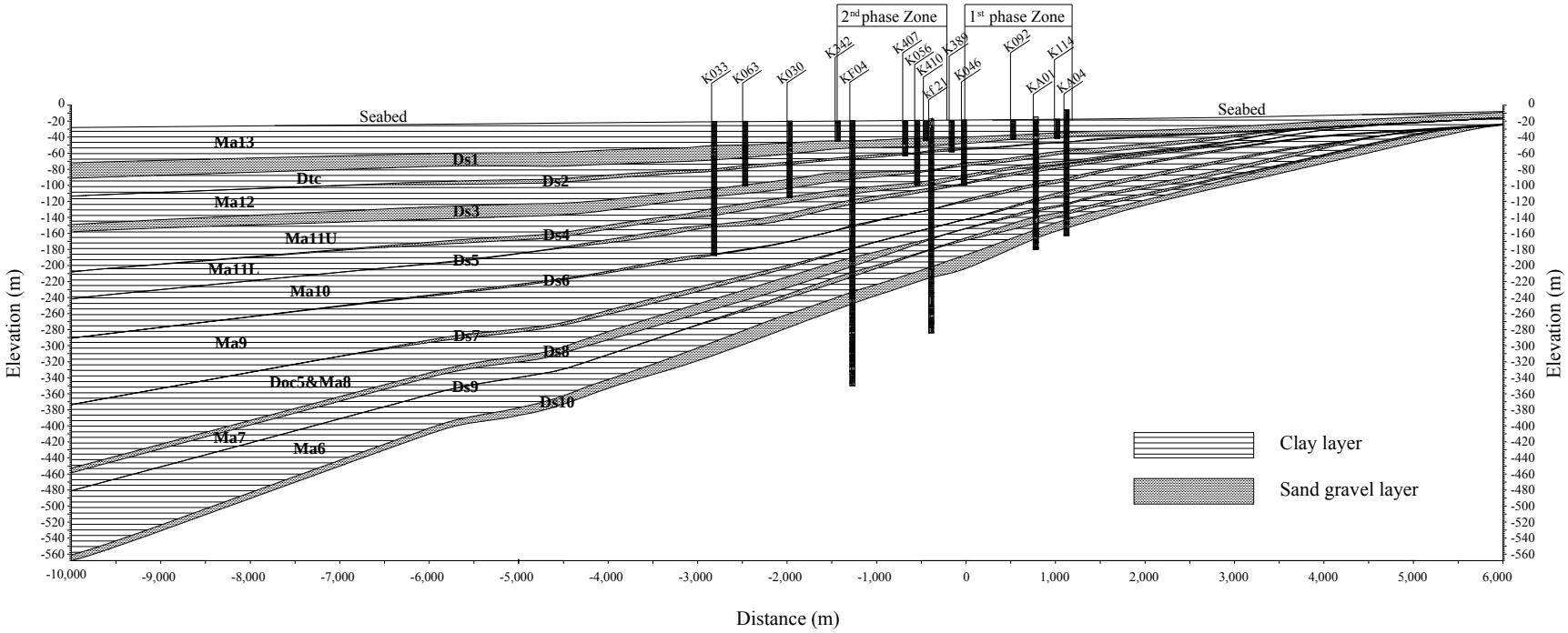

Fig. 6.2 Geological layer configuration along the section in A-A' line with boring logs

6.2.2 Foundation model and framework of numerical assessment

A series of elasto-viscoplastic finite element analyses is performed for geologically genuine foundation model of KIX. Figure 6.3(a) schematically shows the geologically genuine foundation model having the inclined base overlain by the inclined Pleistocene layers with irregular thickness that has been developed based on the completed geological layer configuration as shown in Fig.6.2. Although the distribution of sand gravel layers drastically changes in thickness horizontally, the continuity of the individual layers is still guaranteed even for the geologically genuine foundation model in the present study. The representative ground model proposed in chapter 4 as the horizontally even foundation model with constant thickness based on the monitoring point 1 is shown in Fig. 6.3 (b) with adding the 2^{nd} phase island. The thickness of the individual layers at the monitoring point 1 is exactly the same for the both foundation models.

The effect of the drastic change in thickness for the sand gravel layers in the geologically genuine foundation model is investigated by comparing with the calculated results for the horizontally even ground model. Here, the condition adopted for the finite element analysis except the foundation model, namely, the individual names of the layers, the condition of ground improvement for Ma13 by sand drains, the assumption of the hydraulic boundary, the applied construction sequence and the reclaimed stress of the both islands, is exactly the same that were used in the previous chapter. The used soil parameters are also exactly the same as the representative ones for the foundations of the two islands that are adopted in chapter 5.

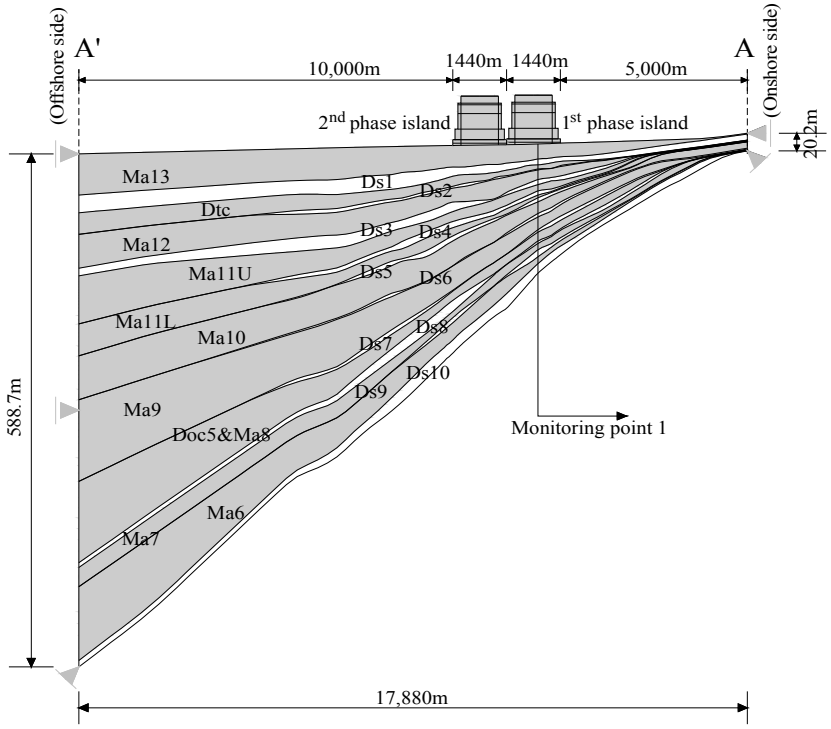

(a) Geologically genuine foundation model

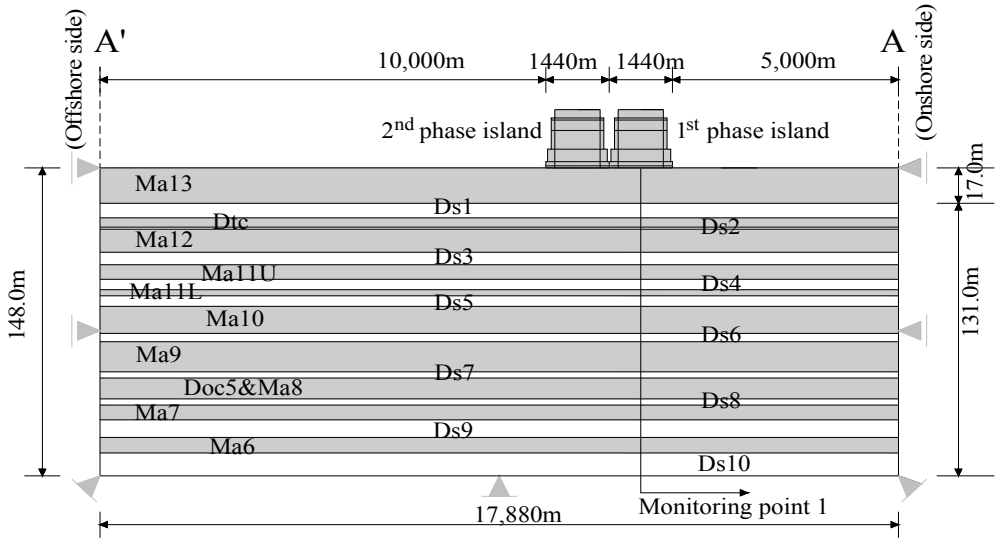

(b) Horizontally even foundation model

Fig. 6.3 Schematic cross-section of the both foundation models for finite element analysis

6.3 Simulation Results and Discussion

6.3.1 Comparison of the calculated distribution of excess pore water pressure.

The calculated distribution of excess pore water pressure at four different times is shown in Fig. 6.4 for the both foundation models. Figure 6.4 (a, b, c, d) denotes the calculated results at the completion of the construction of the 1st phase island (after 5years), before the construction of the 2nd phase island (after 13years), at the completion of the 2nd reclamation (after 19years) and after 50 years since the start of the project respectively. As shown in Fig 6.4, the distribution tendency of excess pore water pressure shows the similarity for the both foundation models. As is explained in the previous chapter 4 and 5, the distribution of them in the foundation is strongly influenced by the permeability of the adjoining sand gravel layers. It should be noted that a large amount of excess pore water pressure at the completion of the 1st and 2nd reclamations generates in the middle Pleistocene layers beneath the corresponding islands and they still remains even after 50years since the start of the project because of the poor permeability of the sand gravel layers, Ds6 and 7. In contrast, the excess pore water pressure in the upper and lower Pleistocene layers, such as Dtc, Ma12, 11, 7, 6 and Ds1, 3, 5, 9, 10 are monotonically dissipated with time because of the high permeability of the sand gravel layers, Ds1, 3 and 10.

As shown in Fig.6.4 (c), it should be noted that the increased excess pore water pressure beneath the foundation of the 2nd phase island due to construction of the 2nd phase island is also propagated to the foundation of the 1st phase island for the geologically genuine foundation model. The propagation of excess pore water pressure is also dependent upon the permeability of the adjoining sand gravel layers. A larger amount of excess pore water pressure in the upper and the lower Pleistocene layers is propagated compared to the one in the middle layers of the foundation beneath the 1st phase island.

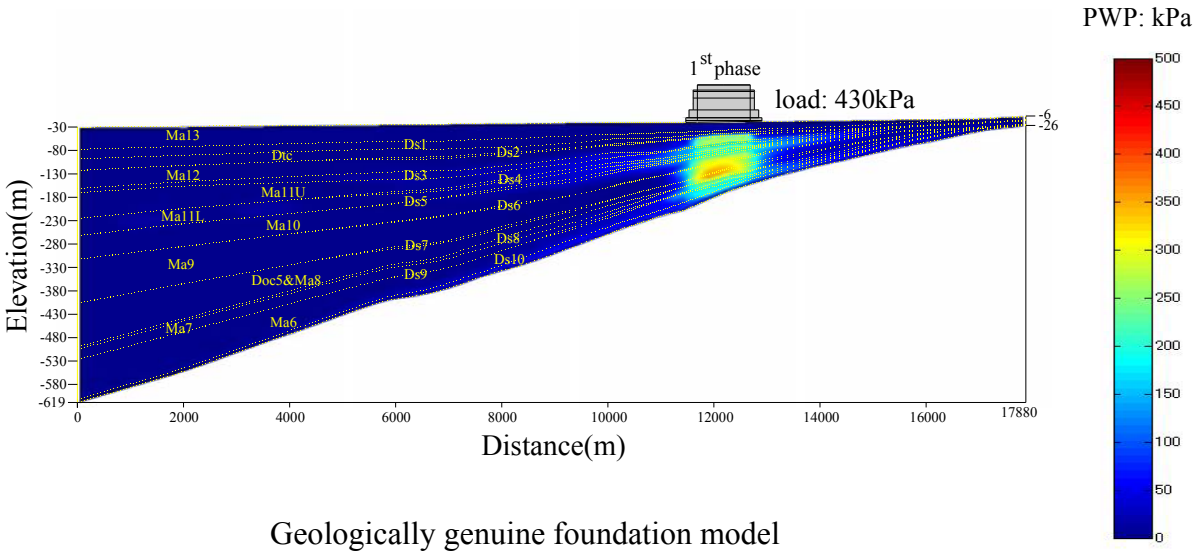

Geologically genuine foundation model

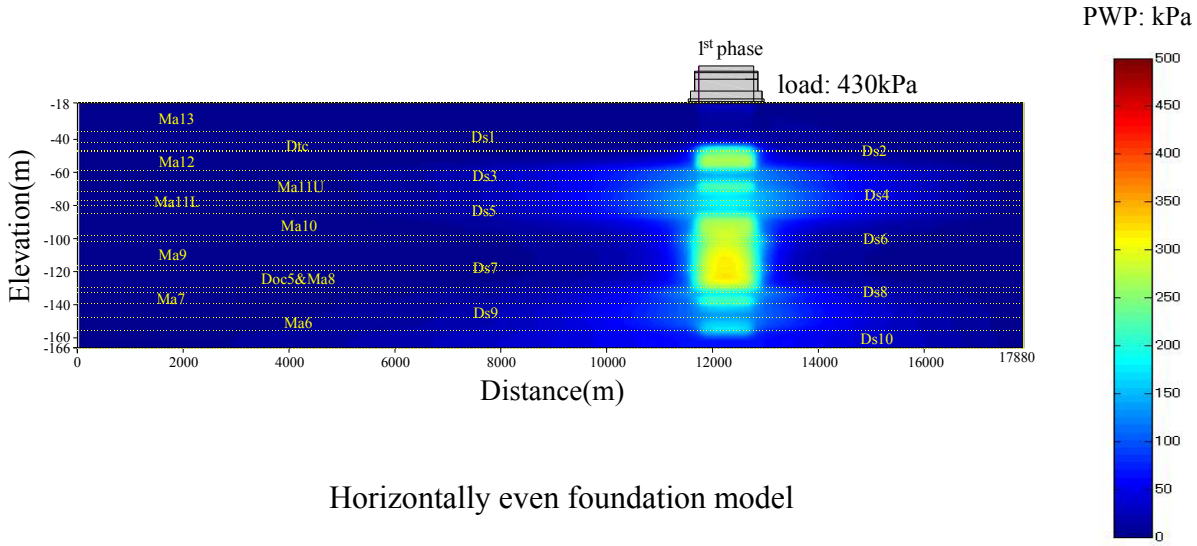

Horizontally even foundation model

(a) at completion of the 1st reclamation (after 5years)

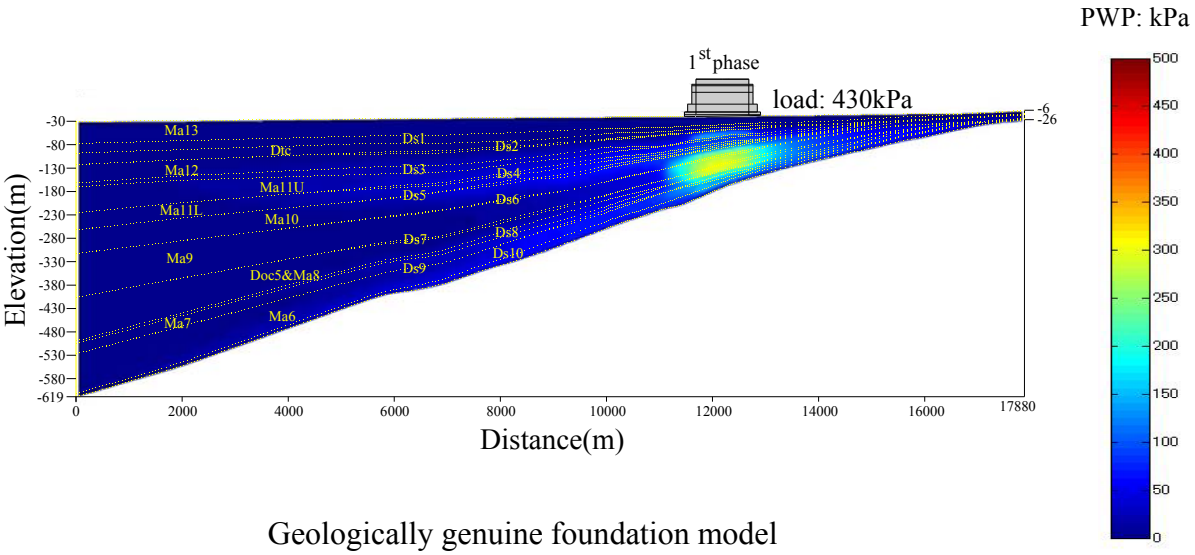

Geologically genuine foundation model

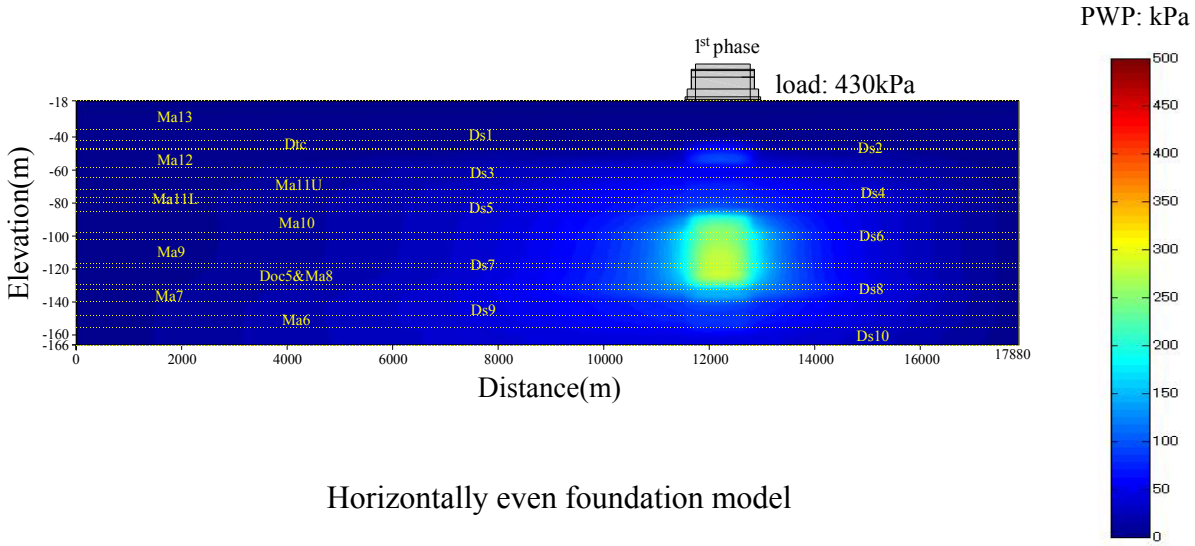

Horizontally even foundation model

(b) before construction of the 2nd reclamation (after 13years)

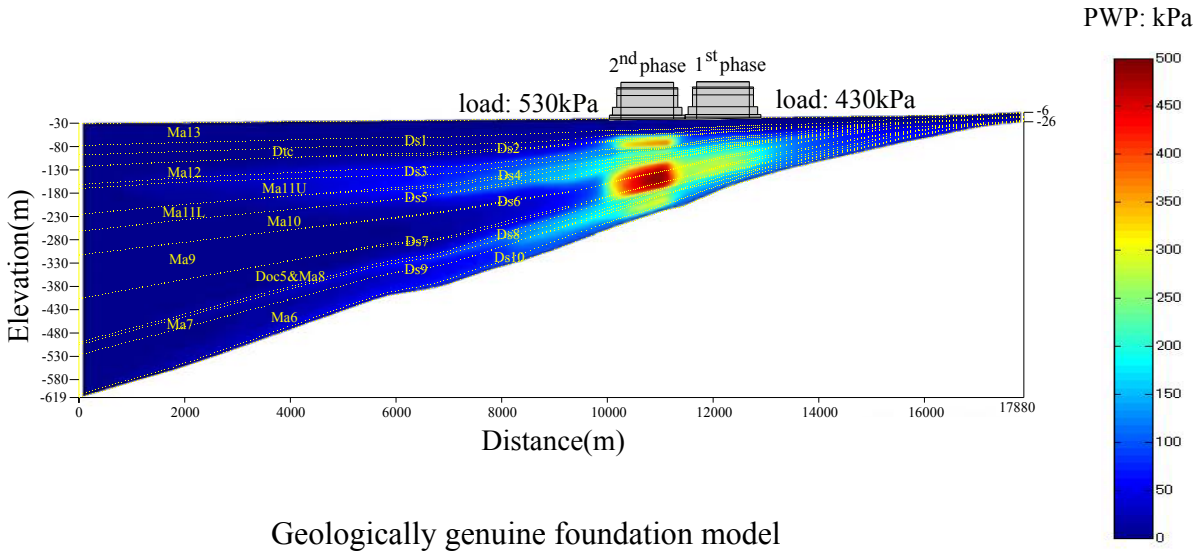

Geologically genuine foundation model

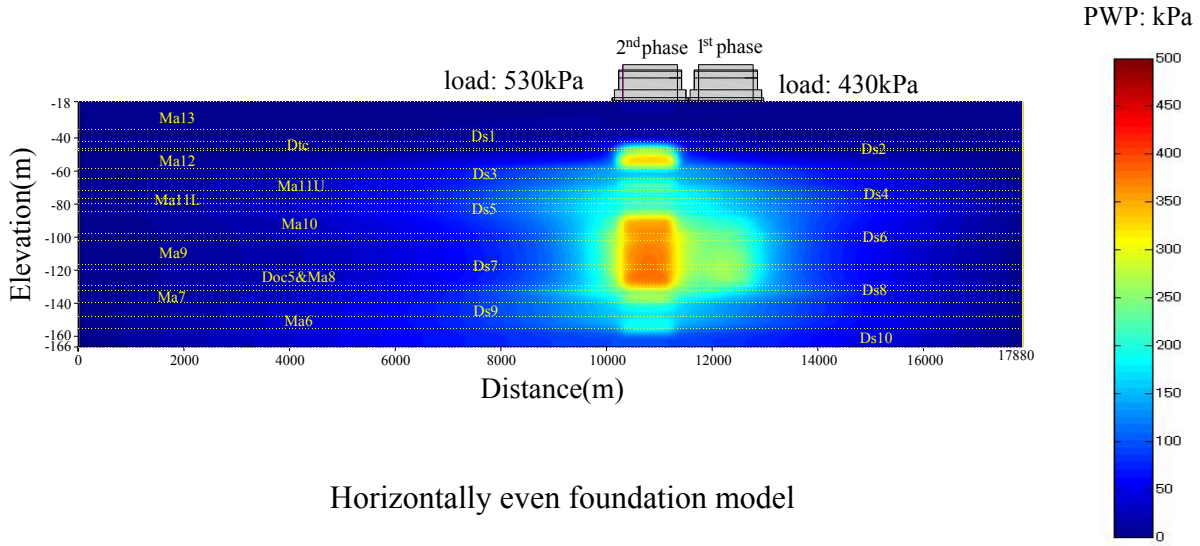

Horizontally even foundation model

(c) at completion of the 2nd reclamation (after 19years)

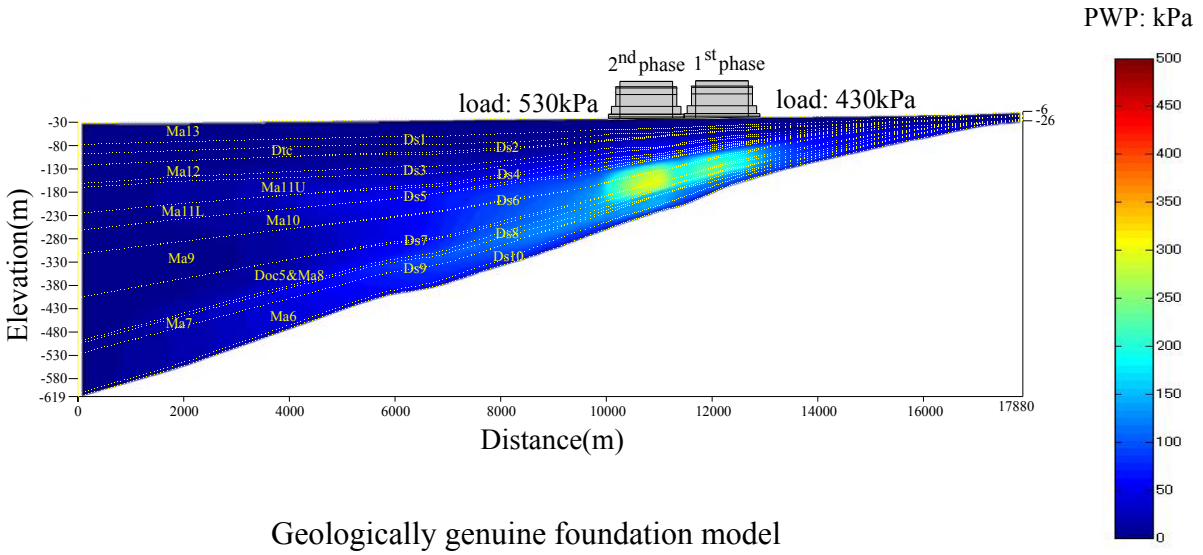

Geologically genuine foundation model

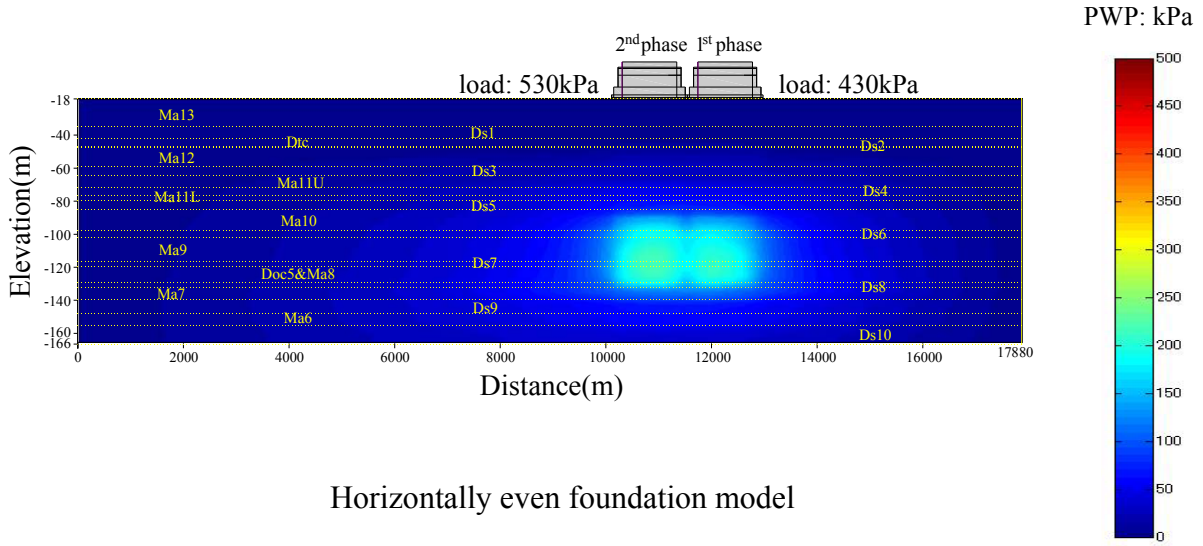

Horizontally even foundation model

(d) after 50years from the start of project

Fig. 6.4 Comparison of calculated contours of excess pore water pressure for the geologically genuine and horizontally even foundation models

The comparison of the two foundation models in Fig 6.4, however, shows that the mode of distribution of excess pore water pressure is dependent upon the permeability as well as the change in thickness of the sand gravel layers. As is shown in Fig 6.4, a larger amount of excess pore water pressure in the geologically genuine foundation model remains undissipated with the lapse of time than that in the horizontally even foundation model at four difference times. In particular, because the thickness of the middle Pleistocene sand gravel layers, such as Ds 4, 5, 6 and 7, drastically decreases towards the offing in the geologically genuine foundation (see Fig 6.3 (a)), this phenomenon is definitely found in the middle Pleistocene layer beneath the 2nd phase island. The decrease in thickness of the permeable Pleistocene sand gravel layers obstructs the smooth dissipation of excess pore water pressure towards the offing. The drastic change in thickness of the sand gravel layers between the both islands also obstructs the propagation of it. It means that the predominant factor for the mechanism of generation/dissipation and propagation of excess pore water pressure is the mode of the distribution in thickness as well as the permeability coefficient of the permeable Pleistocene sand gravel layers.

The calculated horizontal distribution of excess pore water pressure and the distribution in the thickness of the individual Pleistocene sand gravel layers are shown in Fig 6.5 at the time before and after the construction of the 2nd phase island for the both foundation models. The difference between the both foundation models is attributed to the wide-range distribution of the Pleistocene sand gravel layers, such as the drastic change in thickness. The horizontally even foundation model has the horizontally uniform layers with constant thickness, whereas the irregular change in thickness of layers appears for the geologically genuine foundation model. The horizontal distribution of excess pore water pressure in the horizontally even foundation model exhibits the smooth parabolic shape of bilateral symmetry without any constriction of excess pore water pressure with constant thickness of layer. However, in the geologically

genuine foundation, the constricted part of the Pleistocene sand gravel layers obstructs the dissipation of it. A rate of excess pore water pressure dissipation towards the outside of the reclaimed areas is hence very slow. As a result, a larger amount of excess pore water pressure in almost all of the Pleistocene sand gravel layers of geologically genuine foundation model is derived compared to the one of horizontally even foundation model at the time before and after construction of the 2nd phase island.

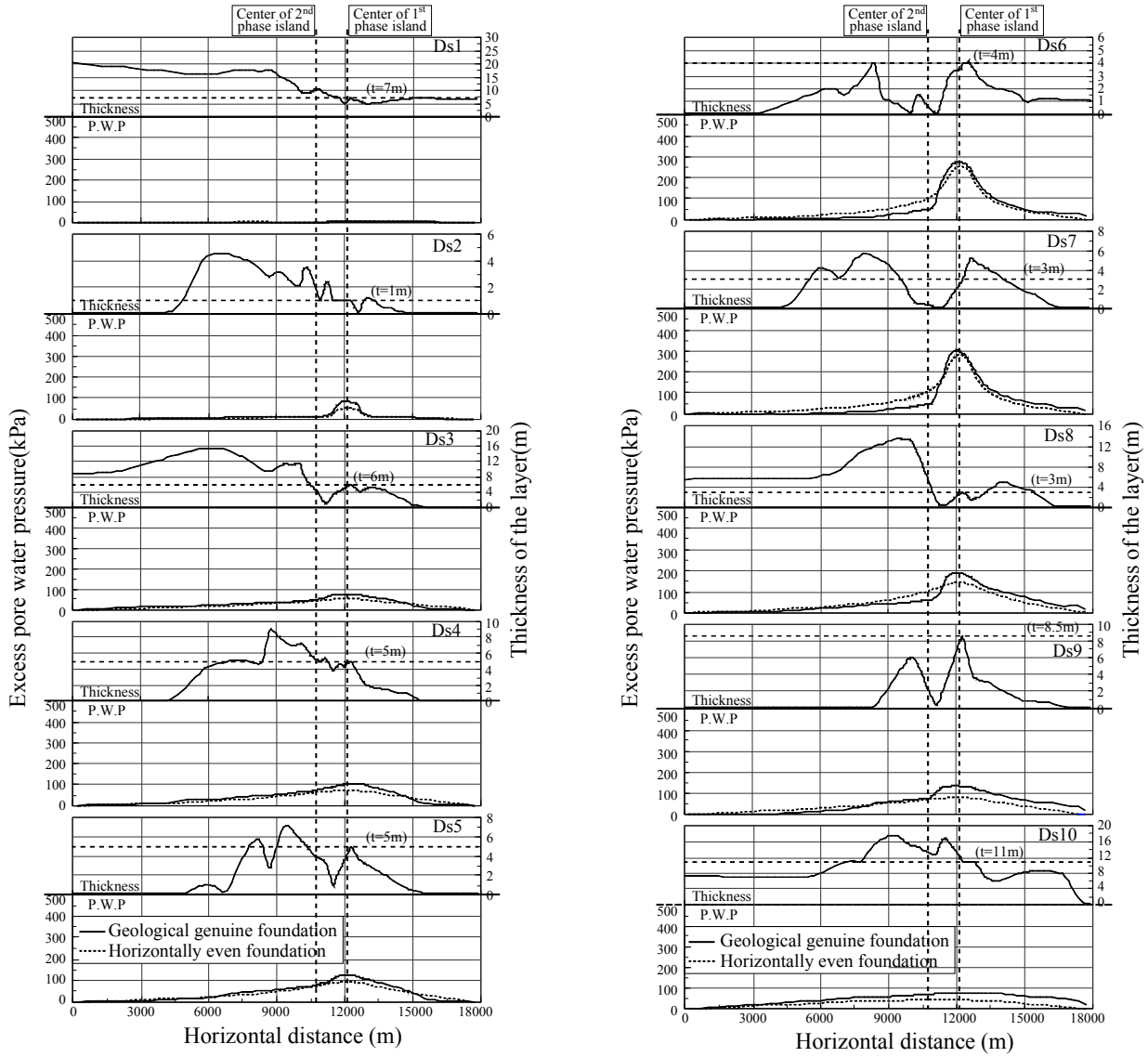

(a) before construction of the 2nd phase reclamation

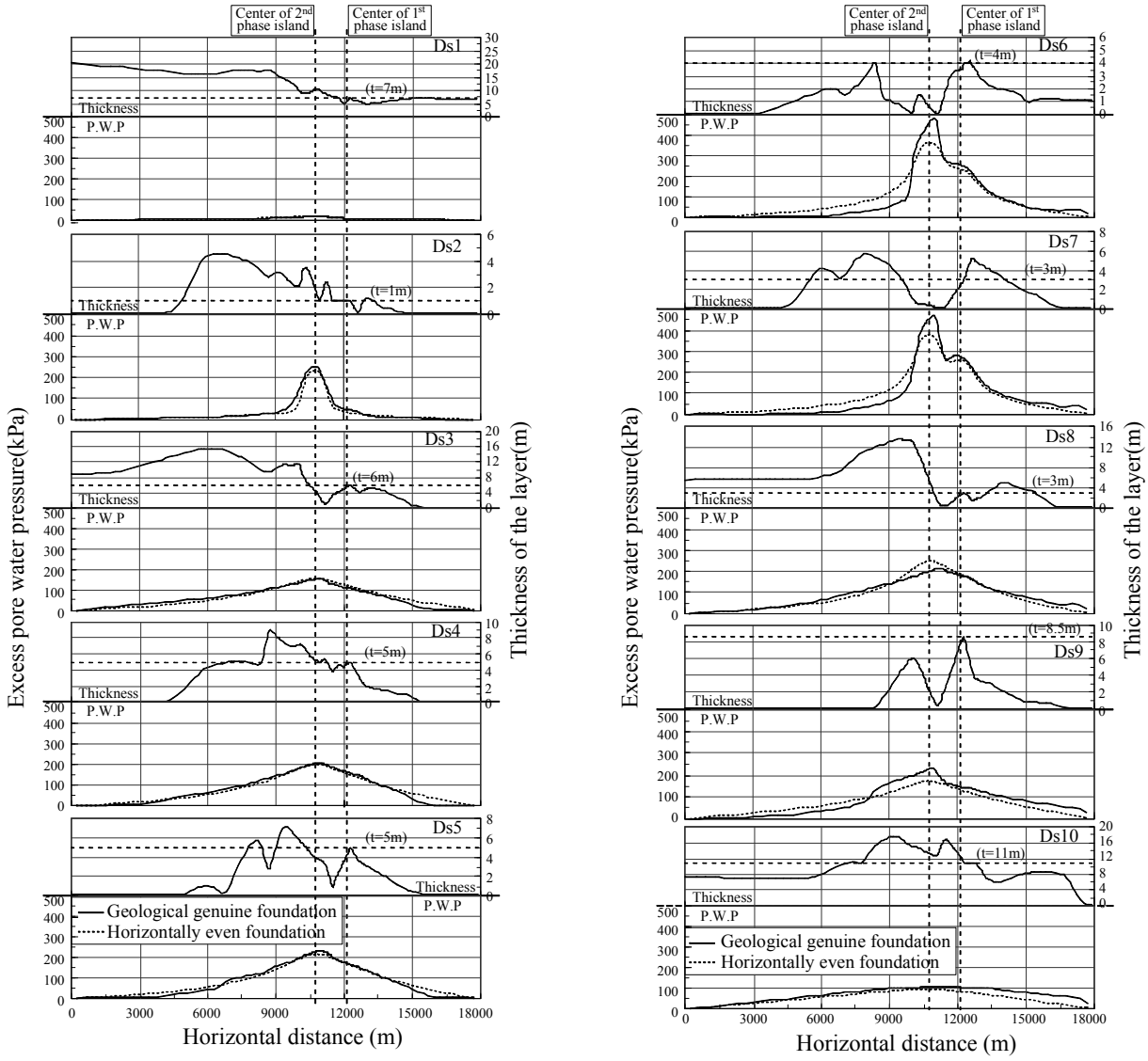

(b) at completion of the 2nd phase reclamation

Fig. 6.5 Comparison of calculated horizontal distribution of excess pore water pressure for the individual Pleistocene sand gravel layers in a horizontal position for the both foundation models

6.3.2 Comparison of the calculated excess pore water pressure-time relations.

Calculated excess pore water pressure - time relations for the both foundation models are shown in Fig. 6.6 together with the measured results for the individual Pleistocene sand gravel layers at the monitoring point 1. The behavior of excess pore water pressure that is dependent upon the permeability of sand gravel layer is identical with that explained in chapter 4 and 5. Here, it is noteworthy that a larger amount of excess pore water pressure generates in the geologically genuine foundation model than that in the horizontally even foundation model at completion of the 1st phase reclamation and a rate of dissipation is also slower in the geologically genuine foundation model. In particular, during the construction of the 2nd phase island, amount of excess pore water pressure propagation is smaller in the geologically genuine foundation model than that in the horizontally even foundation model. That is because the constricted part of the Pleistocene sand gravel layer in the geologically genuine foundation model obstructs the dissipation and propagation of excess pore water pressure as shown in Fig.6.5. Attention should be paid to the fact that the mode of propagation of excess pore water pressure in Ds3, 5 and 10 due to construction of the adjacent 2nd phase island is also well simulated even in the geologically genuine foundation model. Figure 6.7 shows the comparison for the individual Pleistocene clay layers at the monitoring point 1. The process of dissipation and propagation of excess pore water pressure is similar to that of the adjoining Pleistocene sand layers. For the clay layers having the measured results, the calculated results well describe the process of dissipation and propagation of excess pore water pressure even in the geologically genuine foundation model.

In general, the calculated performance for the excess pore water pressure can well describe the measured results not only in the horizontally even foundation model but also in the geologically genuine foundation model with the present numerical procedure. However, the calculated performance for the horizontally even foundation model shows the better prediction

for the measured results than that of the geological genuine foundation model because the equivalent coefficient of permeability was set for the horizontally even foundation model. In order to get better prediction for the geologically genuine foundation model, the new concept and procedure to define "mass permeability" for the Pleistocene sand gravel layers having the changing thickness of layers is required.

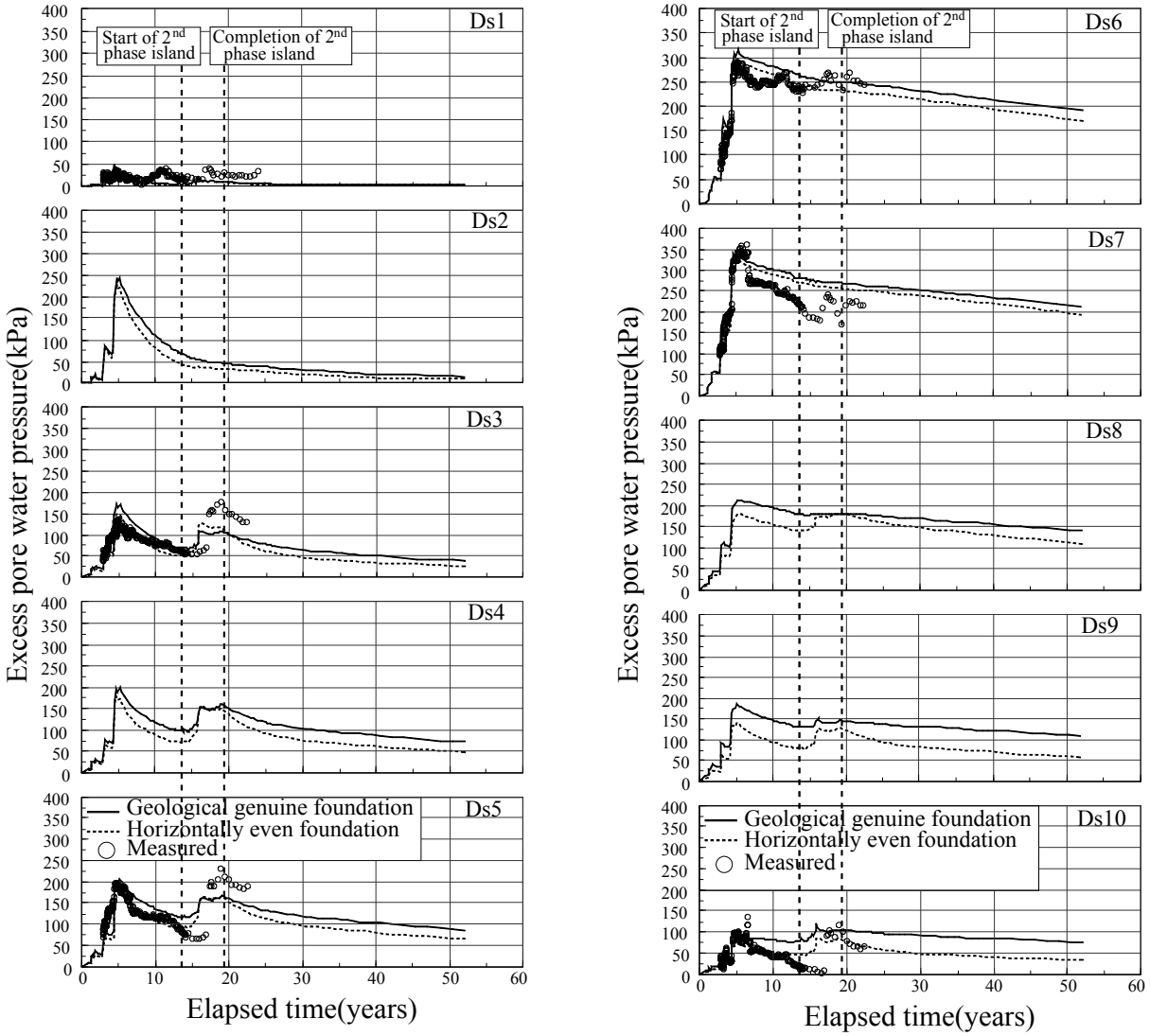

Fig. 6.6 Comparison of calculated excess pore water pressure-time relations in the both foundation models with measured results for the individual Pleistocene sand gravel layers at the monitoring point 1

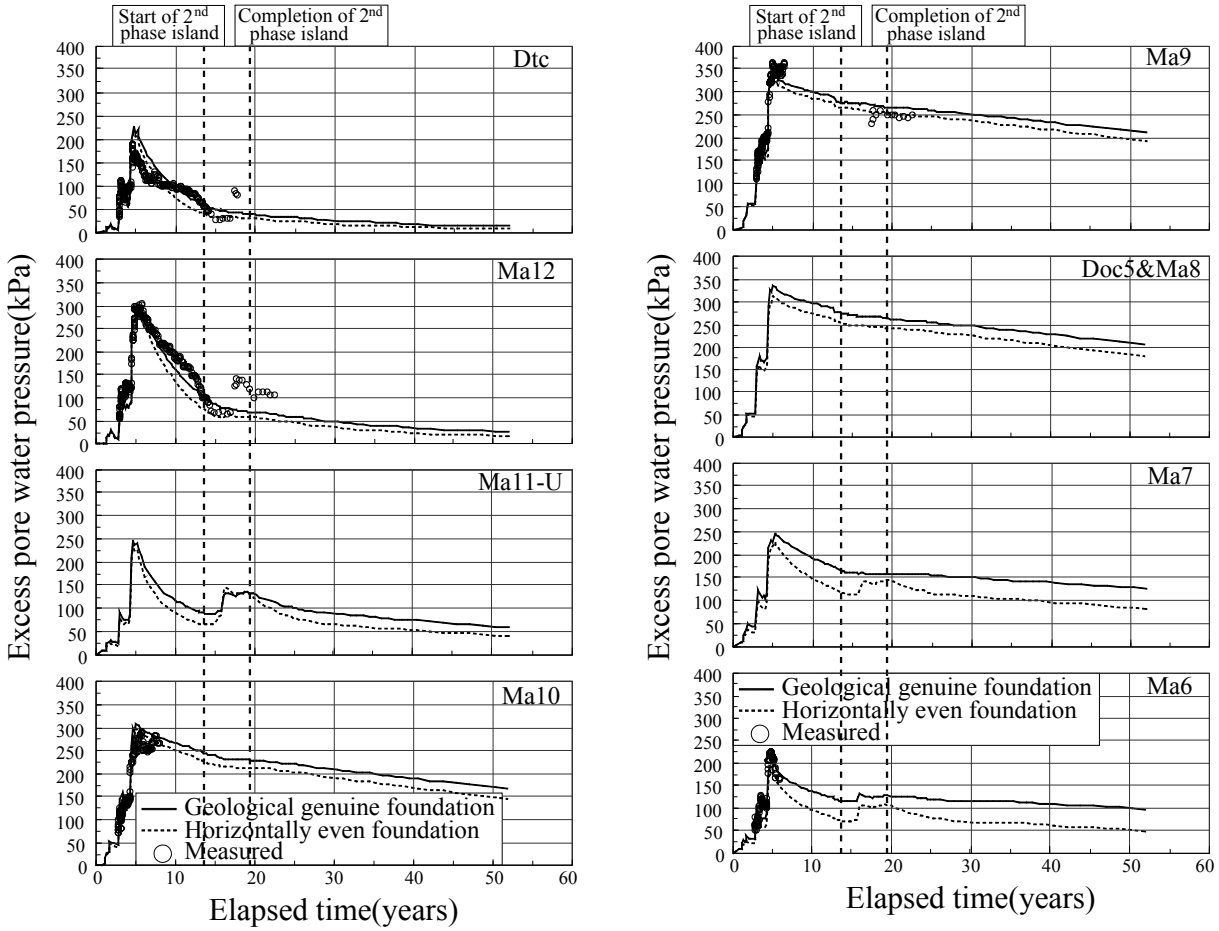

Fig. 6.7 Comparison of the calculated excess pore water pressure-time relations in the both foundation models with measured results for the individual Pleistocene clay layers at the monitoring point 1

6.3.3 Comparison of the calculated compression - time relations of the Pleistocene clay layers

The calculated long-term settlement associated with the dissipation and propagation of excess pore water pressure is shown for the both foundation models in Fig.6.8 together with the measured results at monitoring point 1. The behavior of long-term settlement that is dependent upon the rate of excess pore water pressure dissipation for the individual Pleistocene clay layers is also identical to that is explained in chapter 4 and 5. As is shown in Figs. 6.6 and 6.7, when the amount of excess pore water pressure propagation increases or the dissipation of it is hindered due to construction of the 2nd phase island, the settlement is also retarded or slight upheaval can happen for the both foundation models (see Fig. 6.8). It is also found that because a rate of excess pore water pressure dissipation in the geologically genuine foundation model is slower than that of the horizontally even foundation model, the rate of settlement for the geological genuine foundation model is also slower than that for the horizontally even foundation model. Attention should be paid to the fact that the mode of long-term settlement after completion of the 2nd phase island exhibits a similar tendency for the both foundation models.

The calculated performance including the interactive behavior due to construction of the adjacent 2nd phase island can well describe the measured results not only in the horizontally even foundation model but also in the geologically genuine foundation model. However, the performed results for the horizontally even foundation model also show better prediction for the measured results

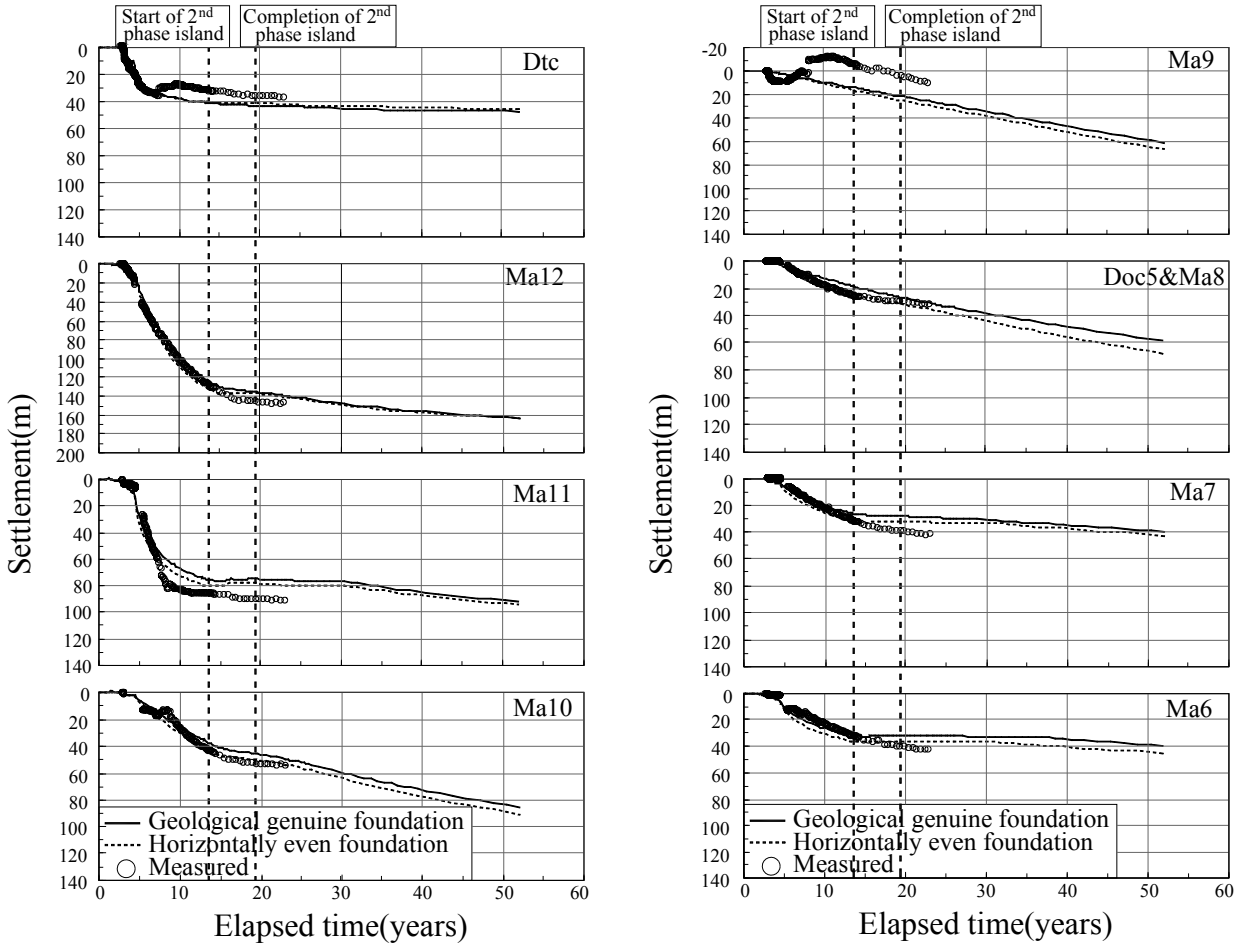

Fig. 6.8 Comparison of the calculated compression – time relations in the both foundation models with measured results for the individual Pleistocene clay layers at the monitoring point 1

6.4 Effect on the Thickness in the Permeable Sand Gravel Layers near the Boundary for the Finite Element Analysis

6.4.1 Outline of Numerical analysis

Figure 6.9 shows the enlarged description of the mesh near the onshore boundary. As is already mentioned in the previous section, when the distance to the boundary is set to be about 10 times of the loading area, the effect of the hydraulic boundary condition can be ruled out (Mimura and Jang, 2005b). In the present study, however, the distance towards the onshore side can not be set to be 10 times of the loading area because that is actually 5km from the main land. The hydraulic boundary condition of the onshore side is hence expected to affect the behavior of excess pore water pressure. The lateral hydraulic boundary was set to be that the clay layers are assumed to be undrained while the sand gravel layers are assumed to be fully drained. However, as is shown in Fig. 6.5, it is found that although the hydraulic boundary condition of the sand gravel layers is set to be fully drained, the excess pore water pressure near the boundary on the onshore side has not yet fully dissipated from Ds6 to Ds10 layers in the geologically genuine foundation model. Due to the insufficient function as the permeable sand gravel layers near the boundary surface, the overall calculated performance towards the onshore side in the geologically genuine foundation model is overestimated compared to that of the horizontally even foundation model. The effect of boundary condition in the horizontally even foundation model can be ignored because of their sufficient thickness as permeable layers, while the effect of that in the geologically genuine foundation model can not be ignored because of the drastic constriction of the permeable sand gravel layers as shown in Fig.6.9.

As is shown in Fig.6.9, the permeable sand gravel layers near the boundary on the onshore side are divided into two groups by the clay layer, Ma10. Because the thickness of layers near boundary surface becomes seriously thin, the layers near boundary surface behave as if they are one continuous layer. The permeable behavior of the groups from Ds1 to Ds5 and Ds6 to Ds10

is mainly controlled by the sand gravel layers Ds1 and Ds10 respectively that have sufficient permeability. As is shown Fig. 6.5, from Ds1 to Ds5, the behavior of excess pore water pressure near the boundary surface exhibits that the excess pore water pressure is almost dissipated because the sand gravel layer Ds1 sufficiently functions as a permeable layer with a sufficient thickness. In contrast, the second group from Ds6 to Ds10 does not function as a permeable layer mainly because the responsible layer Ds10 has an insufficient thickness.

In this section, the effect of the hydraulic boundary condition due to the variation in thickness of the permeable sand gravel layers near the boundary on the onshore side is investigated by changing the thickness in Ds10 layer near boundary surface. The calculated results for the modified foundation model with the geological knowledge are compared with the ones for the original foundation model that has the constriction for Ds10 near the boundary as well as the ones for the horizontally even foundation model.

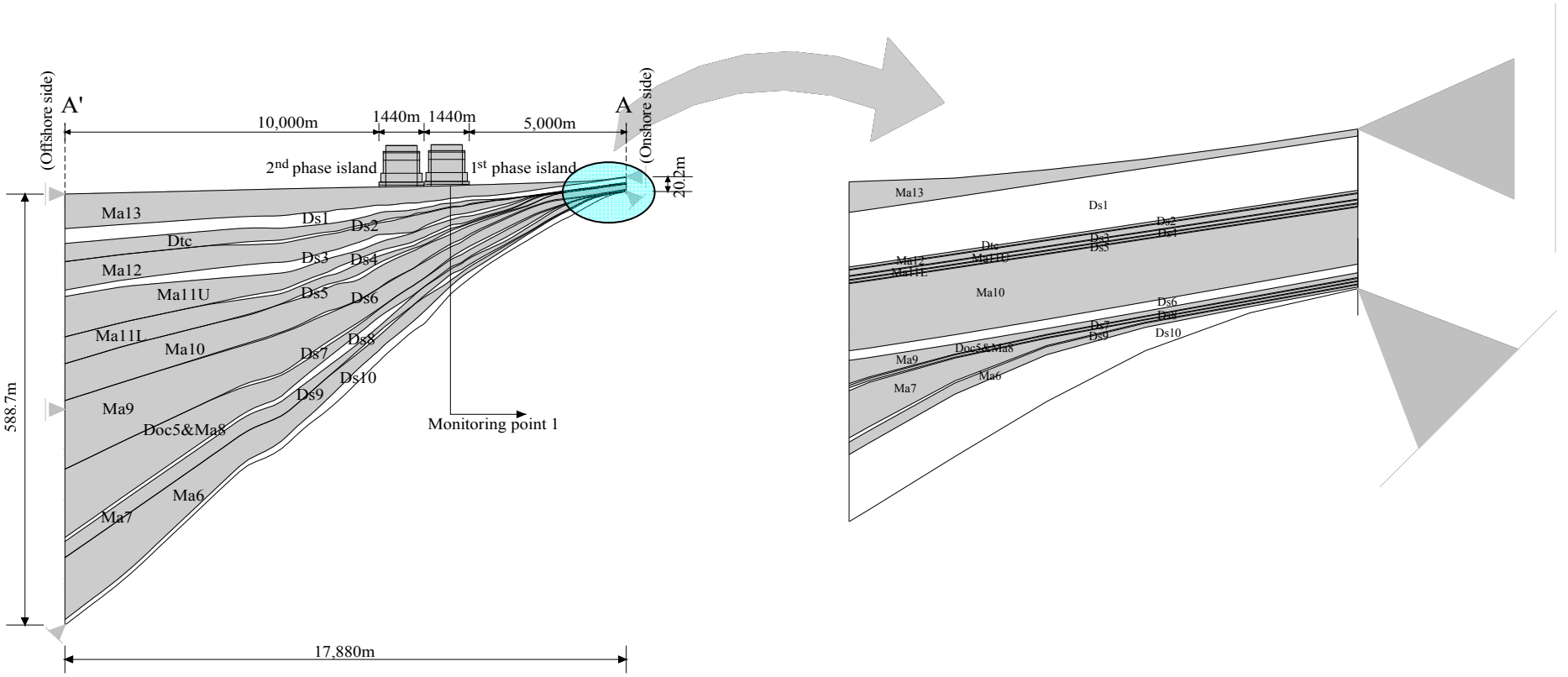

Fig. 6.9 Distribution of the thickness in layers near the boundary on the onshore side

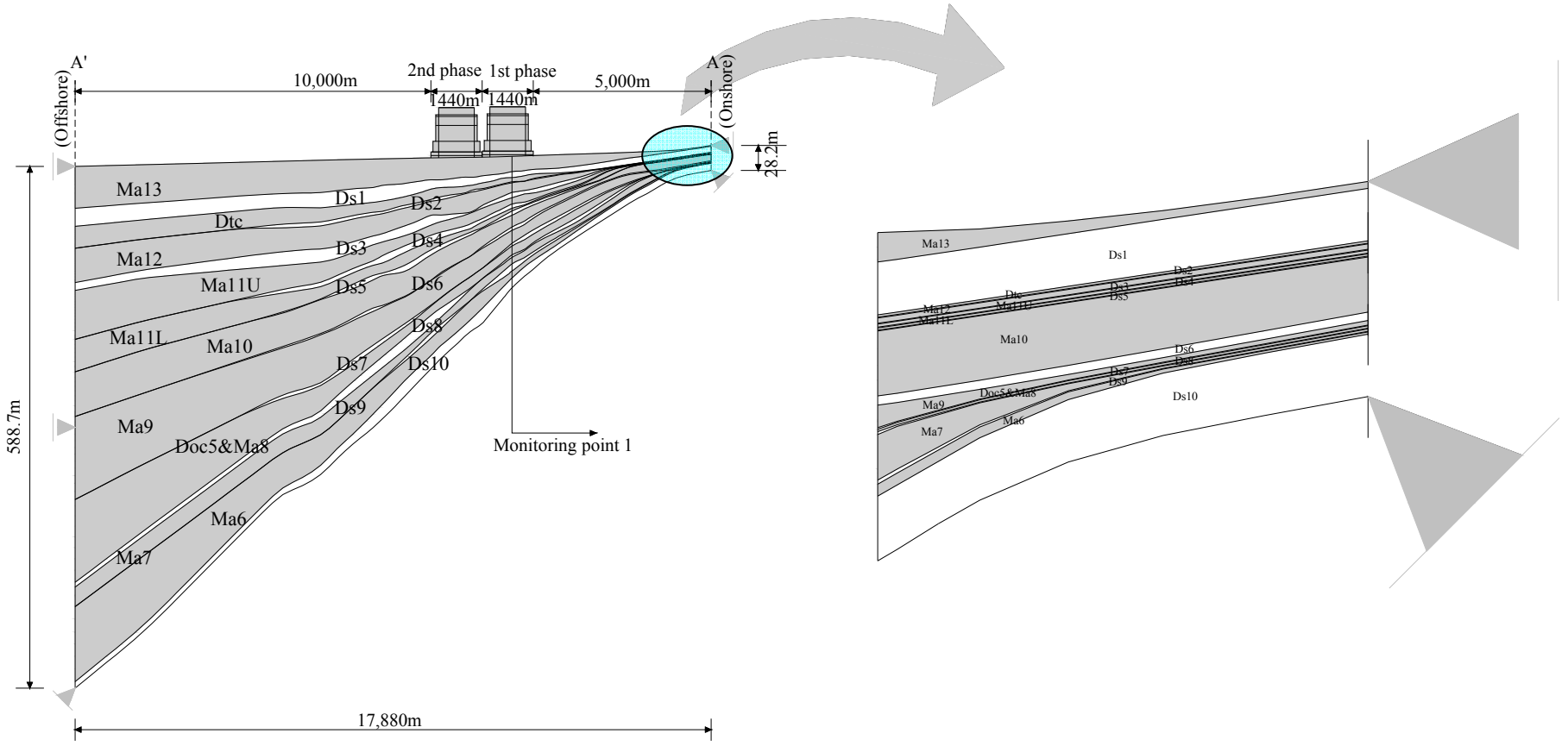

Fig. 6.10 Modified foundation model for the thickness of Ds10 layer near the boundary on the onshore side

6.4.2 Modified foundation model near the boundary on the onshore side

Figure 6.10 shows the modified foundation model for the thickness of Ds10 layer near the boundary on the onshore side. As is mentioned above, the existence of the constriction for Ds10 near the boundary on the onshore side affects the overall behavior of excess pore water pressure. It is noteworthy that the subsurface model near the boundary on the onshore side was developed only on the basis of the acoustic exploration because there is no boring data. Because during the process of development of the subsoil model, the overlain layers cover up the underlain layers near the boundary, the bottom layer, Ds10 has to be trapped completely. The area close to the onshore boundary should however become a coarser deposit because of the effect of rivers. Based on this finding, the hydraulic boundary of the second group from Ds6 to Ds10 is set to be drained by enlarging the thickness of Ds10 for the modified foundation model.

6.4.3 Comparison of the calculated results and discussion

The calculated horizontal distribution of excess pore water pressure and the distribution of the thickness in the individual Pleistocene sand gravel layers are shown in Fig. 6.11 at the time before and after the construction of the 2^{nd} phase island for the geologically genuine foundation model before and after modification of the onshore hydraulic boundary condition, and the horizontally even foundation model respectively. As shown in the hatched area of Fig.6.11, it is confirmed that the effect of the hydraulic boundary condition due to the drastic constriction of the permeable layers was ruled out in the modified foundation model from Ds6 to Ds10 by increasing in thickness of Ds10 near the boundary on the onshore side. It is also found that the excess pore water pressure near the boundary on the onshore side is almost dissipated with the hydraulic boundary condition to be fully drained in the modified foundation model, similar to the calculated results for the horizontally even foundation model.

Figures 6.12 and 6.13 show the calculated excess pore water pressure - time relations for the three foundation models together with the measured results for the individual Pleistocene sand gravel and clay layers at the monitoring point 1. It is also found that the rate of excess pore water pressure dissipation in the modified foundation model from Ds8 to Ds10 for the sand gravel layers and from Doc5&Ma8 to Ma6 for the clay layers becomes a little faster compared to the results before modification of the foundation model due to increase in thickness of Ds10. Due to this effect, it is found that the rate of settlement advances a little faster in the modified foundation model from Doc5&Ma8 to Ma6 (see Fig. 6.14). Although the effect of the hydraulic boundary due to drastic constriction of the permeable layer is ruled out by modifying the thickness in the permeable layer near the boundary on the onshore side, the rate of excess pore water pressure dissipation and the settlement in the geologically genuine foundation model is still slower than that of the horizontally even foundation model because the net thickness of the individual sand gravel layers for the geologically genuine foundation model is still much smaller compared to that for the horizontally even foundation model.

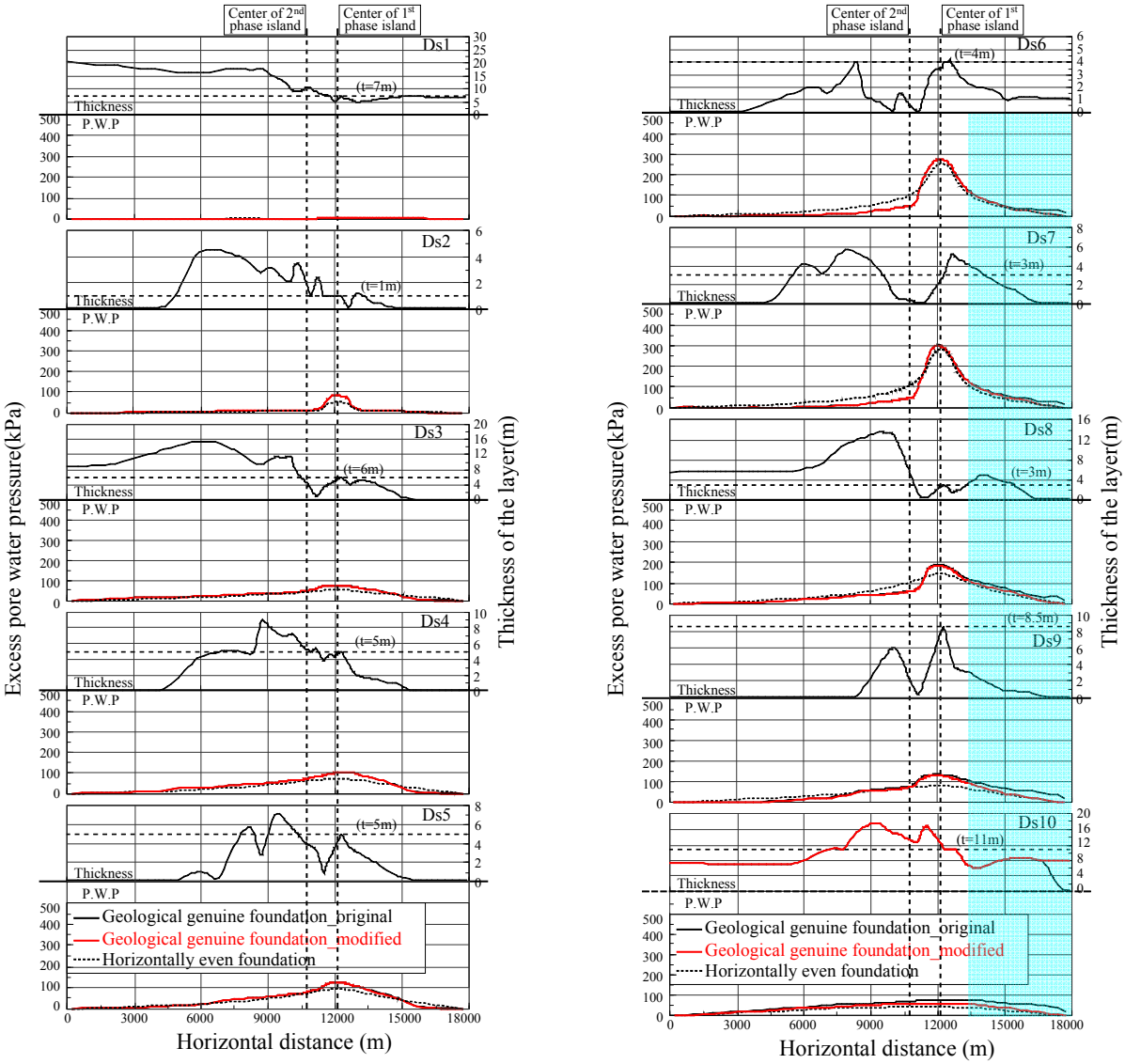

(a) before construction of the 2nd phase reclamation

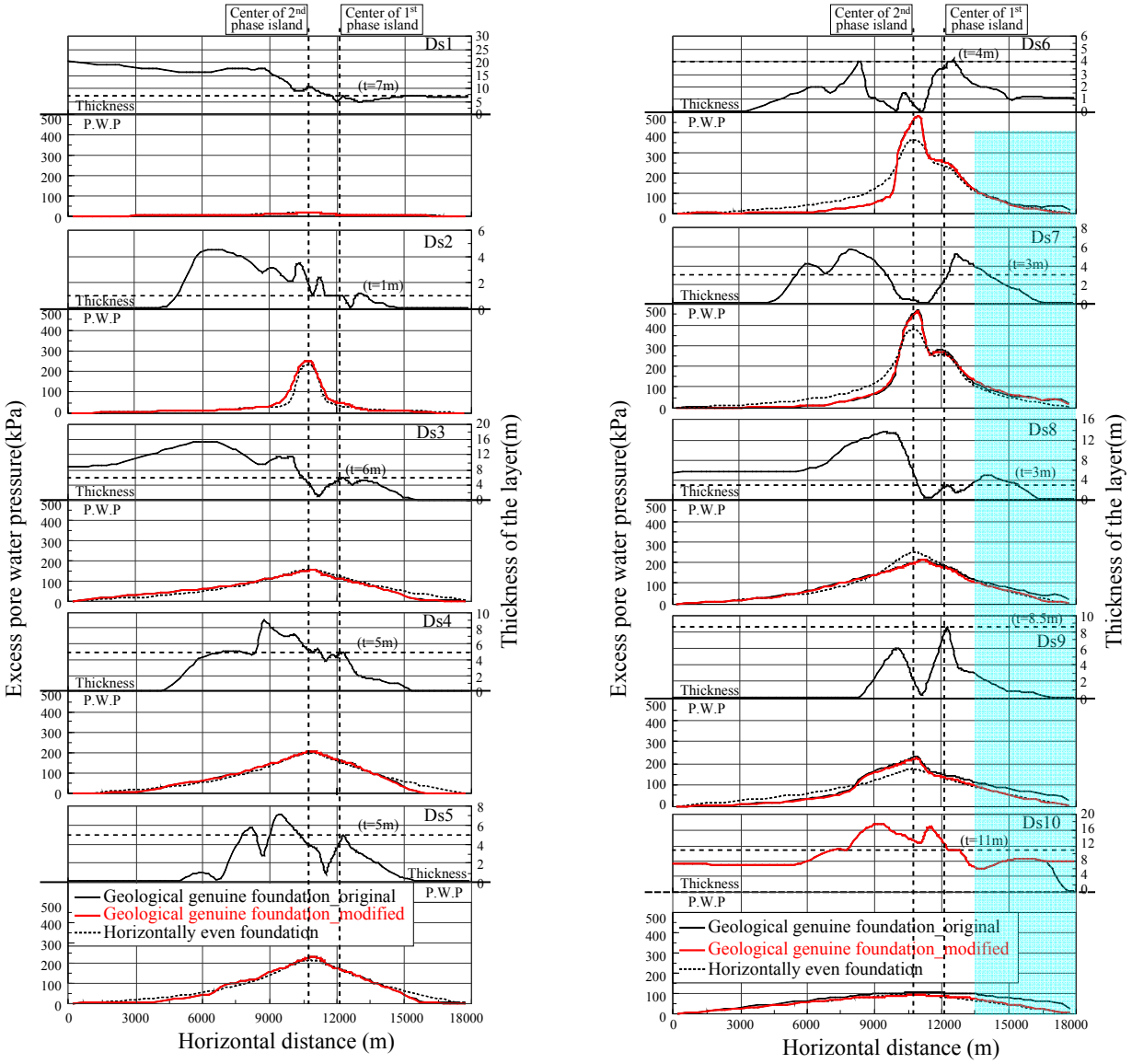

(b) at completion of the 2nd phase reclamation

Fig. 6.11 Comparison of calculated horizontal distribution of excess pore water pressure for the individual Pleistocene sand gravel layers in a horizontal position for the modified foundation model

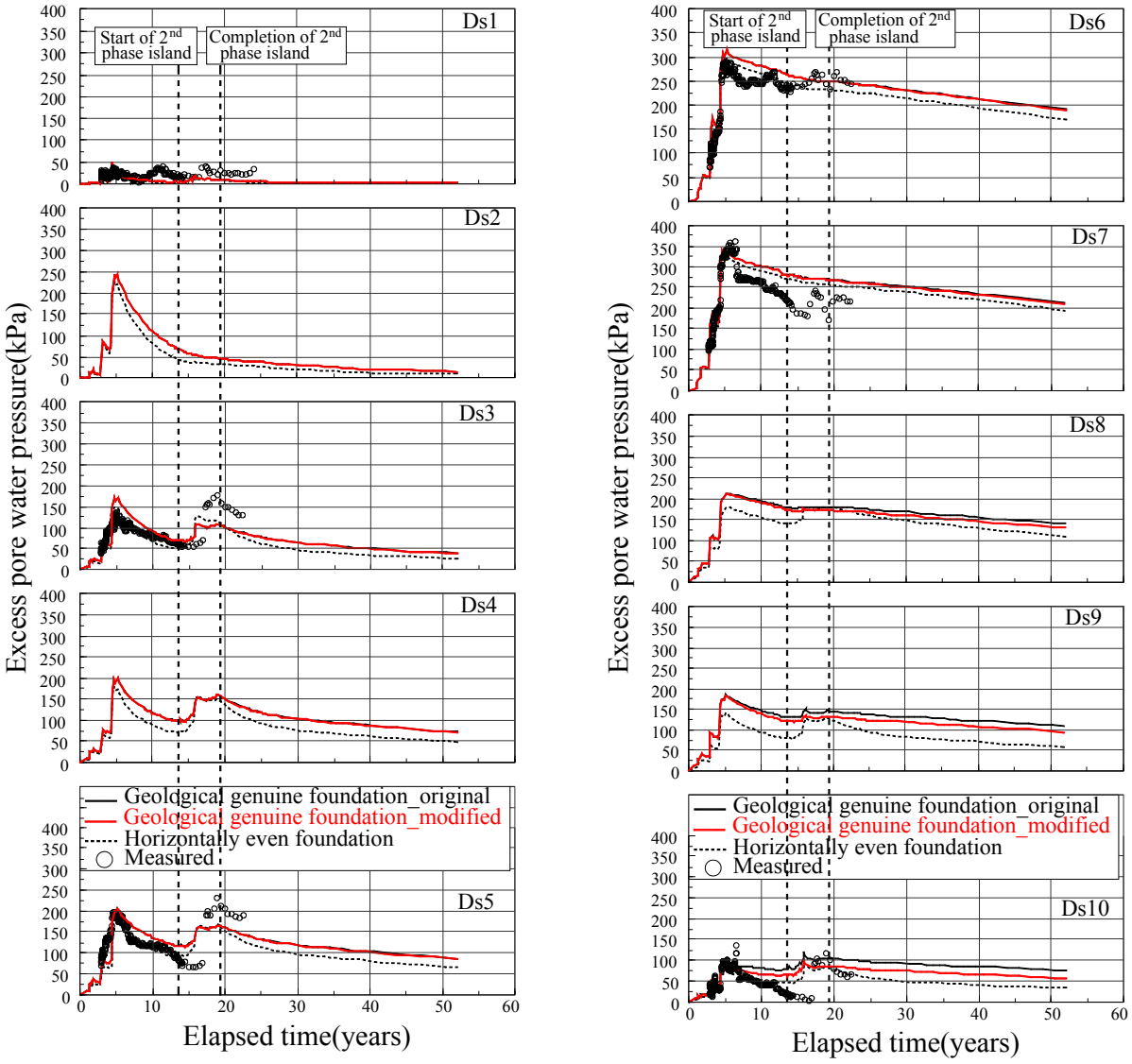

Fig. 6.12 Comparison of calculated excess pore water pressure – time relations in the modified foundation model with measured results for the individual Pleistocene sand gravel layers at monitoring point 1

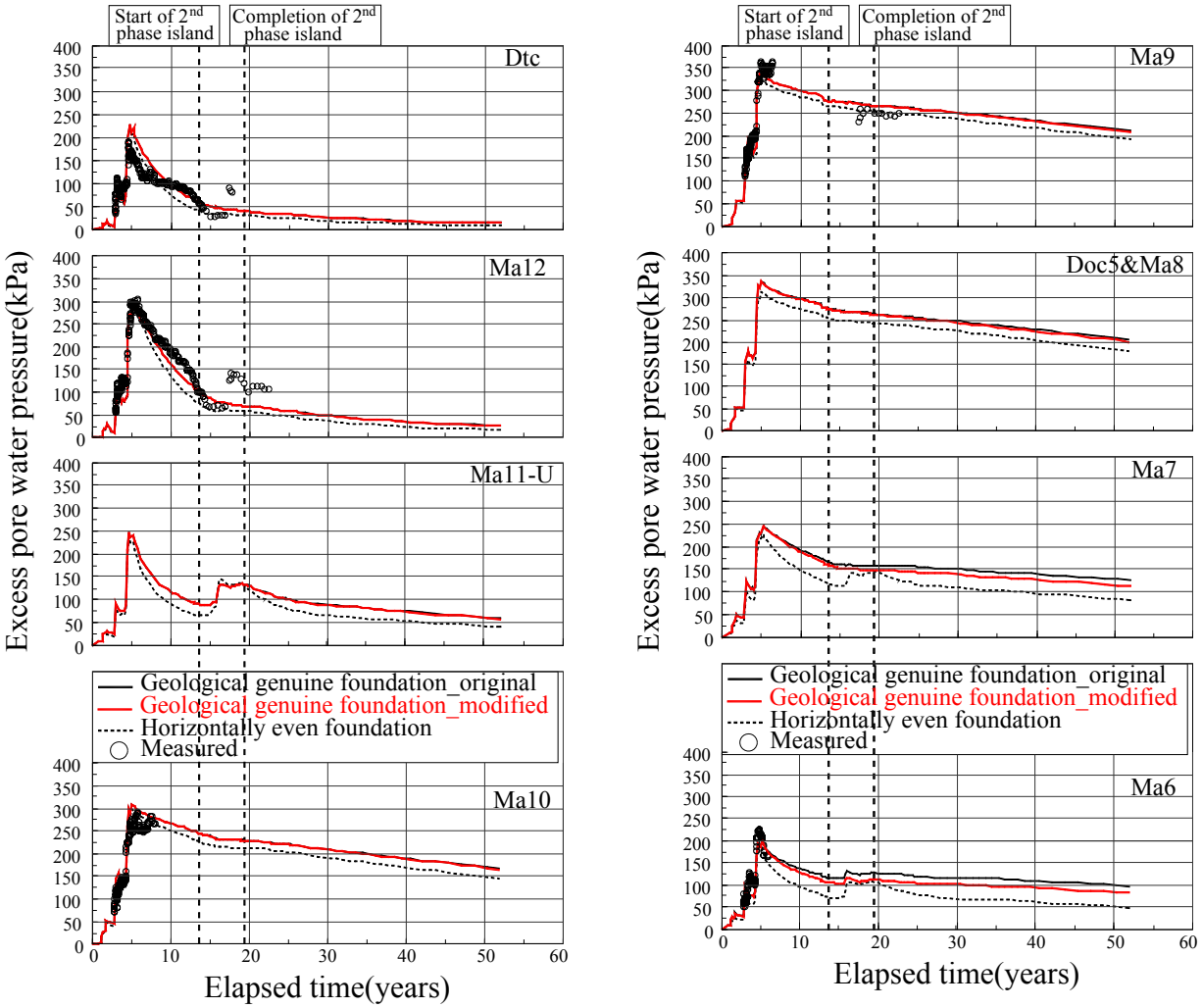

Fig. 6.13 Comparison of calculated excess pore water pressure – time relations in the modified foundation model with measured results for the individual Pleistocene clay layers at monitoring point 1

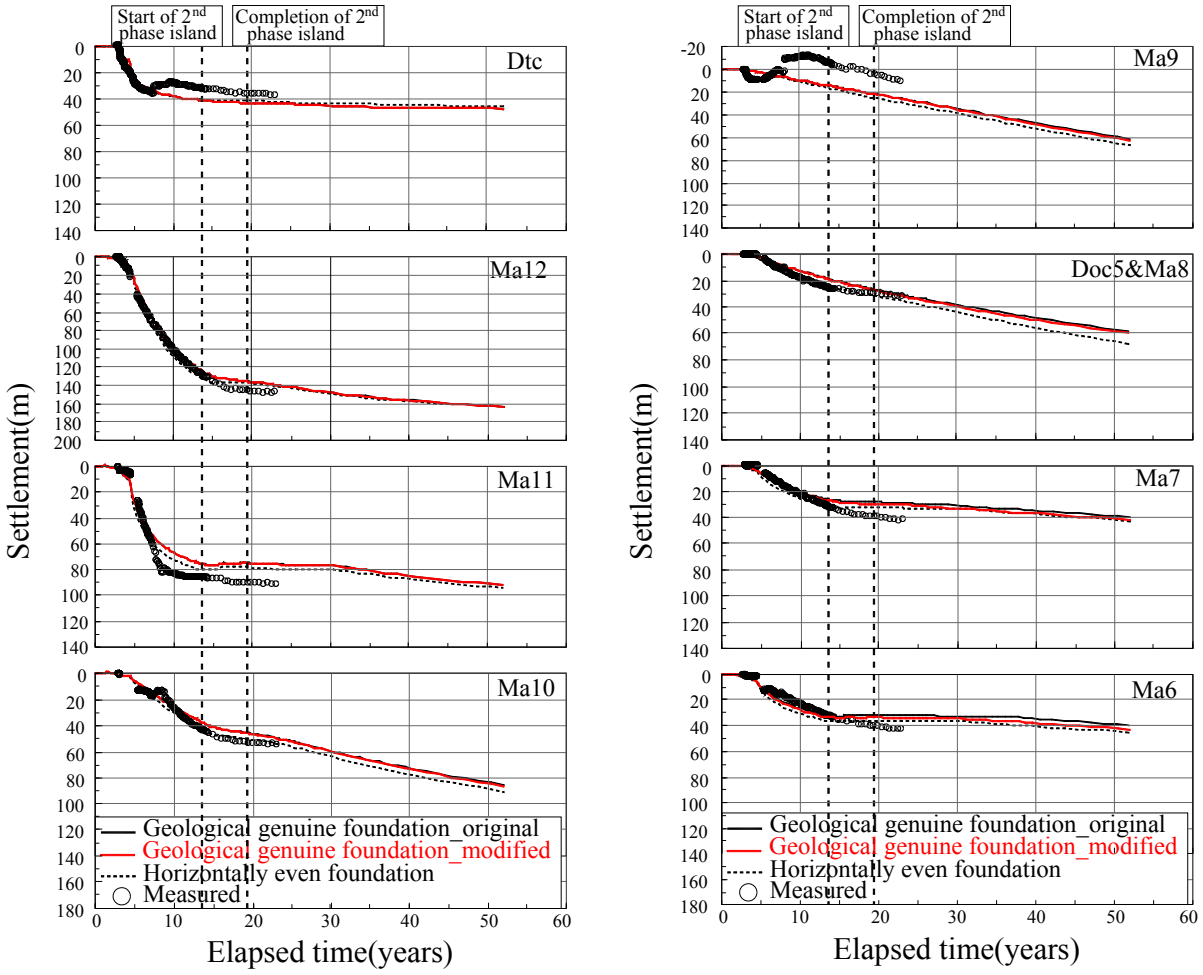

Fig. 6.14 Comparison of calculated compression – time relations in the modified foundation model with measured results for the individual Pleistocene clay layers at monitoring point 1

6.5 Evaluation of Mass Permeability for the Pleistocene Sand Gravel Layers with Irregular Thickness

6.5.1 Outline of evaluation of mass permeability

As is investigated in the previous section 6.3, the adopted numerical procedure with "Compression model for quasi-overconsolidated Pleistocene clays" as well as "mass permeability for the Pleistocene sand gravel layers" was found to well function to assess the long-term and interactive behavior not only in the horizontally even foundation model but also in the geologically genuine foundation model. It was also found that the constriction of the permeable sand gravel layers in the drastic change of thickness affects the process of dissipation and propagation of excess pore water pressure by comparing the performed results between the both foundation models. Although the calculated performance for the geologically genuine foundation model can well describe the measured results, as long as the equivalent coefficient of permeability for the Pleistocene sand gravel layers is set for the ideal foundation model having horizontally even layers, it is natural that the calculated performance for the horizontally even foundation model shows better prediction for the measured results.

Originally, the concept of "mass permeability" was proposed to evaluate the permeability not for each element but for the whole layer as one body. It was regarded as the macroscopic capability of permeability for the individual sand gravel layers by considering the horizontal continuity, the change in thickness and the degree of fine contents of them. Author evaluated the mass permeability of the Pleistocene sand gravel layers using the simple foundation model having horizontally even layers. The distribution of sand gravel layers not only in the loading area but also in the surrounding area that is developed to avoid the effect of the hydraulic boundary condition should be considered to assess the mechanism of the propagation/dissipation of excess pore water pressure in the coupled stress-flow analysis. Here, on the basis of the assumption that the hydraulic gradient derived in the representative foundation model having horizontally even

layers with constant thickness is regarded as the standard one for the individual Pleistocene sand gravel layers. Then, the evaluated mass permeability can be the representative of the capacity of permeability for the individual Pleistocene sand gravel layers at KIX. The standard hydraulic gradient is hence applied to the geologically genuine foundation model that has been developed to consider the actual stress level not only of the monitoring point but also of the considered area for the numerical analysis. Due attention should be paid to the fact that this assumption is only considered in horizontal position for the individual Pleistocene sand gravel layers.

6.5.2 Concept of standard hydraulic gradient

The pore water flow is assumed to obey isotropic Darcy's law in the present study. As is already expressed in the appendix C.2, the flow rate q for individual element of the FE mesh is simply defined by obeying isotropic Darcy's law in the following form:

$$q = v \times Sy = k \times i \times Sy \tag{6.1}$$

where v is the discharge velocity, Sy denotes the thickness of layer in the element of FE mesh, k and i are the permeability coefficient and the hydraulic gradient respectively. Here, if the flow rate q due to reclaimed load is determined, the hydraulic gradient i as unknown is calculated by the known values, k and Sy. For the case of geologically genuine foundation model with irregular thickness, if the identical flow rate q is assumed to generate with that of the ideal foundation model having the horizontally even layer with constant thickness, the relation between Sy and i is in inverse proportion for the given parameter, k. In comparing the pore water flow between the horizontally even foundation and the geologically genuine foundation models, first, the flow rate q generated due to the reclaimed load is assumed to be identical for the corresponding individual element of the Pleistocene sand gravel layers of both

foundation models in the following form:

$$q = k_s \times i_s \times Sy_s = k_{geo} \times i_{geo} \times Sy_{geo} \tag{6.2}$$

in which subscripts s and geo mean the standard values for the horizontally even foundation model and the values for the geologically genuine foundation model respectively. Here, in order to apply the permeable capacity of the sand gravel layer evaluated from the horizontally even foundation model to the corresponding sand gravel layer of the geologically genuine foundation model, the identical hydraulic gradient is assumed as follows:

$$i_s = i_{geo} \tag{6.3}$$

Then, the permeability coefficient, k_{geo} in the geological genuine foundation model is calculated as follows:

$$k_{geo} = \frac{k_s \times Sy_s}{Sy_{geo}} \tag{6.4}$$

Here, the standard values k_s and Sy_s in the horizontally even foundation model are constant and the value, Sy_{geo} in the geological genuine foundation model exhibits the changing value with irregular thickness of the individual layers. Therefore, to express the identical permeable capacity of sand gravel layers for both foundation models, the permeability coefficient, k_{geo} in the geologically genuine foundation model is programmed for the individual Pleistocene sand gravel elements in the finite element analysis code as automatically calculating the value by the change in thickness of the mesh. Eventually, the derived coefficient B to determine the matrix $[K_3]$ associated with the pore water flow becomes the same values for both foundation models. As is expressed in the appendix C.12, the coefficient B_1 consisting of B is calculated in the horizontally even foundation model as follows:

$$B_1 = \frac{\Delta t}{\gamma_w} \times \left(k_{si} \times Sy_s\right) / \left\{ \left(AL_1 - A_1\right) \times \frac{k_{si}}{k_{sj}} + A_1 \right\} \tag{6.5}$$

Here, the expressed notations were already explained in the appendix C. Then, the coefficient B_1 for the geologically genuine foundation model is also expressed as follows:

$$B_1 = \frac{\Delta t}{\gamma_w} \times \left(k_{geoi} \times Sy_{geo}\right) / \left\{ \left(AL_1 - A_1\right) \times \frac{k_{geoi}}{k_{geoj}} + A_1 \right\} \tag{6.6}$$

Substituting Eq. (6.4) into Eq. (6.6) yields

$$B_1 = \frac{\Delta t}{\gamma_w} \times \left(\frac{k_{si} \times Sy_s}{Sy_{geo}} \times Sy_{geo} \right) / \left\{ \left(AL_1 - A_1\right) \times \frac{\dfrac{k_{si} \times Sy_{si}}{Sy_{geoi}}}{\dfrac{k_{sj} \times Sy_{sj}}{Sy_{geoj}}} + A_1 \right\} \approx \frac{\Delta t}{\gamma_w} \times \left(k_{si} \times Sy_s\right) / \left\{ \left(AL_1 - A_1\right) \times \frac{k_{si}}{k_{sj}} + A_1 \right\} \tag{6.7}$$

As is shown in Eq. (6.5) and Eq. (6.7), the derived coefficient B becomes the same values for both foundation models with the assumption for the identical flow rate q and hydraulic gradient i. This assumption is only considered in the horizontal position for the Pleistocene sand gravel layers because the permeable capacity in vertical position by change in thickness of the permeable sand gravel layer almost does not affect the behavior of excess pore water pressure due to the adjoining impermeable clay layer. It is noteworthy that the assumption of the identical flow rate for both foundation models is actually validated when the volumetric strain of the element is identical, namely, that is validated in the monitoring point 1 where the thickness of layer is identical. In particular, because the geologically genuine foundation model has the inclined layers with increasing in thickness of clay layer towards the offing, the behavior of excess pore water pressure for both foundation models is not always agreed in the region except the monitoring point 1 due to the effect of the change in thickness of clay layers. However, the permeable capacity of sand gravel layers evaluated in the horizontally even foundation model

can be intactly applied to the geologically foundation model by deriving the same coefficient B with the assumption for the identical flow rate and hydraulic gradient.

6.5.3 Comparison of the calculated results and discussion

The calculated horizontal distribution of excess pore water pressure and the distribution in the thickness of layer for the individual Pleistocene sand gravel layers are shown in Fig 6.15 at the time before and after the construction of the 2nd phase island. For comparison, the calculated results with the original and proposed methods of the geologically genuine foundation model are shown together with the horizontally even foundation model. It is found that the calculated results for the proposed method of geologically genuine foundation model is similar to the ones for the horizontally even foundation model. It is confirmed that the identical permeable capability for the individual Pleistocene sand gravel layers in both foundation models is applied by considering the concepts of "mass permeability" and "standard hydraulic gradient". However, as shown in Fig. 6.15, it should be noted that the distribution of excess pore water pressure near the 1st phase island almost shows a good match for both foundation models by applying the concept of "standard hydraulic gradient", whereas the one of the region outside the reclaimed area shows the different distribution with the change in the thickness of clay layers. The thickness of layers beneath the foundation of the 1st phase island is almost the same for both foundation models because the horizontally even foundation model was developed based on the stratigraphy at the monitoring point 1, whereas the one beneath the foundation of the 2nd phase island is different each other due to the increase in thickness of clay layers towards the offing in the geologically genuine foundation model. It is noteworthy that although the identical permeable capability for the individual Pleistocene sand gravel layers was applied, the calculated results of excess pore water pressure show the difference with the change in the

thickness of clay layers. It is also found that the effect of constriction in the permeable layer due to the drastic change in the thickness of the sand gravel layers disappears by considering the proposed method, similar to the calculated results for the horizontally even foundation model.

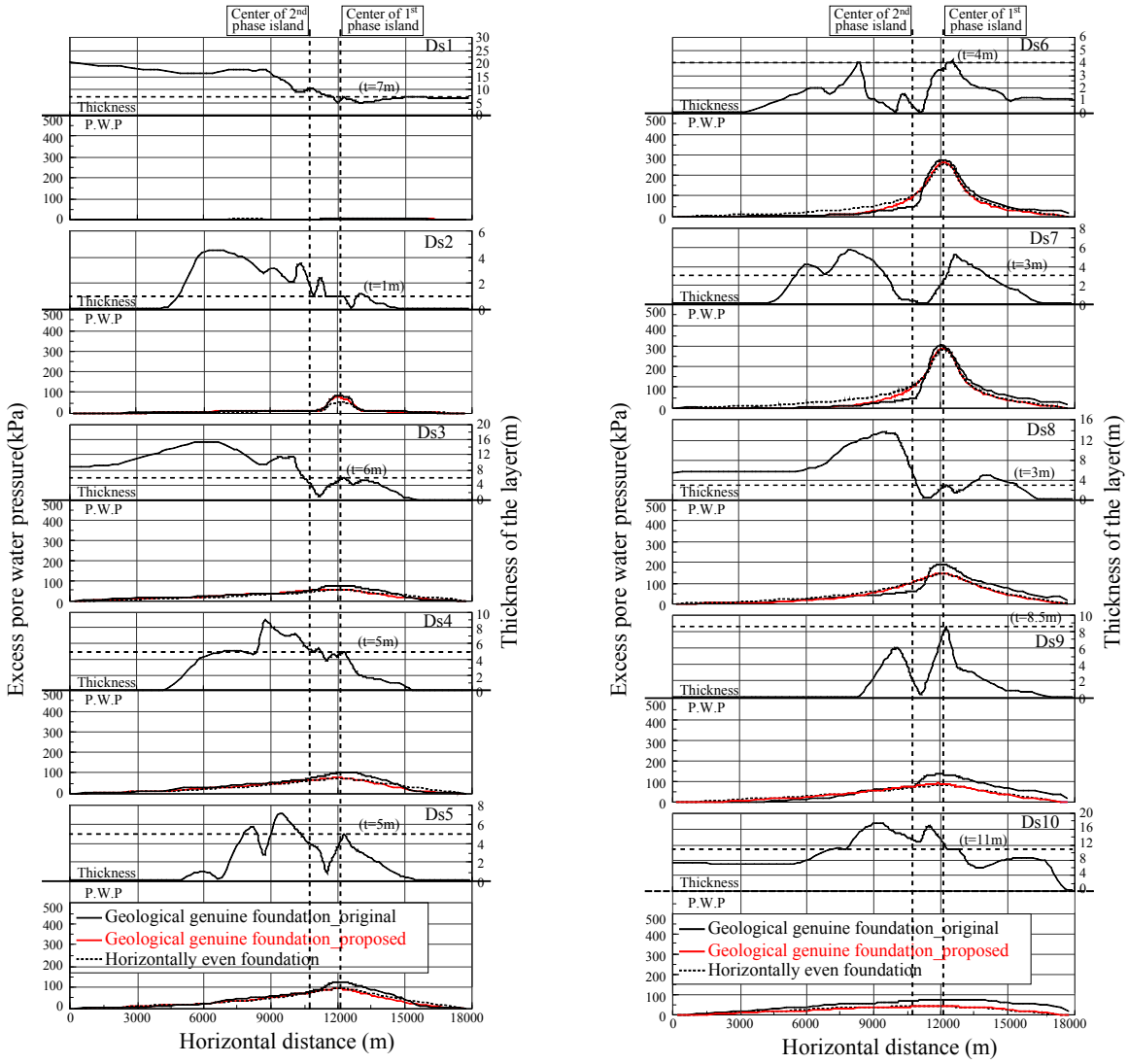

(a) before construction of the 2nd phase reclamation

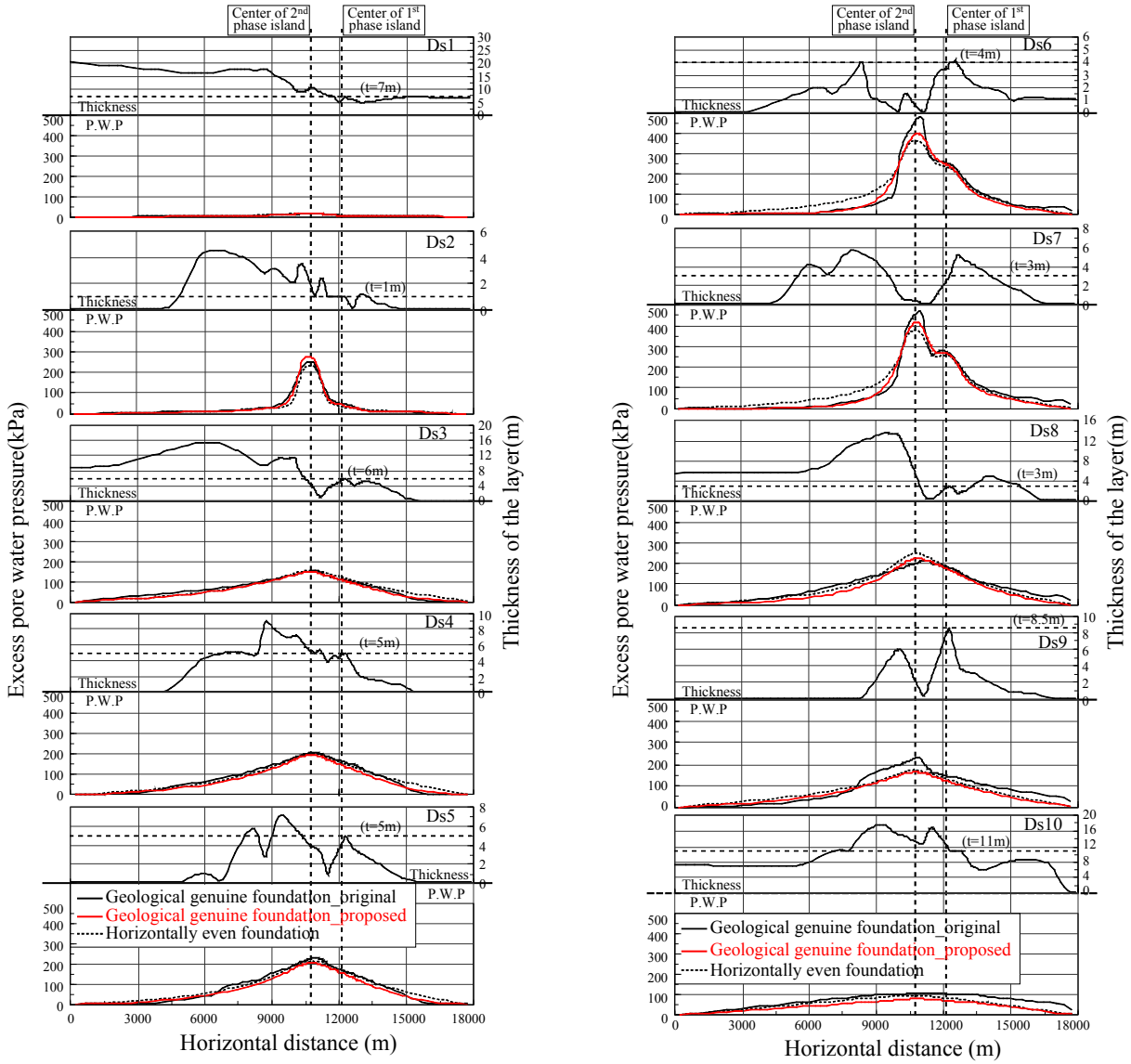

(b) at completion of the 2nd phase reclamation

Fig. 6.15 Comparison of calculated horizontal distribution of excess pore water pressure for the individual Pleistocene sand gravel layers in a horizontal position with concept of standard hydraulic gradient

Calculated excess pore water pressure-time relations for both foundation models are shown in Figs. 6.16 and 6.17 together with the measured results for the individual Pleistocene sand gravel and clay layers at the monitoring point 1. Although a little discrepancy can be seen for the calculated behavior of excess pore water pressure propagation between the proposed method of the geologically genuine foundation model and the horizontally even foundation model during the construction of the 2nd phase island, the overall behavior for the proposed method is almost identical to that for the horizontally even foundation model. The calculated long-term of settlement for the proposed method of the geologically genuine foundation model also shows a good match with the ones for the horizontally even foundation model (see Fig. 6.18). Therefore, by applying the concept of "standard hydraulic gradient", it is confirmed that the evaluated permeable capacity of the sand gravel layers for the horizontally even foundation model can be well reproduced for the geologically genuine foundation model having the drastic change in thickness of the permeable layers.

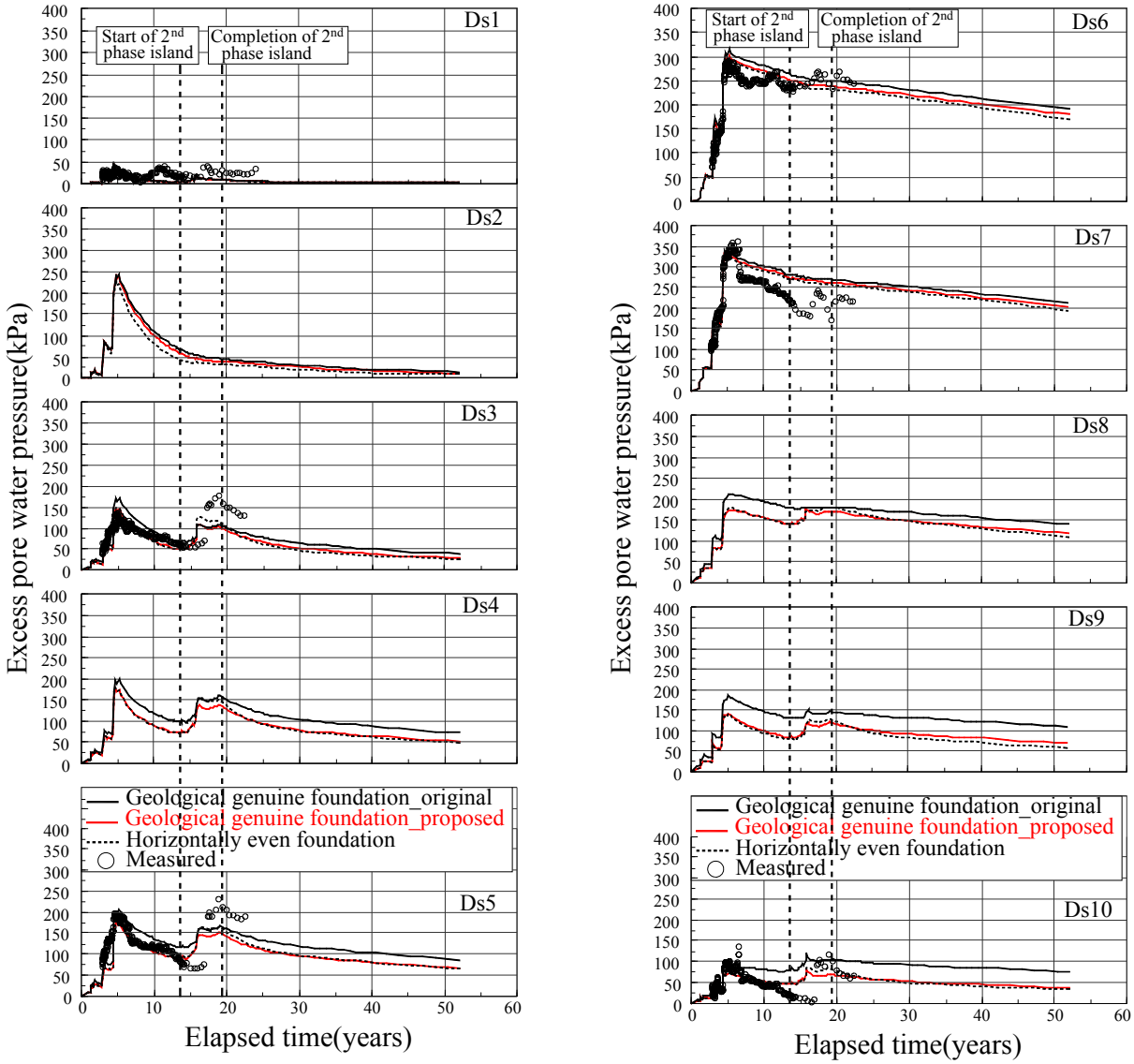

Fig. 6.16 Comparison of the calculated excess pore water pressure – time relations in concept of standard hydraulic gradient with measured results for the individual Pleistocene clay layers at monitoring point 1

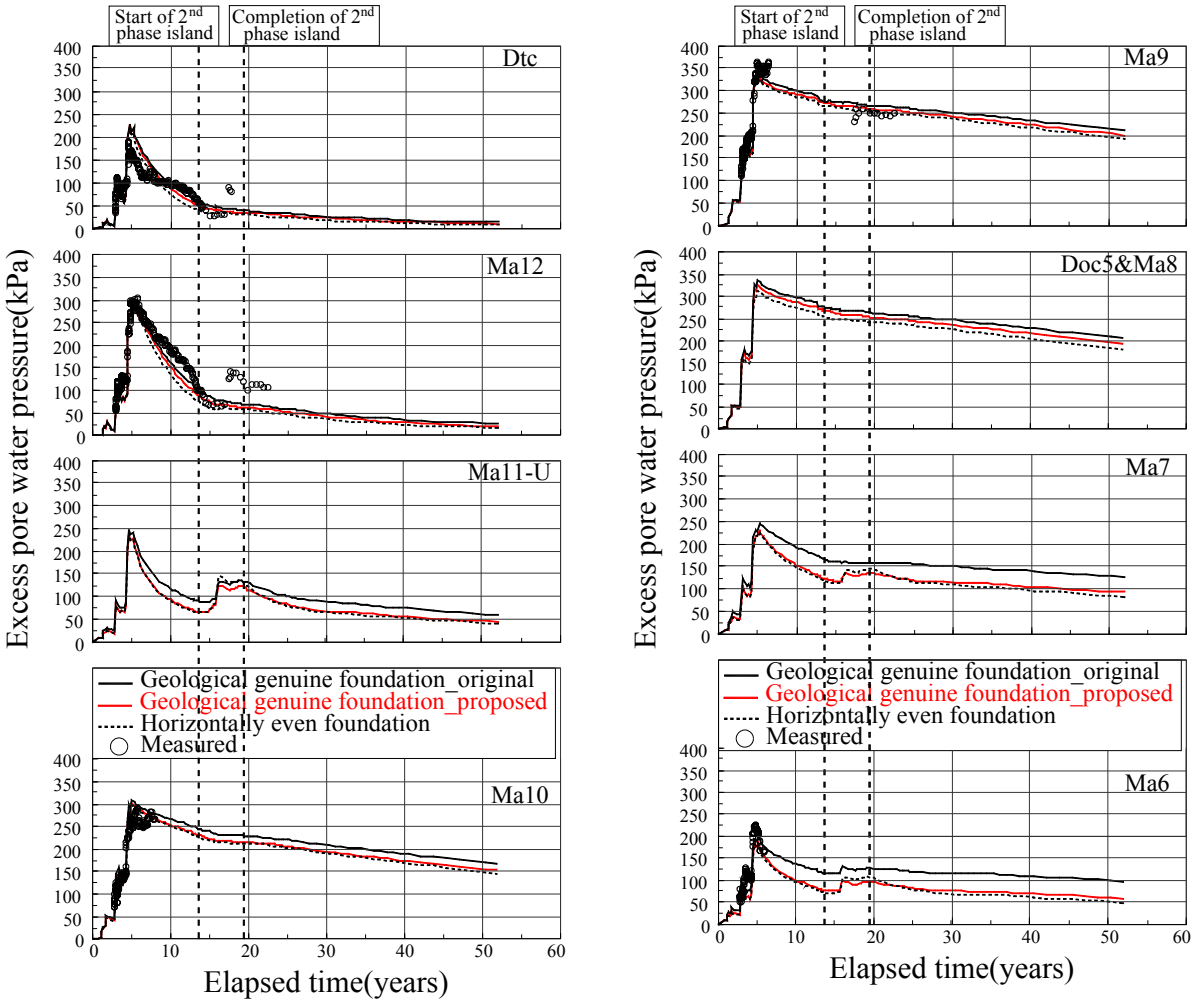

Fig. 6.17 Comparison of the calculated excess pore water pressure – time relations in concept of standard hydraulic gradient with measured results for the individual Pleistocene clay layers at monitoring point 1

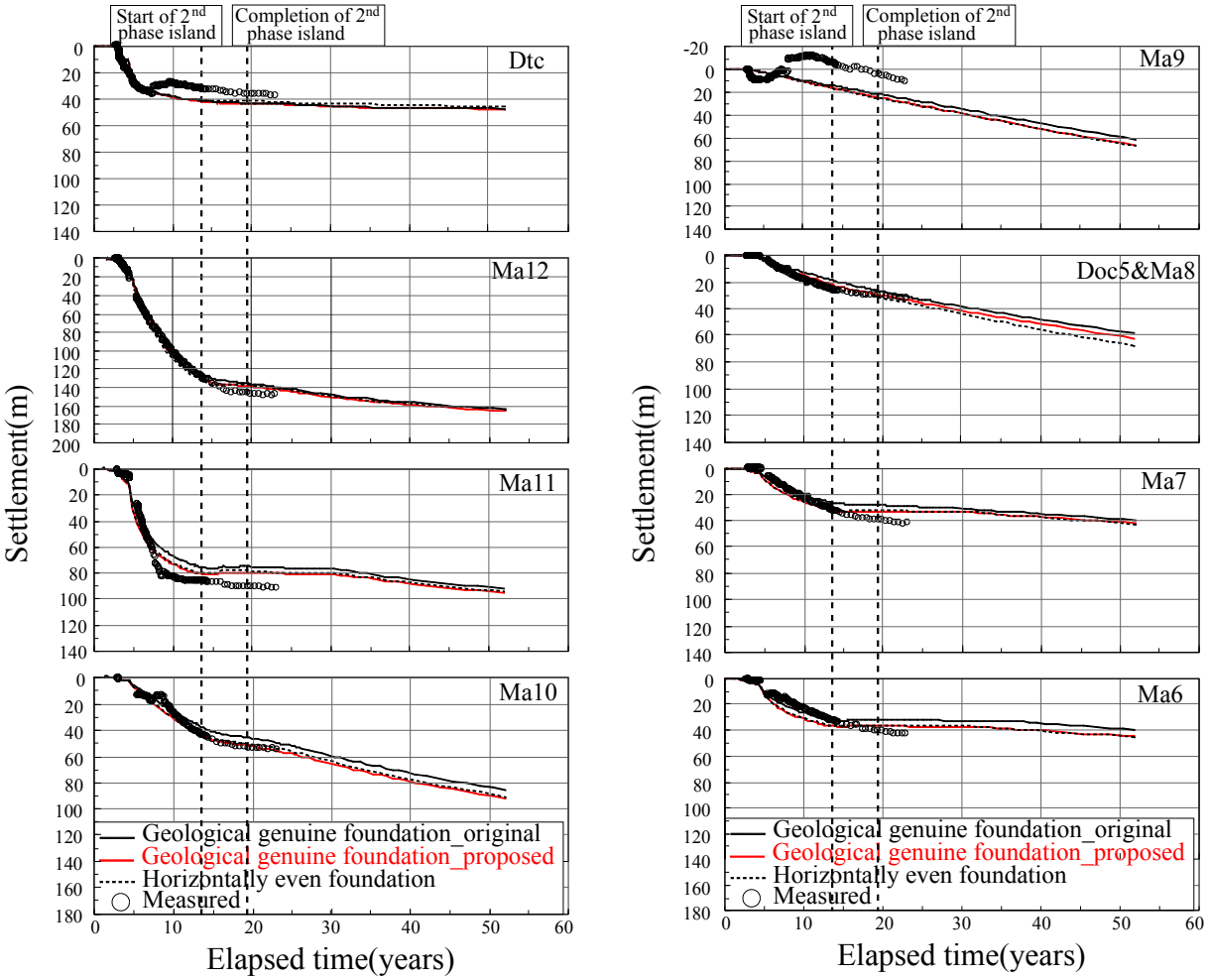

Fig. 6.18 Comparison of the calculated compression – time relations in concept of standard hydraulic gradient with measured results for the individual Pleistocene clay layers at monitoring point 1

6.6 Summary

Long-term behavior of the reclaimed Pleistocene foundation of the 1st phase island of KIX was numerically evaluated for the geologically genuine foundation model through the elasto-viscoplastic finite element analyses. The geologically genuine foundation model has the inclined base overlain by the inclined Pleistocene deposits with irregular thickness. The proposed numerical procedure in which non-elastic behavior in the quasi-overconsolidated region for the Pleistocene clays and the equivalent coefficient of permeability evaluated as the concept of "mass permeability" for the Pleistocene sand gravel layers are assumed, was found to well function even for the geologically genuine foundation model. However, by comparing with the performed results for the horizontally even foundation model that has constant thickness horizontally, the constriction of the permeable layers due to drastic change in thickness of the sand gravel layers was found to affect the process of dissipation and propagation of excess pore water pressure. Therefore, the thickness and the permeability in the sand gravel layers were found to play significant roles for the mode of dissipation and propagation of excess pore water pressure. Dissipation rate of the excess pore water pressure for the geologically genuine foundation model was evaluated to be smaller than that for the horizontally even foundation model because of the effect of constriction of the permeable layers. The rate of the consolidation associated with dissipation of excess pore water pressure was also underestimated compared to the horizontally even foundation model.

The adopted foundation model was set to have the sufficient distance to avoid the effect of the hydraulic boundary on the offshore side, whereas to have insufficient distance on the onshore side because of the exact modeling based on the actual distance between the main land and KIX. The effect of the hydraulic boundary is hence of concern. It was found that although the hydraulic boundary condition of send gravel layers was set to be fully drained, due to the

drastic constriction of the permeable layers near the boundary on the onshore side, the calculated excess pore water pressure has not yet fully dissipated from Ds6 to Ds10 near the boundary on the onshore side. However, the hydraulic boundary near the onshore side could be set to be fully drained for the all Pleistocene layers because the coarser deposits is actually predominant due to the effect of rivers. It was then found that the effect of the hydraulic boundary condition could be ruled out by enlarging the thickness of Ds10 layer near the boundary on the onshore side.

On the basis of the findings by comparing for two foundation models, which are the geologically genuine and the horizontally even foundation models, it was found that as long as the equivalent coefficient of permeability for the Pleistocene sand gravel layers is set for the horizontally even foundation, the calculated performance for the horizontally even foundation model shows better prediction for the measured data. Originally, the concept of "mass permeability" was evaluated as representative permeable capacity of sand gravel layers for the ideal foundation model that was developed to be the horizontally even foundation model to determine the numerical procedure and the soil parameters. The representative permeable capacity of the sand gravel layers evaluated for the horizontally even foundation model was applied to the geologically genuine foundation model by introducing the concept of "standard hydraulic gradient" for the coupled stress-flow analysis. The concept of "standard hydraulic gradient" was found to well reproduce the representative permeable capacity by comparing the calculated results for the both foundation models.

7. Numerical Assessment for the Additional Monitoring Points with the Proposed Procedure

7.1 Introduction

The permeability of the Pleistocene sand gravel layers was evaluated using the concept of "mass permeability" to consider the practical permeability to control the rate of consolidation in the filed. Mimura and Jang (2005a) reported that when the permeability of sand gravel layer is considered as perfectly drained, one-dimensional analysis can be adopted for the consolidation problem without considering the effect of permeability loss in the those sand gravel layers. If a sand gravel layer plays a sufficient role as a permeable layer, long-term behavior in the reclaimed marine foundations could be well explained by conducting one-dimensional analysis only considering the characteristics of clayey soils. However, the sand gravel layers sandwiched by the Pleistocene clay layers that can be seen at KIX were recognized not to function as fully permeable layers through the in-situ measurement of excess pore water pressure. In the case, multi-dimensional consolidation analysis is definitely required to assess the long-term behavior of the reclaimed Pleistocene foundation because the distribution of excess pore water pressure in the Pleistocene sand gravel layers with finite permeability has to be taken into account. The influential factors to determine the permeability of sand gravel layer are the thickness, the horizontal continuity and the fine contents of the sand gravel layers. The permeability of them is different with places even if they are categorized as the identical ones. But, it is impossible to evaluate the permeability of the sand gravel layers at every point. It is also very difficult to confirm how the sand gravel layers in the Pleistocene marine foundation are distributed in practice. Therefore, the author proposed the concept of mass permeability to evaluate the permeability of the individual sand gravel layers by considering the horizontal continuity, the change in thickness and the degree of fine contents of them. The evaluated mass permeability

through the numerical analysis using the ideal foundation model was adjusted to reproduce the measured results at the representative section. The evaluated mass permeability was regarded as the representative of the capacity of permeability for the individual Pleistocene sand gravel layers at KIX by considering the distribution of the sand gravel layers not only in the loading area but also outside of the loading area.

In the present study, the two-dimensional analysis is performed due to the difficulties in developing the three-dimensional distribution model for the reclaimed marine foundation and time constrains in performing the numerical analysis. Direct substitution of the equivalent coefficient of permeability determined for the horizontally uniform foundation model with constant thickness to the corresponding Pleistocene sand gravel layers of the geological genuine foundation model is not rational because it is determined as an average value for the specific foundation model as the horizontally uniform foundation model. The concept of "standard hydraulic gradient" has hence been proposed to rationally determine the mass permeability of the Pleistocene sand gravel layers of the geological genuine foundation model by using the prescribed equivalent coefficient of permeability for the horizontally uniform foundation model. In this chapter, a series of finite element analyses for the additional review sections is conducted to validate the proposed concept of "standard hydraulic gradient" and to confirm the objectivity of the proposed procedure in terms of the elasto-viscoplastic finite element analysis with the assumption of the mass permeability and quasi-overconsolidation.

Figure 7.1 shows the flow to evaluate the representative permeable capacity of the sand gravel layers at KIX by considering the concepts of "mass permeability" and "standard hydraulic gradient". In this chapter, the validity and objectivity of the proposed numerical procedure are investigated by applying them to the additional review sections. In particular, the applicability of the representative permeable capacity evaluated for representative foundation model using the concept of "mass permeability" for the Pleistocene sand gravel layers is

carefully discussed. The representative permeable capacity of the sand gravel layers is applied to the additional review sections by using the concept of standard hydraulic gradient. The validity of the procedure is also discussed by comparing with the in-situ measured results.

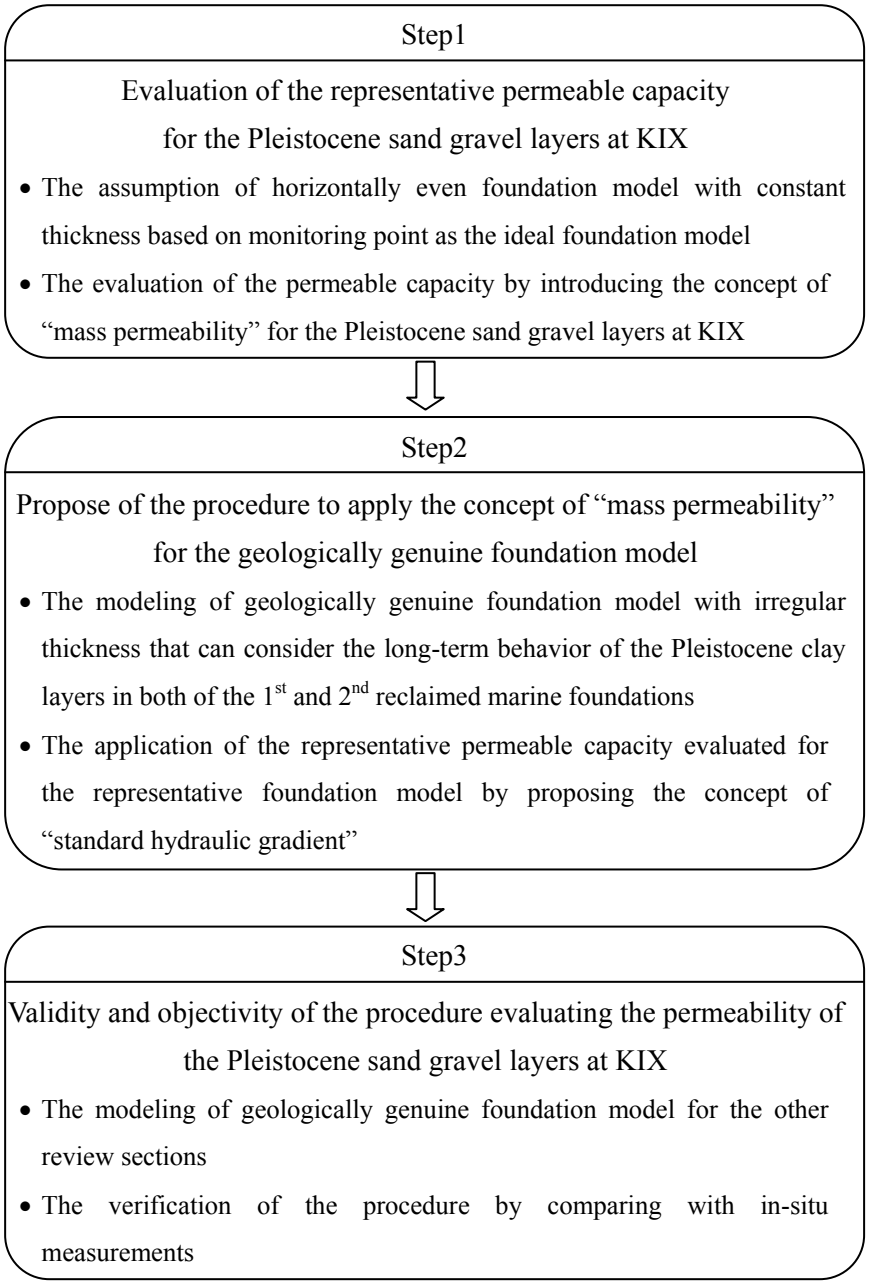

Fig. 7.1 Flow to evaluate the permeability of the Pleistocene sand gravel layers at KIX

7.2 Foundation Model and Framework of Numerical Assessment

7.2.1 Foundation model considering the subsurface stratigraphy

The differential settlement of the individual Pleistocene clay layers as well as the excess pore water pressure at various depths, both in the clay and the sand gravel layers, have been measured at various points of KIX to perform the stable operation of the airport, the maintenance program and the disaster risk management. Figure 7.2 shows the plan view of KIX together with the additional review sections, along where there are the monitoring points, S2 and S3. The settlement and excess pore water pressure have been measured for the monitoring point S3, whereas, the excess pore water pressure has been only measured for the monitoring point S2.

A series of elasto-viscoplastic finite element analyses is carried out along the two sections shown by B-B' and C-C' and the calculated performance is compared with the measured results at the monitoring points S2 and S3. The geologically genuine foundation models that have been developed based on the date from acoustic explorations and in-situ boring logs are shown in Fig. 7.3 together with the location of S2 and S3 respectively. The Pleistocene clay layers also increase in thickness towards the offing and the Pleistocene sand gravel layers drastically change in thickness horizontally for both cross-sections B-B' and C-C', similar to the geologically genuine foundation model of the representative section A-A' as shown in Fig. 6.2.

In order to apply the permeable capacity of the Pleistocene sand gravel layers evaluated for the representative foundation model as the concept of "mass permeability", the same condition with the representative foundation model is satisfied for the two geologically genuine foundation model used in the present study. Even number of the nodal points and elements and width of elements are exactly the same with the representative foundation model.

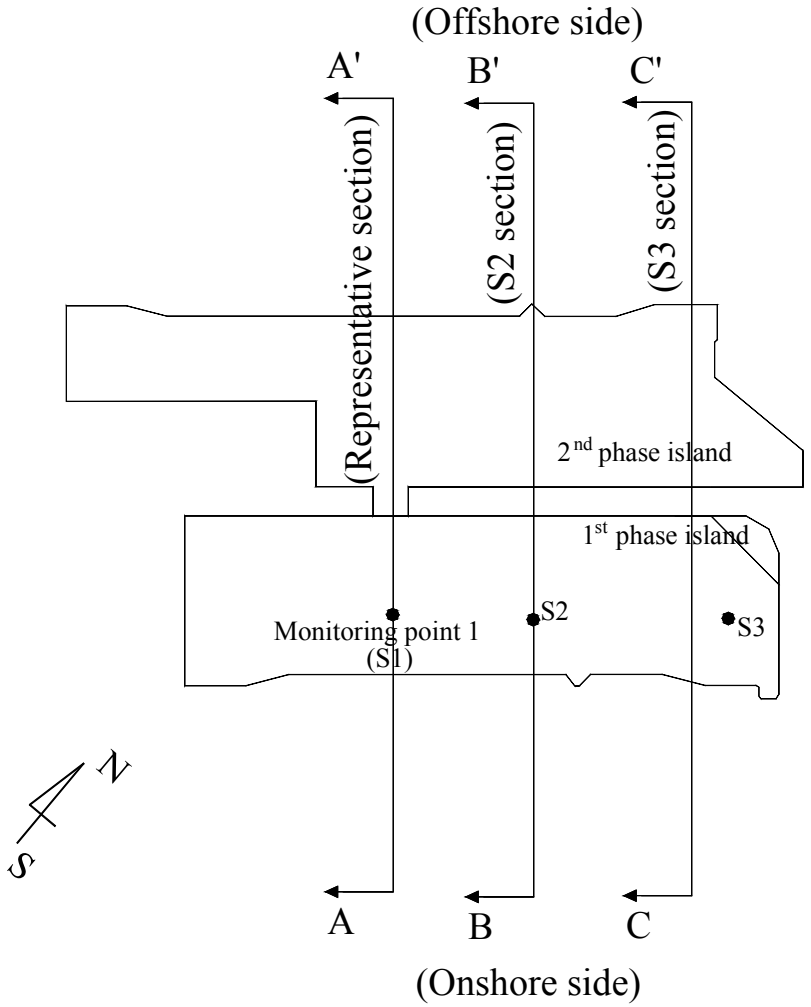

Fig. 7.2 Plan view of Kansai International Airport with the location of the monitoring points at the additional review sections

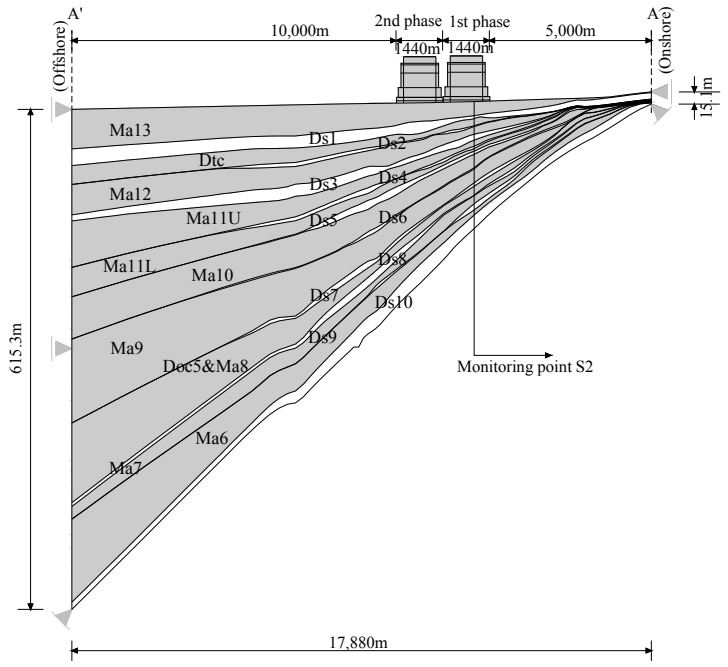

(a) B-B' section with the monitoring point S2

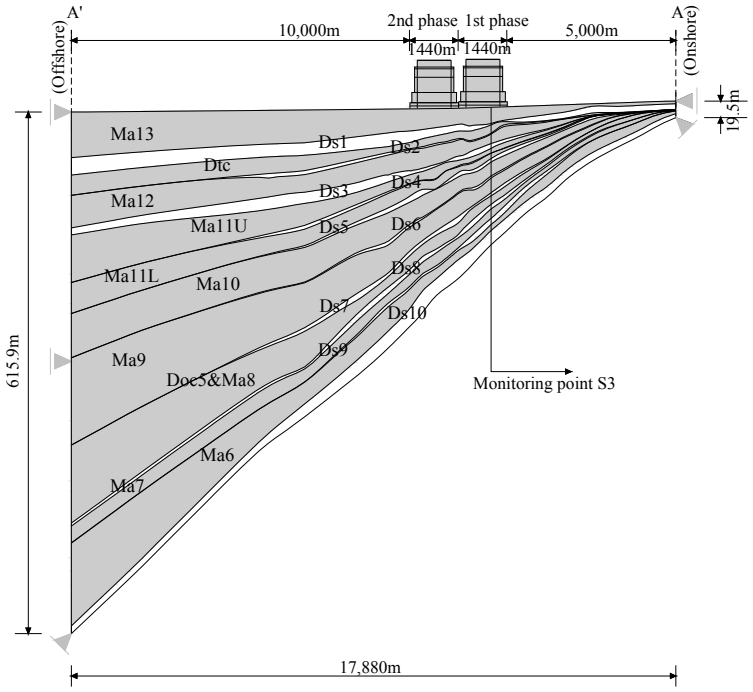

(b) C-C' section with the monitoring point S3

Fig. 7.3 Schematic cross-section of the geologically genuine foundation models of Kansai International Airport for finite element analysis

7.2.2 Framework of numerical assessment and soil parameters

The proposed procedure in terms of the elasto-viscoplastic finite element analysis is adopted. Attention should be also paid to the fact that the assumption of non-elastic behavior in the quasi-overconsolidated region for the Pleistocene clays and the concept of "mass permeability" of the Pleistocene sand gravel layers are also considered in the present analysis. The evaluated mass permeability for the representative foundation model is applied to the two geologically genuine foundation models by considering the concept of "standard hydraulic gradient" proposed in chapter 6. Therefore, the coefficient of matrix to simulate the horizontal flow of the sand gravel layers in the coupled stress-flow analysis becomes identical with that of the representative foundation model.

The construction sequence is the same that introduced in the previous chapters (see fig. 2.8) and the reclaimed stress measured at the monitoring points S2 and S3 is shown in Fig. 7.4. For the monitoring points S2, the prescribed final overburden due to airport fill construction amounts to about 410 kPa for the 1^{st} phase island and about 510kPa for the 2^{nd} phase island respectively. For the monitoring points S3, the final overburden amounts to about 460kPa and 540kPa respectively. The period of reclamation is about 4years for the 1^{st} phase island and about 6years for the 2^{nd} phase island respectively. The 2^{nd} phase reclamation is started after about 13years from the 1^{st} reclamation.

The parameters for the Pleistocene clay layers at KIX were already evaluated for the distinguished 4 blocks in section 4.2 (see Fig. 4.1). In the present study, as shown in Figs. 4.1 and 7.2, the corresponding blocks, A-N and B-N are used in the present numerical analysis for S2 and S3 sections. The value of the principal soil parameters of both groups for the Pleistocene clay layers were summarized in Table 4.3 and 4.4. It is noteworthy that the coefficient of permeability of Dtc layer in the section S3 is adopted in the order of 10^{-3} m/day because that is evaluated as the sandy clay based on the liquid limit.

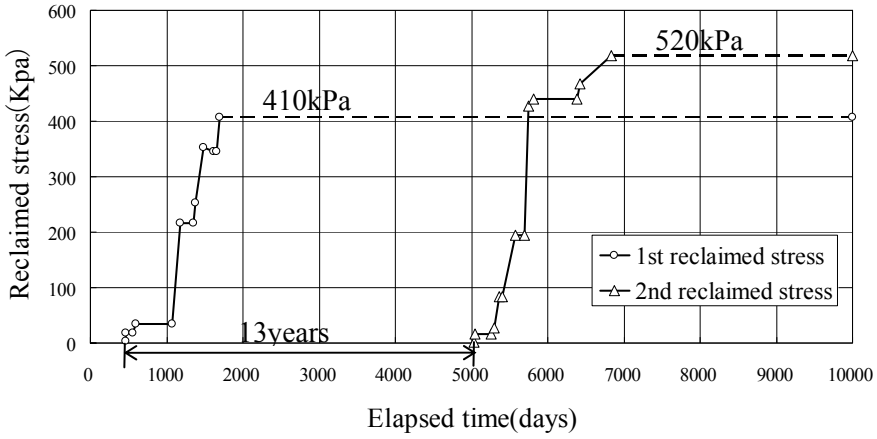

(a) At monitoring point S2

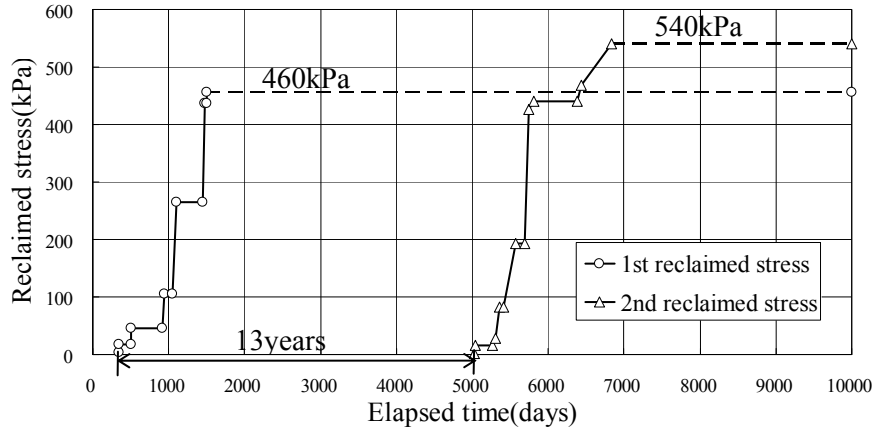

(b) At the monitoring point S3

Fig. 7.4 Reclaimed stress with time for the 1st and 2nd phase reclamations at the additional review sections

7.3 Simulation Results and Discussion

7.3.1 Performance of excess pore water pressure

Calculated excess pore water pressure - time relations are shown in Fig. 7.5 together with the measured results for the individual Pleistocene sand gravel layers at the monitoring points S2 and S3 respectively. Note that the comparison is only shown for the individual Pleistocene sand gravel layers, where the pore pressure cells have survived, to confirm the reproducibility for the different cross-sections. Although the calculated performance at Ds3 layer underestimates the measured excess pore water pressure, the overall process of generation/ dissipation and propagation of excess pore water pressure is well described by adopting the representative permeable capacity determined for the horizontally uniform foundation model. Calculated excess pore water pressure for Ds3 of both monitoring points underestimates the measured results. It means that Ds3 has the lower permeability than the setup one. Detailed investigation is necessary about the local difference in the geometry of the layers as well as the mechanical properties in terms of permeability of the sand gravel layers.

The evaluated mass permeability at the representative section could be recognized well to function as representative permeable capability for the Pleistocene sand gravel layer through the performed results for the section S2 and S3. Local characteristics of the geometry, the physical and mechanical properties may have serious influence on the performance of excess pore water pressure. Detailed investigation is required to derive the realistic foundation model. The behavior of excess pore water pressure due to construction of the adjacent twin islands is similar to that explained for the cross-section A-A’.

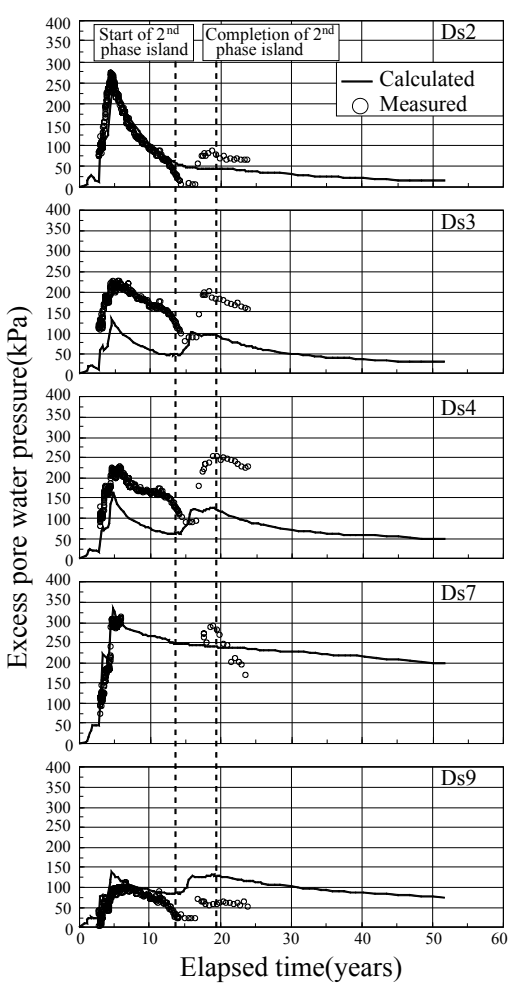

(a) At monitoring point S2

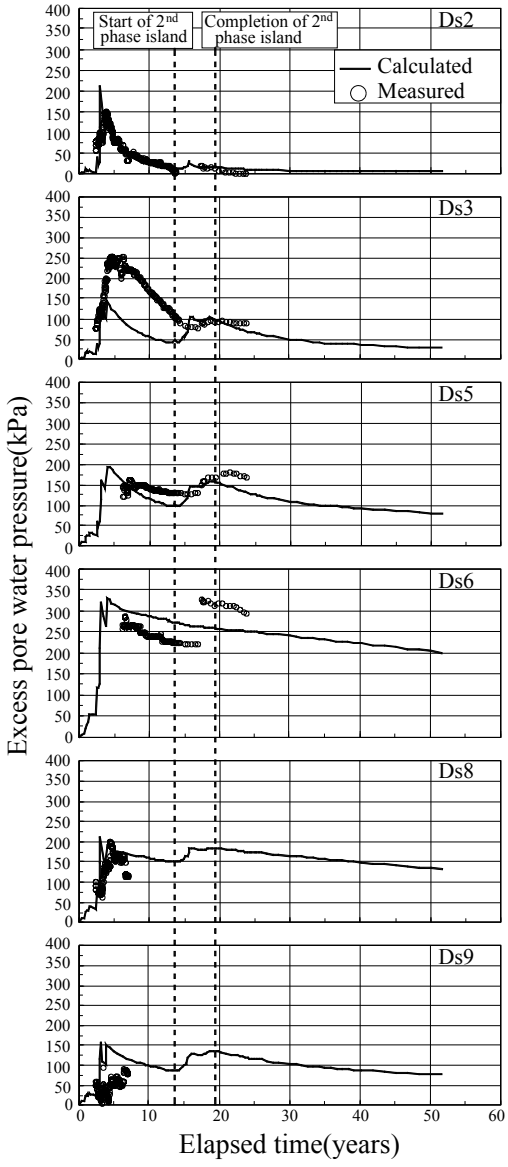

(b) At monitoring point S3

Fig. 7.5 Comparison of measured and calculated excess pore water pressure with time for the Pleistocene sand gravel layers at the additional monitoring points

7.3.2 Compression of the Pleistocene clay layers

Calculated compression - time relations for the individual Pleistocene clay layers are shown in Fig. 7.6 together with measured results at monitoring point S3. It should be also noted that comparison is only shown for the monitoring point S3 because the differential settlement of the individual Pleistocene clay layers have not been measured at the monitoring point S2. The mode of compression also shows the similar behavior with that explained in the previous chapter 4 and 5. Although the validity of the present procedure is not accurately evaluated for the middle Pleistocene layers such as Ma11, 10, 9 and Doc5&Ma8 due to insufficient measurements, long-term settlement for Dtc, Ma12, 7 and 6 is found to be well simulated with the present numerical procedure even at the section S3.

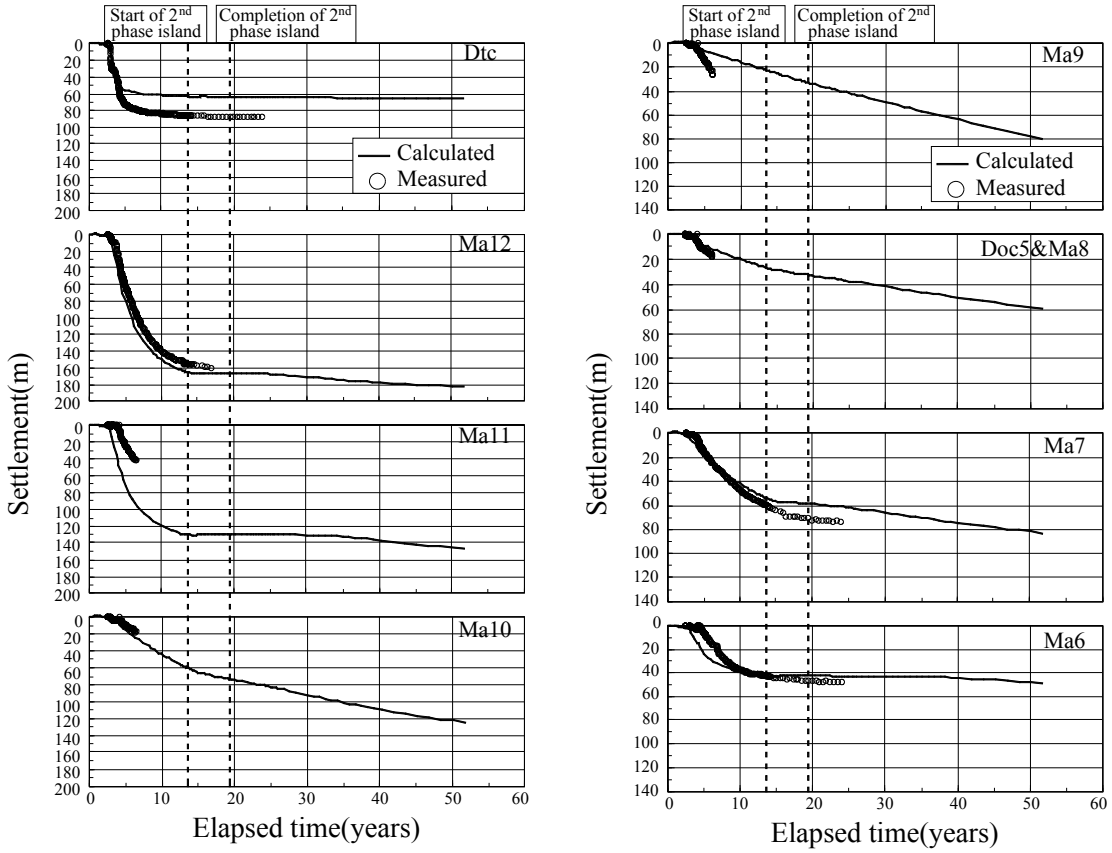

Fig. 7.6 Comparison of measured and predicted settlement for the Pleistocene clay layers at monitoring point S3

7.4 Summary

Applicability of the proposed numerical procedure in this study was validated through the elasto-viscoplastic finite element analyses for the additional review sections. The assumption of non-elastic behavior in the quasi-overconsolidated region for the Pleistocene clays and the concept of “mass permeability” of the Pleistocene sand gravel layers were adopted for the numerical analyses. In particular, on the basis of the assumption that the hydraulic gradient derived in the developed horizontally uniform foundation model with constant thickness is regarded as the standard one for the individual Pleistocene sand gravel layers, the evaluated mass permeability could be the representative of the permeable capacity for the individual Pleistocene sand gravel layers at KIX. The evaluated representative permeable capacity of the representative section was applied to the section S2 and S3 by applying the concept of “standard hydraulic gradient”.

Comparison of excess pore water pressure was conducted for the individual Pleistocene sand gravel layers where the pore pressure cells have survived at monitoring points S2 and S3. The representative permeable capacity for the Pleistocene sand gravel layers at KIX was found to well function to describe the in-situ measured results even at the sections S2 and S3. It was found that the permeability of Ds3 layer has a lower value than the representative one due to the local variation of geometrical condition and material properties.

The compression model for quasi-overconsolidated Pleistocene clays and the representative permeable capacity in the concept of “mass permeability” for the Pleistocene sand gravel layers was also found to well describe the measured settlement at the monitoring point S3.

On the basis of these findings, it is cofirmed that the proposed numerical procedure is versatile to assess the long-term behavior of the reclaimed marine foundations that have been measured at a lot of monitoring points of KIX.

8. Conclusions

In the present study, long-term behavior of the reclaimed Pleistocene foundations due to a large-scale offshore reclamation was investigated based on the elasto-viscoplastic finite element analyses. The modeling for the quasi-overconsolidated Pleistocene clay and the evaluation of permeability for the Pleistocene sand gravel deposits are the significant factors to assess the long-term behavior of the reclaimed Pleistocene foundations. The time-dependent behavior associated with insufficient dissipation of excess pore water pressure and the interactive behavior of the reclaimed Pleistocene foundations due to construction of the adjacent twin islands were investigated through performance of the elasto-viscoplastic finite element analyses that consider non-elastic behavior in the quasi- overconsolidated region for the Pleistocene clay and the concept of "mass permeability" for the Pleistocene sand gravel layers. The proposed numerical procedure was validated by comparing the calculated performance with the measured results for over 24years from start of construction in the field. The main results of this thesis are summarized as follows:

In chapter 2, the structure of foundation ground in Kansai International Airport (KIX) was investigated based on the acoustic exploration and geological survey. The marine deposits at KIX consist of the very complicated geological layers that have the Holocene clay underlain by the alternated Pleistocene clay and sand gravel layers. The Pleistocene clay deposits have the distinguished structure so-called "quasi-overconsolidated clay" exhibiting slight overconsolidation with OCR of 1.1 to 1.6 in average. It was verified that the Pleistocene sand gravel deposits are not always distributed uniformly and consistently in thickness and they do not play a role as perfect drainage layer through in-situ measurement of excess pore water pressure. The primary and secondary consolidation for the Pleistocene clay deposits was found

to take place at the same time depending on the permeability of the adjoining Pleistocene sand gravel deposits through the brief evaluation using in-situ measurements.

In chapter 3, the constitutive models used in this study were introduced. The concrete forms of elasto-viscoplastic and elasto-plastic constitutive models for the finite element analysis were described to assess the time-dependent behavior in the measured results by comparing the performed results for two constitutive models. The compression model for the quasi-overconsolidated Pleistocene clays proposed by Mimura and Jang (2004) was also introduced. In order to assess long-term behavior considering the permeability of the sand gravel layer, the concrete form of the coupled stress-flow analysis obeying isotropic Darcy's law was also described.

In chapter 4, a series of elasto-viscoplastic finite element analyses was performed to propose the numerical procedure for the construction of the 1st phase island using the simple foundation model assumed to be horizontally even layer that have a constant thickness and continuous layer based on the boring data at monitoring point1. A compression model assuming the non-elastic behavior in the quasi- overconsolidated region for the Pleistocene clays and the concept of "mass permeability" introduced to model the actual process of dissipation of excess pore water pressure in the filed for the Pleistocene sand gravel deposits were implemented in the numerical analysis. The concept of "mass permeability" for the Pleistocene sand gravel layers was proposed to evaluate the permeability not of each element but of the whole layer in one body by considering the horizontal continuity, the change in thickness and the degree of fine contents of them. On the basis of the findings by Itoh et al. (2001), Kitada et al. (2011a), Inoue et al. (2011) and the calculated results, the relatively high mass permeability was evaluated for Ds1, 3 and10 because they have been evaluated as gravelly, horizontally continuous and having enough

thickness. On the other hand, very low mass permeability was evaluated for Ds6 and 7 that have been evaluated to be the insufficient thickness with high degree of fine contents and poorly continuous. The other sand gravel layers were evaluated as the ordinary permeable layers.

The calculated performance for the Pleistocene deposits was found to well describe the actual process of settlement as well as excess pore water pressure both in the clay and the sand gravel layers by adopting the compression model for the quasi-overconsolidated Pleistocene clay deposits and the concept of mass permeability for the Pleistocene sand gravel deposits.

The time-dependent behavior that actually has taken place in the field was evaluated by comparing the calculated results between the elasto-viscoplastic and elasto-plastic constitutive models. It was found that the calculated performance in terms of the elasto-viscoplasitc constitutive model well describes the time-dependent behavior associated with insufficient dissipation of excess pore water pressure that has taken place in the Pleistocene clays of the foundation of Kansai International Airport.

The reclaimed marine deposits of KIX consist of the inclined foundation as having the gradient of from 0.3% to 2.0%. A series of elasto-viscoplastic finite element analyses was also performed to investigate the effect of the gradient of the reclaimed marine foundation for the inclined foundation model with the adopted numerical procedure. It was confirmed that the gradient of them almost does not affect the long-term behavior due to large-scale offshore reclamation by comparing the calculated results between the horizontally even and the inclined foundation models because the slope of foundation is not so steep in practice.

The long-term behavior of the deeper Pleistocene deposits than Ds10 layer, until which the foundation model was considered to propose the numerical procedure in the present study, was investigated based on the elasto-viscoplastic finite element analyses. Although the deformation of the deep foundation due to reclamation load was calculated not to be so large in this particular case, the amount of settlement in the deeper Pleistocene deposits than Ds10 layer was found not

to able to be ignored for the operation of the airport fill. Such large settlement in those deep Pleistocene layers should be a coming important topic.

In chapter 5, the numerical procedure proposed in chapter4 was extended to assess the interactive behavior due to the adjacent construction of the both islands. A series of elasto-viscoplastic finite element analyses was performed to assess the long-term settlement and generation/propagation/dissipation process of excess pore water pressure for the Pleistocene foundations of the 1st and 2nd phase islands of KIX considering the effect of adjacent construction of the both islands. The Pleistocene marine foundations integrating the 1st and 2nd phase islands were modeled as to have continuous, horizontally even layers with constant thickness independently for the both islands.

It was found that the excess pore water pressure generated due to the construction of the adjacent 2nd phase island tends to propagate to the foundation beneath the 1st phase island through the permeable Pleistocene sand gravel layers. Decrease in effective stress due to returning excess pore water pressure caused the tentative decrease in the rate of compression or slight swelling in the some Pleistocene clay layers beneath the foundation of the 1st phase island. Here, the permeability of the sand gravel layers was found to play a significant role for the mode of propagation. Propagation of excess pore water pressure did not take place in the highly permeable sand gravel layers such as Ds1 and 10 because the generated excess pore water pressure easily dissipated in these layers. It is also noteworthy that propagation of excess pore water pressure did not take place in the poorly permeable sand gravel layers such as Ds6 and 7 because of their low permeability. Serious propagation of excess pore water pressure was found to occur in the ordinary permeable sand gravel layers such as Ds3 and 5 in the Pleistocene foundation at KIX.

In the foundation beneath the 2nd phase island, the decrease in the initial effective stress

before the start of reclamation for the 2nd phase island occurred due to propagation of excess pore water pressure from the foundation of the 1st phase island. The condition of effective stress then remained in the quasi-overconsolidated region for the longer time than the initial condition during the 2nd phase reclamation. It was also found that the rate of excess pore water pressure dissipation was relatively low compared to that in the foundation of the 1st phase island because the initial stress level with increase in thickness of clay deposits is higher than that in the foundation of the 1st phase island and the permeable sand gravel layers decrease in thickness towards the offing. It is also noteworthy that the time-dependent compression associated with insufficient dissipation of them was generally predominant in the foundation of the 2nd phase island.

It was confirmed that the foundations of the 1st and 2nd phase islands are seriously affected each other by the reclamation of the adjacent islands with 200m distance through the elasto-viscoplastic finite element analyses with the proposed numerical procedure.

In chapter 6, the long-term behavior of the inclined Pleistocene deposits with irregular thickness at KIX due to the adjacent construction of the two airport islands was investigated based on the elasto-viscoplastic finite element analyses with the proposed numerical procedure. The geologically genuine foundation model that has the inclined base overlain by the inclined Pleistocene deposits with irregular thickness was adopted for the numerical analysis. Comparing with the calculated results for the horizontally even foundation model that has a constant thickness horizontally, the drastic change in thickness of the permeable layers was found to affect the process of dissipation and propagation of excess pore water pressure. It was then found that the thickness as well as the permeability of sand gravel layers plays a significant role for the mode of dissipation and propagation of excess pore water pressure and advance in settlement associated with the process of them.

The effect of the change in thickness of permeable sand gravel layers near the boundary was also investigated based on the finite element analysis considering the change in thickness near the boundary on the onshore side. It was found that although the hydraulic boundary condition of the sand gravel layers was set to be fully drained, the drastic constriction of permeable sand gravel layers near the boundary seriously affects the calculated results of the finite element analysis as long as the lateral distance is not enough to rule out the effect of the hydraulic boundary effect.

Originally, the concept of “mass permeability” for the Pleistocene sand gravel layers was introduced for the ideal foundation model having the horizontally even layer with constant thickness to evaluate the permeability not of each element but of the whole layer in one body by considering the horizontal continuity, the change of thickness horizontally, the degree of fine contents and three-dimensional distribution of layer. In order to reasonably evaluate the mass permeability of the Pleistocene sand gravel layer for the geologically genuine foundation model, the evaluated mass permeability for the ideal horizontally even foundation model was applied to the geologically genuine foundation model by introducing the concept of “standard hydraulic gradient”. The concept of “standard hydraulic gradient” was found to well reproduce the mass permeability evaluated for the ideal horizontally even foundation model by comparing the calculated results for the two foundation models.

In chapter 7, on the basis of the assumption that the hydraulic gradient derived in the initially developed horizontally uniform foundation model with constant thickness at the representative section is regarded as the standard one for the individual Pleistocene sand gravel layers, the evaluated mass permeability for the horizontally uniform foundation model can be the representative of the capacity of permeability for the individual Pleistocene sand gravel layers at KIX. The representative permeable capacity of sand gravel layers was applied to the additional

monitoring sections with the geologically genuine foundation model by introducing the concept of “standard hydraulic gradient” for the coupled stress-flow analysis.

It was confirmed that the compression model for the quasi-overconsolidated Pleistocene clays and the representative capacity of permeability in the concept of “mass permeability” for the individual Pleistocene sand gravel layers well describe the measured results even at the additional monitoring sections.

On the basis of these findings, it is concluded that the proposed numerical procedure in this study can be applied to assess the long-term behavior of the reclaimed marine foundations due to construction of large-scale offshore reclamation in the other project as well as Kansai International Airport (KIX).

REFERENCES

Adachi, T. and Oka, F. (1982): Constitutive Equations for Normally Consolidated Clays Based on Elasto-viscoplasticity, Soils and Foundations, 22(4), pp. 57-70.

Akai, K. and Sano, I. (1981): Long-term Consolidation of Osaka Upper Diluvial Clay, Tsuchi-To-Kiso, Vol.29, No.3, pp. 43-47 (in Japanese).

Akai, K., Sano, I., Ma, S. D. and Ishiguro, T. (1984): Experimental Studies on Delayed Consolidation, Annuals DPRI, Kyoto University, 27(B-2), pp. 49-63 (in Japanese).

Akai, K. and Tamura, T. (1976): An Application of Nonlinear Stress-strain Relations to Multi-dimensional Consolidation Problems, Annuals DPRI, Kyoto University, 21(B-2), pp.19-35 (in Japanese).

Akai, K. and Tanaka, Y. (1999): Settlement Behaviour of An Off-shore Airport KIA, Proc. 12th ECSMGE, 2, pp. 1041-1046.

Baladi, G. Y. and Rohani, B. (1984): Development of an Elastic- viscoplastic Constitutive Relationship for Earth Materials, Mechanics of Engineering Materials, pp. 23-43, John Wiley & Wiley Ltd.

Calladaine, C. R. (1971): A microstructural view of the mechanical properties of saturated clay, Geotechnique, 15(4), 345-415.

Christian, J.T. (1968): Undrained Stress Distribution By Numerical Method. Journal of Soil Mech. and Foundation Div., ASCE, 94 (SM6), pp.1333-1345.

Dragon, A. and Mroz, Z. (1979): A Model for Plastic Creep of Rock-like Materials Accounting for the Kinematics of Fracture, Int. Jour. Rock Mech. Min. Sci. & Geomech. Abstr., 16, pp.253-259.

Duncan, J.M., Rajot, J-P. and Perrone, V.J. (2005): Factors Affecting Magnitude of Clay Settlement, proceedings of the Symposium on Geotechnical Aspects of Kansai International Airport, pp. 1-6.

Endo, H., Oikawa, K., Komatsu, A. and Kobayashi, M. (1991): Settlement of Diluvial Clay Layers Caused by a Large Scale Man-made Island, Proceedings of International Conference on Geotechnical Engineering for Coastal Development.

Imai, G., Ohmukai, N. and Tanaka, H (2005): An Isotaches-type Compression Model for Predicting Long Term Consolidation of KIA Clays, proceedings of the Symposium on Geotechnical Aspects of Kansai International Airport, pp. 49-64.

Inoue, N., Kitada, N., Takemura, K., Fukuda, K. and Emura, T. (2011): Three-dimensional subsurface structure model of Kansai International Airport by integration of boring data and seismic profiles, Proc. Int. Symp. on Advances in Ground technology and Geo-information, pp. 121-126.

Ishii, I., Ogawa, F. and Zen, K. (1984): Engineering properties of marine clays in Osaka Bay(Part 2) physical properties, consolidation characteristics and permeability, Technical Note of the Port and Harbour Resarch Institute Ministry of Transport, Japan, 498, 47-86 (in Japanese).

Itoh, Y., Takemura, K., Kawabata, D., Tanaka, Y. and Nakaseko, K. (2001): Quaternary Tectonic Warping and Strata Formation in the Southern Osaka Basin Inferred from Reflection Seismic Interpretation and Borehole Sequences, Journal of Asian Earth Science, 20, pp. 45-58.

Jang, W.Y. and Mimura, M. (2005): Effect of Permeability and Compressibility of Sandwiched Gravelly Sand Layers on Subsequent Settlement of Pleistocene Deposits, Soils and Foundations, 45(6), pp. 111-119.

Kansai International Co. Ltd. (2002): Committee Report on Investigation of the Behavior of the Reclamation Foundation at Kansai International Airport -2nd Phase Island (in Japanese).

Karube, D. (1975): Procedure and problems of non-standard triaxial test, Proc. 20th JSSMFE Symposium, 45-60(in Japanese).

Katona, M. G. (1984): Evaluation of Viscoplastic Cap Model, Jour. Geotech. Eng., ASCE, 110(8), pp. 1106-1125.

Kitada, N., Inoue, N., Takemura, K., Fukuda, K. and Emura, T (2011a): Subsurface structure model around Kansai Airport according to re-interpretation of borehole data based on result of KIX18-1 core, Proc. Int. Symp. on Advances in Ground technology and Geo-information, pp. 137-142.

Kitada, N., Inoue, N., Takemura, K., Mimura, M., Nakatani, Y. and Matsui, K. (2011b): Subsurface structure model around Kansai Airport for estimation of subsidence behavior, 66th JSCE Annual Meeting, Ⅲ-143 (in Japaness)

Kitada, N., Takemura. K., Inoue, N., Itoh, H., Masuda, F., Hayashida, A., Emura, T. and Fukuda, K. (2009): Stratigraphy of the drilling cores in Kansai International Airport (KIX18-1), Programme and Abstract, 39 Japan Association for Quaternary Research Meeting pp. 104-105 (in Japanese).

Kiyama, M. (1991): Settlement of the Reclaimed Land at the Coastal Area, Proc. Int. Conf. On Geotech. Engng. For Coastal Development-Theory and Practice on Soft Ground-, 1, pp. 207-212.

Kobayashi, G., Mitamura, M. and Yoshikawa, S. (2001): Lithofacies and Sedimentation Rate of Quaternary Sediments from Deep Drilling Cores in the Kobe Area, Southwest Japan, Earth Science, 55, pp. 131-143 (in Japanese).

Kobayashi, M., Furudoi, T., Suzuki, S. and Watabe, Y. (2005): Modeling of Consolidation Characteristics of Clays for Settlement Prediction of Kansai International Airport, proceedings of the Symposium on Geotechnical Aspects of Kansai International Airport, pp. 65-76.

Leonards, G.A. and Altschaeffl, A.G. (1964): Time Effects in the Consolidation of Clays, Journal of the Soil Mech. And Found. Div., ASCE, 90(SM5), pp. 133-155.

Leroueil, S., Kabbaj, M., Tavenas, F. and Bouchard, R. (1985): Stress-strain-strain rate relation for the compressibility of sensitive natural clays. Geotechnique, 35(2), pp. 159-180.

Leroueil, S., Tavenas, F., Brucy, F., La Rochelle, P. and Roy, M. (1979): Behavior of Destructured Natural Clays, Journal of the Geotech. Eng. Div., ASCE, 105(GT6), pp. 759-778.

Marques, M.E.S., Leroueil, S. and Almeida, M.S.S. (2004): Viscous behaviour of St-Roch-de-I'Achigan clay, Quebec, Can. Geotech.J., 41(1), 25-38.

Matsui, T. and Abe, N. (1985): Elasto/viscoplastic Constitutive Equation of Normally Consolidated Clays Based on Flow Surface Theory, Proc. 5th Int. Conf. Numerical Methods in Geomechanics, 1, pp.407-413.

Mesri, G. and Godlewski, P. M. (1977): Time and stress compressibility interrelationship, Journal of the Geotechnical Engineering Division, ASCE, 103(GT5), 417-430.

Mikasa, M. and Takada, N. (1977): Observation of the Settlement at the Reclaimed Marine Foundations, Proc. 52th National Conf., JSCE, pp.184-185 (in Japanese).

Mimura, M. and Jang, W.Y. (2004): Description of time-dependent behavior of quasi-overconsolidated Osaka Pleistocene clays using elasto-viscoplastic finite element analyses, Soils and Foundations, 44(4), pp. 41-52.

Mimura, M. and Jang, W.Y. (2005a): Verification of the Elasto-viscoplastic Approach Assessing the Long-term Deformation of the Quasi-overconsolidated Pleistocene Clay Deposits, Soils and Foundations, 45(1), pp. 37-49.

Mimura, M. and Jang, W.Y. (2005b): Long-term Settlement of the Pleistocene Deposits due to Construction of KIA, proceedings of the Symposium on Geotechnical Aspects of Kansai International Airport, pp. 77-85.

Mimura, M., Ohshima, A., Takeda, K., Yoshikawa, M., Suwa, S. and Nagaya, J. (2001): Settlement Behavior of Pleistocene Deposits due to Reclamation in Osaka Port, Proc. National Conf., JGS, 1007-1008 (in Japanese).

Mimura, M. and Sekiguchi, H. (1986): Bearing Capacity and Plastic Flow of A Rate-sensitive Clay Under Strip Loading. Bulletin of DPRI, Kyoto University, 36(2), pp. 99-111.

Mimura, M., Shibata, T., Nozu, M. and Kitazawa, M. (1990): Deformation analysis of a reclaimed marine foundation subjected to land construction, Soils and Foundations, 30(4), pp. 119-133.

Mimura, M., Shibata, T. and Watanabe, K. (1994): Post Yield Modeling of Compression for Pleistocene Clays and Its Application to Finite Element Analysis, Proc. Pre-failure Deformation of Geomaterials, 1, pp. 517-522.

Mimura, M. and Sumikura, Y. (2000): Deformation and Excess Pore Water Pressure of the Pleistocene Marine Deposits due to Offshore Reclamation, Proc. Int. Symp. on Coastal Geotechnical Engineering in Practice, 1, pp.339-344.

Mimura, M., Takeda, K., Yamamoto, K., Fujiwara, T. and Jang, W.Y. (2003): Long-term Settlement of the Reclaimed Quasi-overconsolidated Pleistocene Clay Deposits in Osaka Bay, Soils and Foundations, 43(6), pp. 141-153.

Murayama, S. and Shibata, T. (1966): Flow and stress relaxation of clays, I.U.T.A.M., Symposium on Rheology and Soil Mechanics, Springer –Verlag, Grenoble, 99-129.

Murayama, S. and Shibata, T. (1956): On the Rheological Characters of Clay, Transaction of JSCE, No. 40, pp. 1-31 (in Japanese).

Nakase, A. (1992): Settlement of Kansai International Airport Island, Proc. of JSCE No.454/III-20, pp. 1-9.

Nishigaki, M. and Imai, T. (2005): A New Method for Predicting Three Dimensional (3-D) Settlement Using Groundwater Flow Analysis, proceedings of the Symposium on Geotechnical Aspects of Kansai International Airport, pp. 23-29.

Nova, R. (1982): A Viscoplastic Constitutive Model for Normally Consolidated Clay, Proc. IUTAM Conference on Deformation and Failure of Granular Materials, pp. 287-295.

Oda, K., Tokida, K., Matusui, T. and Ono, M. (2005): Elasto-viscoplastic Model for Expressing Strain Rate Dependency of Creep Behavior and Its Applicability to One-dimensional Consolidation Behavior of Pleistocene Clays in Osaka Bay, proceedings of the Symposium on Geotechnical Aspects of Kansai International Airport, pp. 41-48.

Olszak, W. and Perzyna, P. (1966): The Constitutive Equations of the Flow Theory for a Non-stationary Yield Condition, Applied Mechanics, Proc. 11th Int. Congress of Applied Mechanics, pp. 545-553, Springer – Verlag.

Perzyna, P. (1963): The Constitutive Equations for Rate Sensitive Plastic Materials, Quart. Appl. Math., 20(4), pp.321-332.

Research Committee on Ground in Osaka Bay. (2002): Ground and Construction of Bay Area, Association of Research on Geotechnical Information in Osaka Bay, 660p. (in Japanese).

Schofield, A.N. and Wroth, C.P. (1968): Critical State Soil Mechanics, McGraw-Hill, London.

Sekiguchi, H. (1983): Applicability of the Plane-strain Viscoplastic Model for Clay, Proc. Annual Conf. of Chubu Brance, JSCE, pp. 342-343.

Sekiguchi, H. (1985): Macrometric Approaches -Static- Intrinsically Time-dependent, Constitutive Laws of Soils, Proc. Discussion Session 1A, 11thICSMFE, pp. 66-98.

Sekiguchi, H. (1977): Rheological Characteristics of Clays, Proc. 9th ICSMFE, 1, pp.289-292.

Sekiguchi, H., Nishida, Y. and Kanai, F. (1982): A Plane-strain Viscoplastic Constitutive Model for Clay, Proc. 37th Natl. Conf., JSCE, pp. 181-182 (in Japanese).

Sekiguchi, H., Shibata, T., Fujimoto, A. and Yamaguchi, H. (1986): A Macro-element Approach to Analyzing the Plane-strain Behaviour of Soft Foundation with Vertical Drains, Proc. 31th Symp., JSSMFE, pp. 111-120 (in Japanese).

Sekiguchi, H., Shibata, T., Mimura, M. and Sumikura, K. (1988): Behavior of the Seawall and Bridge Abutment at the Edge of an Offshore Airport Fill, Annuals, Disaster Prevention Research Institute, 31 (B-2), pp. 123-145 (in Japanese).

Sekiguchi, H., Shibata, T. and Mimura, M. (1991): Long-term Deformation of Pleistocene Clays, Proc. 10th European Conf. on SMFE, 1, pp. 261-264.

Sekiguchi, H. and Toriihara, M. (1976): Theory of One-Dimensional Consolidation of Clays with Consideration of their Rheological Properties, Soils and Foundations, 16(1), pp. 27-44.

Shibata, T. (1963): On the Volume Changes of Normally-Consolidated Clays, Annuals DPRI, Kyoto University, 6, pp.128-134 (in Japanese).

Shibata, T. and Karube, D. (2005): Settlement Prediction of Kansai International Airport, proceedings of the Symposium on Geotechnical Aspects of Kansai International Airport, pp. 87-96.

Suzuki, S., Emura, T., Mizukami, J. and Ono, M. (2008): Geotechnical Issue Due to Construction of Kansai International Airport , Geotechnical Engineering Magazine of JGS, vol.56, No. 8 Ser. No. 607, pp.78-85 (in Japanese).

Takemura, K. (1985): The Plio-Pleistocene Tokai Group and the Tectonic Development around Ise Bay of Central Japan since Pliocene, Mem. Fac. Sci. Kyoto Univ. Ser. Geol. Mineral, 51, pp. 21-96.

Takemura, K. and Nakaseko, K. (2005): Subsurface geology of Kansai International Airport, central Japan, proceedings of the Symposium on Geotechnical Aspects of Kansai International Airport, pp. 17-22.

Terzaghi, K., Peck, R.B. and Mesri, G. (1996): Analysis of Consolidation by Rate Process Theory, Journal of the Soil Mechanics and Foundations Division, ASCE, 92(SM6), pp. 229-248.

Tsuchida, T. (2005): Structure Due to Cementation of Osaka Bay Clay and Its Mathematical Modeling, proceedings of the Symposium on Geotechnical Aspects of Kansai International Airport, pp. 31-40.

Yokokura, T., Kano, N., Yamaguchi, K., Miyazaki, T., Ikawa, T., Ohta, Y., Kawanaka, T. and Abe, S. (1998): Seismic Profiling of Deep Geological Structure in the Osaka Bay Area, Bull. Geol. Surv. Japan, 49, pp. 571-590.

Yoshinaka, R. (1968): Lateral Coefficient of Subgrade Reaction, Civil Engineering Journal, 10(1), pp. 32-37 (in Japanese).

APPENDIX A

The concrete form of the model for plane-strain version is expressed as follows in Eq. (3.22):

$$\{\Delta\sigma'\} = [D^{evp}]\{\Delta\varepsilon\} - \{\Delta\sigma^R\} \tag{A.1}$$

Equation (A.1) can be expressed in matrix notation as

$$\begin{pmatrix} \Delta\sigma'_{xx} \\ \Delta\sigma'_{yy} \\ \Delta\sigma'_{xy} \\ \Delta\sigma'_{zz} \end{pmatrix} = \left[\begin{bmatrix} \tilde{\lambda}+2\tilde{\mu} & \tilde{\lambda} & 0 \\ \tilde{\lambda} & \tilde{\lambda}+2\tilde{\mu} & 0 \\ 0 & 0 & \tilde{\mu} \\ \tilde{\lambda} & \tilde{\lambda} & 0 \end{bmatrix} - \frac{C_1}{C_3} \begin{bmatrix} A_{xx}^2 & A_{xx}A_{yy} & A_{xx}A_{xy} \\ A_{xx}A_{yy} & A_{yy}^2 & A_{yy}A_{xy} \\ A_{xx}A_{xy} & A_{yy}A_{xy} & A_{xy}^2 \\ A_{xx}A_{zz} & A_{yy}A_{zz} & A_{xy}A_{zz} \end{bmatrix} \right] \begin{pmatrix} \Delta\varepsilon_{xx} \\ \Delta\varepsilon_{yy} \\ \Delta\gamma_{xy} \end{pmatrix} - \frac{C_2}{C_3} \begin{pmatrix} A_{xx} \\ A_{yy} \\ A_{xy} \\ A_{zz} \end{pmatrix} \Delta t \tag{A.2}$$

where the elasto-viscoplastic constitutive matrix, $[D^{evp}]$, the effective stress increment vector, $\{\Delta\sigma'\}$, the strain increment vector, $\{\Delta\varepsilon\}$ and relaxation stress vector, $\{\Delta\sigma^R\}$ are defined as follows:

$$[D^{evp}] = \left[\begin{bmatrix} \tilde{\lambda}+2\tilde{\mu} & \tilde{\lambda} & 0 \\ \tilde{\lambda} & \tilde{\lambda}+2\tilde{\mu} & 0 \\ 0 & 0 & \tilde{\mu} \\ \tilde{\lambda} & \tilde{\lambda} & 0 \end{bmatrix} - \frac{C_1}{C_3} \begin{bmatrix} A_{xx}^2 & A_{xx}A_{yy} & A_{xx}A_{xy} \\ A_{xx}A_{yy} & A_{yy}^2 & A_{yy}A_{xy} \\ A_{xx}A_{xy} & A_{yy}A_{xy} & A_{xy}^2 \\ A_{xx}A_{zz} & A_{yy}A_{zz} & A_{xy}A_{zz} \end{bmatrix} \right] \tag{A.3}$$

$$\{\Delta\sigma'\} = \begin{pmatrix} \Delta\sigma'_{xx} \\ \Delta\sigma'_{yy} \\ \Delta\sigma'_{xy} \\ \Delta\sigma'_{zz} \end{pmatrix} \tag{A.4}$$

$$\{\Delta\varepsilon\} = \begin{pmatrix} \Delta\varepsilon_{xx} \\ \Delta\varepsilon_{yy} \\ \Delta\gamma_{xy} \end{pmatrix} \tag{A.5}$$

$$\{\Delta\sigma^R\} = \frac{C_2}{C_3} \begin{pmatrix} A_{xx} \\ A_{yy} \\ A_{xy} \\ A_{zz} \end{pmatrix} \Delta t \tag{A.6}$$

in which

$$A_{ij} = \tilde{\lambda}\frac{\partial f}{\partial \sigma_{kk}}\delta_{ij} + 2\tilde{\mu}\frac{\partial f}{\partial \sigma_{ij}}, \ (i,j = x,y,z), \qquad \frac{\partial f}{\partial \sigma_{kk}} = \frac{\partial f}{\partial \sigma_{xx}} + \frac{\partial f}{\partial \sigma_{yy}} + \frac{\partial f}{\partial \sigma_{zz}} \tag{A.7}$$

$$C_1 = 1 - exp(-\frac{\varepsilon_v^{vp}}{\alpha}), \qquad C_2 = \dot{v}_o \, exp(\frac{f - \varepsilon_v^{vp}}{\alpha}) \tag{A.8}$$

$$C_3 = \left[\tilde{\lambda} \left(\frac{\partial f}{\partial \sigma_{kk}} \right)^2 + 2\tilde{\mu} \left\{ \left(\frac{\partial f}{\partial \sigma_{xx}} \right)^2 + \left(\frac{\partial f}{\partial \sigma_{yy}} \right)^2 + 2 \left(\frac{\partial f}{\partial \sigma_{xy}} \right)^2 + \left(\frac{\partial f}{\partial \sigma_{zz}} \right)^2 \right\} \right] C_1 + \frac{\partial f}{\partial \sigma_{kk}} \tag{A.9}$$

Where $\tilde{\lambda}$ and $\tilde{\mu}$ denote Lame's constant and the shear modulus, ε_v^{vp} is the viscoplastic volumetric strain, α is the secondary compression index, and f is the yield function. $\tilde{\lambda}$ and $\tilde{\mu}$ can be expressed in the following form:

$$\tilde{\lambda} = K - \frac{2}{3}G, \qquad \tilde{\mu} = G = \frac{3(1-2\nu)}{2(1+\nu)}K \tag{A.10}$$

Here, ν is Poisson's ratio, K is the bulk modulus expressed in the following form:

$$K = \frac{1+e_o}{\kappa} p' \tag{A.11}$$

in which e_o and κ are the initial value of void ratio and the compression and swelling index.

APPENDIX B

The concrete form of the model for plane-strain version is expressed as follows in Eq. (3.31):

$$\{\Delta\sigma'\} = [D^{ep}]\{\Delta\varepsilon\} \tag{B.1}$$

Equation (B.1) can be expressed in matrix notation as

$$\begin{pmatrix} \Delta\sigma'_{xx} \\ \Delta\sigma'_{yy} \\ \Delta\sigma'_{xy} \\ \Delta\sigma'_{zz} \end{pmatrix} = \left[\begin{bmatrix} \tilde{\lambda}+2\tilde{\mu} & \tilde{\lambda} & 0 \\ \tilde{\lambda} & \tilde{\lambda}+2\tilde{\mu} & 0 \\ 0 & 0 & \tilde{\mu} \\ \tilde{\lambda} & \tilde{\lambda} & 0 \end{bmatrix} - \frac{1}{C_4} \begin{bmatrix} A_{xx}^2 & A_{xx}A_{yy} & A_{xx}A_{xy} \\ A_{xx}A_{yy} & A_{yy}^2 & A_{yy}A_{xy} \\ A_{xx}A_{xy} & A_{yy}A_{xy} & A_{xy}^2 \\ A_{xx}A_{zz} & A_{yy}A_{zz} & A_{xy}A_{zz} \end{bmatrix} \right] \begin{pmatrix} \Delta\varepsilon_{xx} \\ \Delta\varepsilon_{yy} \\ \Delta\gamma_{xy} \end{pmatrix} \tag{B.2}$$

where the elasto-plastic constitutive matrix, $[D^{ep}]$ is defined as follows:

$$[D^{ep}] = \left[\begin{bmatrix} \tilde{\lambda}+2\tilde{\mu} & \tilde{\lambda} & 0 \\ \tilde{\lambda} & \tilde{\lambda}+2\tilde{\mu} & 0 \\ 0 & 0 & \tilde{\mu} \\ \tilde{\lambda} & \tilde{\lambda} & 0 \end{bmatrix} - \frac{1}{C_4} \begin{bmatrix} A_{xx}^2 & A_{xx}A_{yy} & A_{xx}A_{xy} \\ A_{xx}A_{yy} & A_{yy}^2 & A_{yy}A_{xy} \\ A_{xx}A_{xy} & A_{yy}A_{xy} & A_{xy}^2 \\ A_{xx}A_{zz} & A_{yy}A_{zz} & A_{xy}A_{zz} \end{bmatrix} \right] \tag{B.3}$$

in which

$$A_{ij} = \tilde{\lambda}\frac{\partial f}{\partial \sigma_{kk}}\delta_{ij} + 2\tilde{\mu}\frac{\partial f}{\partial \sigma_{ij}}, \ (i,j = x,y,z), \qquad \frac{\partial f}{\partial \sigma_{kk}} = \frac{\partial f}{\partial \sigma_{xx}} + \frac{\partial f}{\partial \sigma_{yy}} + \frac{\partial f}{\partial \sigma_{zz}} \tag{B.4}$$

$$C_4 = \tilde{\lambda}\left(\frac{\partial f}{\partial \sigma_{kk}}\right)^2 + 2\tilde{\mu}\left\{\left(\frac{\partial f}{\partial \sigma_{xx}}\right)^2 + \left(\frac{\partial f}{\partial \sigma_{yy}}\right)^2 + 2\left(\frac{\partial f}{\partial \sigma_{xy}}\right)^2 + \left(\frac{\partial f}{\partial \sigma_{zz}}\right)^2\right\} + \frac{\partial f}{\partial \sigma_{kk}} \tag{B.5}$$

Where $\tilde{\lambda}$ and $\tilde{\mu}$ denote Lame's constant and the shear modulus expressed in the following form:

$$\tilde{\lambda} = K - \frac{2}{3}G, \qquad \tilde{\mu} = G = \frac{3(1-2\nu)}{2(1+\nu)}K \tag{B.6}$$

Here, ν is Poisson's ratio, K is the bulk modulus expressed in the following form:

$$K = \frac{1+e_o}{\kappa}p' \tag{B.7}$$

in which e_o and κ are the initial value of void ratio and the compression and swelling index.

APPENDIX C

The Figure schematically shows the elements surrounding i element for finite element analysis.

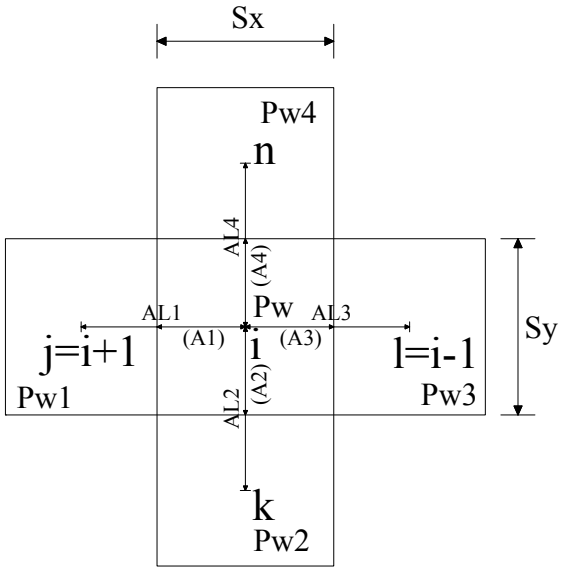

in Eq. (3.49), the divergence of the vector of flow rate $q_{i,i}$ is expressed as follows:

$$-\Delta t q_{i,i} = -\Delta t\left[\left(q_j - q_l\right) + \left(q_k - q_n\right)\right] \tag{C.1}$$

where, the flow rate q is defined by obeying isotropic Darcy's law in the following form:

$$q_j = v_j \times S_y = k_{x(eq)} \times \frac{p_w - p_{wl}}{\gamma_w \times AL_l} \times S_y = k_{xi} \times \frac{p_w - p_{wl}}{\gamma_w} \times S_y \Big/ \left\{\left(AL_l - A_l\right) \times \frac{k_{xi}}{k_{xj}} + A_l\right\} \tag{C.2}$$

in which the discharge velocity v is defined as:

$$v_j = k_{x(eq)} \times i_j \tag{C.3}$$

Here, the equivalent coefficient of permeability $k_{x(eq)}$ and the hydraulic gradient i are defined as follows:

$$k_{x(eq)} = \frac{AL_1}{\dfrac{A_1}{k_{xi}} + \dfrac{AL_1 - A_1}{k_{xj}}} AL_1 \times k_{xi} \Big/ \left\{ (AL_1 - A_1) \times \frac{k_{xi}}{k_{xj}} + A_1 \right\} \tag{C.4}$$

$$i_j = \frac{p_w - p_{w1}}{\gamma_w \times AL_1} \tag{C.5}$$

where k_{xi} and k_{xj} denote the permeability coefficient of x-direction of i and j element respectively, γ_w is the unit weight of water.

The flow rate q components for the other elements are defined by the same procedure with Eq. (C.2) in the following forms:

$$q_l = v_l \times S_y = k_{x(eq)} \times \frac{p_{w3} - p_w}{\gamma_w \times AL_3} \times S_y = k_{xi} \times \frac{p_{w3} - p_w}{\gamma_w} \times S_y \Big/ \left\{ (AL_3 - A_3) \times \frac{k_{xi}}{k_{xl}} + A_3 \right\} \tag{C.6}$$

$$q_k = v_k \times S_x = k_{y(eq)} \times \frac{p_w - p_{w2}}{\gamma_w \times AL_2} \times S_x = k_{yi} \times \frac{p_w - p_{w2}}{\gamma_w} \times S_x \Big/ \left\{ (AL_2 - A_2) \times \frac{k_{yi}}{k_{yk}} + A_2 \right\} \tag{C.7}$$

$$q_n = v_n \times S_x = k_{y(eq)} \times \frac{p_{w4} - p_w}{\gamma_w \times AL_4} \times S_x = k_{yi} \times \frac{p_{w4} - p_w}{\gamma_w} \times S_x \Big/ \left\{ (AL_4 - A_4) \times \frac{k_{yi}}{k_{yn}} + A_4 \right\} \tag{C.8}$$

Substitution Eqs. (C.2), (C.6), (C.7) and (C.8) into Eq. (C.1) yields

$$\begin{aligned} -\Delta t q_{i,i} = & -\frac{\Delta t}{\gamma_w} \left[\begin{array}{l} (k_{xi} \times S_y) \Big/ \left\{ (AL_1 - A_1) \times \dfrac{k_{xi}}{k_{xj}} + A_1 \right\} + (k_{yi} \times S_x) \Big/ \left\{ (AL_2 - A_2) \times \dfrac{k_{yi}}{k_{yk}} + A_2 \right\} \\ + (k_{xi} \times S_y) \Big/ \left\{ (AL_3 - A_3) \times \dfrac{k_{xi}}{k_{xl}} + A_3 \right\} + (k_{yi} \times S_x) \Big/ \left\{ (AL_4 - A_4) \times \dfrac{k_{yi}}{k_{yn}} + A_4 \right\} \end{array} \right] p_w \\ & + \frac{\Delta t}{\gamma_w} \left[\begin{array}{l} (k_{xi} \times S_y) \Big/ \left\{ (AL_1 - A_1) \times \dfrac{k_{xi}}{k_{xj}} + A_1 \right\} \times p_{w1} + (k_{yi} \times S_x) \Big/ \left\{ (AL_2 - A_2) \times \dfrac{k_{yi}}{k_{yk}} + A_2 \right\} \times p_{w2} \\ + (k_{xi} \times S_y) \Big/ \left\{ (AL_3 - A_3) \times \dfrac{k_{xi}}{k_{xl}} + A_3 \right\} \times p_{w3} + (k_{yi} \times S_x) \Big/ \left\{ (AL_4 - A_4) \times \dfrac{k_{yi}}{k_{yn}} + A_4 \right\} \times p_{w4} \end{array} \right] \end{aligned} \tag{C.9}$$

Eq. (C.9) can be written as expressed in Eq. (3.55) by using coefficient B in the following form:

$$-\Delta t q_{i,i} = B p_w + \sum_{i=1}^{4} B_i p_{wi} \tag{C.10}$$

where,

$$B = -\left(B_1 + B_2 + B_3 + B_4\right) \tag{C.11}$$

$$B_1 = \frac{\Delta t}{\gamma_w} \times \left(k_{xi} \times S_y\right) / \left\{ \left(AL_1 - A_1\right) \times \frac{k_{xi}}{k_{xj}} + A_1 \right\} \tag{C.12}$$

$$B_2 = \frac{\Delta t}{\gamma_w} \times \left(k_{yi} \times S_x\right) / \left\{ \left(AL_2 - A_2\right) \times \frac{k_{yi}}{k_{yk}} + A_2 \right\} \tag{C.13}$$

$$B_3 = \frac{\Delta t}{\gamma_w} \times \left(k_{xi} \times S_y\right) / \left\{ \left(AL_3 - A_3\right) \times \frac{k_{xi}}{k_{xl}} + A_3 \right\} \tag{C.14}$$

$$B_4 = \frac{\Delta t}{\gamma_w} \times \left(k_{yi} \times S_x\right) / \left\{ \left(AL_4 - A_4\right) \times \frac{k_{yi}}{k_{yn}} + A_4 \right\} \tag{C.15}$$